

**SUPRAMOLECULAR SELF-ASSEMBLY OF HOMO- AND
HETERO-LEPTIC METAL COMPLEXES USING
DIPYRRROMETHENE LIGANDS**

by

LI MA

B.Sc., Nankai University, 2002

A THESIS SUBMITTED IN PARTIAL FULFILLMENT OF THE
REQUIREMENTS FOR THE DEGREE OF
DOCTOR OF PHILOSOPHY

in

THE FACULTY OF GRADUATE STUDIES

(Chemistry)

THE UNIVERSITY OF BRITISH COLUMBIA

(Vancouver)

October 2010

© Li Ma, 2010

Abstract

Dipyrromethenes (dipyrins) have been widely studied as important precursors for the synthesis of porphyrins for decades. More recently, bisdipyrins, constructed through the controlled linkage of two dipyrins, have drawn considerable attention in the field of supramolecular chemistry where supramolecular structures have exhibited potential application in the areas of gas storage and separation, catalysis and drug delivery. Bisdipyrin metal complexes featuring double-, triple-helical or triangular structures have been previously reported by our group. The primary goal of this project was to synthesize new bisdipyrin ligands to explore their applicability to the construction of novel homoleptic and heteroleptic metal complexes, such as circular helicates, grids, racks and ladders.

The key to the successful synthesis of the homoleptic metal complexes (circular helicates and grids) is the spacer linking two dipyrin units. Phenylodiacetylene and carbazolediacetylene were introduced to generate dinuclear circular helicates, whereas ligands with diacetylene as the spacer formed even higher nuclear oligomers. In the case of grids, the two central pyrrole rings were fused to a ring to allow the two dipyrin units to be parallel to each other to eliminate unwanted circular helicates. Furthermore, both hexagons and grids are formed when phenyl groups were introduced to the dipyrin ligands, and they show channel structures in their crystalline frameworks. Studies on driving forces such as π - π stacking and F-F interactions were conducted.

A series of heteroleptic anti-parallel and parallel racks were prepared. Surprisingly, zigzag racks along with the parallel racks were generated without unwanted grids when the ligand with bulky phenyl groups was introduced. During the preparation of ladders, two heteroleptic metal complexes emerged that act as both the ligand and metal ion source. A Cu^{II} rigid ladder and a Zn^{II} flexible ladder were synthesized and characterized by X-ray diffraction analysis. Both ladders display rectangular channel structures in the solid state, which were guided by intermolecular CH/ π and/or CH \cdots O interactions.

Preface

The inspiration for this project was provided by my supervisor, Prof. David Dolphin. I established the key parameters of this project through an exhaustive search of the literature and initial investigations. I designed, synthesized, purified and fully characterized the bisdipyrrin ligands which successfully resulted in the desired circular helicates, grids, racks and ladders. One paper (Ma, L.; Shin, J.-Y.; Patrick, B. O.; Dolphin, D. *CrystEngComm*, **2008**, *10*, 1539–1541) has been published from this work thus far (from Chapter Two). Six figures from the paper have been incorporated into Chapter Two. I conducted the entire research work and was the primary writer of the paper. Dr. Ji-Young Shin provided useful suggestions for the packing of the three circular helicates in the solid state and some picture-drawing techniques in the paper. Dr. Brian O. Patrick solved the crystal structures. Prof. David Dolphin offered constructive guidance and invaluable suggestions during the entire course of research and paper preparation.

Table of Contents

Abstract	ii
Preface	iv
Table of Contents	v
List of Tables	ix
List of Figures	xi
List of Schemes	xviii
List of Abbreviations	xix
Acknowledgements	xxii
Chapter One: Introduction	1
1.1 Supramolecular Chemistry	2
1.2 Self-Assembly	2
1.3 Inorganic Self-Assembly	3
1.4 Circular Helicates	4
1.5 Grid-Type Metal Complexes	11
1.6 Rack-Type Metal Complexes	18
1.7 Ladder-Type Metal Complexes	22
1.8 Dipyrrromethene (Dipyrin) Metal Complexes	24
1.9 Goals and Scope of the Thesis	28

Chapter Two: Homoleptic Circular Helicates.....	31
2.1 Design Strategy	32
2.2 Results and Discussion.....	34
2.2.1 Phenylodiacetylene Bisdipyrrin Co ^{II} Complex.....	34
2.2.1.1 Synthesis of Phenylodiacetylene Bisdipyrrin Co ^{II} Complex	34
2.2.1.2 X-Ray Analysis of Phenylodiacetylene Bisdipyrrin Co ^{II} Complex	36
2.2.2 Carbazolediacetylene Bisdipyrrin Co ^{II} Complex.....	38
2.2.2.1 Synthesis of Carbazolediacetylene Bisdipyrrin Co ^{II} Complex.....	38
2.2.2.2 X-Ray Analysis of Carbazolediacetylene Bisdipyrrin Co ^{II} Complex.....	40
2.2.3 Diacetylene Bisdipyrrin Metal Complexes.....	43
2.2.3.1 Synthesis of Diacetylene Bisdipyrrin Metal Complexes	43
2.2.3.2 ¹ H NMR Spectra of Diacetylene Bisdipyrrin Zn ^{II} Complexes	46
2.2.3.3 X-Ray Analysis of Diacetylene Bisdipyrrin Zn ^{II} Complexes.....	48
2.2.4 α,β -Ethyl Diacetylene Bisdipyrrin Metal Complexes.....	52
2.2.4.1 Synthesis of α,β -Ethyl Diacetylene Bisdipyrrin Metal Complexes.....	53
2.2.4.2 ¹ H NMR Spectra of α,β -Ethyl Diacetylene Bisdipyrrin Zn ^{II} Complex ...	55
2.2.4.3 X-Ray Analysis of α,β -Ethyl Diacetylene Bisdipyrrin Zn ^{II} Complex	57
2.2.5 Electronic Absorption Spectra of Diacetylene Bisdipyrrin Metal Complexes	59
2.3 Conclusions	62
Chapter Three: Homoleptic Grids and Hexagons.....	63
3.1 Design Strategy	64

3.2 Results and Discussion.....	66
3.2.1 Ring Fused Bisdipyrrin Metal Complexes	66
3.2.1.1 Synthesis of Ring Fused Bisdipyrrin Metal Complexes.....	66
3.2.1.2 ¹ H NMR Spectra of Ring Fused Bisdipyrrin Zn ^{II} Complexes.....	71
3.2.1.3 X-Ray Analysis of Ring Fused Bisdipyrrin Zn ^{II} Complexes.....	76
3.2.1.3.1 X-Ray Analysis of Ring Fused Bisdipyrrin [2×2] Zn ^{II} Grids	76
3.2.1.3.2 X-Ray Analysis of Ring Fused Bisdipyrrin Zn ^{II} Hexagon	80
3.2.1.4 Electronic Absorption Spectra of Ring Fused Bisdipyrrin Metal Complexes	82
3.3 Conclusions.....	86
Chapter Four: Heteroleptic Racks and Ladders.....	87
4.1 Design Strategy	88
4.2 Results and Discussion.....	90
4.2.1 Rack-Type Metal Complexes	90
4.2.1.1 Synthesis of Rack-Type Metal Complexes.....	90
4.2.1.2 ¹ H NMR Spectra of Zn ^{II} Rack-Type and Zigzag Rack-Type Complexes	95
4.2.1.3 X-Ray Analysis of Zn ^{II} Rack IV-16-3.....	97
4.2.1.4 Electronic Absorption Spectra of Metal Racks and Zigzag Racks.....	99
4.2.2 Rigid Ladder-Type Metal Complexes.....	102
4.2.2.1 Synthesis of Rigid Ladder-Type Metal Complexes.....	103
4.2.2.2 X-Ray Analysis of Cu ^{II} Rigid Ladder IV-23-L.....	106

4.2.2.3 Electronic Absorption Spectra of Metal Rigid Ladders.....	110
4.2.3 Flexible Ladder-Type Metal Complexes	112
4.2.3.1 Synthesis of Flexible Ladder-Type Metal Complexes.....	112
4.2.3.2 ¹ H NMR Spectra of Zn ^{II} Flexible Ladder-Type Complexes.....	115
4.2.3.3 X-Ray Analysis of Zn ^{II} Flexible Ladder IV-42-L.....	117
4.2.3.4 Electronic Absorption Spectra of Zn ^{II} Flexible Ladders.....	121
4.3 Conclusions	123
Chapter Five: Experimental Sections	124
5.1 General Information	125
5.2 Experimental Procedure and Data.....	127
5.3 Crystal Data.....	198
Chapter Six: Conclusions and Future Work	209
6.1 Conclusions	210
6.2 Future Work.....	211
References.....	214

List of Tables

Table 2-1 Metal-to-ligand charge transfer transition band λ_{\max} (nm) for tri-, tetra- and/or pentameric metal complexes in chloroform.	60
Table 3-1 Spin-allowed ligand-centered transition band $\lambda_{\max 1}$ (nm) and metal-to-ligand charge transfer transition band $\lambda_{\max 2}$ (nm) for the metal grids and/or hexagons in chloroform.....	85
Table 4-1 Metal-to-ligand charge transfer transition bands λ_{\max} (nm) for the Zn ^{II} racks in chloroform.	100
Table 4-2 Metal-to-ligand charge transfer transition bands $\lambda_{\max 1}$ and $\lambda_{\max 3}$ (nm) and spin-allowed ligand-centered transition band $\lambda_{\max 2}$ (nm) for the metal racks and zigzag racks in chloroform.	102
Table 4-3 Intermolecular CH/ π interactions in the crystal structure of Cu ^{II} rigid ladder IV-23-L	110
Table 4-4 Ligand-centered transition band λ_{\max} (nm) for the ligands and metal-to-ligand charge transfer transition bands λ_{\max} (nm) for metal complexes in chloroform.....	111
Table 4-5 Intermolecular CH/O and CH/ π interactions in the crystal structure of Zn ^{II} flexible ladder IV-42-L	120
Table 4-6 Metal-to-ligand charge transfer transition band(s) λ_{\max} (nm) for Zn ^{II} ladders in chloroform.	122
Table 5-1 Crystal data and structure refinement for II-7-2	198
Table 5-2 Crystal data and structure refinement for II-13-2	199
Table 5-3 Crystal data and structure refinement for II-25-3	200

Table 5-4 Crystal data and structure refinement for II-26-3	201
Table 5-5 Crystal data and structure refinement for II-35-3	202
Table 5-6 Crystal data and structure refinement for III-27-4	203
Table 5-7 Crystal data and structure refinement for III-33-4	204
Table 5-8 Crystal data and structure refinement for III-36-6	205
Table 5-9 Crystal data and structure refinement for IV-16-3	206
Table 5-10 Crystal data and structure refinement for IV-23-L	207
Table 5-11 Crystal data and structure refinement for IV-42-L	208

List of Figures

Figure 1-1 Diagram of (a) trimeric circular helicate; (b) tetrameric circular helicate and (c) grid.	5
Figure 1-2 Synthetic route for preparation of trinuclear circular helicate I-2 (counterions omitted for clarity).	6
Figure 1-3 Synthetic route for preparation of trinuclear circular helicate I-4 (counterions omitted for clarity).	7
Figure 1-4 Synthetic route for preparation of trinuclear circular helicate I-6 (counterions omitted for clarity).	8
Figure 1-5 Synthetic route for preparation of tetranuclear circular helicate I-8 (counterions omitted for clarity).	9
Figure 1-6 Synthetic route for preparation of tetranuclear circular helicate I-10 (counterions omitted for clarity).	9
Figure 1-7 Synthetic route for preparation of hexanuclear circular helicate I-12 (counterions omitted for clarity).	10
Figure 1-8 Synthetic route for preparation of Cu ^{II} [2×2] grid I-14 (counterions omitted for clarity).	12
Figure 1-9 Synthetic route for preparation of Cu ^I pseudo[3×3] grid I-16 (counterions omitted for clarity).	13
Figure 1-10 Synthetic route for preparation of Pb ^{II} [2×2] grid I-20 (counterions omitted for clarity).	14

Figure 1-11 Synthetic route for preparation of Cu ^{II} [2×2] grid I-22 (counterions omitted for clarity).....	15
Figure 1-12 Synthetic route for preparation of Ag ^I [3×3] grid I-24 (counterions omitted for clarity).....	16
Figure 1-13 Synthetic route for preparation of Pb ^{II} [4×4] grid I-26 (counterions omitted for clarity).....	17
Figure 1-14 Synthetic route for preparation of Cu ^I rack I-29 (crown ether chain and counterions omitted for clarity).....	19
Figure 1-15 Synthetic route for preparation of Ru ^{II} rack I-32 (counterions omitted for clarity).....	20
Figure 1-16 Synthetic route for preparation of parallel Ru ^{II} rack I-34 (counterions omitted for clarity).....	21
Figure 1-17 Synthetic route for preparation of anti-parallel Ru ^{II} rack I-36 (counterions omitted for clarity).....	21
Figure 1-18 Synthetic route for preparation of heteroleptic Cu ^I ladder I-39 (counterions omitted for clarity).....	22
Figure 1-19 Synthetic route for preparation of heteroleptic Zn ^{II} ladder I-42 (counterions omitted for clarity).....	23
Figure 1-20 IUPAC-recommended (left) and the commonly simplified (right) numbering systems for dipyrins.....	24
Figure 1-21 Bipyridine, dipyrin ligands and their M ²⁺ complexes.....	25
Figure 1-22 Bisdipyrin ligands for preparation of Zn ^{II} or Co ^{II} double-stranded helicates.....	26
Figure 1-23 Synthetic route for preparation of Co ^{III} triple-stranded helicate I-44 and mesocate	

I-45	27
Figure 1-24 Synthetic route for preparation of Zn ^{II} trinuclear circular helicate I-47	28
Figure 2-1 Reported bisdipyrrin ligands for double- and triple-stranded helicates.	32
Figure 2-2 ¹ H NMR spectrum of dimeric Co ^{II} complex II-7-2 in CD ₂ Cl ₂ (300 MHz).	36
Figure 2-3 ORTEP diagram of dimeric Co ^{II} complex II-7-2 (thermal ellipsoids are scaled to the 50 % probability level): (a) top view and (b) side view.	37
Figure 2-4 (a) Top view of the molecular space-filled packing of II-7-2 ; (b) top view and (c) side view of the twin-tunnel structure of II-7-2 (reprinted with permission of the RSC).	37
Figure 2-5 ¹ H NMR spectrum of dimeric Co ^{II} complex II-13-2 in CD ₂ Cl ₂ (300 MHz).	40
Figure 2-6 ORTEP diagram of dimeric Co ^{II} complex II-13-2 (thermal ellipsoids are scaled to the 50 % probability level): (a) top view and (b) side view.	41
Figure 2-7 (a) Top view of the molecular space-filled packing of II-13-2 ; (b) side view and (c) top view of the single tunnel structure of II-13-2 (reprinted with permission of the RSC); (d) π - π stacking interactions between the carbazole rings of the adjacent molecules (distance = 3.32 Å) by stick representation.	42
Figure 2-8 ¹ H NMR spectra (alkyl region) of ligand II-21 (top), trimeric II-25-3 (middle) and tetrameric II-25-4 (bottom) Zn ^{II} complexes in CDCl ₃ (300 MHz).	47
Figure 2-9 ORTEP diagram of trimeric Zn ^{II} complex II-25-3 (thermal ellipsoids are scaled to the 50 % probability level).	49
Figure 2-10 Stepwise packing pattern of the individual layers for II-25-3 ; positions of tunnels were displayed as yellow spheres in the last figure for clarity (reprinted with permission of the RSC).	49

Figure 2-11 Space-filled packing of II-25-3 : without (left) and with solvent molecules in space-filling (right) or stick (center) representations showing 3-fold axis disorder (reprinted with permission of the RSC).....	50
Figure 2-12 ORTEP diagram of trimeric Zn ^{II} complex II-26-3 (thermal ellipsoids are scaled to the 50 % probability level).	51
Figure 2-13 Space-filled packing of II-26-3 : (a) top view; (b) and (c) side views.	51
Figure 2-14 Diagram of (a) Zn ^{II} trimeric circular helicate; (b) Zn ^{II} tetrameric circular helicate and (c) Zn ^{II} grid.	52
Figure 2-15 ¹ H NMR spectra (alkyl region) of ligand II-34 (top) (400 MHz), trimeric II-35-3 (middle) and tetrameric II-35-4 (bottom) Zn ^{II} complexes in CDCl ₃ (300 MHz).....	56
Figure 2-16 ORTEP diagram of trimeric Zn ^{II} complex II-35-3 (thermal ellipsoids are scaled to the 33 % probability level).	58
Figure 2-17 Space-filled packing of II-35-3 : (a) top view; (b) and (c) side views.	58
Figure 2-18 Electronic absorption spectra of bisdipyrrin metal complexes in chloroform: (a) II-25 , (b) II-26 , (c) II-27 , (d) II-28 , (e) II-29 , (f) II-30 , (g) II-35 and (h) II-36	61
Figure 3-1 Ligands based on bipyridine introduced by Lehn and Siegel for preparation of grid-type metal complexes.....	64
Figure 3-2 Different conformations of the dipyrin units in one strand linked by diacetylene (left) and a fused ring (right).	65
Figure 3-3 ¹ H NMR spectra (aromatic region) of ligand III-24 (top) and Zn ^{II} grid III-33-4 (bottom) in CDCl ₃ (400 MHz).....	72
Figure 3-4 ¹ H NMR spectra (alkyl region) of ligand III-24 (top) and Zn ^{II} grid III-33-4 (bottom)	

in CDCl ₃ (400 MHz).....	72
Figure 3-5 ¹ H NMR spectra (aromatic region) of ligand III-26 (top), Zn ^{II} grid III-36-4 (middle) and Zn ^{II} hexagon III-36-6 (bottom) in CDCl ₃ (400 MHz).....	74
Figure 3-6 ¹ H NMR spectra (alkyl region) of ligand III-26 (top), Zn ^{II} grid III-36-4 (middle) and Zn ^{II} hexagon III-36-6 (bottom) in CDCl ₃ (400 MHz).....	75
Figure 3-7 Equilibrium between [2×2] Zn ^{II} grid III-36-4 and Zn ^{II} hexagon III-36-6 in CDCl ₃ .	76
Figure 3-8 Crystal structure of [2×2] Zn ^{II} grid III-27-4 : (a) ORTEP diagram (thermal ellipsoids are scaled to the 50% probability level) and (b) space-filled representation.....	77
Figure 3-9 Stick-packing of [2×2] Zn ^{II} grid III-27-4 : (a) top view; (b) and (c) side views.	78
Figure 3-10 Crystal structure of [2×2] Zn ^{II} grid III-33-4 : (a) ORTEP diagram (thermal ellipsoids are scaled to the 50% probability level) and (b) space-filled representation.....	79
Figure 3-11 Stick-packing of [2×2] Zn ^{II} grid III-33-4 : (a) top view; (b) side view (with hexane molecules in red) and (c) π-π stacking interactions between the phenyl rings (distance = ~ 3.5 Å).	80
Figure 3-12 Crystal structure of Zn ^{II} hexagon III-36-6 : (a) ORTEP diagram (thermal ellipsoids are scaled to the 50% probability level); (b) space-filled representation and (c) stick representation with CHCl ₃ molecules.	81
Figure 3-13 Stick packing of Zn ^{II} hexagon III-36-6 : (a) top view; (b) side view; (c) F-F interactions between neighbouring <i>p</i> -fluorophenyl groups of the adjacent molecules (alkyl groups omitted for clarity) and (d) side view (with CHCl ₃ molecules in red/blue).	82
Figure 3-14 Electronic absorption spectra of cyclohexane bisdipyrrin metal complexes in chloroform: (a) III-27-4 , III-29-4 through III-33-4 and III-35-4 ; (b) III-34 and (c) III-36	84

Figure 4-1 Rack-type Cu ^I complexes using bipyridine ligands synthesized by Lehn (counterions omitted for clarity).....	88
Figure 4-2 Ladder-type Cu ^I and Zn ^{II} complexes using bipyridine/terpyridine ligands reported by Lehn and Schmittel (counterions omitted for clarity).....	89
Figure 4-3 ¹ H NMR spectra (aromatic region) of ligand III-24 (400 MHz) and IV-2 (300 MHz) (top), Zn ^{II} rack IV-16-3 (300 MHz) (middle) and zigzag Zn ^{II} rack IV-16-2 (400 MHz) (bottom) in CDCl ₃	96
Figure 4-4 Crystal structure of Zn ^{II} rack IV-16-3 : (a) ORTEP diagram (thermal ellipsoids are scaled to the 50% probability level) and (b) space-filled representation.....	98
Figure 4-5 Stick-packing of Zn ^{II} rack IV-16-3 : (a) top view and (b) side view.	98
Figure 4-6 Electronic absorption spectra of rack-type Zn ^{II} complexes in chloroform: (a) IV-9-2 through IV-11-2 ; (b) IV-12-1 through IV-15-2 ; (c) IV-16 and (d) IV-17	100
Figure 4-7 Crystal structure of Cu ^{II} ladder IV-23-L : (a) ORTEP diagram (thermal ellipsoids are scaled to the 50% probability level) and (b) space-filled representation.....	107
Figure 4-8 Stick-packing of Cu ^{II} ladder IV-23-L : (a) top view; (b) and (c) side views.	108
Figure 4-9 Five types of CH/π interactions (A to E) in IV-23-L with stick representation: (a) top view and (b) side view.	109
Figure 4-10 Electronic absorption spectra of rigid ladder-type metal complexes in chloroform: (a) Zn ^{II} ladder IV-22-L with ligand IV-18 and complex IV-20 ; (b) Cu ^{II} ladder IV-23-L with ligand IV-19 and complex IV-21	111
Figure 4-11 Partial ¹ H NMR spectra of ligand IV-18 , Zn ^{II} ladders IV-40-L , IV-42-L and IV-43-L in CDCl ₃ (400 MHz).	116

Figure 4-12 Crystal structure of Zn ^{II} ladder IV-42-L : (a) ORTEP diagram (thermal ellipsoids are scaled to the 50% probability level) and (b) space-filled representation.....	118
Figure 4-13 Stick-packing of Zn ^{II} ladder IV-42-L : (a) top view; (b) and (c) side views.	119
Figure 4-14 Two types of CH/O interactions (A and B) and two types of CH/ π interactions (C and D) in IV-42-L with stick representation: (a) top view and (b) side view.	120
Figure 4-15 Electronic absorption spectra of flexible ladder-type Zn ^{II} complexes in chloroform: (a) Zn ^{II} ladder IV-40-L through IV-44-L ; (b) Zn ^{II} ladder IV-42-L and IV-45-L through IV-48-L ; (c) Zn ^{II} ladder IV-42-L and dimer IV-42-D	122

List of Schemes

Scheme 2-1 Synthetic route for preparation of dimeric Co ^{II} complex II-7-2	35
Scheme 2-2 Synthetic route for preparation of dimeric Co ^{II} complex II-13-2	39
Scheme 2-3 Synthetic route for preparation of tri-, tetra- and/or pentameric metal complexes.....	45
Scheme 2-4 Synthetic route for preparation of tri- and tetrameric metal complexes.....	54
Scheme 3-1 Synthetic route for preparation of pyrrole-2-carbaldehyde derivatives.....	67
Scheme 3-2 Synthetic route for preparation of [2×2] metal grids and/or hexagons.....	69
Scheme 4-1 Synthetic route to the ligands for preparation of rack-type metal complexes.....	91
Scheme 4-2 Synthetic route for preparation of rack-type metal complexes.....	94
Scheme 4-3 Synthetic route for preparation of the heteroleptic Cu ^{II} dipyrin complex by Cohen.	104
Scheme 4-4 Synthetic route for preparation of the heteroleptic Zn ^{II} and Cu ^{II} bisdipyrin complexes.....	104
Scheme 4-5 Synthetic route for preparation of rigid ladder-type metal complexes.....	105
Scheme 4-6 Synthetic route for preparation of pyrrole-2-carbaldehyde derivatives.....	113
Scheme 4-7 Synthetic route for preparation of flexible ladder-type Zn ^{II} complexes.....	114
Scheme 6-1 Synthetic route for preparation of unsymmetric ring fused bisdipyrin ligand and its corresponding Zn ^{II} grid.....	212
Scheme 6-2 Synthetic route for preparation of heteroleptic Zn ^{II} complexes using bisdipyrin ligand III-24 and IV-8	213

List of Abbreviations

Ac	acetyl
acac	acetylacetonate
anal.	analytical
Ar	aryl
Bn	benzyl
br	broad
Calcd	calculated
d	doublet
dd	doublet of doublets
DCE	dichloroethane
DCTB	2-[(2 E)-3-(4- <i>tert</i> -butylphenyl)-2-methylprop-2-enylidene]malononitrile
DME	dimethoxyethane
DMF	N,N'-dimethylformamide
DMSO	dimethyl sulfoxide
DNA	deoxyribonucleic acid
EI	electron impact
ESI	electrospray ionization
Et	ethyl
GPC	gel permeation chromatography
h	hour(s)

HRMS	high resolution mass spectrometry
MLCT	metal-to-ligand charge transfer
IUPAC	International Union of Pure and Applied Chemistry
LC	ligand-centered
m	meta
m	multiplet
MALDI-TOF	matrix-assisted laser desorption/ionization-time of flight
Me	methyl
min	minute(s)
MS	mass spectrometry
NIS	N-iodosuccinimide
nm	nanometer(s)
NMR	nuclear magnetic resonance
ORTEP	Oak Ridge Thermal Ellipsoid Plot
Ph	phenyl
ppm	parts per million
RSC	Royal Society of Chemistry
s	singlet
t	triplet
TFA	trifluoroacetic acid
THF	tetrahydrofuran
TLC	thin-layer chromatography

TMOF trimethyl orthoformate

TMS trimethylsilyl

UV/Vis ultraviolet/visible

Acknowledgements

First of all, my foremost sincere gratitude goes to my supervisor, Prof. David Dolphin, for his constructive guidance, kindness, patience and invaluable support during the course of my entire research work.

I would also like to thank all of the members of Dolphin's group, past and present. My life in UBC would never been so fruitful and enjoyable without their sincere help. Special thanks go to Dr. Yan Li and Dr. Ji-Young Shin for their encouragement and help during the early stage of this project. My great appreciation goes to Ms. Qing Miao for her unreserved help and support during my entire research. Special thanks give to Mr. Andrew Tovey for his kindness and time for proofreading and precious suggestions for this thesis. I also deeply thank Dr. Lingyun Zhang, Dr. Zhan Zhang, Dr. Hua Yang and Dr. Xin Liu for their concerns and help all along the time.

I truly appreciate the help from Prof. Mark MacLachlan for his time for reading the thesis and valuable advice. Thanks also go to Dr. Brian O. Patrick for X-ray crystal structures; to Dr. Yun Ling and the analysis group for Mass Spectrometry service; to Dr. Paul Xia, Dr. Maria Ezhova and Ms. Zorana Danilovic for their help on NMR analysis.

Last, but not least, I would like to express my deep sense of gratitude to my parents, Mr. Ruihe Ma and Ms. Xiuling Hui, for their love, support and concern over the years.

Chapter One

Introduction

1.1 Supramolecular Chemistry

Molecular chemistry has developed into a very powerful tool for making complex molecules and materials by covalent synthesis. Supramolecular chemistry, chemistry beyond the molecule, focuses on constructing highly-sophisticated chemical systems driven by intermolecular noncovalent interactions such as hydrogen-bonding, π - π stacking interactions, metal-ligand coordination and hydrophobic interactions.¹ Through proper manipulation of these interactions, the information stored at the molecular level can be recovered, transferred, and processed at the supramolecular level through molecular recognition. Supramolecular chemistry aims at obtaining progressive control over the sophisticated structural and dynamic features of chemical systems through self-organization.

1.2 Self-Assembly

Self-assembly is the spontaneous, self-directed arrangement of components into structures without human interference. It is one of the few practical methods for constructing groups of nanostructures.² Self-assembly is a highly-convergent synthetic strategy, which requires fewer steps to achieve final complex products from easily accessible starting materials compared to that of a conventional sequential synthetic protocol.³ There are three main stages in a self-assembly process: (i) molecular recognition for the selective binding of the fundamental components; (ii) sequential growth and ultimate binding of multiple components in the correct relative orientation; (iii) termination of the process, a built-in stop signal required to show the completion of the process.⁴ Self-assembly defines an algorithm through interactions between the

components based on the interpretation of the information stored in the structure of the precursor. It follows the algorithm to access a variety of supramolecules with extraordinary structural complexity, many of which were recently considered impossible to make.

1.3 Inorganic Self-Assembly

One of the most extensively investigated fields of self-assembly is the spontaneous formation of well-defined metallo-supramolecular architectures from specific interactions between carefully constructed covalent organic ligands and metal ions.⁵ These ligands should have: (i) a few binding units along the strand allowing the recognition and coordination of different metal ions, and (ii) appropriate spacers which are rigid enough to abandon the coordination of binding units within one strand to the same metal ion to form stable polynuclear complexes. Metal ions are systematically selected since they play a significant role in the assembly process: (i) a set of coordination numbers and stereochemical preferences relying on their size, charge and electronic structure; (ii) different affinities for different binding units; and (iii) explicit electronic, spectroscopic and magnetic properties exhibited in the final metal complexes.¹

An enormous variety of self-assembled organic and inorganic systems have been investigated over the last two decades. Of special interest are functional multimetallic superstructures due to their potential application in the field of nanotechnology as molecular-scale sensors, switches and information storage devices.⁶⁻⁸ A wide range of

three-dimensional inorganic supramolecular architectures has recently been successfully constructed, such as double-⁹⁻¹¹ and triple-¹² stranded helicates, circular helicates,¹³⁻¹⁷ grids,¹⁸⁻²¹ racks^{22, 23} and ladders.^{24, 25}

1.4 Circular Helicates

One of the most fascinating topics of metallo-supramolecular chemistry is that of helicates, and many investigations have focused on these systems.^{26, 27} Circular helicates, unlike their acyclic counterparts, are polynuclear complexes with a cyclic arrangement of the metal ions which are wrapped by several bridging ligands. Most of the ligands share a common structural feature: the strands have two anti-parallel bidentate or tridentate-chelating sites. Thus, for each strand, one coordinate vector is above (+) and the other is below (-) the average plane of the metal ions. However, the anti-parallel geometry of the two binding units on each strand is not rigidly locked, and the two coordinate vectors may adapt either a trans or a cis arrangement. The [2×2] grid-type geometry can be formed with tetrahedral/octahedral metal ions and the cis strands. In this case, the two coordination vectors for each strand are either above or below the mean plane of the four metal ions (Figure 1-1).

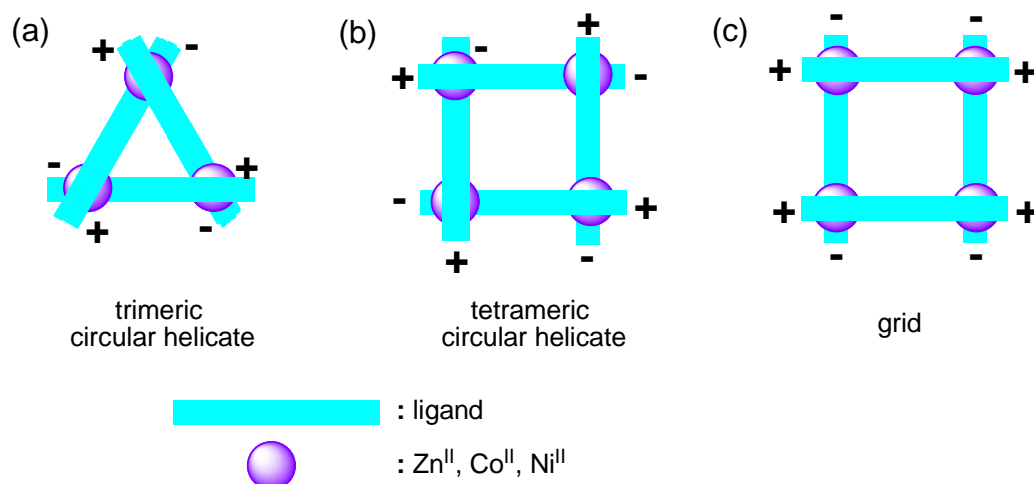


Figure 1-1 Diagram of (a) trimeric circular helicate; (b) tetrameric circular helicate and (c) grid.

Thummel has synthesized trinuclear circular helicate **I-2**, which was formed by treatment of diphenanthrolylpyrene-bridged ligand **I-1** with 1 equivalent of $[\text{Cu}(\text{MeCN})_4]\text{ClO}_4$ in $\text{MeCN}/\text{CH}_2\text{Cl}_2$ (3/4) (Figure 1-2).¹³ Cu^{I} ion is of particular interest because the lability of its diimine complexes allows the formation of the most thermodynamically-stable products by ligand interchange.²⁸ Unfortunately, only a preliminary X-ray structure could be obtained due to the poor quality of the crystal. It has D_3 symmetry which indicates that all three ligands are identical and possess the same helical twist. A donut-shaped structure could be observed due to a pyrene being positioned between two phenanthrolines to generate three sandwiches. The structure is stabilized by strong π - π stacking interactions between these three aromatic rings.

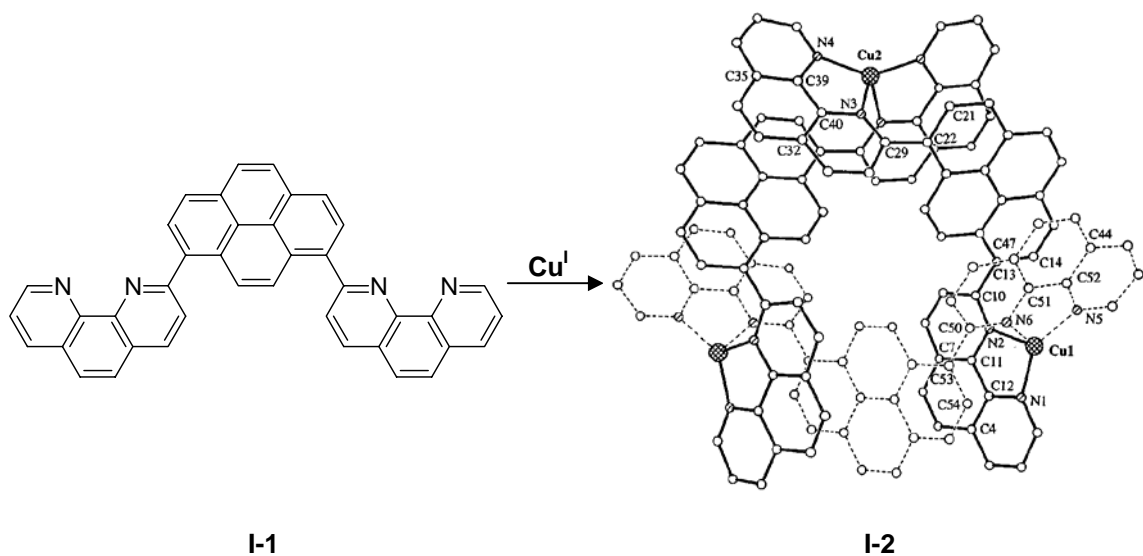


Figure 1-2 Synthetic route for preparation of trinuclear circular helicate **I-2** (counterions omitted for clarity).

Another type of ligand in which the two pyridylimine chelating sites are connected directly through the nitrogen atoms from the imine group has been introduced to the circular helicate family by Hannon. Ligand **I-3** in MeOH treated with equimolar $[\text{Cu}(\text{MeCN})_4]\text{PF}_6$ leads to complex **I-4** (Figure 1-3).¹⁴ Complex **I-4** was characterized as a trinuclear circular helicate by X-ray analysis. The structure is racemic owing to the existence of two enantiomers in equal amounts. The pyridylimine binding units are essentially planar (dihedral angles $1.8\text{-}6.2^\circ$), but there is a significant twisting about the central N-N bonds (dihedral angles $81\text{-}101^\circ$).

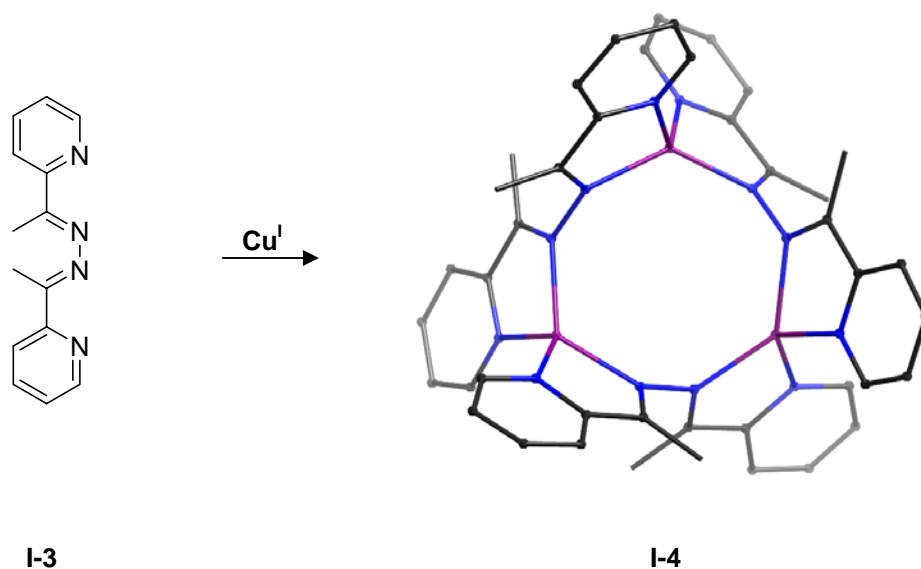


Figure 1-3 Synthetic route for preparation of trinuclear circular helicate **I-4** (counterions omitted for clarity).

Hannon has also designed ligand **I-5** in which two pyridylimine units are linked by sterically-hindered aryl groups. Combination of ligand **I-5** and $[\text{Cu}(\text{MeCN})_4]\text{PF}_6$ in MeOH afforded complex **I-6** as a dark red solid. The solid-state structure of the single crystal obtained by diffusion of Et_2O into a MeNO_2 solution of **I-6** shows a trinuclear circular helicate (Figure 1-4).¹⁵ There are six CH- π interactions (CH-centroid 2.9-3.0 Å) between the methyl groups of one ligand and the phenyl rings of a neighbouring ligand, which probably stabilize the structure. The side view of **I-6** indicates that the triangle is not planar, but is instead slightly bent to form a bowl-shaped structure due to proper adjustment for the CH- π interactions and steric twisting of the ligands. Remarkably, a tetrameric ball-shaped array is formed by four bowl-shaped triangles **I-6** through CH- π interactions.

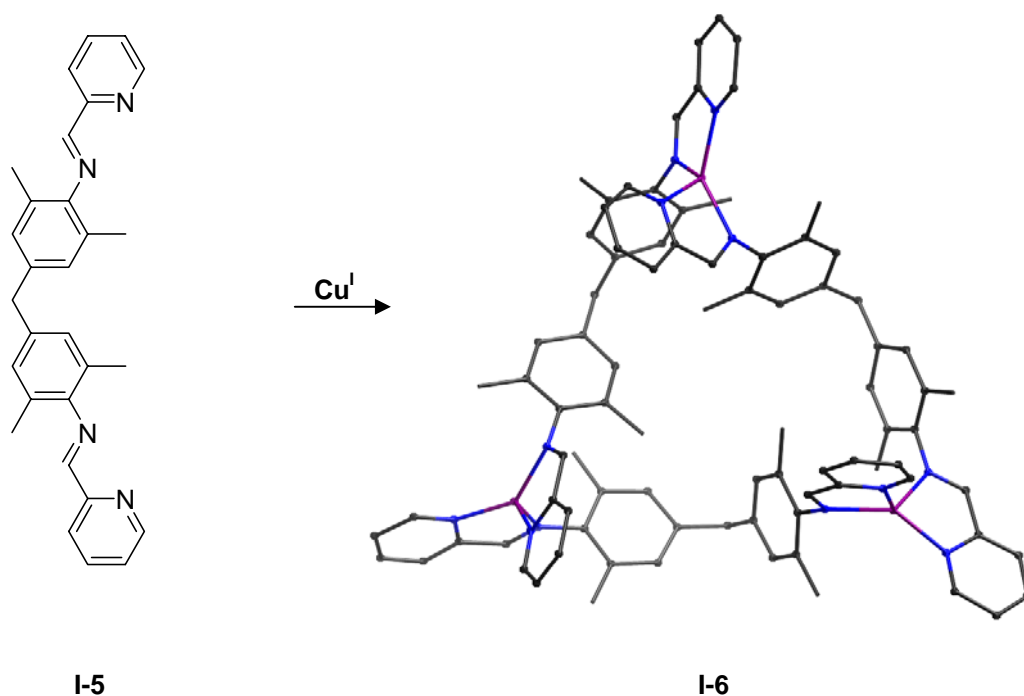


Figure 1-4 Synthetic route for preparation of trinuclear circular helicate **I-6** (counterions omitted for clarity).

Tetranuclear circular helicates have been accomplished by von Zelewsky. Geometrically rigid bisterpyridine ligands **I-7** and **I-9** in which two terpyridine units are anti-parallel to each other were treated with $\text{Zn}(\text{ClO}_4)_2 \cdot 6\text{H}_2\text{O}$ in MeCN, followed by addition of an aqueous NH_4PF_6 solution to precipitate the final metal complexes **I-8** and **I-10** as hexafluorophosphate salts (Figure 1-5).¹⁶ Diffusion of Et_2O into a MeNO_2 solution of **I-8** afforded an X-ray quality crystal, which shows racemic property and C_2 symmetry. In order to only obtain one isomer, pinene moieties (chiral centers) were introduced into ligand **I-9** to achieve chiral derivatization. Complex **I-10**, unlike **I-8**, crystallized from MeCN/MeOH/ Et_2O only contains one diastereomer (Figure 1-6).

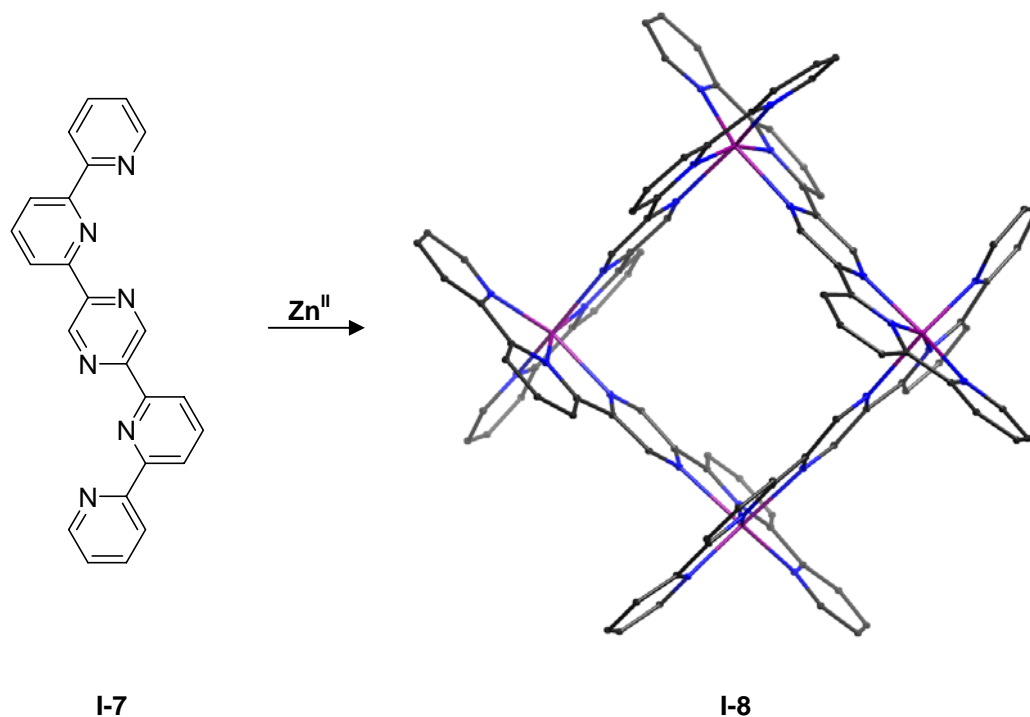


Figure 1-5 Synthetic route for preparation of tetranuclear circular helicate **I-8** (counterions omitted for clarity).

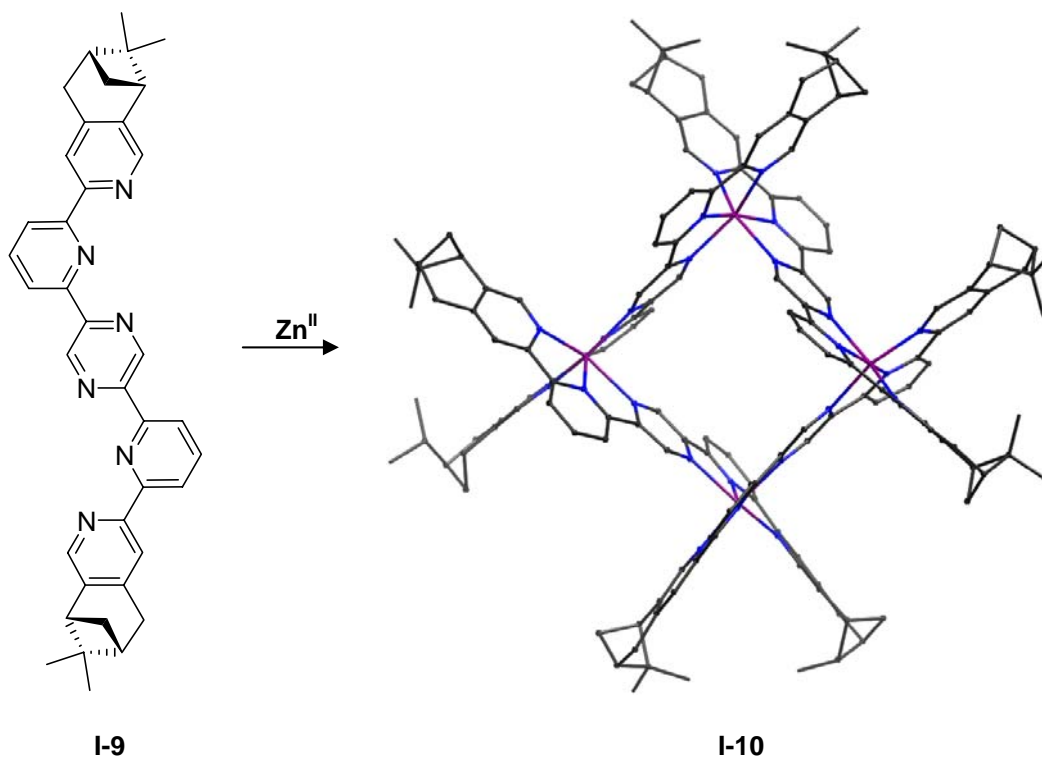


Figure 1-6 Synthetic route for preparation of tetranuclear circular helicate **I-10** (counterions omitted for clarity).

The first example of a completely stereospecific hexanuclear circular helicate was also successfully represented by von Zelewsky. Ligand **I-11** contains two bipyridine binding units and pinene moieties. Slow diffusion of Et₂O into a MeCN solution of ligand **I-11** and AgPF₆ in a 1:1 molar ratio afforded complex **I-12** as a hexafluorophosphate salt (Figure 1-7).¹⁷ X-ray analysis of **I-12** shows that it has a crystallographic C₆ axis, and the pinene groups, containing the chiral centers of the ligands, are pointed to the center of the circular structure constructing two different layers, surrounding the chiral cavity. All the xylene linkers are almost parallel (1.5°) to the C₆ axis and generate the walls of the hexagon (the distance between two opposite xylene moieties is about 18.1 Å) while the terminal pyridines act as the outer shell of the hexagon. The outside diameter of the hexagon is about 30 Å and inside is about 8.4 Å. The hexagonal box is about 14 Å in depth. Helicate **I-12** with the chiral cavity may become a potential candidate for the study of chiral recognition and stereoselective catalysis.

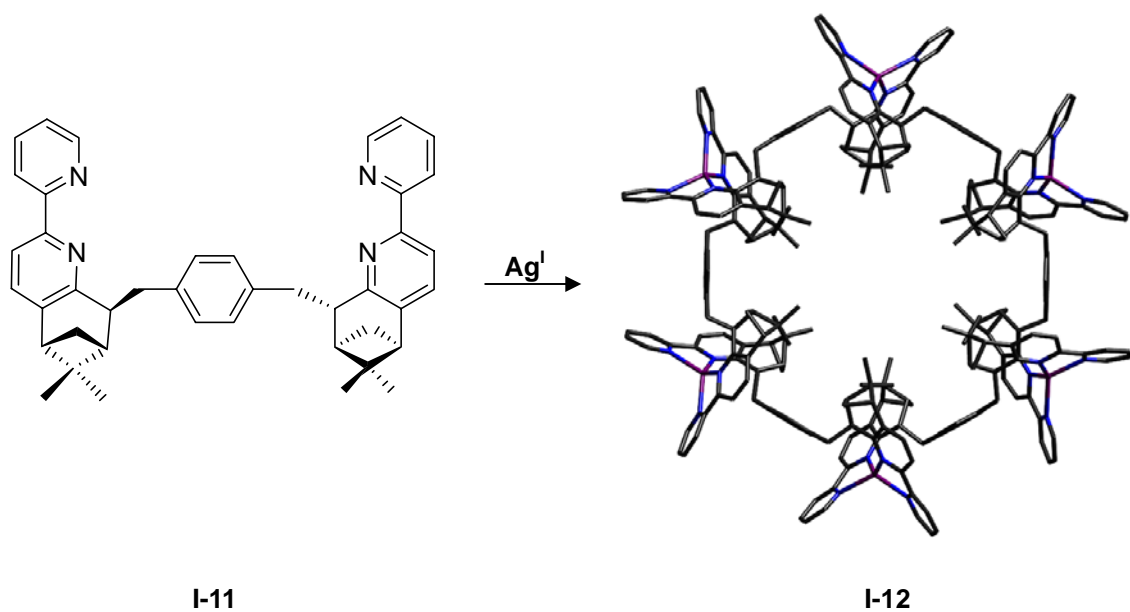


Figure 1-7 Synthetic route for preparation of hexanuclear circular helicate **I-12** (counterions omitted for clarity).

1.5 Grid-Type Metal Complexes

In the last decade, nano-electronic devices have been of special interest, which has resulted in an enormous number of designs and explorations into molecular switches, sensors and information storage devices.^{7, 8, 26, 29} Suitable candidates for molecular data storage must: (i) contain two or more easily switched physicochemically-distinct states triggered by external factors such as electromagnetic fields or thermodynamic parameters and (ii) be switchable and addressable within the nanometer system. Toward this end, grid-type metal ion arrays, in which perpendicular organic ligands wrap around a set of metal ions, show several exciting features: (i) well-documented magnetic, redox and spin-state transitions; (ii) strong similarity to the binary coded matrices and cross-bar architectures used in data storage and processing technology; and (iii) potential arrangement into extended two-dimensional aggregates by solid-surface deposition.

In the design of grid-type metal ion arrays, the selection of organic ligands depends on the coordination chemistry of the metal ions. In most cases, the metal ion with tetrahedral or octahedral coordination geometries (the coordination number is 4 or 6, respectively) is usually observed. It is crucial for the successful design of the systems that the chosen ligand should possess an adequate number of chelating sites in the coordination unit to fill the coordination sphere of the metal ion.

Osborn has synthesized Cu^{II} $[2 \times 2]$ grid-type complex **I-14**. Combining 2 equivalents of bis(pyridyl)pyridazine ligand **I-13** and 1 equivalent of $[\text{Cu}(\text{CF}_3\text{SO}_3)_2] \cdot \text{C}_6\text{H}_6$ in benzene afforded a brown solid (Figure 1-8).³⁰ A single crystal was grown from a mixture of MeOH/acetone/EtOH (1/1/1), whose structure is confirmed as a rhombus. The structure of the complex cation has C_2 symmetry about the Cu1-Cu2 diagonal. The distance between the pairs of ligands which are parallel to each other is 3.47 Å, which suggests the existence of strong π - π stacking interactions.

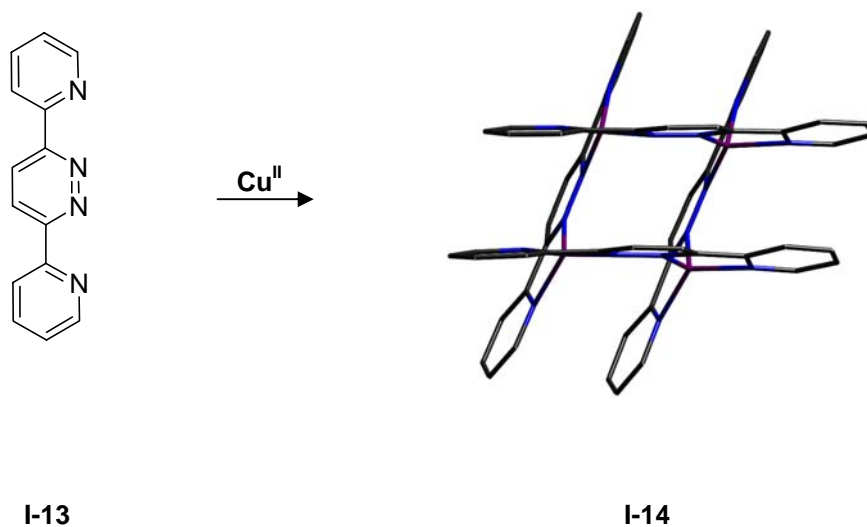


Figure 1-8 Synthetic route for preparation of Cu^{II} $[2 \times 2]$ grid **I-14** (counterions omitted for clarity).

Another bidentate ligand, bisphenanthroline ligand **I-15**, has been introduced to construct grid-type metal complexes by Siegel.³¹ Treatment of a suspension of **I-15** in MeCN with CuBF_4 generates a red solution of grid-type metal complex **I-16**. Surprisingly, X-ray analysis shows that **I-16** is a pseudo $[3 \times 3]$ grid containing a $[2 \times 2]$ grid as host and two additional ligands as

guests filling the interstitial spaces (Figure 1-9). The distance between two host biphenanthroline ligands is about 7.5 Å, which is enough to accommodate an additional ligand as an aromatic guest by intercalation. The unique supramolecular structure of **I-16** also receives contributions from strong π - π stacking interactions between the ligands.

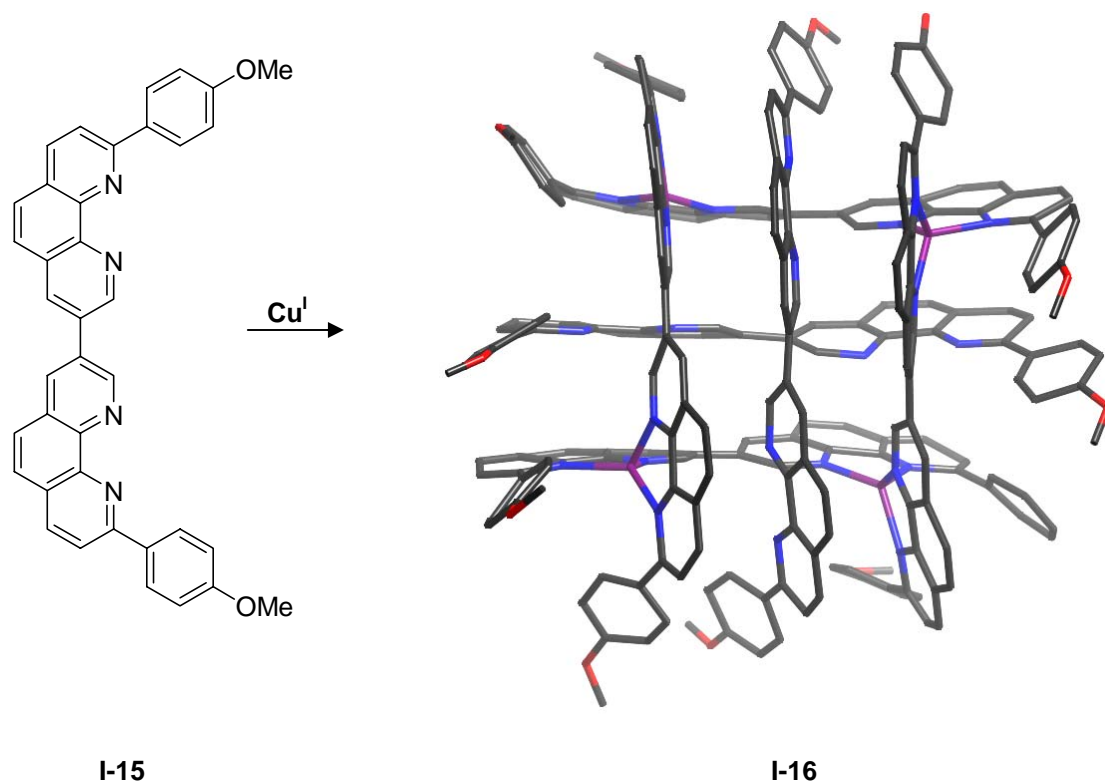


Figure 1-9 Synthetic route for preparation of Cu^{I} pseudo[3x3] grid **I-16** (counterions omitted for clarity).

Other than pairing tetrahedrally coordinated metal ions with bidentate ligands, combination of octahedrally coordinated metal ions and tridentate ligands has also been investigated for the construction of grid-type complexes by Lehn. Treatment of ligand **I-17** ($\text{R}=\text{Me}$) with an equimolar amount of $\text{Co}(\text{OAc})_2 \cdot 4\text{H}_2\text{O}$ in methanol at reflux, followed by addition of an aqueous solution of NH_4SbF_6 afforded the [2x2] grid-type metal complex **I-18**, and its structure was

confirmed by X-ray crystallography.¹⁸ In addition to transition metal ions, Pb^{II} ion was selected to react with ligand **I-19** (R=H) in MeCN for formation of [2×2] grid-type metal complex **I-20**. A single crystal was grown from slow diffusion of Et₂O into a solution of **I-20** in MeCN, whose structure is confirmed by X-ray analysis (Figure 1-10).³² The metal ions lie almost in a plane and form a square. The bonds to the ligands in each coordination site are pushed to one part of the coordination sphere due to the existence of a stereochemically-active electron lone pair in the lead ions.³³ The average M-M distance is similar in **I-18** and **I-20**, although the Pb-N distance is much longer than Co-N due to the larger radius of the Pb^{II} ion.

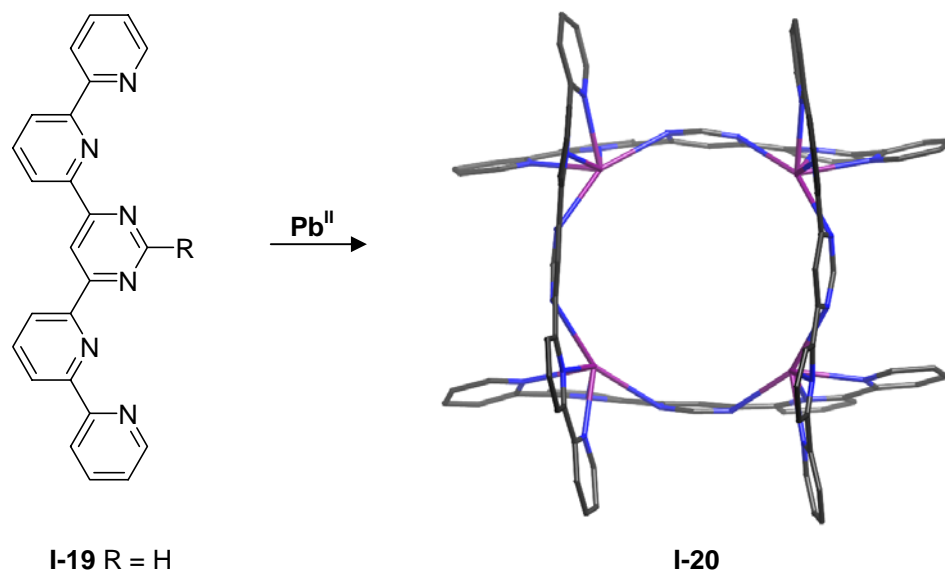


Figure 1-10 Synthetic route for preparation of Pb^{II} [2×2] grid **I-20** (counterions omitted for clarity).

Brooker has successfully presented the synthesis of a new kind of [2×2] grid-type metal complex **I-22** which was generated by combination of equimolar amounts of bistridentate diamide ligand **I-21**, Cu(BF₄)₂·xH₂O and NEt₃ in MeCN (Figure 1-11).³⁴ X-ray analysis of **I-22**

demonstrates both deprotonated amide nitrogen atoms in each ligand are engaged in the tridentate coordination in addition to the pyridine nitrogen atoms, resulting in a distorted octahedral coordination geometry for all of the Cu^{II} ions. Remarkably, one amide proton of each ligand is left behind due to the addition of only 1 equivalent base, and then, likely, positioned in symmetrical $\text{O}\cdots\text{H}\cdots\text{O}$ hydrogen bonds between the two amide oxygen atoms of each ligand strand.

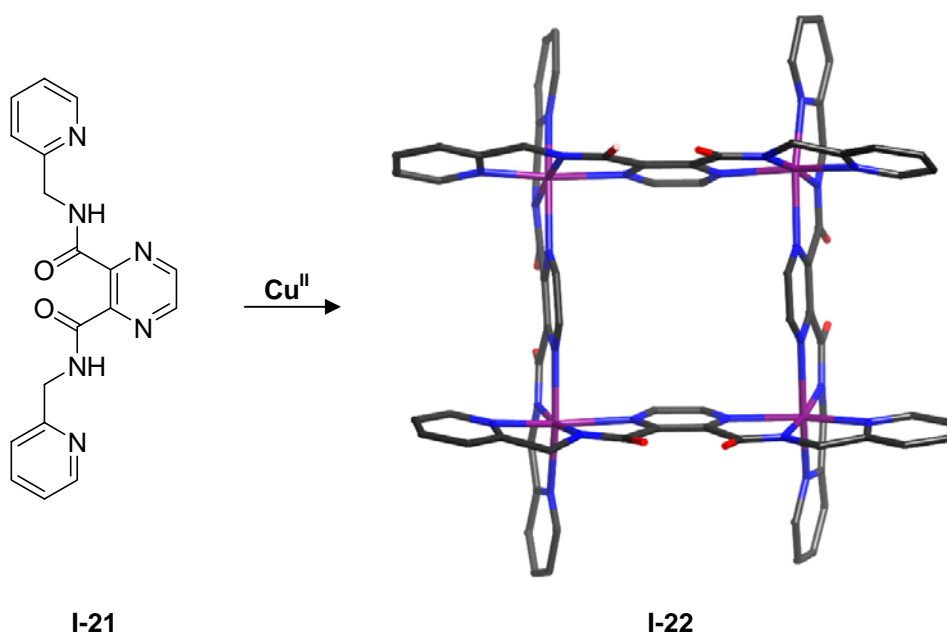


Figure 1-11 Synthetic route for preparation of Cu^{II} $[2\times 2]$ grid **I-22** (counterions omitted for clarity).

A much larger $[3\times 3]$ grid-type metal complex has been introduced into the inorganic grid family by Lehn.³⁵ Combination of 1 equivalent tritopic bipyridine ligand **I-23** with 1.5 equivalents AgCF_3SO_3 in MeNO_2 leads to the Ag^{I} $[3\times 3]$ grid **I-24** (Figure 1-12). Two sets of signals in a 2:1 ratio in ^1H NMR spectrum of **I-24** indicate ligand **I-23** is in two different environments, which is consistent with a $[3\times 3]$ grid-type structure. The ^{109}Ag NMR spectrum

displays three peaks for Ag^{I} ions positioned at the corners, the centers of the edges and the center of the $[3 \times 3]$ grid in 4:4:1 ratio, which further confirms the grid structure. The solid state structure of **I-24** shows that the grid is a distorted rhombus, and all Ag^{I} ions are in a distorted tetrahedral geometry with the same dihedral angle of approximately 72° . The geometry of the pyridazine ring, which is not a regular hexagon, may be partially responsible for the slight bending of the ligand in **I-24**.

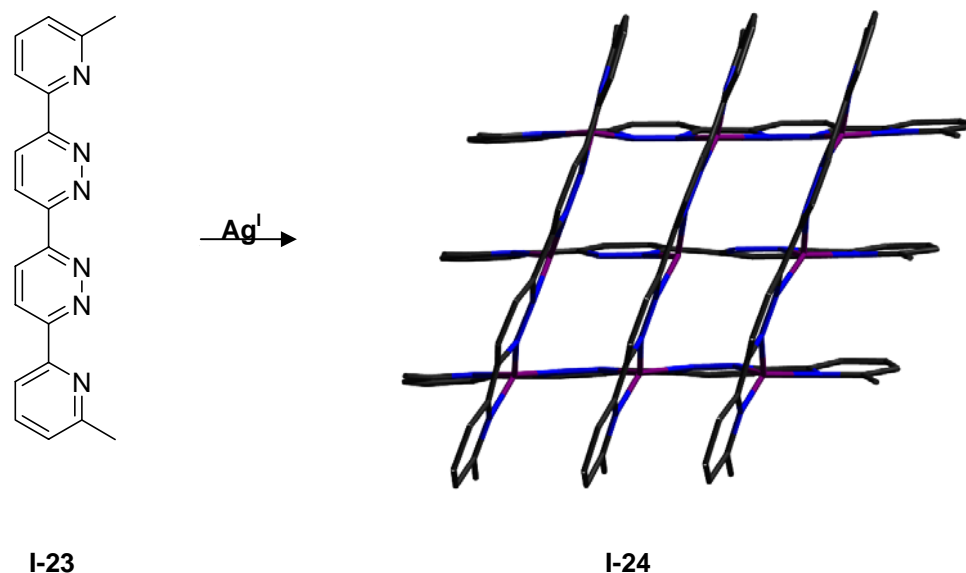


Figure 1-12 Synthetic route for preparation of Ag^{I} $[3 \times 3]$ grid **I-24** (counterions omitted for clarity).

An expanded Pb^{II} $[4 \times 4]$ grid **I-26** has also been accomplished by Lehn.³⁶ Treatment of polyterpyridine ligand **I-25** with $\text{Pb}(\text{CF}_3\text{SO}_3)_2$ in 1:2 stoichiometry results in complex **I-26** which is confirmed by X-ray crystallography (Figure 1-13). Like Pb^{II} $[2 \times 2]$ grid **I-20**, the coordination geometry around Pb^{II} ions displays a hemi-directed structure.³⁷ All eight ligands are divided into two sets of four, one of which is inner and the other is outer within the grid.

Thus, rather than a normal [4×4] grid, **I-26** acts more as a set of four [2×2] subgrids. A strong π - π stacking interaction can be achieved due to substantial overlap between the aromatic rings in the inner ligands (centroid-centroid distance of 3.6 Å).³⁸ All available void space in the four [2×2] subgrids is filled by triflate counterions and water molecules.

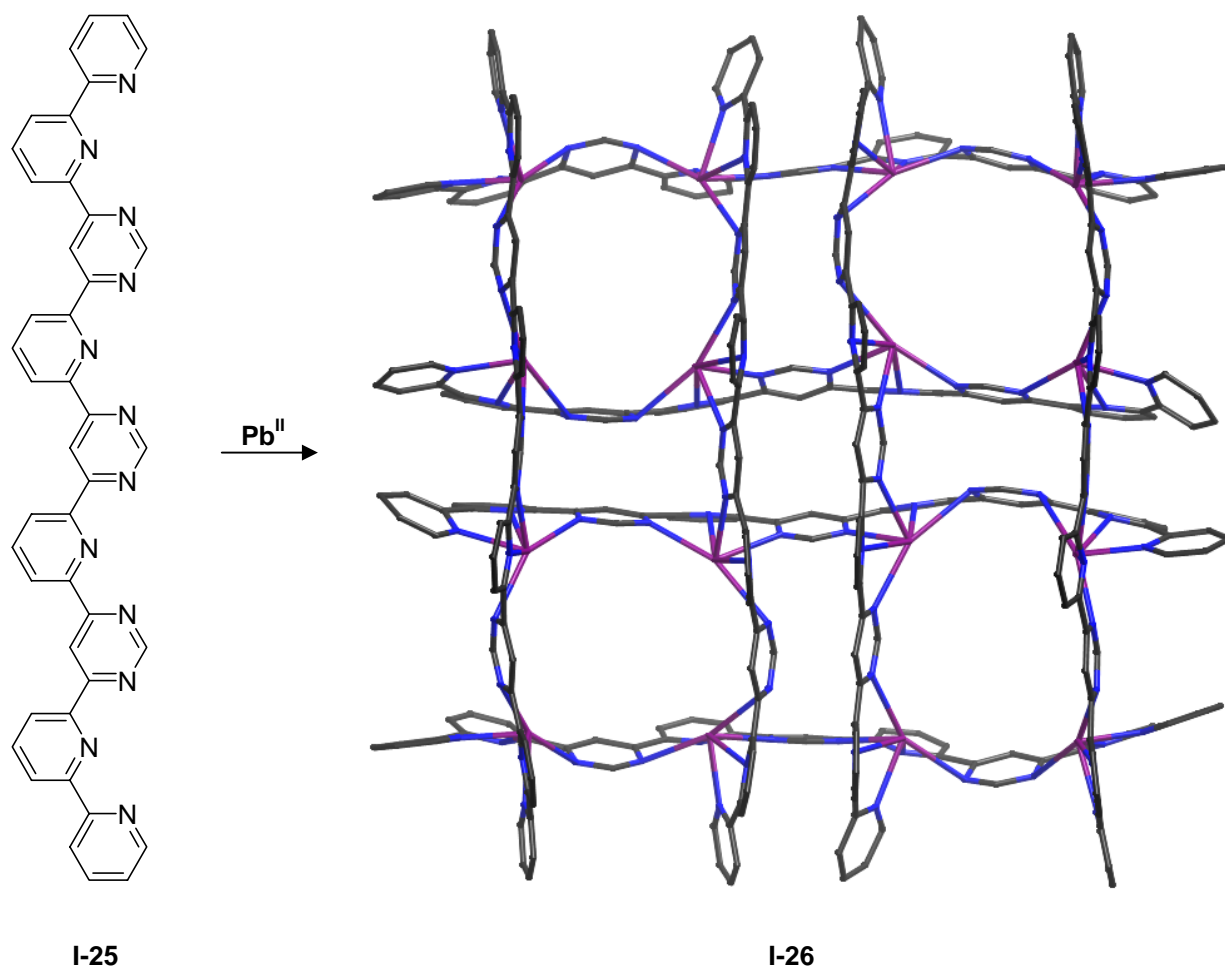


Figure 1-13 Synthetic route for preparation of Pb^{II} [4×4] grid **I-26** (counterions omitted for clarity).

1.6 Rack-Type Metal Complexes

Rack-type metal complexes are multinuclear heteroleptic species possessing one polytopic ligand chelating several metal ions, each of which is also coordinated by one or more monotopic ligands.²³ The polytopic molecular strands, the backbones, can be either flexible or rigid. The appropriate metal-based monotopic ligands play an important role in constructing a linear and rigid conformation in the synthesis of inorganic racks.^{22, 39, 40}

Lehn has explored a new class of rack-type multimetallic pseudorotaxane complexes. Treatment of a mixture containing bis-bipyridine ligand **I-27** and phenanthroline macrocycle **I-28** with $[\text{Cu}(\text{MeCN})_4]\text{PF}_6$ in 1:2:2 ratio in $\text{CH}_2\text{Cl}_2/\text{MeCN}$ under argon afforded a dark red solid. A single crystal was obtained by slow diffusion of toluene into a nitromethane solution of complex **I-29**, and the structure is confirmed by X-ray crystallography (Figure 1-14).⁴¹ The two threaded phenanthroline macrocycles **I-28** are in a cisoid conformation on the rigid backbone of ligand **I-27**. A weak π - π stacking interaction between two phenanthroline rings from **I-28** can be observed in **I-29**. Furthermore, another set of weak π - π stacking interactions exist between the terminal phenyl group from ligand **I-27** and the phenanthroline group from macrocycle **I-28**. Ligand **I-27** are slightly bent in **I-29** due to the shorter N=N bond in the pyridazyl ring which is not a regular hexagon.

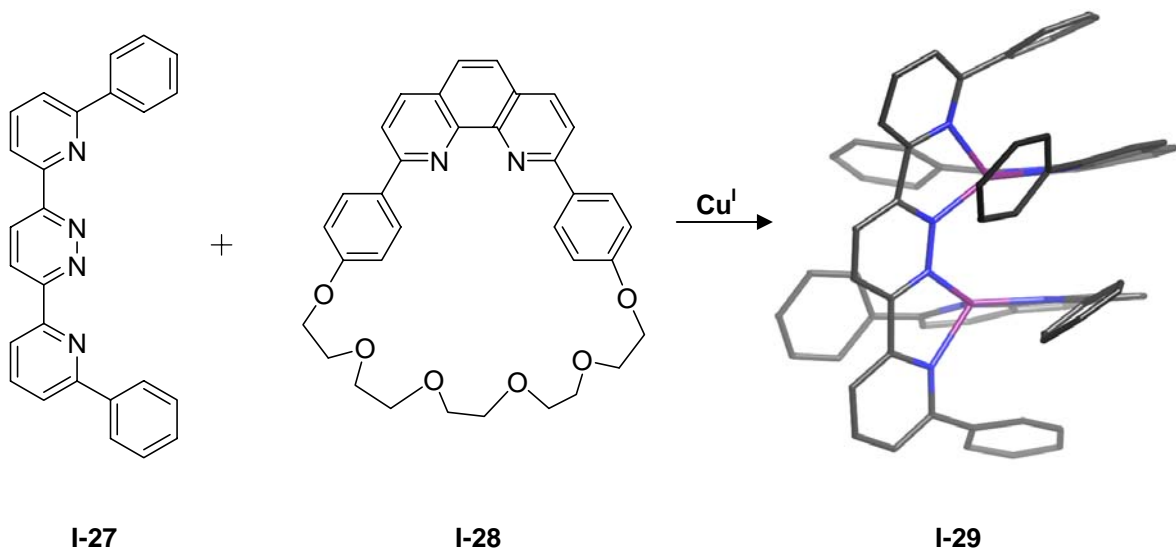


Figure 1-14 Synthetic route for preparation of Cu^{I} rack **I-29** (crown ether chain and counterions omitted for clarity).

Terpyridine ligands, together with bipyridine ligands, are good coordination units for the generation of stable complexes. Both high and low oxidation states of metal ions can be stabilized by coordination to the aforementioned ligands since they are good σ - and π -donors and π -acceptors.^{42, 43} Combination of bistridentate ligand **I-30** and 2.5 equivalents of Ru^{III} terpyridine complex **I-31** in refluxing EtOH/ H_2O (1:1), followed by addition of an aqueous solution of NH_4PF_6 afforded a green precipitate. Pure Ru^{II} complex **I-32** was obtained as a green solid through successive recrystallization from MeCN/ C_6H_6 (Figure 1-15).³⁹ The Ru^{III} - Ru^{II} conversion was achieved by the introduction of an electron-donating solvent. X-ray analysis indicates that the two Ru atoms are crystallographically inequivalent and are in pseudooctahedral chelation environments in **I-32**. The π - π stacking interactions can be expected between the phenyl group and terpyridine moieties which are stacked at van der Waals contact

distance in **I-32**.

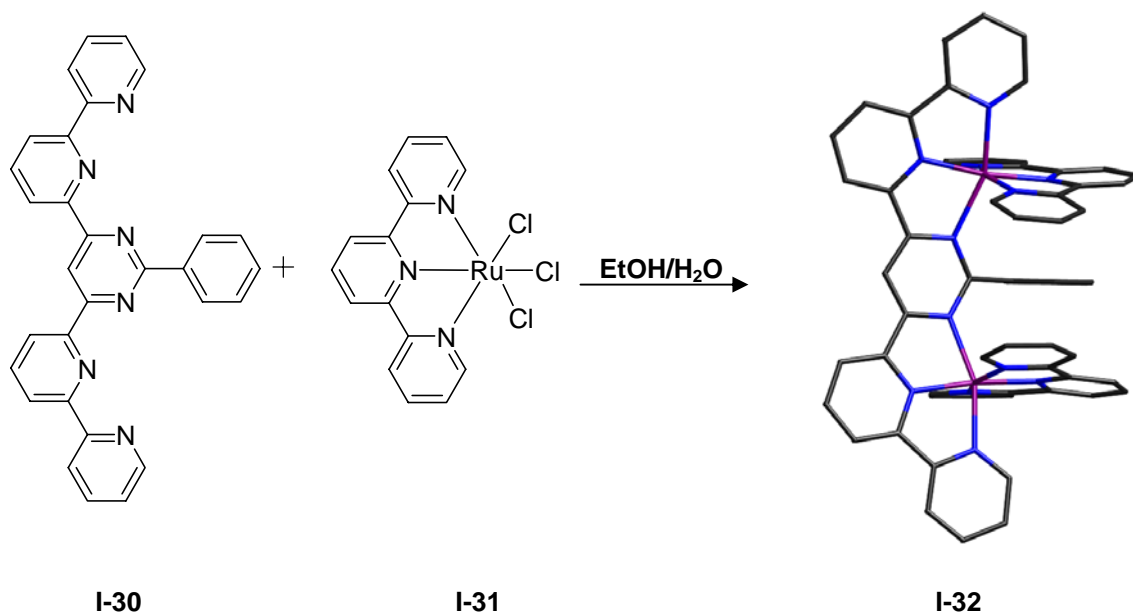


Figure 1-15 Synthetic route for preparation of Ru^{II} rack **I-32** (counterions omitted for clarity).

The tridentate ditopic hydrazone ligands have also been introduced as the backbones of the rack-type metal complexes by Lehn. Treatment of ligand **I-33** with Ru^{III} terpyridine complex **I-31**, in a molar ratio of 1:2.2, in a refluxing mixture of protic solvents which can provide electrons to reduce Ru^{III} to Ru^{II}, led to parallel Ru^{II} rack **I-34** as a green solid after recrystallization and reprecipitation (Figure 1-16). Anti-parallel rack **I-36** was synthesized using the same procedure, starting with ligand **I-35** (Figure 1-17).^{40, 44} The crystal structures show that the parallel rack **I-34** exhibits a curved structure while the anti-parallel rack **I-36** is totally linear. The two terpyridine ligands are crystallographically equivalent in rack **I-36** while they are not in rack **I-34**. In contrast to **I-34** in which the planes of terpyridine generate an angle of about 33°, **I-36** possesses two parallel terpyridine planes which are almost perpendicular to the plane of the backbone **I-35**.

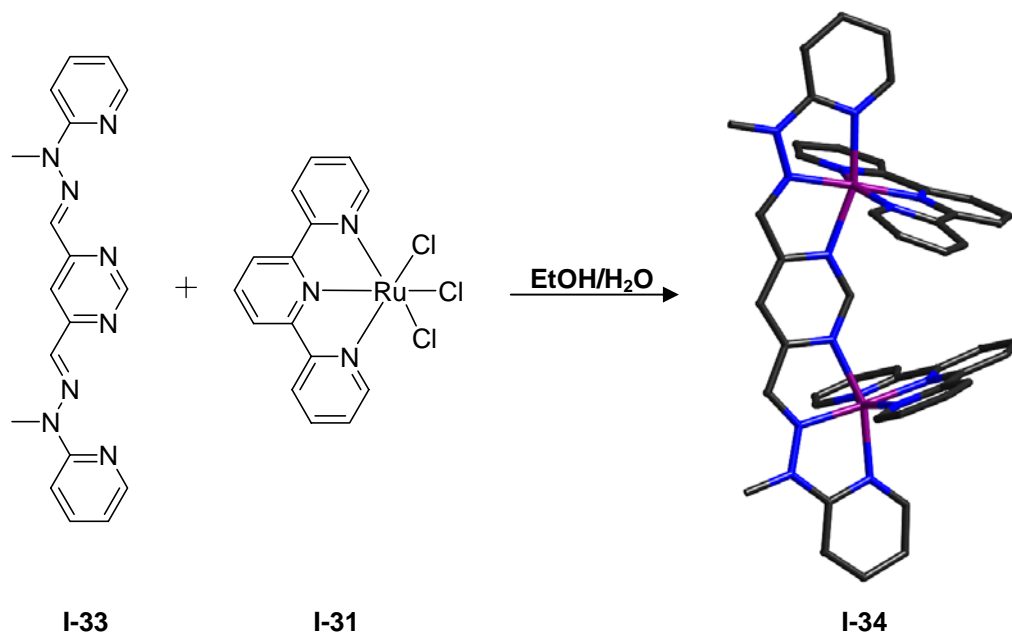


Figure 1-16 Synthetic route for preparation of parallel Ru^{II} rack **I-34** (counterions omitted for clarity).

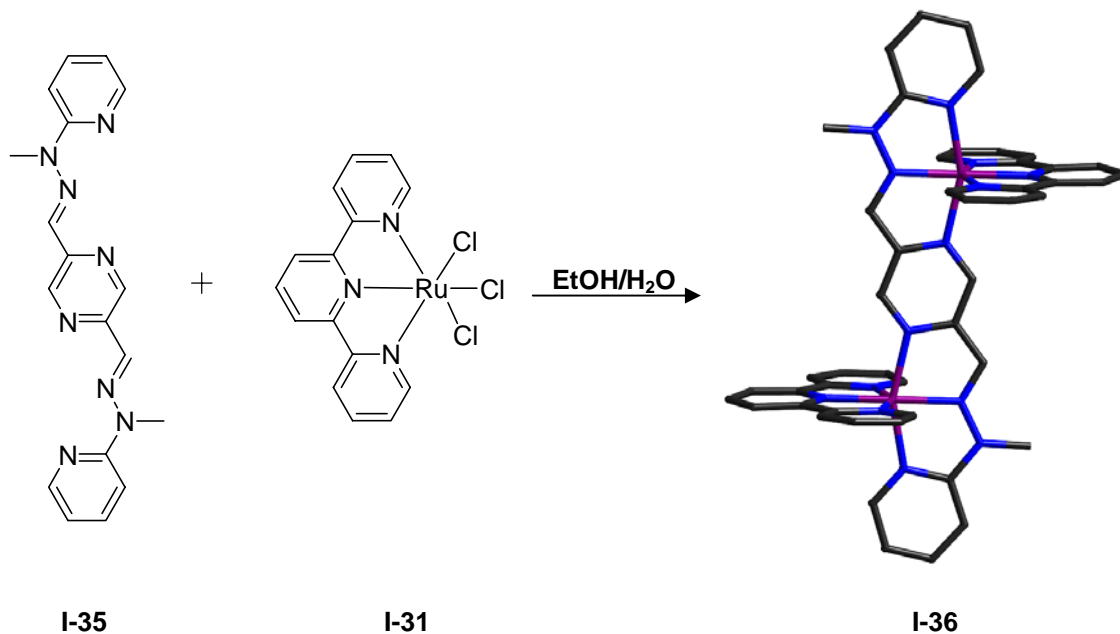


Figure 1-17 Synthetic route for preparation of anti-parallel Ru^{II} rack **I-36** (counterions omitted for clarity).

1.7 Ladder-Type Metal Complexes

The ladder-type metal complexes, in contrast to grid-type ones, are generated through combination of heteroleptic ligands with metal ions. The rack-type metal complexes can be considered as the half-ladders. Lehn has presented the formation of the first ladder complex **I-39** which is synthesized through treatment of bis-bipyridine ligand **I-37** (the rail) and the bipyrimidine ligand **I-38** (the rung) with $[\text{Cu}(\text{MeCN})_4]\text{PF}_6$ in a 1:1:2 stoichiometry (Figure 1-18).²⁴ The extreme simplicity of ^1H and ^{13}C NMR spectra of **I-39** suggested the presence of a highly symmetric complex in solution. The ladder-shaped structure of **I-39** was further supported by ESI-MS (electrospray ionization) measurements. However, no solid state structure of **I-39** is available at this point.

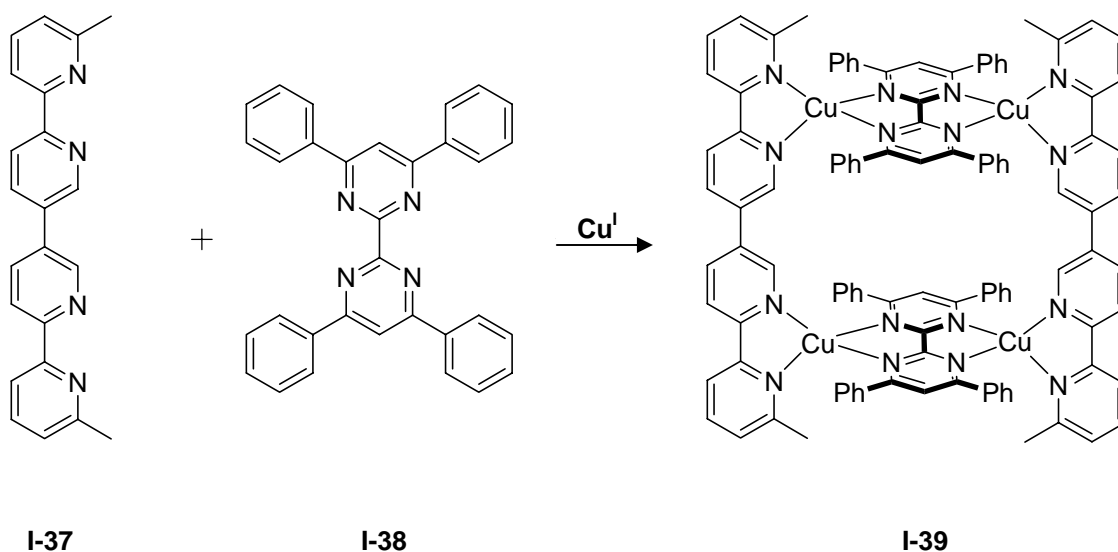


Figure 1-18 Synthetic route for preparation of heteroleptic Cu^I ladder **I-39** (counterions omitted for clarity).

Schmittl has synthesized another new inorganic ladder **I-42** which consists of bisphenanthroline ligand **I-40**, bisterpyridine ligand **I-41** and Zn^{II} ions in a 1:1:2 stoichiometry (Figure 1-19).²⁵ Like **I-39**, the ladder-shaped structure of **I-42** was supported by 1H and ^{13}C NMR spectra and ESI-MS measurements. Due to poor quality of the crystal, only the solid state structure with a high R_1 value (0.2315) could be obtained, but the structure shows that **I-42** possesses a nanoscale ladder arrangement. Strong π - π stacking interactions can be observed between the terpyridine units from ligand **I-41** and the aryl groups attached to 2- and 9-positions of phenanthrolines from ligand **I-40**. The Zn^{II} ions were forced to adapt a heavily distorted trigonal bipyramidal geometry, instead of their usual tetrahedral geometry, due to the presence of both bidentate (**I-40**) and tridentate (**I-41**) ligands in the Zn^{II} ladder **I-42**.

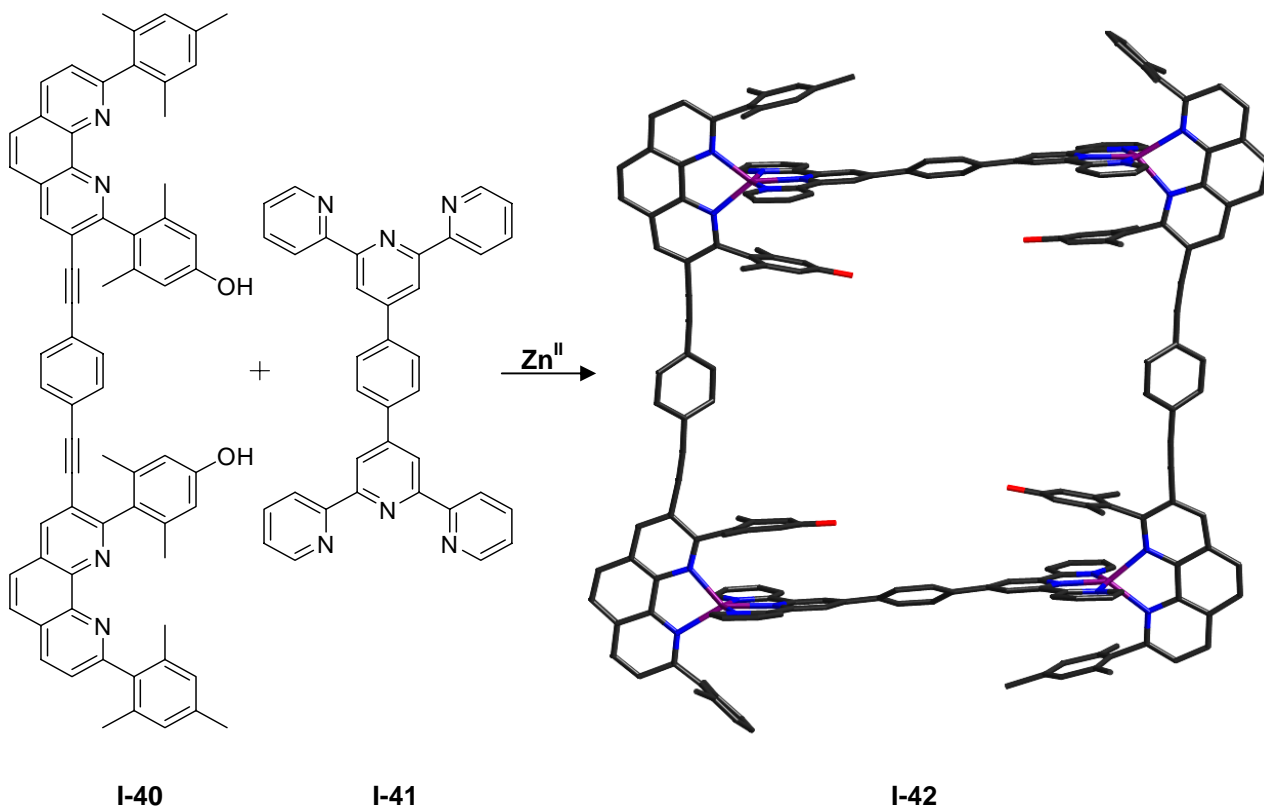


Figure 1-19 Synthetic route for preparation of heteroleptic Zn^{II} ladder **I-42** (counterions omitted for clarity).

1.8 Dipyrrromethene (Dipyrriin) Metal Complexes

Dipyrriin chemistry has been fully investigated by many researchers for decades due to their application for synthesis of porphyrins. Dipyrriins possess two pyrrolic rings linked at the α - and α' -positions by a methine spacer. The two pyrrolic rings and the methine bridge are usually coplanar to achieve maximum conjugation of the π system. Both IUPAC-recommended and commonly simplified numbering systems for dipyrriins are shown in Figure 1-20.

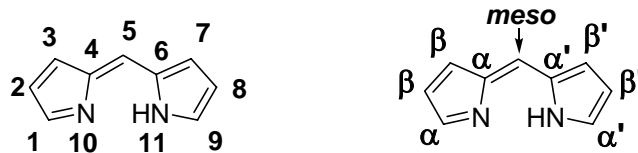


Figure 1-20 IUPAC-recommended (left) and the commonly simplified (right) numbering systems for dipyrriins.

Bipyridines, the major binding units in the ligands introduced into Lehn's work on supramolecular self-assembly, are neutral ligands and generate charged complexes when coordinated to metals at any oxidation state. Therefore, counterions are needed for charge balance. Unfortunately, such counterions can result in disorder in the solid state, and thus lower the chance to obtain the X-ray quality crystals for structural analysis. Furthermore, purification of these metal complexes is often very challenging through traditional separation techniques such as chromatography. Dipyrriins, on the other hand, afford mono-anionic resonance stabilized

ligands which readily coordinate to metal ions (M^{2+}/M^{3+}) to give neutral square planar, tetrahedral or octahedral complexes in which no counterions are required (Figure 1-21). Most dipyrin metal complexes are highly crystalline and soluble in a variety of organic solvents such as methylene chloride, chloroform, THF and toluene.

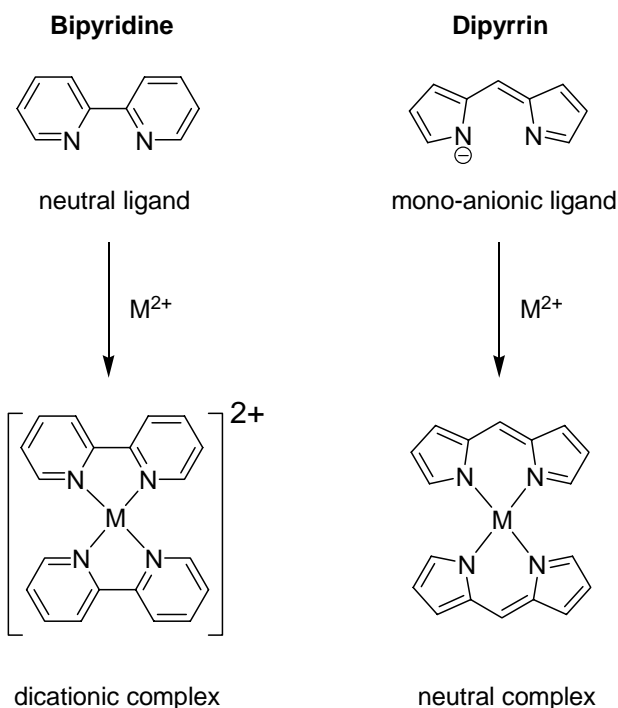


Figure 1-21 Bipyridine, dipyrin ligands and their M^{2+} complexes.

Over the past few decades, dipyrins that can generate neutral complexes with various metal ions have been introduced as versatile ligands in the field of metallo-supramolecular chemistry. Bisdipyrin metal complexes possessing double-,^{45, 46} triple-⁴⁷ stranded helical structures or triangular⁴⁸ structure have been reported so far.

Dolphin has successfully synthesized a series of double-stranded helicates using flexible bisdipyrrin ligands in which the two dipyrin units are linked either directly or by alkylene groups at α - and α' -positions, or by alkylene groups at β - and β' -positions (Figure 1-22). Zn^{II} and Co^{II} ions which favour tetrahedral coordination geometry are commonly selected to coordinate to the ligands. X-ray analysis shows that the metal complexes possess double-stranded helical geometry.^{45, 46}

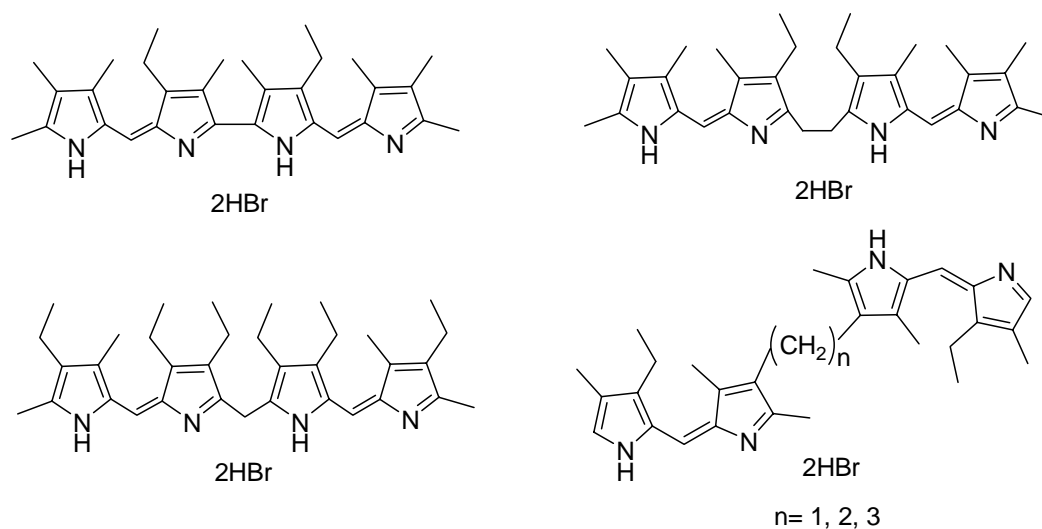


Figure 1-22 Bisdipyrrin ligands for preparation of Zn^{II} or Co^{II} double-stranded helicates.

Recently, the first triple-stranded helicates and mesocates were generated by Dolphin using a novel α -free bisdipyrrin ligand **I-43** in which two dipyrin units are linked by a methylene group at the β - and β' -positions.⁴⁷ Combination of ligand **I-43** and Co^{III} ions afforded a mixture of helicate **I-44** and mesocate **I-45** which can be separated by a one-meter silica gel column. The signal of the linker CH_2 hydrogens is a singlet at 3.51 ppm in 1H NMR spectrum of helicate **I-44**

the metal ions while the other lies below the average plane.

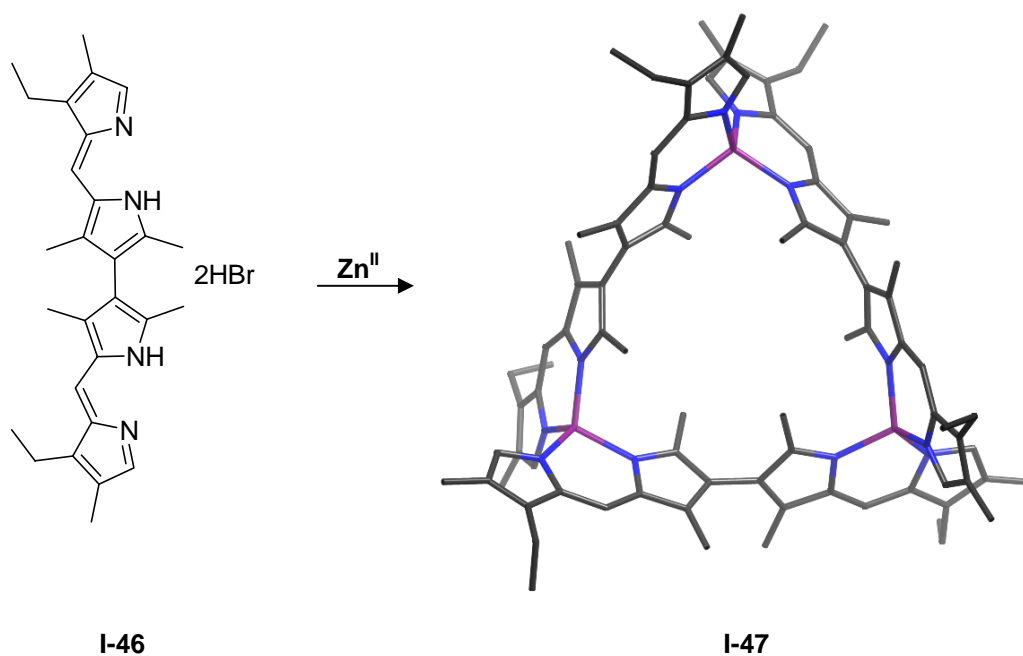


Figure 1-24 Synthetic route for preparation of Zn^{II} trinuclear circular helicate **I-47**.

1.9 Goals and Scope of the Thesis

Metal-organic porous materials with molecule-sized channels have received intense scientific and technological attention because of their various potential applications in many areas, such as gas storage and separation,⁵¹⁻⁵⁴ catalysis^{55, 56} and drug delivery.^{57, 58} Due to such critical requirements as very low temperatures and/or extremely high pressures, storage of large amounts of dihydrogen can be expensive and complex in a conventional context. The interest in storing dihydrogen, which has high energy content and is clean burning, into the cavities of porous materials for mobile fueling applications is substantial. Recently, Yaghi has reported several metal-organic frameworks (MOFs), in which the volumetric and gravimetric storage

densities of H₂ are close to the limit of practical utility.⁵² In terms of catalysis, Raymond has developed a tetrahedral assembly [Ga₄L₆]¹²⁻ as a water-soluble host which captures propargyl enammonium cations, facilitates an aza Cope rearrangement and releases the final products after hydrolysis. The catalytic reaction fits the Michaelis-Menten model of enzyme kinetics well, which indicates the host can act as an enzyme mimic in these tricky catalytic reactions under mild, aqueous conditions.⁵⁵ As well, Ferey has reported that flexible porous MOFs (iron terephthalates) can be used for controlled drug delivery of Ibuprofen. Drug-matrix interactions are optimized since the MOFs can adjust their pore size to fit the dimensions of Ibuprofen, which results in an unusual zero-order kinetics drug release.⁵⁸

One of the goals in this project is to create nano-sized channels in the solid state using bisdipyrrin ligands and metal ions. Very limited work has been done to study circular helicates using rigid linear *meso*-unsubstituted bisdipyrrin ligands and their porosities. Therefore, new ligands and multinuclear circular helicates were prepared and studied in great detail. Surprisingly, the synthesis and characterization of grid-type metal complexes using bisdipyrrin ligands is still a deserted area. In order to construct these neutral metal complexes, a variety of ring fused bisdipyrrin ligands were designed and investigated. Their interesting channel structures and corresponding driving forces in the solid state were explored in detail.

Over the past few decades, considerable interest has been drawn to the generation of multicomponent functional architectures through noncovalent self-assembly to mimic the diversity and complexity of biological systems and to study the specific biological functions.⁵⁹⁻⁶¹

To the best of our knowledge, heteroleptic racks and ladders using bisdipyrrin ligands are unprecedented. Therefore, another goal of this project is to perform controlled synthesis of novel heteroleptic racks and ladders by self-sorting.²⁹ In order to achieve this goal, the steric interaction and reactivity of the reactants were investigated for the directed synthesis. Many *meso*-aryl dipyrins were synthesized based on previously reported procedures for the rack synthesis. Two new heteroleptic metal complexes as the crucial intermediates were created to generate the ladders. The exciting tunnel structures for ladders and the fascinating spectroscopic properties for both racks and ladders were studied in detail.

Chapter Two
Homoleptic Circular Helicates

2.1 Design Strategy

meso-Unsubstituted bisdipyrrins have been incorporated into the field of supramolecular chemistry as flexible and versatile ligands. They can be prepared as HBr salts through condensation of 2-formyl pyrrole and 2-unsubstituted pyrrole or pyrrole-2-carboxylic acid in the presence of HBr. The bisdipyrrin salts are aromatic chromophores, and more stable than their free-base counterparts. While there has been an enormous amount of study on bisdipyrrin metal complexes featuring double-^{45, 46, 50, 62} or triple-⁴⁷ helical structures, in which the two dipyrin units are linked either directly or by alkylene groups at the α -position, or linked by alkylene groups at the β -position (Figure 2-1), there have been relatively few studies on the bisdipyrrin metal complexes possessing multinuclear circular-helical structures.⁴⁸

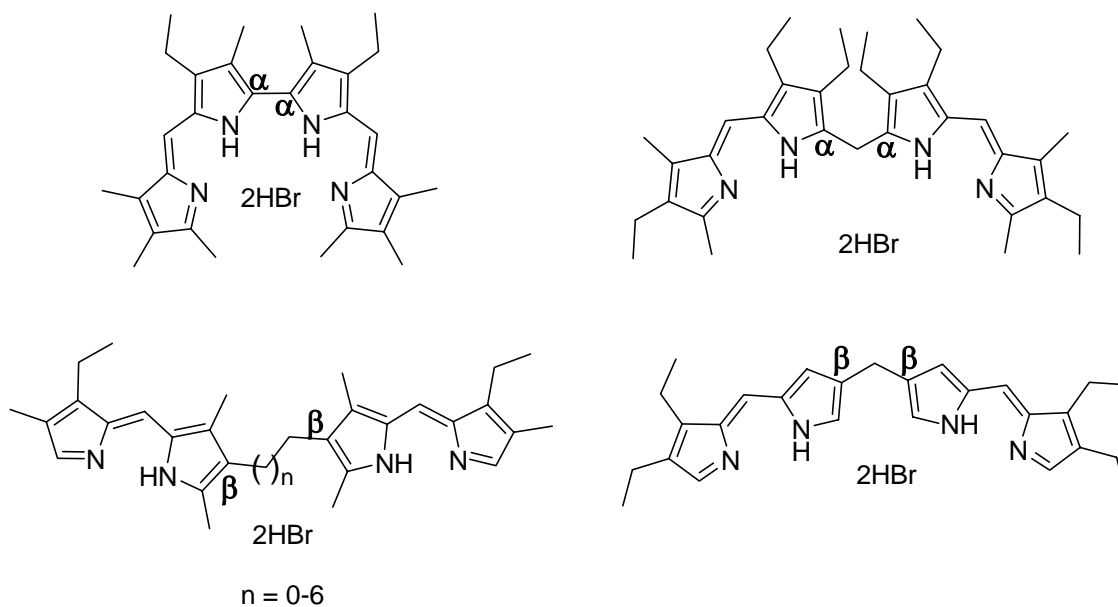


Figure 2-1 Reported bisdipyrrin ligands for double- and triple-stranded helicates.

The spacers linking two dipyrin units play an extremely important role in the design of suitable ligands for circular helicates. Combination of the previously synthesized flexible bisdipyrins linked by alkylene groups with Zn^{II} and Co^{II} ions forms either the expected double helicates and even monomers if the spacer is long enough to allow the dipyrin units to fold back against each other.⁴⁸ Rigid organic spacers, such as phenyldiacetylene, carbazolediacetylene and diacetylene, are introduced to generate rigid bisdipyrins suitable for the construction of circular helicates.

2.2 Results and Discussion

2.2.1 Phenyldiacetylene Bisdipyrrin Co^{II} Complex

2.2.1.1 Synthesis of Phenyldiacetylene Bisdipyrrin Co^{II} Complex

The preparation of the phenyldiacetylene bisdipyrrin ligand **II-6** began with the synthesis of the spacer **II-2** which is the product of a Sonogashira coupling reaction of 1,3-dibromo-5-*t*-butylbenzene and ethynyltrimethylsilane, followed by basic hydrolysis with addition of KOH.⁶³ Compound **II-3** was generated by iodination of 3,5-dimethylpyrrole-2-carbaldehyde.⁶⁴ A second Sonogashira coupling was conducted with **II-2** and **II-3** under hydrogen to give **II-5** in a very low yield.⁶⁵ The electron-withdrawing group attached to R was thought to decrease the electron density between the R group and iodide and thus make it easier to break the R-I bond. Apparently, the aldehyde group is not strong enough to appreciably achieve that goal. Therefore, **II-4** with a more activated R-I bond was synthesized from **II-3** by addition of malononitrile,⁶⁶ followed by a Sonogashira coupling with **II-2**. Basic hydrolysis afforded **II-5** in a good yield which was then condensed with 2,4-dimethylpyrrole in the presence of HBr to afford the rigid bisdipyrrin ligand **II-6** as the HBr salt. Treatment of ligand **II-6** with Co(OAc)₂•4H₂O and NaOAc generates the bisdipyrrin Co^{II} complexes **II-7** (Scheme 2-1). A non-polar fraction containing the desired metal macrocycle was first isolated by flash chromatography on silica gel with a mixed solvent system of CH₂Cl₂ and hexanes (3:2). The generation of the self-assembled oligomers was confirmed by MALDI-TOF mass spectrometry. The pure dimeric Co^{II} complex **II-7-2** was obtained as a slower moving fraction, after fractions of higher oligomeric Co^{II} complexes eluted from a gel permeation

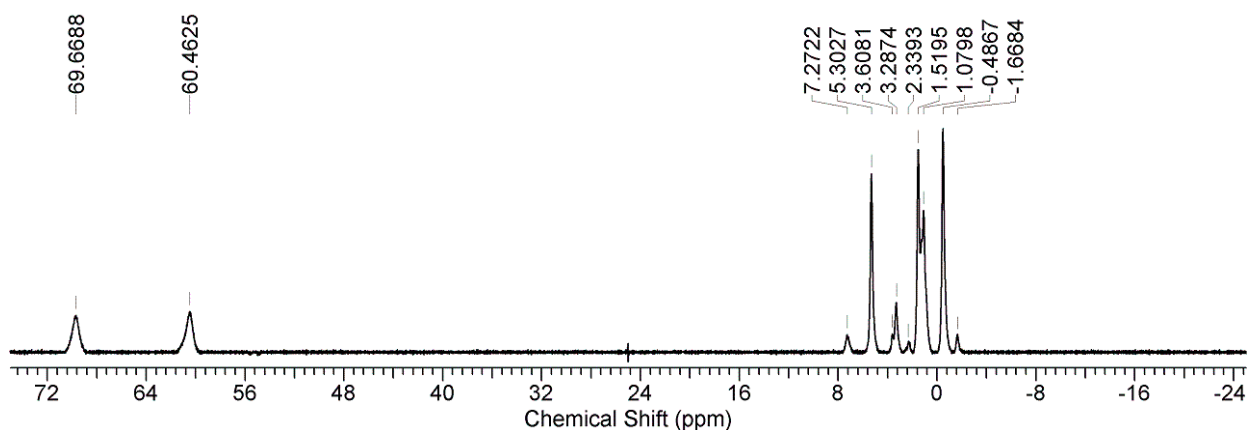


Figure 2-2 ^1H NMR spectrum of dimeric Co^{II} complex **II-7-2** in CD_2Cl_2 (300 MHz).

2.2.1.2 X-Ray Analysis of Phenylodiacetylene Bisdipyrin Co^{II} Complex

A single crystal of dimeric Co^{II} complex **II-7-2** was obtained *via* slow evaporation of a chloroform solution of **II-7-2** and the structure was determined by X-ray diffraction analysis. Surprisingly, instead of a flat, square-shaped arrangement caused by the formation of a mesocate, **II-7-2** displays a bowl-shaped arrangement with a folding angle of 128° due to the generation of a helicate. The distances between Co1 and Co2, C21 and C61 are 14.29 and 8.15 Å, respectively (Figure 2-3). The Co-N bond distances range from 1.96-1.99 Å. The dihedral angles between the mean planes of two dipyrins coordinated to the same Co^{II} ion are 78.8° and 71.7° , which indicates each metal center has a distorted tetrahedral geometry. The mean planes of the two terminal dipyrins and the phenyl spacer in each ligand are tilted by 34.1° and 81.7° for strand with C21, 68.7° and 28.9° for strand with C61. The inter-layer distance between Co^{II} ions is 18.88 Å. The three-dimensional packing structure of **II-7-2** describes a twin tunnel-like structure resulting from the partial overlap, by 3.42 Å, of the

individual molecules (Figure 2-4), which may be explained by the absence of π - π stacking interaction between the phenyl groups due to the repulsion between the bulky *t*-butyl groups. Therefore, a much bigger aromatic system with less bulky substituents may be introduced as the spacer to generate larger tunnels through complete overlap of the individual molecules.

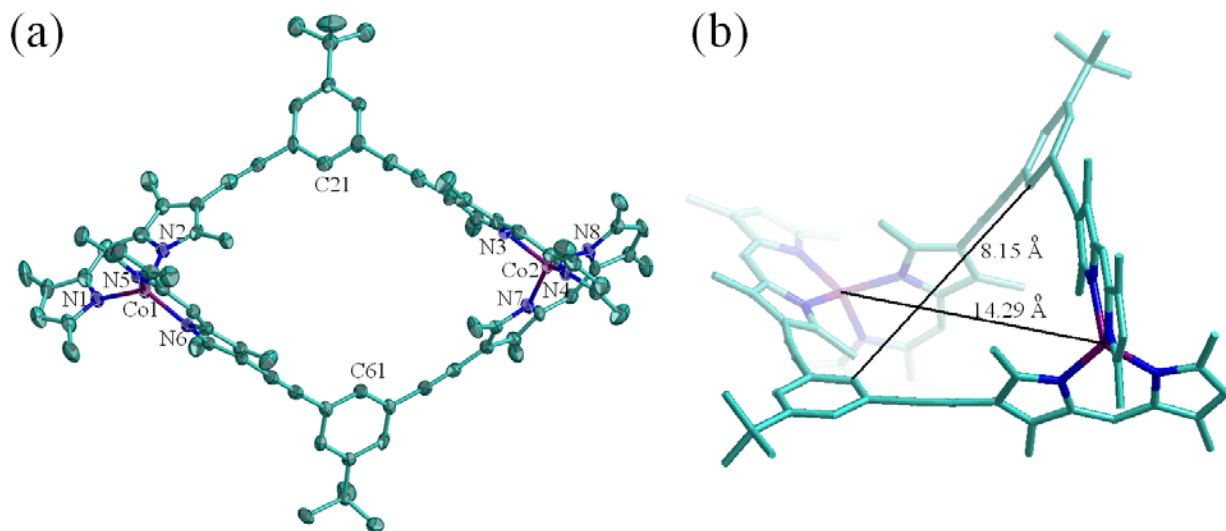


Figure 2-3 ORTEP diagram of dimeric Co^{II} complex **II-7-2** (thermal ellipsoids are scaled to the 50 % probability level): (a) top view and (b) side view.

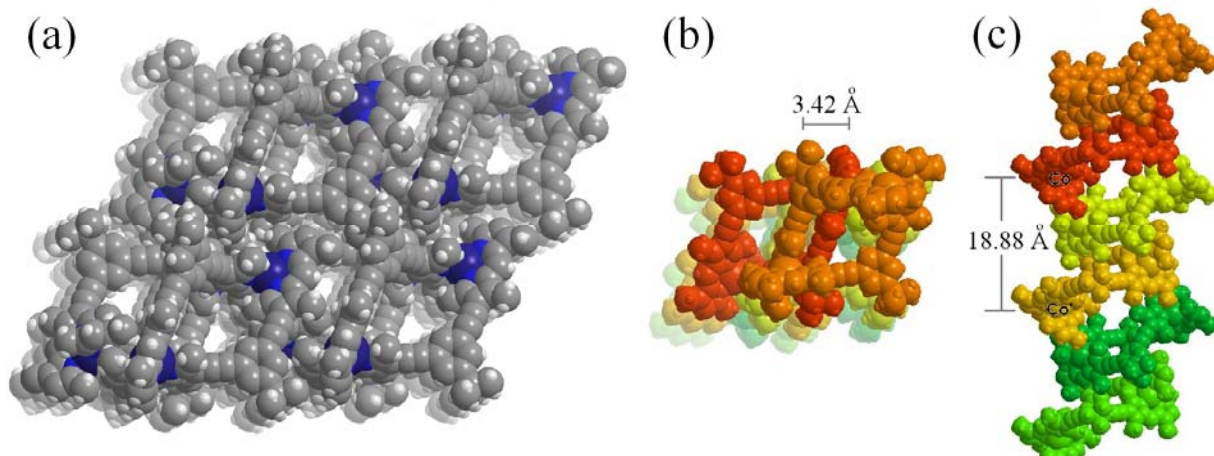
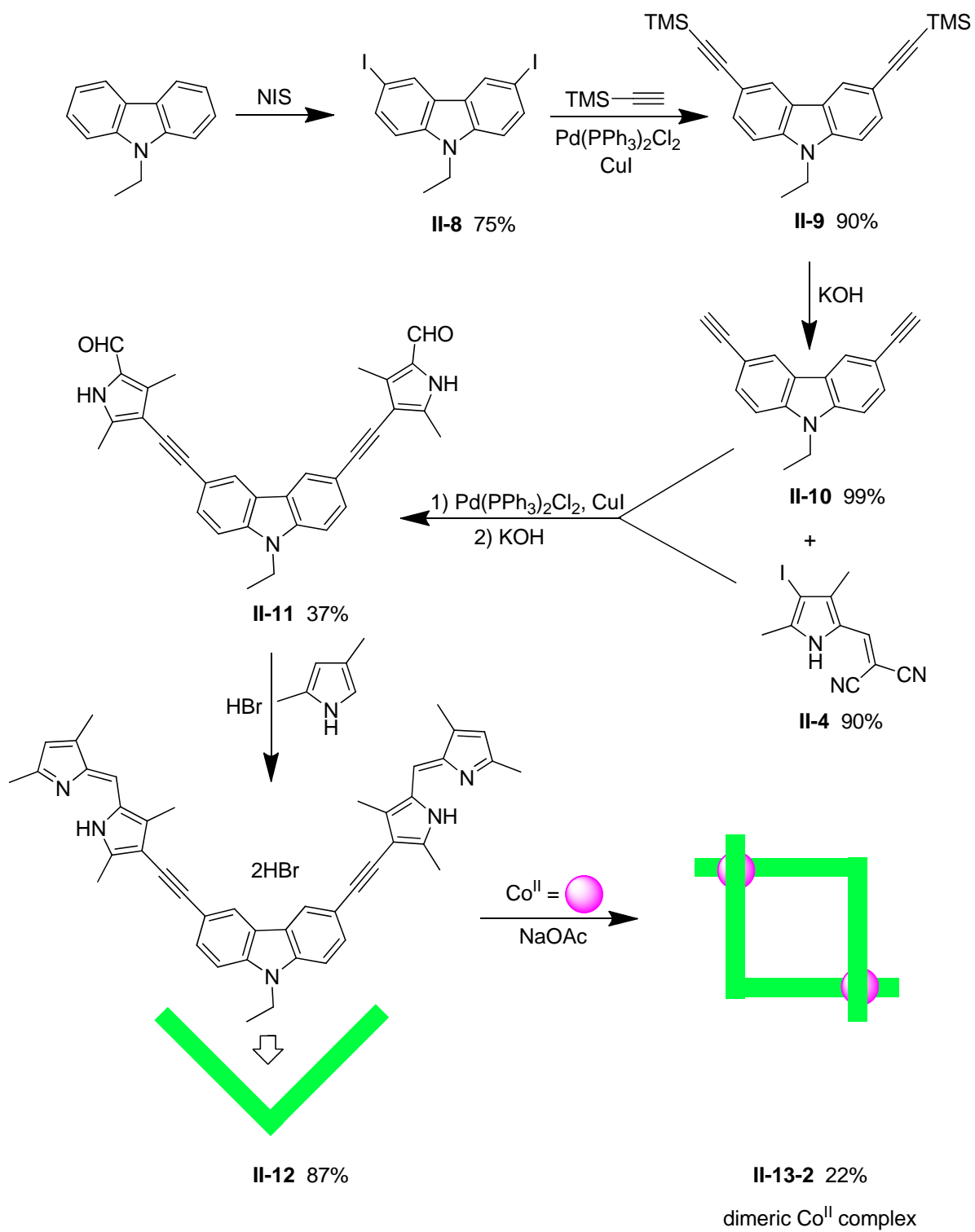


Figure 2-4 (a) Top view of the molecular space-filled packing of **II-7-2**; (b) top view and (c) side view of the twin-tunnel structure of **II-7-2** (reprinted with permission of the RSC).

2.2.2 Carbazolediacetylene Bisdipyrrin Co^{II} Complex

2.2.2.1 Synthesis of Carbazolediacetylene Bisdipyrrin Co^{II} Complex

Carbazole, a much bigger aromatic system, was selected as the spacer in order to form a larger tunnel in the solid state driven by π - π stacking interactions. The N atom of carbazole was protected by an ethyl group to decrease the polarity of the final metal complex for quick flash chromatography on silica gel, and improve the solubility in chloroform for crystal growth. The preparation of the carbazolediacetylene bisdipyrrin ligand **II-12** began with the synthesis of the spacer **II-10** which is the product of Sonogashira coupling of 9-ethyl-3,6-diiodocarbazole **II-8** and ethynyltrimethylsilane, followed by hydrolysis with addition of KOH.⁶⁹ A second Sonogashira coupling was employed with **II-10** and **II-4**,⁶⁵ followed by basic hydrolysis, and condensation with 2,4-dimethylpyrrole in the presence of HBr to afford the rigid bisdipyrrin ligand **II-12** as the HBr salt. Combination of **II-12** with Co(OAc)₂•4H₂O and NaOAc forms the bisdipyrrin Co^{II} complexes **II-13** (Scheme 2-2). The generation of the self-assembled oligomers collected from flash chromatography on silica gel was confirmed by MALDI-TOF mass spectrometry. The pure dimeric Co^{II} complex **II-13-2** was obtained from the same GPC column as for **II-7-2**.⁶⁷ The ¹H NMR spectrum of **II-13-2** again exhibited a large range of signals (-25 ~ 75 ppm), correlating with a paramagnetic structure (Figure 2-5).⁶⁸ However, no non-polar fraction was obtained from combination of either **II-6** or **II-12** with Zn(OAc)₂•2H₂O and NaOAc, which indicates no formation of the expected dimeric Zn^{II} complexes.



Scheme 2-2 Synthetic route for preparation of dimeric Co^{II} complex **II-13-2**.

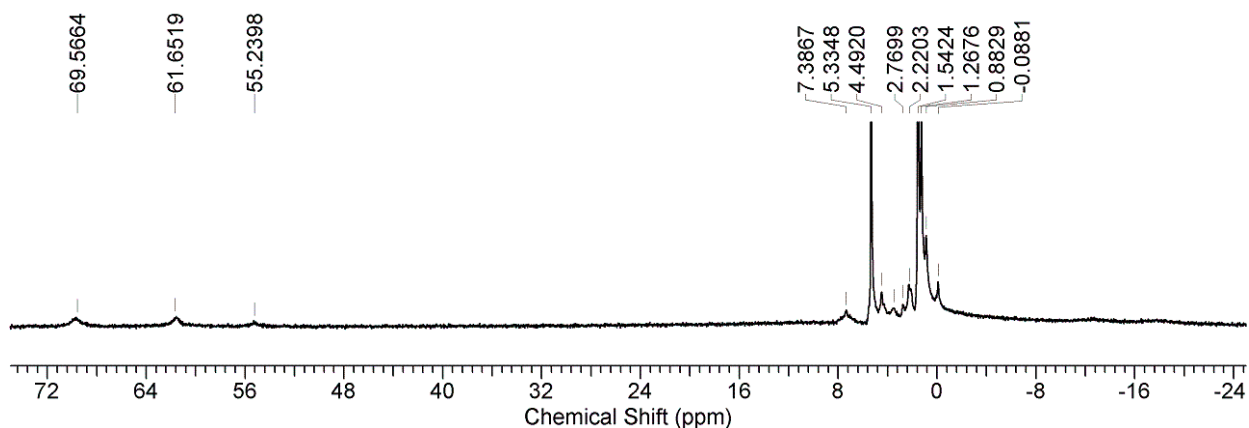


Figure 2-5 ^1H NMR spectrum of dimeric Co^{II} complex **II-13-2** in CD_2Cl_2 (300 MHz).

2.2.2.2 X-Ray Analysis of Carbazolediacetylene Bisdipyrrin Co^{II} Complex

A single crystal of dimeric Co^{II} complex **II-13-2** was grown from a chloroform solution of **II-13-2** and the structure was determined by X-ray diffraction analysis. Complex **II-13-2**, like **II-7-2**, displays a novel bowl-shaped arrangement with a smaller folding angle of 103° due to the formation of helicate. The distances between Co1 and Co2, N9 and N10 are 16.79 and 14.75 Å, respectively (Figure 2-6). The Co-N bond distances range from 1.96-1.98 Å. The dihedral angles between the mean planes of two dipyrins coordinated to the same Co^{II} ion are 81.0° and 81.4° , which show each metal center has a less distorted tetrahedral geometry than that in **II-7-2**. The mean planes of the two terminal dipyrins and the carbazole spacer in each ligand are tilted by 30.1° and 59.4° for the strand with N9 and 68.6° and 22.0° for the strand with N10. The inter-layer distance between Co^{II} ions is 13.59 Å, which is much shorter than that of **II-7-2**. The three-dimensional packing structure of **II-13-2** exhibits a much larger single tunnel

approximately 7.5 Å in diameter, resulting from the complete overlap of the individual molecules in the crystal. The complete overlap of the individual molecules may be driven by the strong π - π stacking interactions between the carbazole rings (distance = 3.32 Å) (Figure 2-7). Therefore, carbazole was proven to be a good spacer to successfully increase the size of the tunnel.

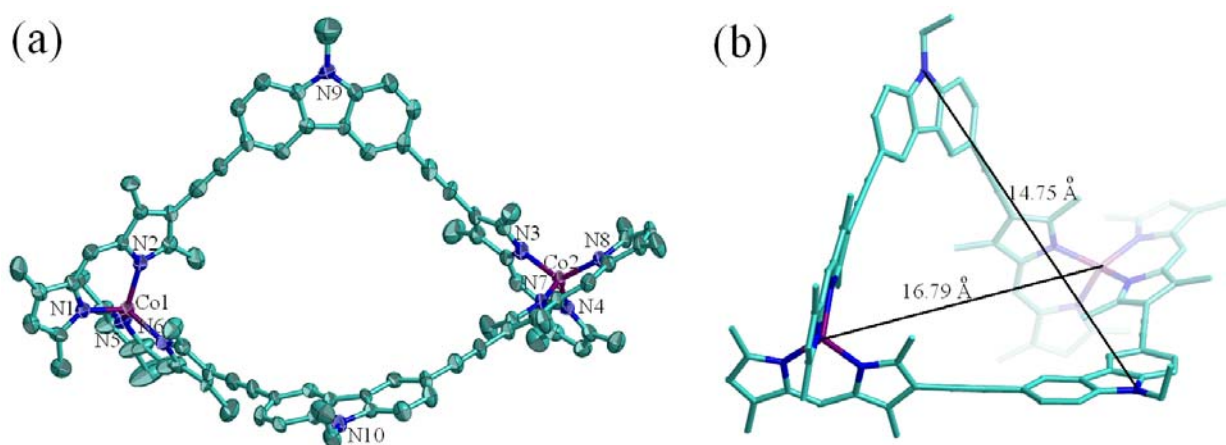


Figure 2-6 ORTEP diagram of dimeric Co^{II} complex **II-13-2** (thermal ellipsoids are scaled to the 50 % probability level): (a) top view and (b) side view.

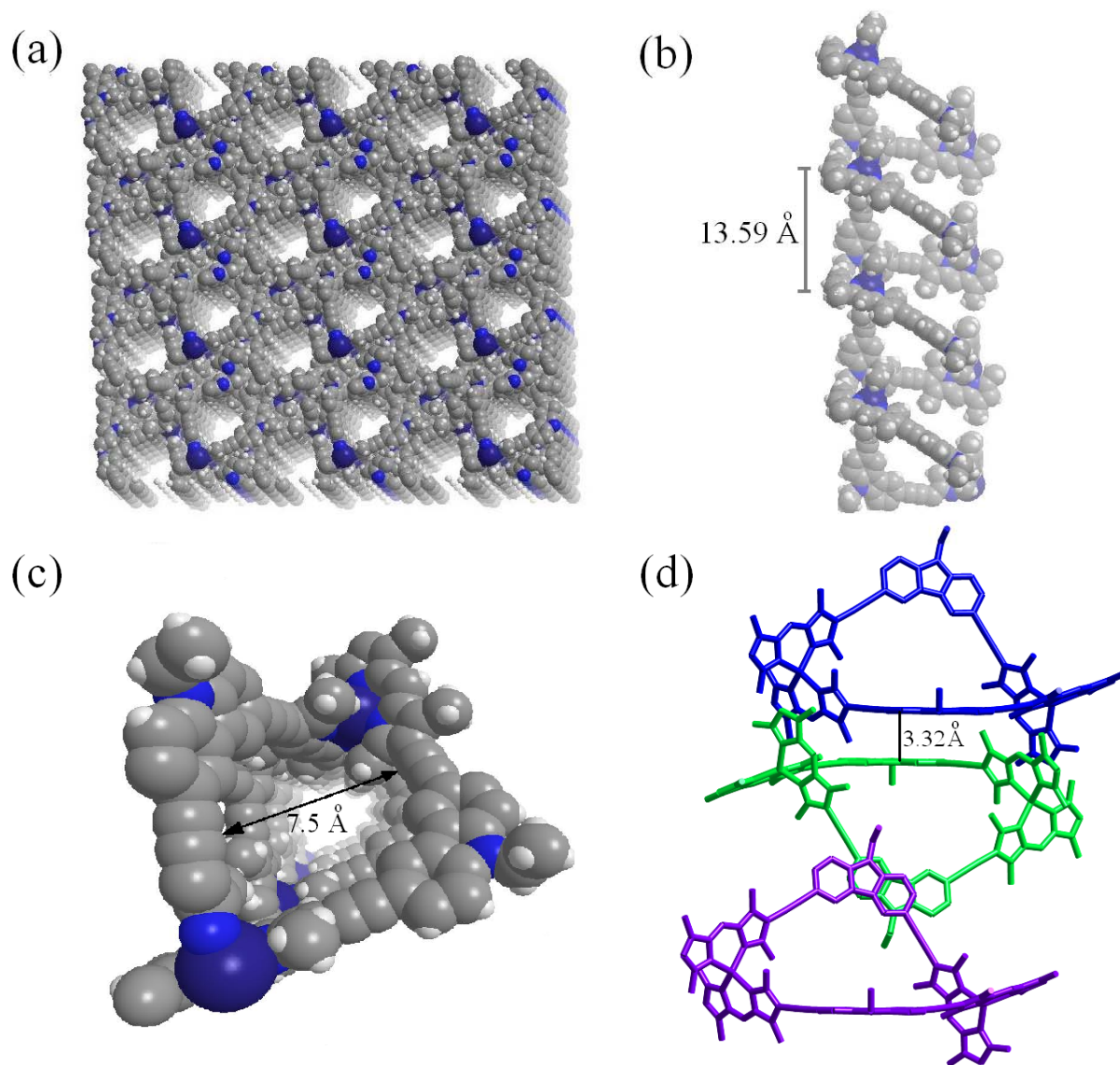


Figure 2-7 (a) Top view of the molecular space-filled packing of **II-13-2**; (b) side view and (c) top view of the single tunnel structure of **II-13-2** (reprinted with permission of the RSC); (d) π - π stacking interactions between the carbazole rings of the adjacent molecules (distance = 3.32 Å) by stick representation.

2.2.3 Diacetylene Bisdipyrin Metal Complexes

The higher nuclearity oligomers in both **II-7** and **II-13** are difficult to characterize due to their extremely low yields (trace). The angular spacers linking the two terminal dipyrins in each ligand limit the chance of generation of the higher nuclearity oligomers to some extent. Diacetylene was introduced as the linear spacer to improve the ligands for formation of higher nuclearity oligomers.

2.2.3.1 Synthesis of Diacetylene Bisdipyrin Metal Complexes

The synthesis of the diacetylene bisdipyrin ligands **II-21–II-24** was based on the preparation of the important intermediate **II-15** which started with decarboxylation of *t*-butyl 4-acetyl-3,5-dimethylpyrrole-2-carboxylate with TFA,⁷⁰ followed by a Vilsmeier reaction.⁷¹ An oxidative coupling of **II-15** afforded homo-coupled dialdehyde **II-16**,⁶⁵ followed by treatment with 4-*t*-butyl-3,5-dimethylpyrrole-2-carboxylic acid or α -free pyrroles in the presence of HBr to form **II-21** through **II-24** as HBr salts. Combination of ligands **II-21** through **II-24** with $\text{Zn}(\text{OAc})_2 \cdot 2\text{H}_2\text{O}$ and NaOAc generates bisdipyrin Zn^{II} complexes **II-25** through **II-28**. Non-polar fractions were collected from flash chromatography on silica gel, followed by elution on a GPC column with toluene to afford three separate red fractions from each reaction. MALDI-TOF mass spectrometry shows the formation of trimeric, tetrameric and pentameric Zn^{II} complexes in all cases except for **II-28**. The Zn^{II} complexes with electron-withdrawing

groups appear to be more stable than their counterparts with electron-donating groups due to electron delocalization caused by inductive effects from the electron-withdrawing groups. However, treatment of ligand **II-22** with either $\text{Co}(\text{OAc})_2 \cdot 4\text{H}_2\text{O}$ or $\text{Ni}(\text{OAc})_2 \cdot 4\text{H}_2\text{O}$ and NaOAc forms only trimeric and tetrameric bisdipyrin metal complexes **II-29** and **II-30** (Scheme 2-3).

2.2.3.2 ^1H NMR Spectra of Diacetylene Bisdipyrin Zn^{II} Complexes

The ^1H NMR spectra of trimeric **II-25-3** and tetrameric **II-25-4** Zn^{II} complexes dissolved in CDCl_3 showed that the two NH signals, previously at δ 13.49 and 13.18 for **II-21**, were no longer present, which supports the formation of the Zn^{II} complexes. Experiments indicated that coordination of **II-21** with a Zn^{II} ion to form **II-25** resulted in upfield shifts for all ^1H signals.⁴⁶ As expected, the α and α' methyl signals shift dramatically (~ 0.8 ppm) (Figure 2-8). X-ray analysis of **II-25-3** demonstrates both the α and α' methyl groups in one dipyrin unit are located either above or below the mean plane of the other dipyrin. Anisotropy results, where the methyl groups are shielded and an upfield-shifting of the signals occurs.¹¹

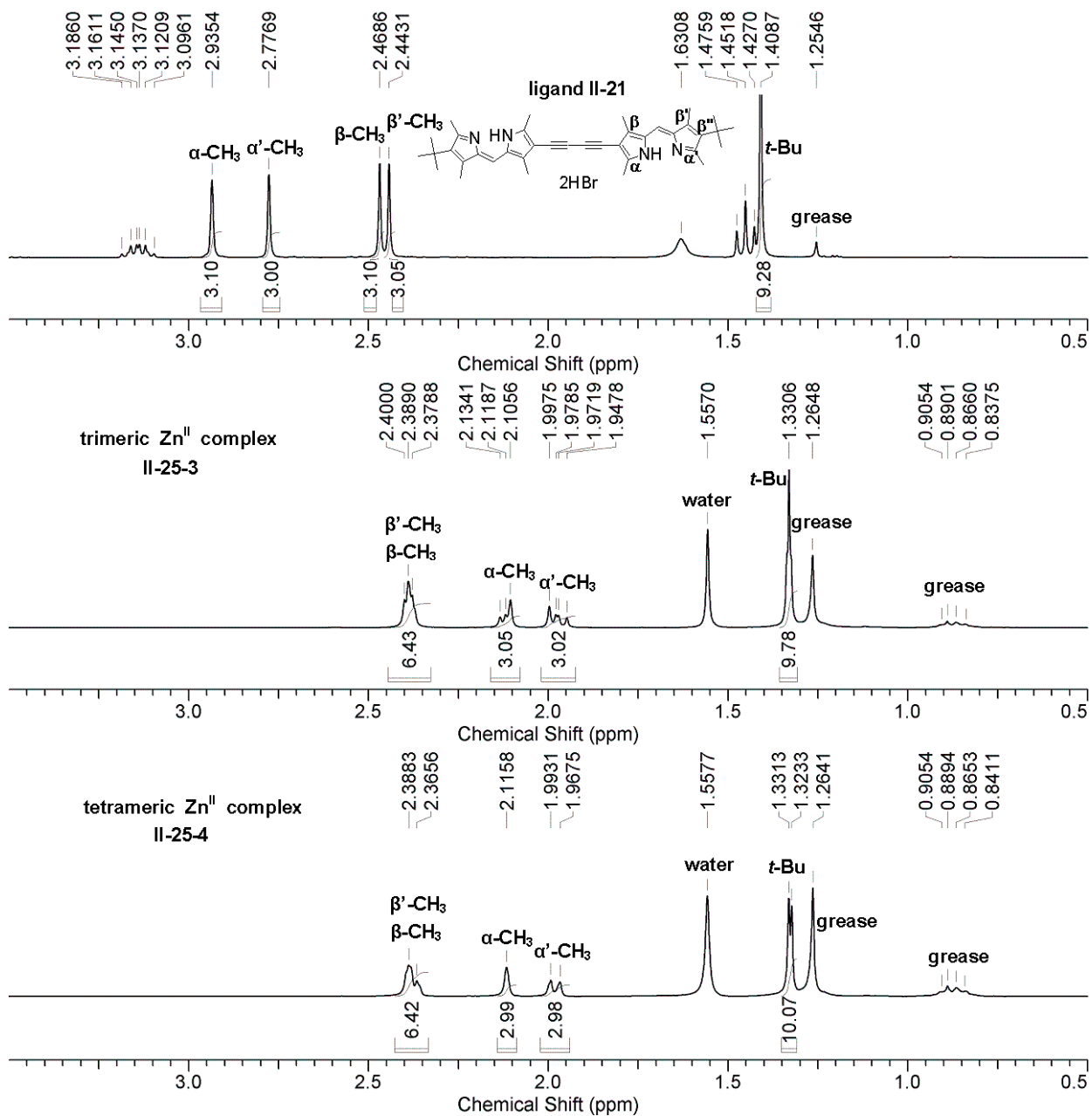


Figure 2-8 ¹H NMR spectra (alkyl region) of ligand **II-21** (top), trimeric **II-25-3** (middle) and tetrameric **II-25-4** (bottom) Zn^{II} complexes in CDCl₃ (300 MHz).

2.2.3.3 X-Ray Analysis of Diacetylene Bisdipyrin Zn^{II} Complexes

A single crystal of trimeric Zn^{II} complex **II-25-3** was obtained from a methylene chloride solution of **II-25-3** and the structure was determined by X-ray diffraction analysis (Figure 2-9). Complex **II-25-3** crystallizes about a three-fold axis located along the crystallographic *c*-axis. The structure also displays high symmetry. The distance between two Zn^{II} ions in one molecule is 14.32 Å. The Zn-N bond distances range from 1.98-1.99 Å. The dihedral angle between the mean planes of two dipyrins coordinated to the same Zn^{II} ion is 79.1°, which shows each metal center has a distorted tetrahedral geometry. The dihedral angle between the mean planes of two dipyrins in each ligand is 70.4°. The distance between the mean planes of each layer was determined to be 10.05 Å. Complex **II-25-3** is almost flat, which suggests it might be a good candidate to produce nano-sized tunnels. However, **II-25-3**, unlike **II-13-2**, did not show a completely overlapped packing pattern due to the bulky terminal *t*-butyl groups (Figure 2-10). In fact, the molecules in complex **II-25-3** adopted a unique packing pattern to minimize steric hindrance with the result being that the three-dimensional structure presents a series of honeycomb-like tunnels approximately 5.7 Å in diameter (Figure 2-11).

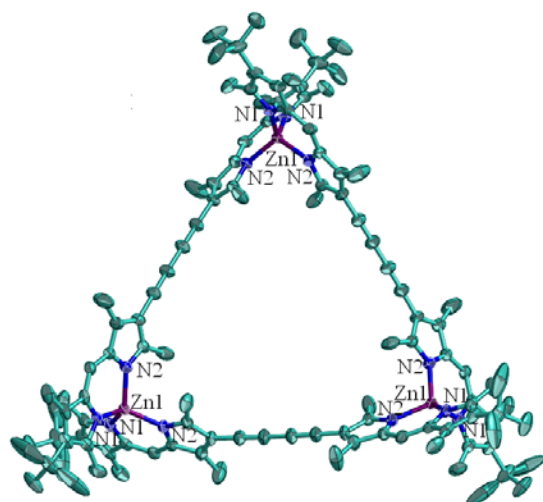


Figure 2-9 ORTEP diagram of trimeric Zn^{II} complex **II-25-3** (thermal ellipsoids are scaled to the 50 % probability level).

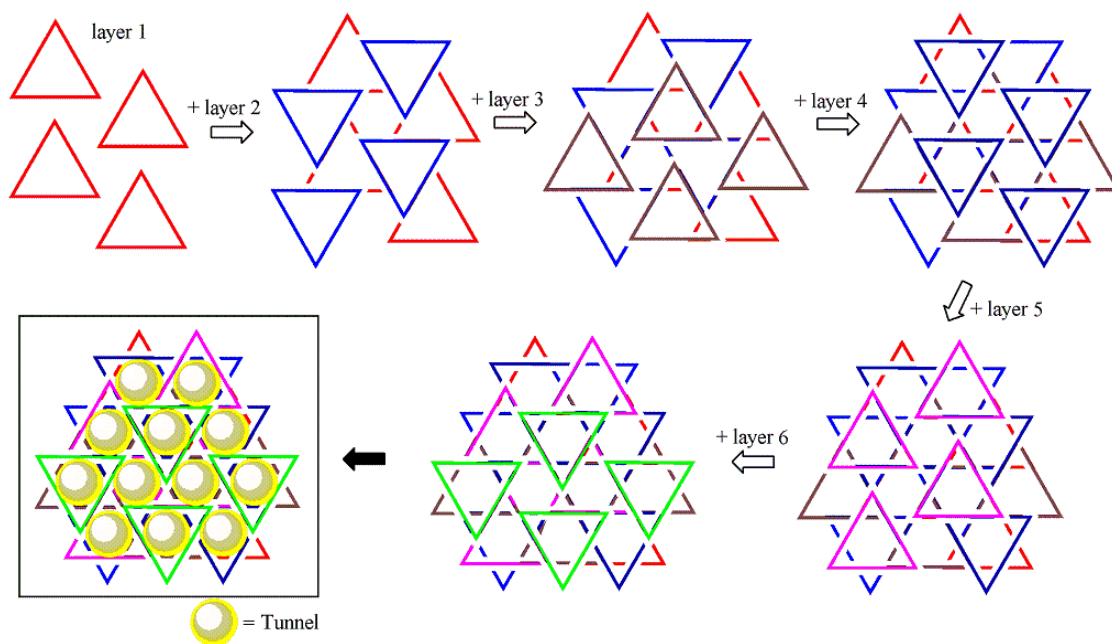


Figure 2-10 Stepwise packing pattern of the individual layers for **II-25-3**; positions of tunnels were displayed as yellow spheres in the last figure for clarity (reprinted with permission of the RSC).

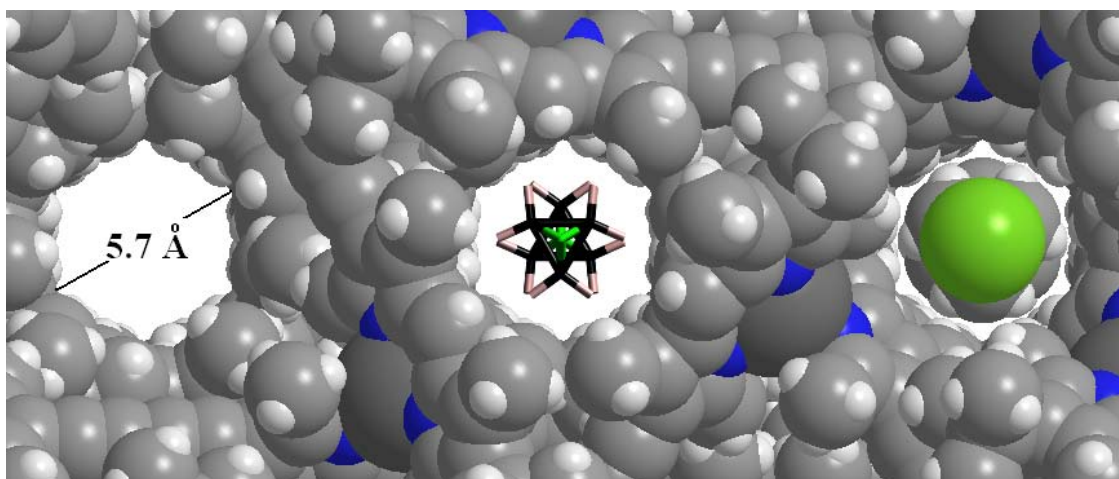


Figure 2-11 Space-filled packing of **II-25-3**: without (left) and with solvent molecules in space-filling (right) or stick (center) representations showing 3-fold axis disorder (reprinted with permission of the RSC).

A single crystal of trimeric Zn^{II} complex **II-26-3** was obtained from slow diffusion of hexane into a dichloromethane solution of **II-26-3** and the structure was again determined by X-ray diffraction analysis (Figure 2-12). Complex **II-26-3** crystallizes with one half-molecule in the asymmetric unit, residing on a two-fold axis of rotation. The distances between two Zn^{II} ions in one molecule are 14.05 and 13.53 Å. The Zn-N bond distances range from 1.96-2.00 Å. Between the mean planes of two dipyrins coordinated to the same Zn^{II} ion are dihedral angles of 79.6 and 78.2°, which show each metal center has a distorted tetrahedral geometry. The dihedral angles between the mean planes of two dipyrins in each ligand are 73.6 and 37.0° and the inter-layer distance between Zn^{II} ions is 16.17 Å. Unlike **II-25-3**, the molecules in complex **II-26-3** adopted a unique packing pattern which displays a series of tunnels (approximately 7.5 Å in diameter) outside the molecule triangles (Figure 2-13).

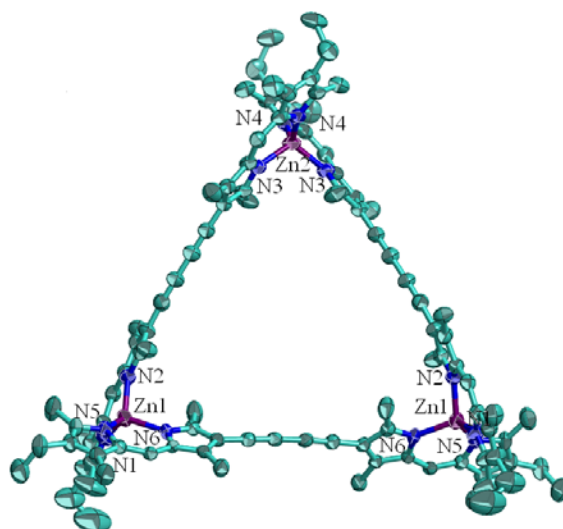


Figure 2-12 ORTEP diagram of trimeric Zn^{II} complex **II-26-3** (thermal ellipsoids are scaled to the 50 % probability level).

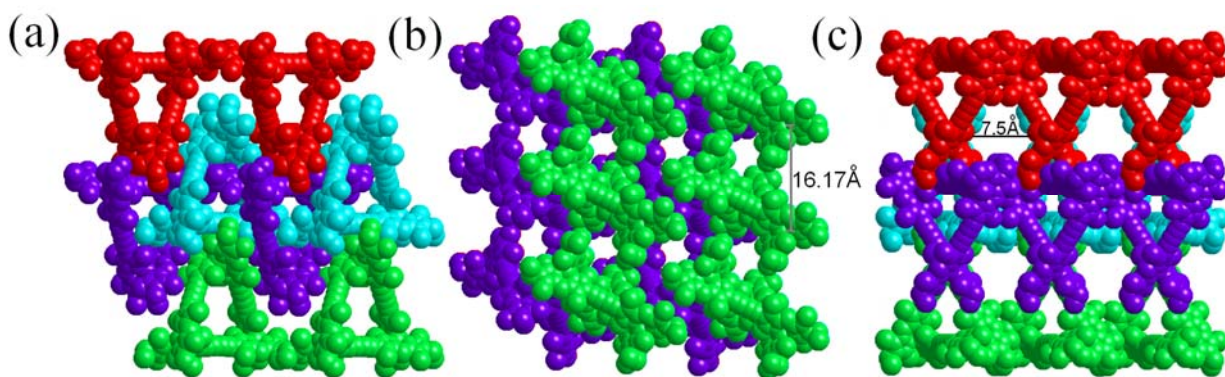


Figure 2-13 Space-filled packing of **II-26-3**: (a) top view; (b) and (c) side views.

The tetrameric Zn^{II} complexes **II-25-4** and **II-26-4**, unlike their trimeric counterparts, are slightly soluble in CH₂Cl₂. Unfortunately, no X-ray structures of tetrameric Zn^{II} complexes have been obtained so far due to unsuccessful single crystal growth, even though several solvent combinations (CHCl₃/hexane, CHCl₃/MeOH and CHCl₃/THF) and growing methods have been investigated. In contrast to the trimeric Zn^{II} complexes which only contain one isomer (circular

helicate), the tetrameric Zn^{II} complexes may possess two isomers (circular helicate and grid) due to the two possible conformations of the two dipyrin units linked by a diacetylene group in one strand to construct the structures. The tetrameric circular helicates contain anti-parallel dipyrin units in all four strands, while the grids instead consist of the parallel dipyrin units (Figure 2-14).¹⁶

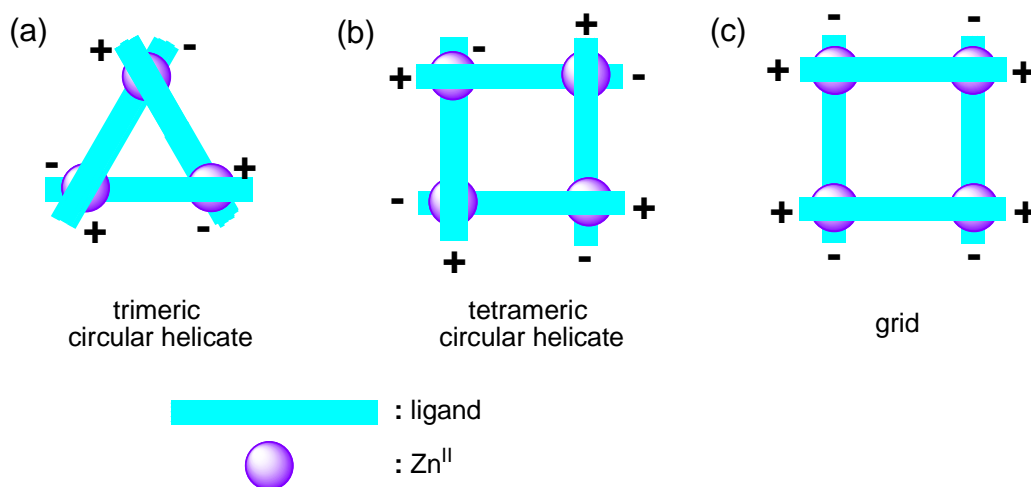


Figure 2-14 Diagram of (a) Zn^{II} trimeric circular helicate; (b) Zn^{II} tetrameric circular helicate and (c) Zn^{II} grid.

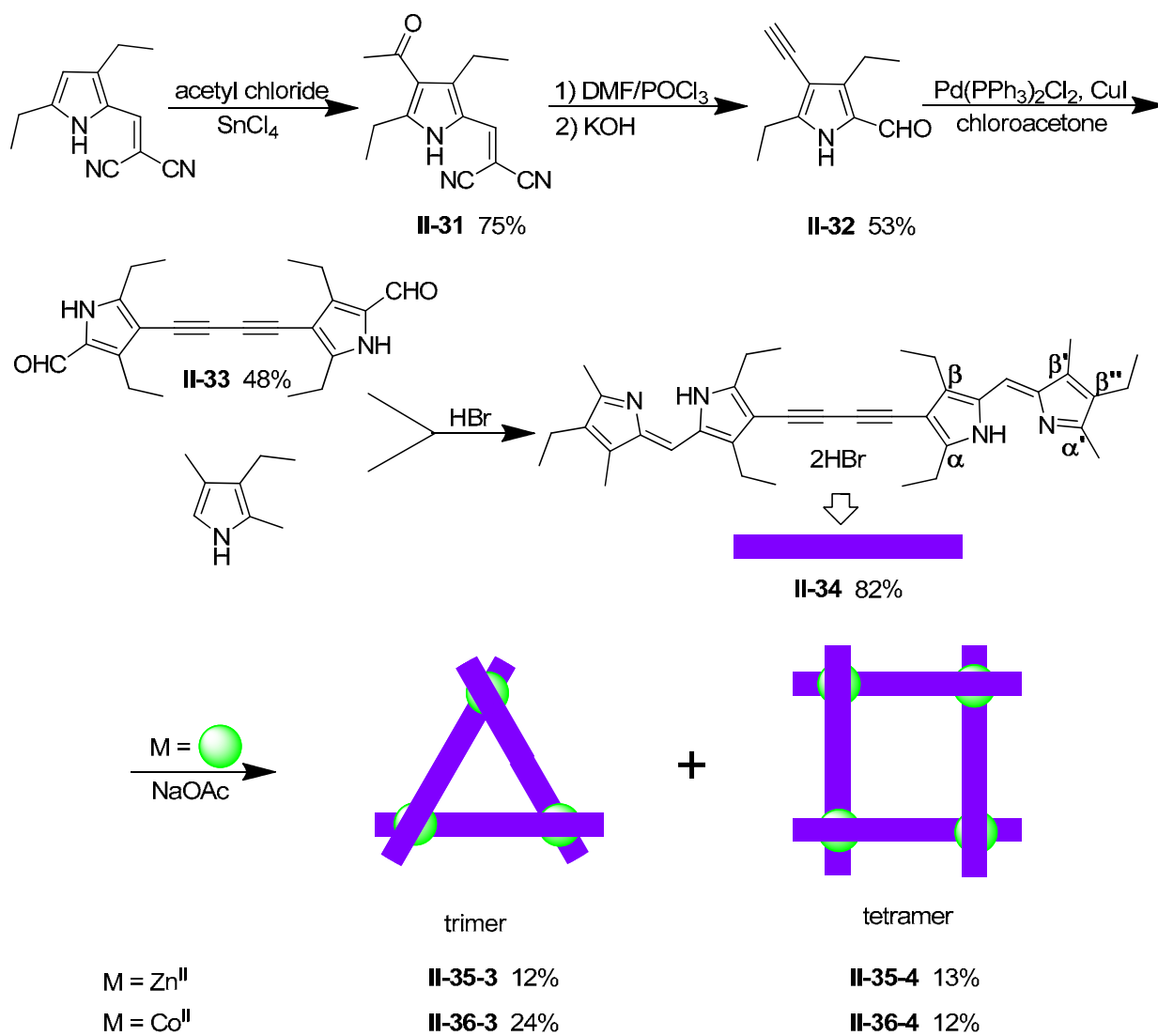
2.2.4 α,β -Ethyl Diacetylene Bisdipyrin Metal Complexes

Reaction conditions were altered for the generation of complex **II-26** including addition of the Zn^{II} ion at various times (adding in one portion to addition over an 8 h period) and variable temperatures (-10 °C to reflux in $CHCl_3/MeOH$). The same trimer was obtained in a high yield in all cases, which implies it is both the kinetically and thermodynamically favoured product. The result of this is that optimization of the ligand is necessary to generate more of the tetramer.

In order to achieve this goal, we introduced ligand **II-34** after replacing the methyl group with ethyl at the α - and β -positions of ligand **II-22**. It was thought that the repulsion between two bulkier ethyl groups at the α -position of ligand **II-34** would encourage the formation of the tetramer.

2.2.4.1 Synthesis of α,β -Ethyl Diacetylene Bisdipyrin Metal Complexes

The synthesis of the α,β -ethyl diacetylene bisdipyrin ligand **II-34** was based on the preparation of the important intermediate **II-32** which began with Friedel-Crafts reaction of 2-((3,5-diethyl-1H-pyrrol-2-yl)methylene)malononitrile with acetyl chloride,⁷⁰ followed by Vilsmeier reaction.⁷¹ An oxidative coupling of **II-32** afforded homo-coupled dialdehyde **II-33**,⁶⁵ followed by treatment with 3-ethyl-2,4-dimethylpyrrole and HBr to form **II-34** as the HBr salt. Combination of ligand **II-34** with either $\text{Zn}(\text{OAc})_2 \cdot 2\text{H}_2\text{O}$ or $\text{Co}(\text{OAc})_2 \cdot 4\text{H}_2\text{O}$ and NaOAc generates the dipyrin metal complexes **II-35** and **II-36**. A non-polar fraction was collected from flash chromatography on silica gel, followed by elution on a gel permeation chromatography (GPC) column with toluene to afford two distinct fractions in each case. MALDI-TOF mass spectrometry indicated the formation of trimer and tetramer in both cases (Scheme 2-4). As expected, the yield of tetramer from ligand **II-34** increased dramatically compared to that from **II-22** (2% to 13% for tetrameric Zn^{II} complex, 4% to 12% for tetrameric Co^{II} complex). Moreover, the introduction of ethyl groups at α -position of ligand **II-34** proved to dramatically increase the solubility of the tetrameric metal complexes (i.e. highly soluble in dichloromethane).



Scheme 2-4 Synthetic route for preparation of tri- and tetrameric metal complexes.

2.2.4.2 ^1H NMR Spectra of α,β -Ethyl Diacetylene Bisdipyrin Zn^{II} Complex

The ^1H NMR spectra of trimeric **II-35-3** and tetrameric **II-35-4** Zn^{II} complexes dissolved in CDCl_3 showed that the two NH signals, previously at δ 13.12 and 13.46 for **II-34**, were no longer present, which indicates the formation of the metal complexes. Experiments displayed that coordination of **II-34** with Zn^{II} ion to form **II-35** led to upfield shifts for all ^1H signals.⁴⁶ The $\alpha\text{-CH}_2$ and CH_3 , $\alpha'\text{-CH}_3$ signals, similar to **II-25**, shift dramatically ($\sim 0.7\text{-}0.85$ ppm) due to the same anisotropic effects mentioned before (Figure 2-15).

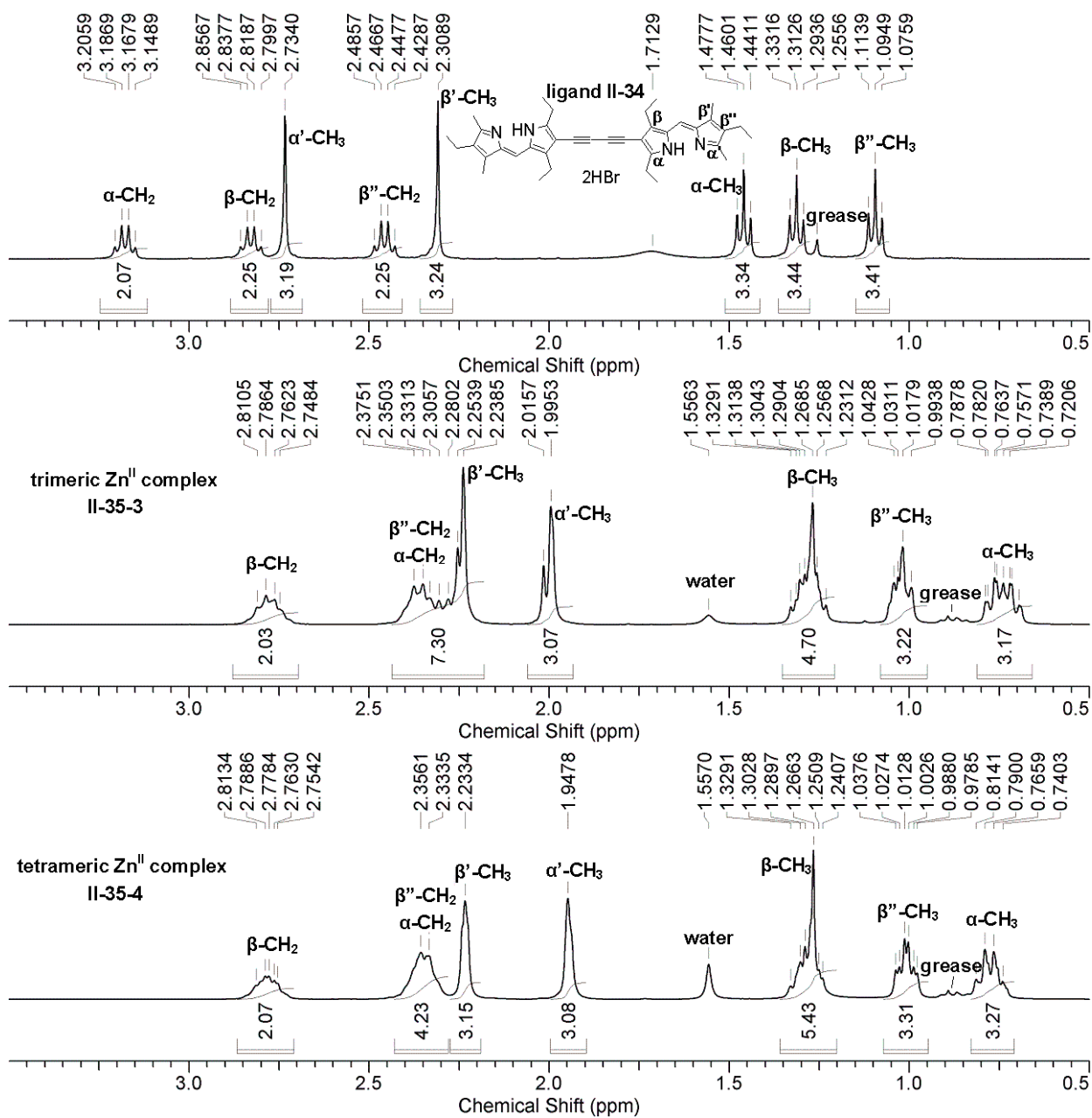


Figure 2-15 ¹H NMR spectra (alkyl region) of ligand **II-34** (top) (400 MHz), trimeric **II-35-3** (middle) and tetrameric **II-35-4** (bottom) Zn^{II} complexes in CDCl₃ (300 MHz).

2.2.4.3 X-Ray Analysis of α,β -Ethyl Diacetylene Bisdipyrin Zn^{II} Complex

A single crystal of trimeric Zn^{II} complex **II-35-3** from ligand **II-34** was obtained from slow diffusion of hexane into a dichloromethane solution of **II-35-3** and the structure was determined by X-ray diffraction analysis (Figure 2-16). The distances between two Zn^{II} ions in one molecule are 14.26, 14.00 and 13.93 Å. The Zn-N bond distances range from 1.91-2.00 Å, which is slightly bigger than those in **II-25-3** and **II-26-3**. The diacetylene bridge is heavily distorted in order to accommodate the bulkier ethyl groups at the α - and β -positions of ligand **II-34**. Therefore, **II-35-3**, unlike **II-25-3** and **II-26-3**, has no symmetry in the crystal structure. The dihedral angles between the mean planes of two dipyrins coordinated to the same Zn^{II} ion are 84.6, 84.3 and 82.2°, which shows each metal center has a slightly distorted tetrahedral geometry. The dihedral angles between the mean planes of two dipyrins in each ligand are 31.7, 44.6 and 38.3°. The inter-layer distance between Zn^{II} ions is 15.08 Å. In contrast to **II-26-3**, the molecules in complex **II-35-3** adopted a partially overlapped packing pattern which leads to a series of smaller tunnels (approximately 3.5 Å in diameter) outside the molecule triangles (Figure 2-17).

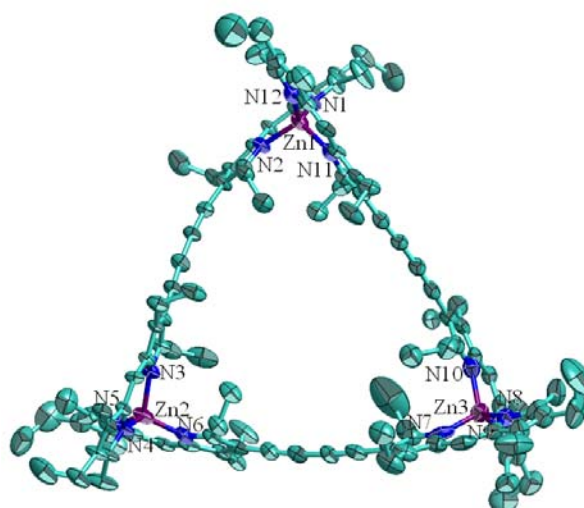


Figure 2-16 ORTEP diagram of trimeric Zn^{II} complex **II-35-3** (thermal ellipsoids are scaled to the 33 % probability level).

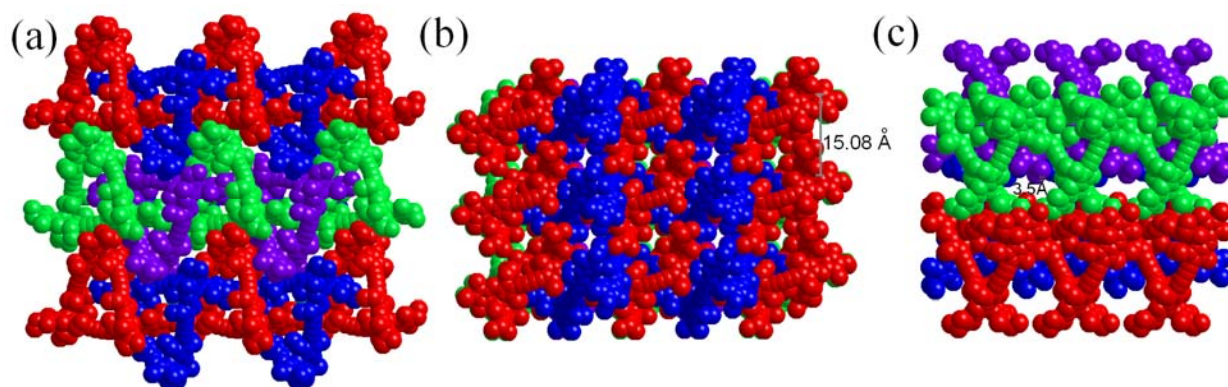


Figure 2-17 Space-filled packing of **II-35-3**: (a) top view; (b) and (c) side views.

2.2.5 Electronic Absorption Spectra of Diacetylene Bisdipyrin Metal Complexes

The diacetylene bisdipyrin Zn^{II} complexes, **II-25-26**, **II-28** and **II-35**, are dichroic red/green solids upon crystallization, but generate red solutions when dissolved in chloroform. Complex **II-27** is a dichroic purple/green solid upon crystallization, but forms a reddish purple solution when dissolved in chloroform. The Co^{II} complexes, **II-29** and **II-36**, are dichroic purple/green solids upon crystallization, but form purple solutions when dissolved in chloroform. However, the Ni^{II} complex **II-30** is a dark brown solid, and generates a dark brown solution. Complexes **II-25-30** and **II-35-36** were analyzed by electronic absorption spectroscopy (Figure 2-18). As expected, the strongest absorption of all complexes in chloroform is a sharp band (λ_{max}) resulting from a metal-to-ligand charge transfer transition (Table 2-1). An ascending trend of λ_{max} can be observed in the Zn^{II} complexes (**II-26** and **II-35**), which may be caused by hyperconjugation effects through replacing methyl groups with ethyl groups.⁷² A large bathochromic shift (~10 nm) occurs with a phenylketone group (**II-27**) on the β ' position of the ligand instead of an alkyl group (**II-26**) owing to the larger π -conjugated systems extended by the electron-withdrawing group.⁷³ However, an ester group seems less effective, only causing a relatively small bathochromic shift (~2 nm). The absorption wavelengths (λ_{max}) of the tri- and tetrameric metal complexes are either the same or marginally shifted (1 to 3 nm) in each case, consistent with similar coordination environments for the metal ions and no major difference between the two distinct π -conjugated systems of the tri- and tetrameric metal complexes. In short, the optical properties of the metal complexes depend much more on the ligand spacer and the metal ions than the substituents present on the pyrrole groups.

Table 2-1 Metal-to-ligand charge transfer transition band λ_{max} (nm) for tri-, tetra- and/or pentameric metal complexes in chloroform.

Complex	λ_{max} (nm)/log ϵ		
	Trimer	Tetramer	Pentamer
II-25	544/5.81	544/5.93	—
II-26	542/5.82	542/5.90	—
II-27	554/5.68	553/5.82	553/5.92
II-28	545/5.77	544/5.84	—
II-29	540/5.54	541/5.73	—
II-30	580/5.40	582/5.50	—
II-35	546/5.82	543/5.93	—
II-36	544/5.66	541/5.74	—

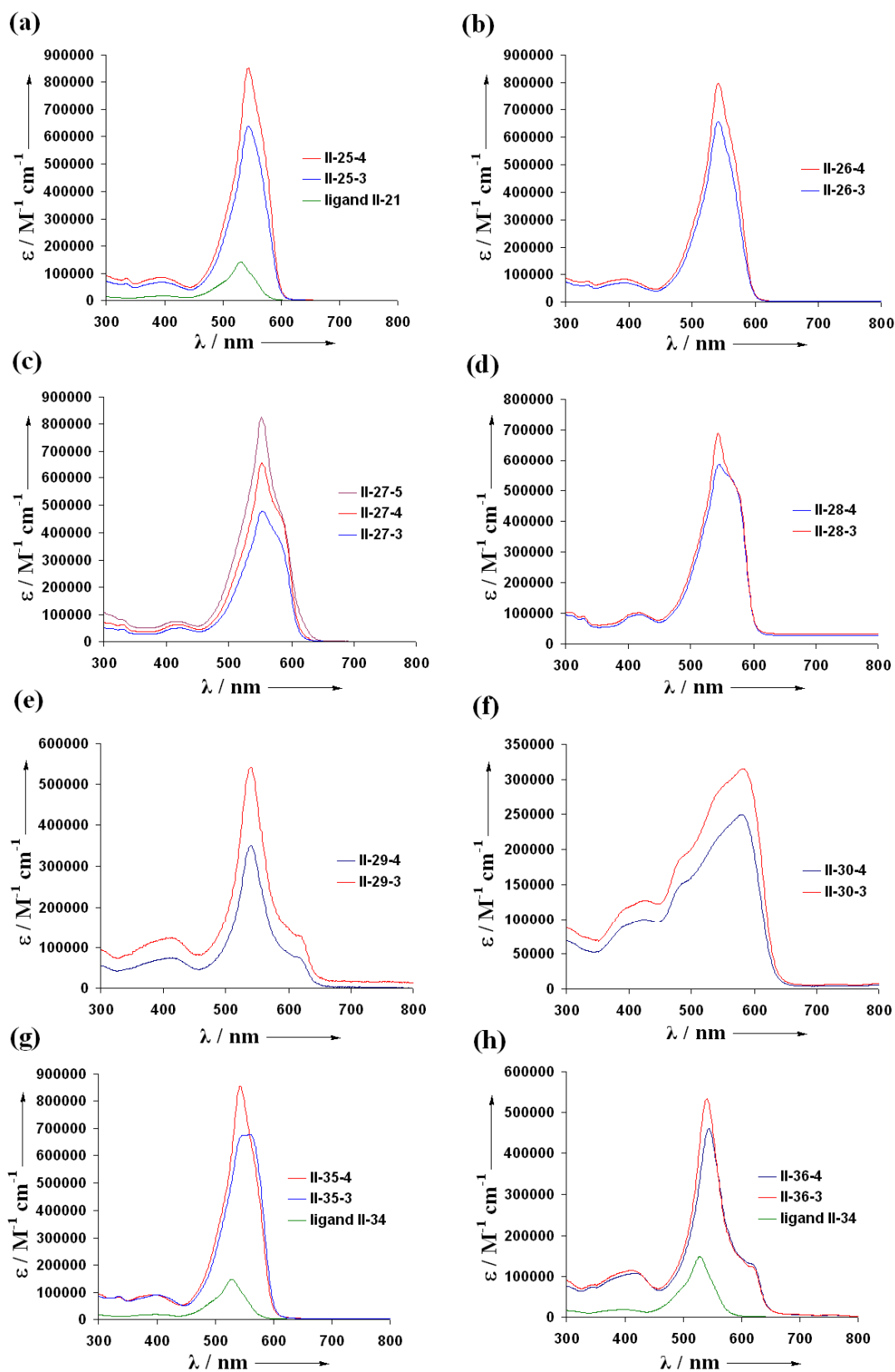


Figure 2-18 Electronic absorption spectra of bisdipyrrin metal complexes in chloroform: (a) **II-25**, (b) **II-26**, (c) **II-27**, (d) **II-28**, (e) **II-29**, (f) **II-30**, (g) **II-35** and (h) **II-36**.

2.3 Conclusions

The bisdipyrrin ligands with diacetylene as their rigid and linear spacer have been prepared, and readily react with different metal ions (Zn^{II} , Co^{II} and Ni^{II}) to afford tri-, tetra- and/or pentameric metal complexes. The trimeric Zn^{II} complexes contain a trinuclear circular-helical structure confirmed by X-ray analysis. The three-dimensional packing of the crystal structures display a variety of tunnel-like structures with different sizes and shapes. No single crystals of the tetrameric Zn^{II} complexes were obtained owing to the unsuccessful separation of the two possible isomers (circular helicate and grid). Therefore, the structures of tetrameric Zn^{II} complexes are still unsolved. By contrast, the grid-type metal complexes with locked parallel dipyrin units contain only one isomer, which easily solved the purification problem. The next chapter will focus on the grid-type metal complexes.

Chapter Three
Homoleptic Grids and Hexagons

3.1 Design Strategy

meso-Unsubstituted bisdipyrrin salts prepared through condensation have been widely studied as ligands for formation of metal complexes featuring double-^{45, 46} or triple-⁴⁷ helical structures. I have already synthesized and characterized the trimeric Zn^{II} circular helicates using rigid linear diacetylene bisdipyrrin ligands in this study. However, no single crystals of the tetrameric Zn^{II} complexes were obtained due to the unsuccessful separation of the two possible isomers (circular helicate and grid). Therefore, the structures of tetrameric Zn^{II} circular helicate and grid are still unsolved. By contrast, the grid-type metal complexes with locked parallel dipyrin units contain only one isomer, which easily solved the purification obstacle. As far as we are aware, no grid-type metal complexes based on bisdipyrrin ligands have been reported thus far. Inspired by the work of Lehn and Siegel on grid-type metal complexes using bipyridine ligands (Figure 3-1),^{19, 31, 35} porous bisdipyrrin metal grids as potential candidates for gas storage, catalysis and drug delivery were thoroughly investigated.

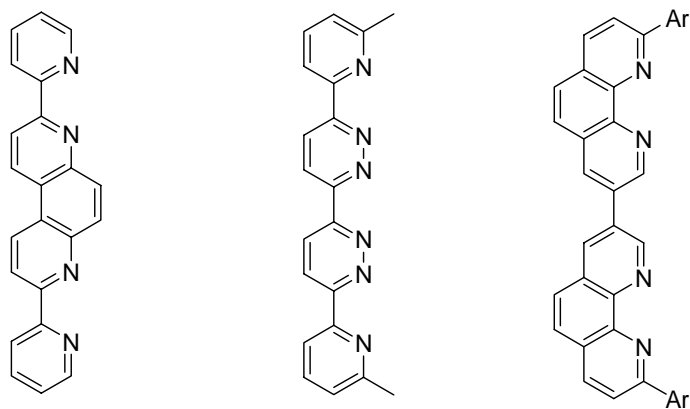


Figure 3-1 Ligands based on bipyridine introduced by Lehn and Siegel for preparation of grid-type metal complexes.

The spacer linking two dipyrin units is the key to the design of appropriate ligands for grid-type metal complexes. Flexible spacers, such as methylene and ethylene, favour the generation of double- or triple-stranded helicates, as expected. The linear rigid spacer, diacetylene, prefers the formation of circular helicates due to the more stable anti-parallel conformation of the dipyrin units in each strand. A spacer which can lock the two dipyrin units in the parallel position is required for the suitable candidates. In order to achieve that goal, a fused ring system was introduced. The two central pyrrole rings from the dipyrin units are fused on the cyclohexane ring to generate a linear bisdipyrin ligand with the two dipyrin units parallel to each other (Figure 3-2).

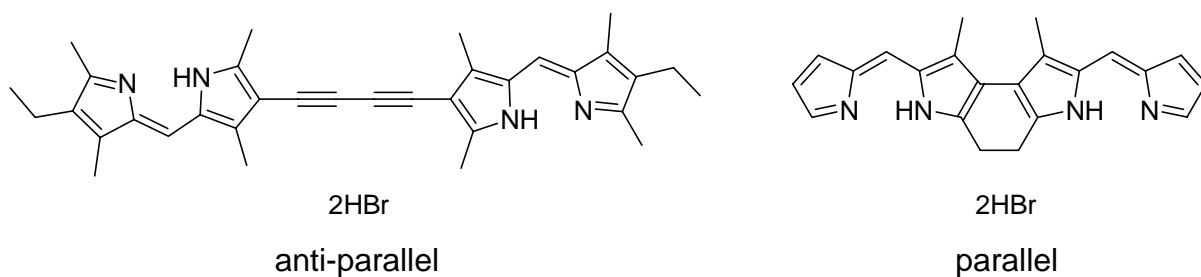


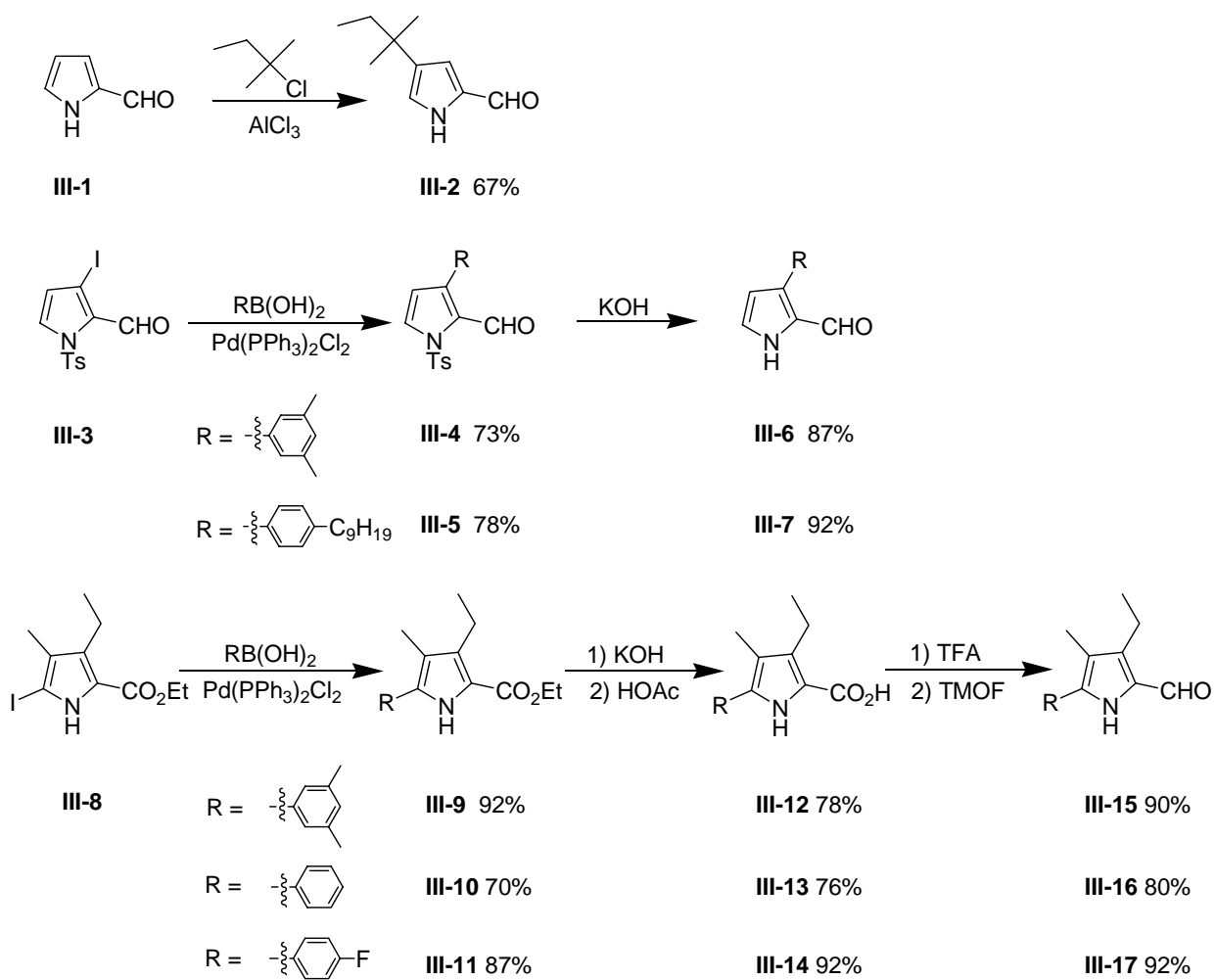
Figure 3-2 Different conformations of the dipyrin units in one strand linked by diacetylene (left) and a fused ring (right).

3.2 Results and Discussion

3.2.1 Ring Fused Bisdipyrrin Metal Complexes

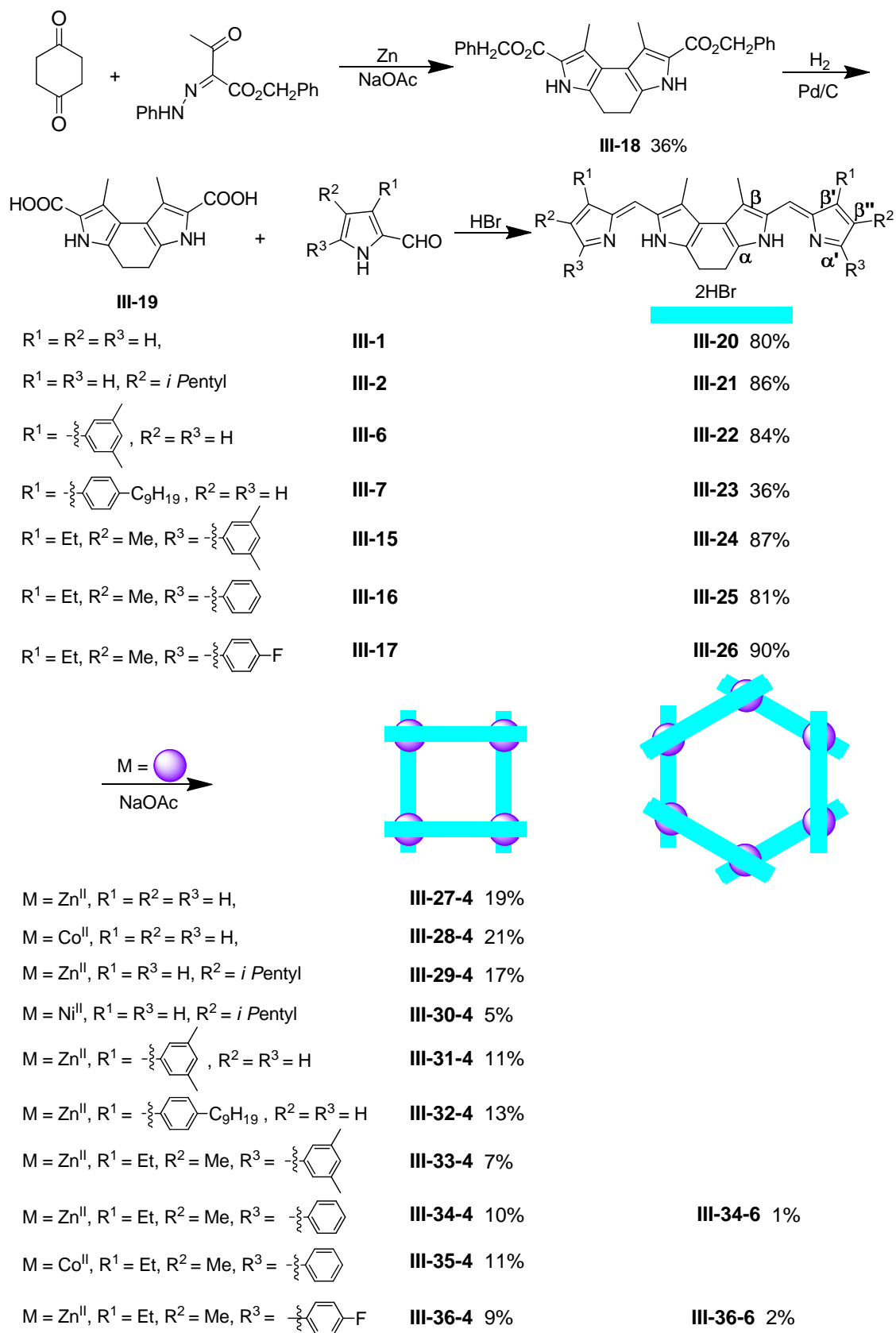
3.2.1.1 Synthesis of Ring Fused Bisdipyrrin Metal Complexes

The preparation of the ring fused bisdipyrrins began with the synthesis of various pyrrole-2-carbaldehyde derivatives (Scheme 3-1). The simplest pyrrole-2-carbaldehyde **III-1** was selected as a starting point. In order to investigate the substituent effects on the pyrrole rings for the generation of metal grids, several pyrrole-2-carbaldehyde derivatives were prepared. **III-2** is the product of Friedel-Crafts reaction of **III-1** and 2-chloro-2-methylbutane in DCE with anhydrous aluminum chloride as the catalyst.⁷⁴ **III-6** was obtained by Suzuki reaction of **III-3**, 3,5-dimethylphenylboronic acid and Pd(PPh₃)₂Cl₂ in DME in the presence of a solution of K₂CO₃ in water, followed by basic hydrolysis.⁷⁵ The same procedure was used to synthesize **III-7**, starting from 4-nonylphenylboronic acid. The same Suzuki reaction condition was performed to generate **III-9** from **III-8**. Basic hydrolysis of **III-9**, followed by addition of acetic acid afforded **III-12** as a grey precipitate. Treatment of dried **III-12** with TFA, followed by addition of TMOF, gave **III-15** as a yellow solid in a high yield.⁷⁶ **III-16** and **-17** were obtained using the same synthetic route.



Scheme 3-1 Synthetic route for preparation of pyrrole-2-carbaldehyde derivatives.

The important starting material **III-18** for the ring fused bisdipyrrins was synthesized based on a previously reported procedure.⁷⁷ Hydrogenation of **III-18** in the presence of palladium on activated carbon as the catalyst,⁴⁶ followed by treatment with pyrrole-2-carbaldehyde derivatives **III-1** and **-2**, **III-6** and **-7**, **III-15-17** and HBr formed ligands **III-20** through **III-26** as their HBr salts. Combination of ligands **III-20** through **III-26** with $\text{Zn}(\text{OAc})_2 \cdot 2\text{H}_2\text{O}$ and NaOAc generates the bisdipyrrin Zn^{II} complexes **III-27**, **III-29**, **III-31-34** and **III-36**. Non-polar fractions were collected from flash chromatography on silica gel eluting with CH_2Cl_2 , followed by elution through a gel permeation chromatography (GPC) column with toluene to afford two separated dark green fractions for both **III-34** and **III-36**, one dark green fraction for **III-33**, and only one dark blue fraction for the others except for **III-27**. Compound **III-27** could not be purified by a GPC column due to very poor solubility in toluene. MALDI-TOF mass spectrometry of **III-34** and **III-36** both show the formation of a tetranuclear $[2 \times 2]$ Zn^{II} grid and a hexameric Zn^{II} hexagon, but only the peak for $[2 \times 2]$ Zn^{II} grid was obtained for the remaining compounds. Furthermore, treatment of ligand **III-20**, **III-21** and **III-25** with either $\text{Co}(\text{OAc})_2 \cdot 4\text{H}_2\text{O}$ or $\text{Ni}(\text{OAc})_2 \cdot 4\text{H}_2\text{O}$ and NaOAc forms only tetranuclear $[2 \times 2]$ metal grids (Scheme 3-2).



Scheme 3-2 Synthetic route for preparation of [2×2] metal grids and/or hexagons.

Ligand **III-20** with no substituents on the terminal pyrrole rings was insoluble in most common solvents (CH_2Cl_2 , CHCl_3 , MeOH, toluene and DMSO) or a solvent mixture due to its large flat structure. Therefore, an alkyl or phenyl group was introduced to the β'' - or β' -position of the terminal pyrrole rings of ligands **III-21** and **-22** which rendered them readily soluble in mixed solvent systems ($\text{CH}_2\text{Cl}_2/\text{MeOH}$ or $\text{CHCl}_3/\text{MeOH}$). The solubility of ligands **III-23** through **III-26** increased dramatically (in CHCl_3), when the phenyl ring with a long chain was attached to the β' -position or the phenyl ring was attached to the α' -position of the terminal pyrrole rings.

To a dark purple suspension of ligand **III-20** in $\text{CHCl}_3/\text{MeOH}$ (2/1) was added $\text{Zn}(\text{OAc})_2 \cdot 2\text{H}_2\text{O}$ and NaOAc. The suspension rapidly changed to a fluorescent blue solution. The $[2 \times 2]$ Zn^{II} grid **III-27-4** was obtained in a moderate yield (~20%) after collection from flash chromatography on silica gel eluting with chloroform. Complex **III-27-4** is very soluble in chloroform. No further purification (GPC) could be conducted due to its poor solubility in toluene. By contrast, the $[2 \times 2]$ metal grids based on ligands **III-21-26** are all soluble in toluene, which allows further purification using a GPC column. The yields of $[2 \times 2]$ Zn^{II} grids based on ligands **III-25** and **III-26** are much lower (9-10%) than that of **III-27-4** due to the inter-ligand crowding caused by the phenyl groups at the α' -position of the terminal pyrrole rings. Moreover, the much bulkier 3,5-dimethylphenyl groups in ligand **III-24** make the yield even lower (7%). The substituents at the β'' - or β' -position of the terminal pyrrole rings show very little effect on the yields of the corresponding $[2 \times 2]$ metal grids.

3.2.1.2 ^1H NMR Spectra of Ring Fused Bisdipyrrin Zn^{II} Complexes

The ^1H NMR spectra of $[2 \times 2]$ Zn^{II} grid **III-33-4** dissolved in CDCl_3 showed the two NH signals, previously at δ 14.27 and 12.52 for **III-24**, were no longer present, which supports the formation of the Zn^{II} grid. Experiments indicated that coordination of **III-24** with Zn^{II} ions to form **III-33-4** resulted in upfield shifts for all ^1H signals. The *meso*-H and *para*-H signals shift about 0.5 ppm while the *ortho*-H signals, remarkably, shift upfield about 1 ppm due to strong anisotropic effects (Figure 3-3). The $\alpha\text{-CH}_2$ signals, as expected, shift dramatically (~ 1.3 ppm) owing to the same anisotropic effects (Figure 3-4). X-ray analysis of **III-33-4** demonstrates both the $\alpha\text{-CH}_2$ group and *ortho*-H in one dipyrrole unit are located either above or below the mean plane of the other dipyrrole unit in one coordination center leading to strong anisotropic effects, which may explain the dramatic upfield-shifting observed.

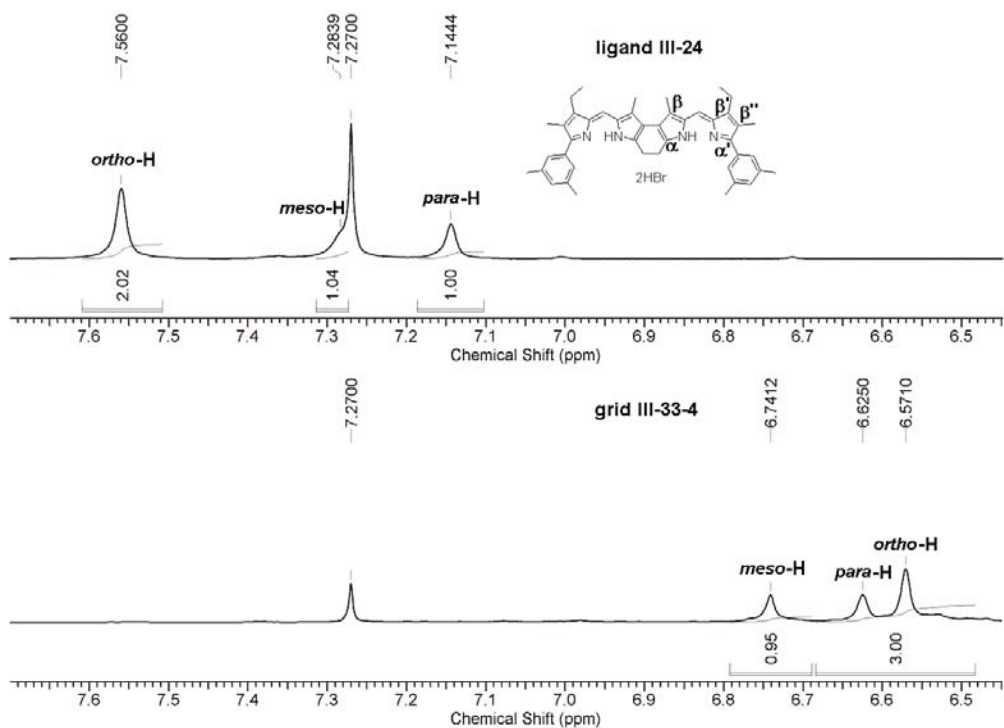


Figure 3-3 ^1H NMR spectra (aromatic region) of ligand **III-24** (top) and Zn^{II} grid **III-33-4** (bottom) in CDCl_3 (400 MHz)

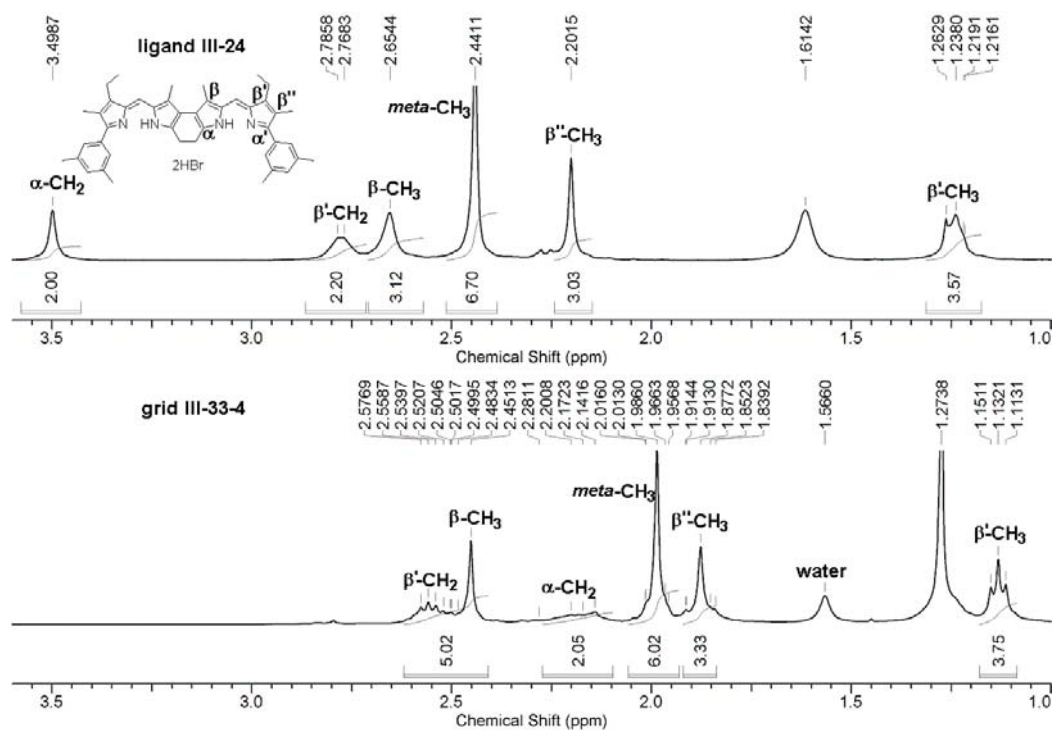


Figure 3-4 ^1H NMR spectra (alkyl region) of ligand **III-24** (top) and Zn^{II} grid **III-33-4** (bottom) in CDCl_3 (400 MHz).

The ^1H NMR spectra of $[2 \times 2]$ Zn^{II} grid **III-36-4** and Zn^{II} hexagon **III-36-6** dissolved in CDCl_3 , like that of **III-33-4**, indicated that the two NH signals, previously at δ 14.25 and 12.61 for **III-26**, were no longer present, which indicates the generation of the Zn^{II} grid and hexagon. Experiments showed that coordination of **III-26** with Zn^{II} ions to form **III-36-4** and **III-36-6** led to upfield shifts for all ^1H signals. The *meso*-H and *meta*-H signals in **III-36-4** shift upfield 0.51 ppm and 0.61 ppm, respectively. However, in **III-36-6**, both signals showed even further upfield shifts (0.53 ppm and 0.65 ppm, respectively), compared to those in **III-36-4**. By contrast, the *ortho*-H signal shifts the opposite way. The signal in **III-36-6** showed a little smaller upfield shift than that in **III-36-4** (0.97 ppm to 1.04 ppm). Theoretically, the *ortho*-H in one dipyrin unit in **III-36-4** should lie right above or below the center of the mean plane of another dipyrin unit from the same coordination center due to the two orthogonal dipyrin planes, while that in **III-36-6** slides away from the center slightly owing to the dihedral angle (60°) between the two mean planes of the dipyrin units in one coordination site. Therefore, the former was thought to suffer much stronger anisotropic effects than the latter, which may be a suitable explanation for the uncommon upfield shift observed (Figure 3-5). The opposite phenomena occur for the $\alpha\text{-CH}_2$ and $\beta\text{-CH}_3$ signals, both of which in **III-36-6** displayed a slightly larger upfield shift than those in **III-36-4** (1.50 and 0.34 ppm for **III-36-6**, 1.33 and 0.17 ppm for **III-36-4**, respectively) (Figure 3-6).

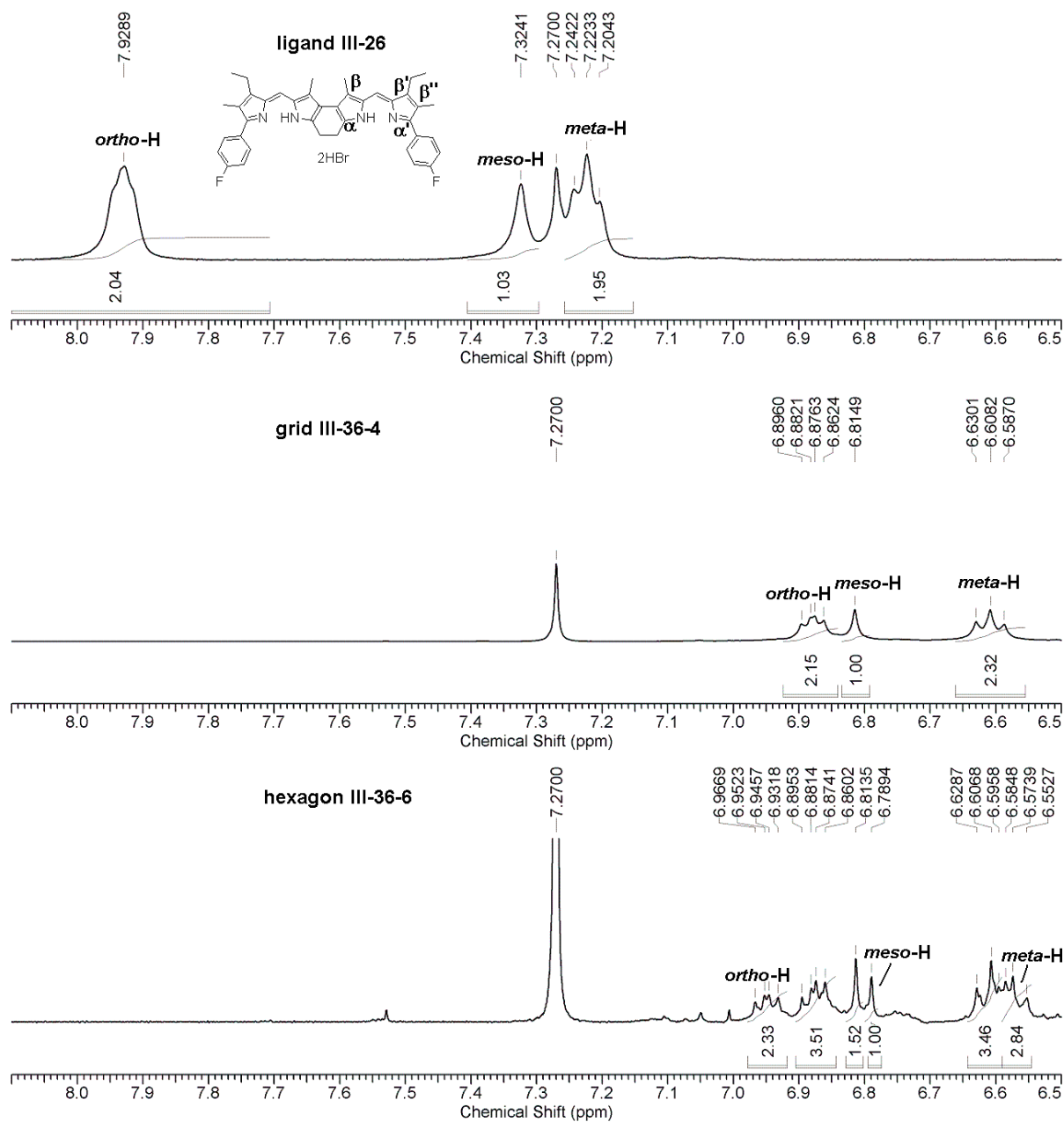


Figure 3-5 ^1H NMR spectra (aromatic region) of ligand **III-26** (top), Zn^{II} grid **III-36-4** (middle) and Zn^{II} hexagon **III-36-6** (bottom) in CDCl_3 (400 MHz).

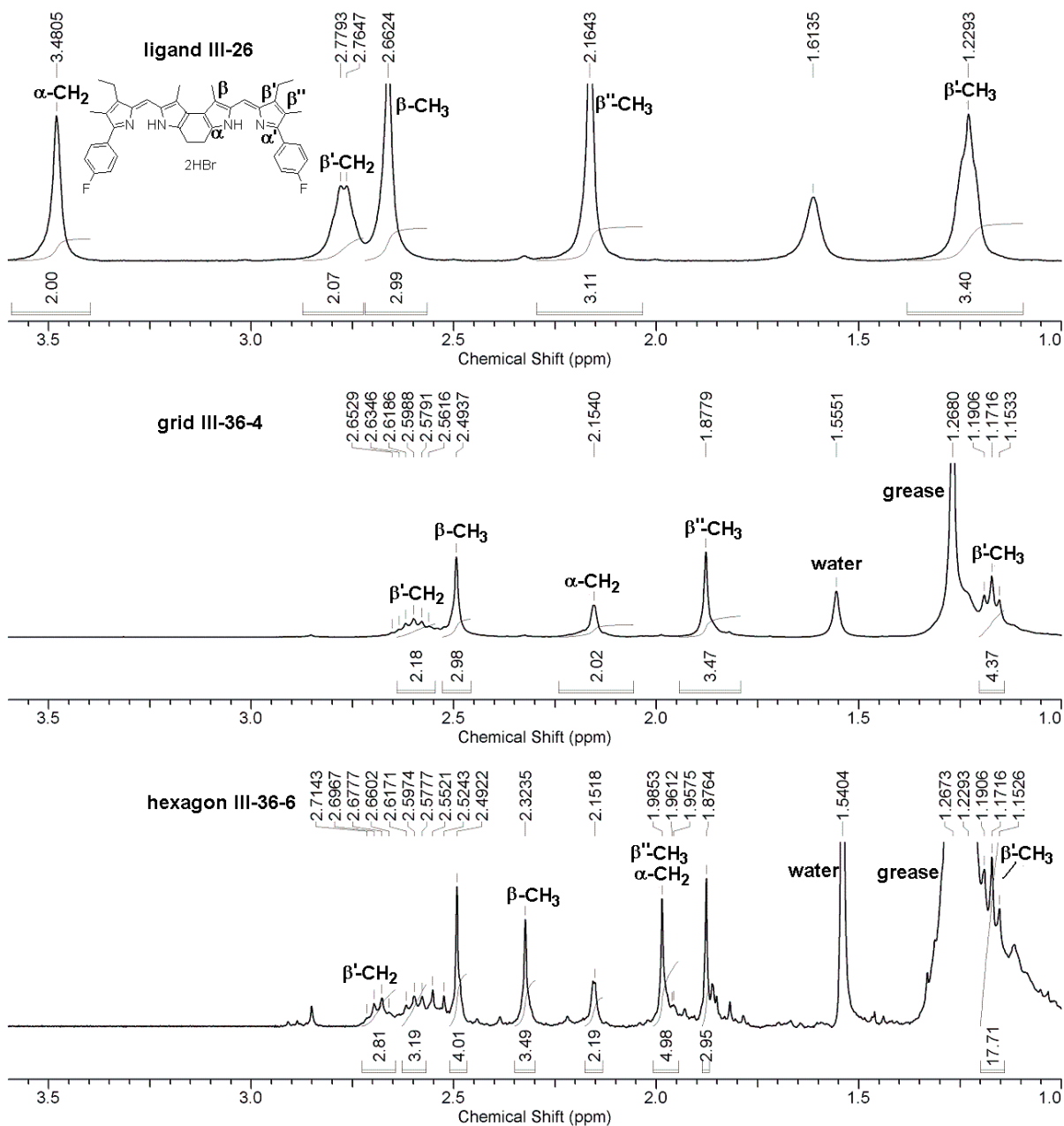


Figure 3-6 ^1H NMR spectra (alkyl region) of ligand **III-26** (top), Zn^{II} grid **III-36-4** (middle) and Zn^{II} hexagon **III-36-6** (bottom) in CDCl_3 (400 MHz).

Surprisingly, the ^1H NMR spectrum of freshly prepared Zn^{II} hexagon **III-36-6** in CDCl_3 , unlike that of **III-34-6** (no fluoride substituent), showed two full sets of signals which can be assigned to grid **III-36-4** and hexagon **III-36-6**. There appears to be an equilibrium between the tetrameric grid and hexameric hexagon (Figure 3-7), though no such equilibrium occurred in the ^1H NMR spectrum of $[2 \times 2]$ Zn^{II} grid **III-36-4** in CDCl_3 .

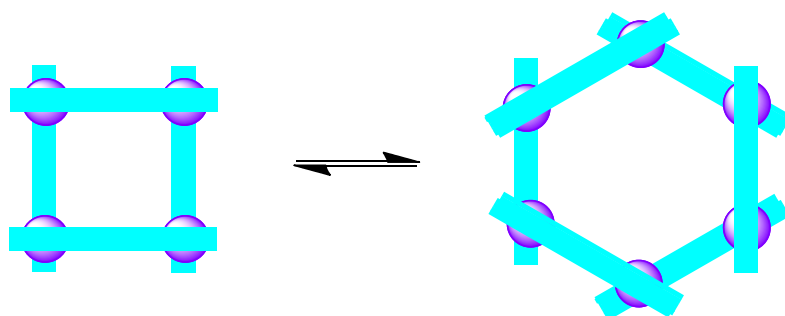


Figure 3-7 Equilibrium between $[2 \times 2]$ Zn^{II} grid **III-36-4** and Zn^{II} hexagon **III-36-6** in CDCl_3 .

3.2.1.3 X-Ray Analysis of Ring Fused Bisdipyrrin Zn^{II} Complexes

3.2.1.3.1 X-Ray Analysis of Ring Fused Bisdipyrrin $[2 \times 2]$ Zn^{II} Grids

A single crystal of **III-27-4** was grown from slow diffusion of hexane into a CHCl_3 solution and the structure was investigated by X-ray diffraction analysis (Figure 3-8). Complex **III-27-4** is indeed a slightly distorted square-like grid consisting of four Zn^{II} ions and four ligand **III-20** components. Ligand **III-20** units are aligned alternately above and below the mean plane through the four Zn^{II} ions.²⁸ The square-shaped **III-27-4** also results from the absence of the substituents at the α' -position of ligand **III-20**. The distances between two adjacent Zn^{II} ions in

one molecule are 8.24, 8.18, 8.37 and 8.22 Å. The distances between two diagonal Zn^{II} ions in one molecule are 11.47 and 11.73 Å. The Zn-N bond lengths range from 1.96-2.01 Å which are close to those in Zn^{II} double helicates.⁴⁶ The dihedral angles between the mean planes of two dipyrrens coordinated to the same Zn^{II} ion are 87.8, 85.3, 85.1 and 87.5°, which indicates each metal center has a slightly distorted tetrahedral geometry owing to the sufficient flexibility of the cyclohexadiene ring. This flexibility allows each ligand to adjust to the stereochemical requirements of the Zn₄ unit and causes each metal center to only slightly deviate from perfect tetrahedral coordination geometry. The dihedral angles between the planes of two dipyrrens within each ligand are 10.1, 27.5, 20.8 and 24.0° due to the same aforementioned reason. The three-dimensional packing structure of **III-27-4** exhibits no tunnel-like structure due to the partial overlap of the individual molecules (Figure 3-9).

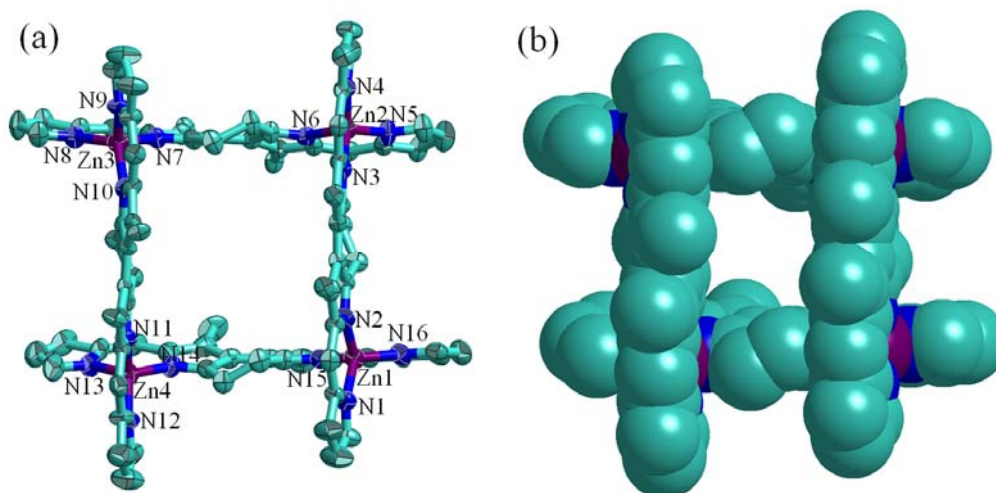


Figure 3-8 Crystal structure of [2×2] Zn^{II} grid **III-27-4**: (a) ORTEP diagram (thermal ellipsoids are scaled to the 50% probability level) and (b) space-filled representation.

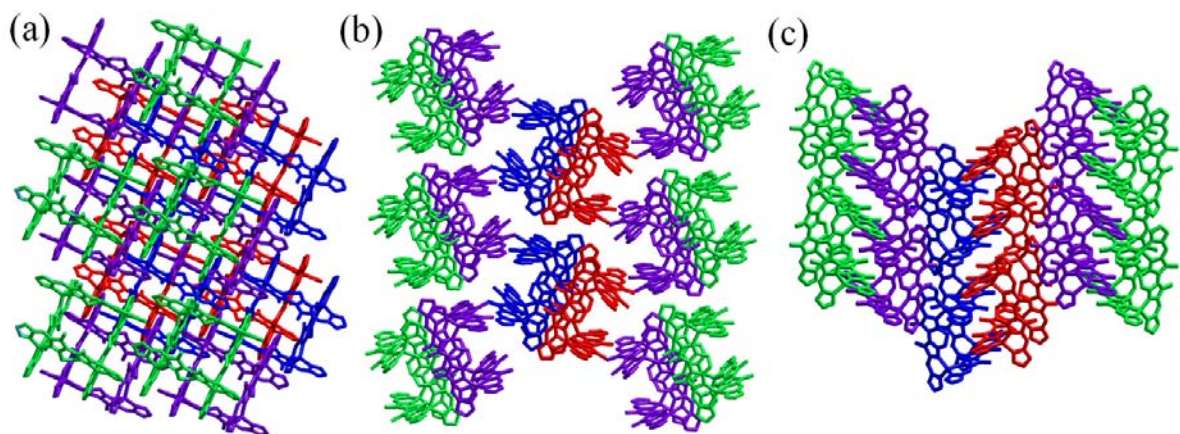


Figure 3-9 Stick-packing of $[2 \times 2]$ Zn^{II} grid **III-27-4**: (a) top view; (b) and (c) side views.

A single crystal of $[2 \times 2]$ Zn^{II} grid **III-33-4** was grown from slow diffusion of hexane into a CHCl_3 solution and the structure was determined by X-ray diffraction analysis (Figure 3-10). Complex **III-33-4** crystallizes with one half-molecule related to another by rotation about a two-fold axis. Unlike **III-27-4**, complex **III-33-4** is not a square but is instead a rhombus. The distance between two adjacent Zn^{II} ions in one molecule is 8.24 Å. The distances between two diagonal Zn^{II} ions in one molecule are 9.19 and 13.80 Å. The Zn-N bond lengths lie in the range of 1.98-2.00 Å which are close to those in **III-27-4**. The dihedral angles between the mean planes of two dipyrrens coordinated to the same Zn^{II} ion are 68.6 and 71.1°, which indicates each metal center has a much more distorted tetrahedral geometry than that in **III-27-4**. It was thought that the interligand crowding caused by the bulky 3,5-dimethylphenyl groups at the α' -position of ligand **III-24** would push the two dipyrren planes away from each other at the corner with Zn1, and consequently push them towards each other at the adjacent corner with Zn2 owing to the same interligand crowding between the two parallel ligands. As a result,

complex **III-33-4** forms a rhombus, which may also be supported by the strong π - π stacking interaction between the phenyl ring in one ligand and the dipyrin plane in another at each corner (distance = ~ 3.5 Å).^{38, 78, 79} The dihedral angles between the phenyl rings and the dipyrin planes attached to them at the corner with Zn2 are much smaller than those at the corner with Zn1 (46.7 and 56.8° for the former, 55.8 and 61.3° for the latter), which result from the larger steric hindrance at the former to force the two phenyl rings to rotate away from each other. The dihedral angles between the mean planes of two dipyrins in each ligand are 9.2, 15.0, 8.5 and 14.3° due to the slight flexibility of the cyclohexadiene ring. The three-dimensional packing structure of **III-33-4**, unlike **III-27-4**, displays a single rhombus-like tunnel (10.5 and 6.0 Å in diameter), resulting from the complete overlap of the individual molecules in the crystal. The complete overlap of the individual molecules may be driven by the strong π - π stacking interactions between the phenyl rings from the adjacent molecules (distance = ~ 3.5 Å) and by the highly-ordered arrangement of the hexane molecules co-crystallized in the lattice (Figure 3-11).

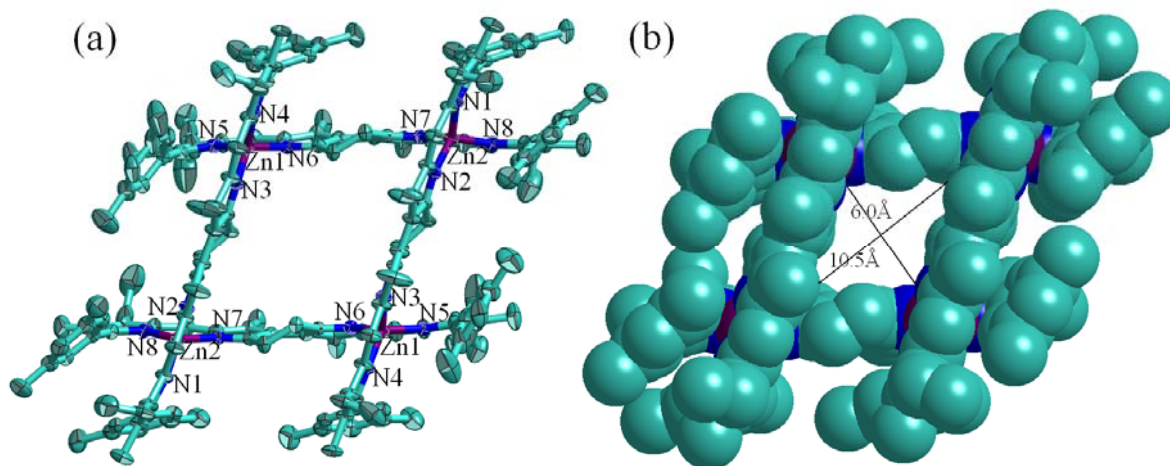


Figure 3-10 Crystal structure of [2x2] Zn^{II} grid **III-33-4**: (a) ORTEP diagram (thermal ellipsoids are scaled to the 50% probability level) and (b) space-filled representation.

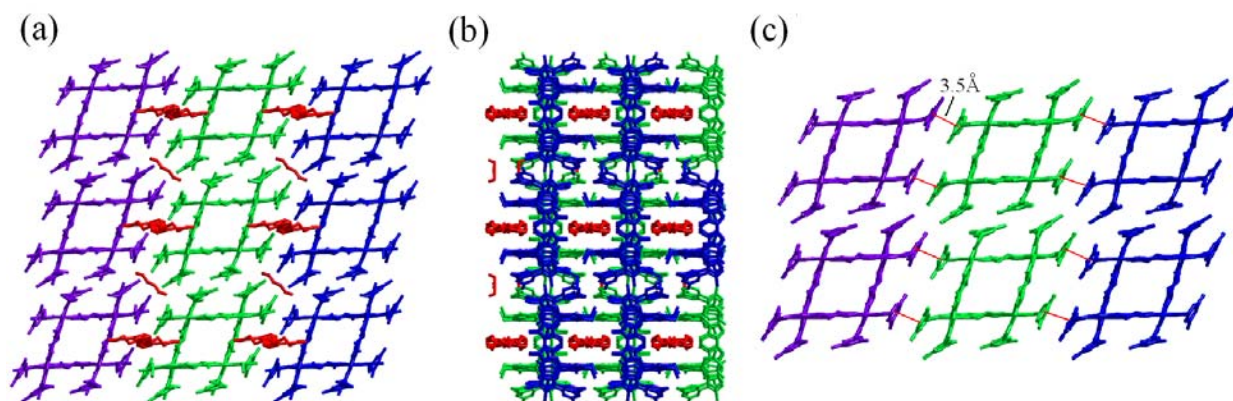


Figure 3-11 Stick-packing of $[2 \times 2]$ Zn^{II} grid **III-33-4**: (a) top view; (b) side view (with hexane molecules in red) and (c) π - π stacking interactions between the phenyl rings (distance = ~ 3.5 Å).

3.2.1.3.2 X-Ray Analysis of Ring Fused Bisdipyrrin Zn^{II} Hexagon

A single crystal of Zn^{II} hexagon **III-36-6** was obtained from slow diffusion of hexane into a chloroform solution of **III-36-6** and the structure was confirmed by X-ray diffraction analysis (Figure 3-12). Complex **III-36-6** is a true hexagon with an S_6 axis perpendicular to the mean plane through the six Zn^{II} ions. The ligand units are divided into two sets, one of which lies above and the other below the mean plane through the six Zn^{II} ions. The distance between two adjacent Zn^{II} ions in one molecule is 8.16 Å. The distance between two diagonal Zn^{II} ions in one molecule is 16.10 Å. The Zn-N bond lengths range from 1.97-1.99 Å which are close to those in **III-33-4**. The dihedral angle between the mean planes of two dipyrins coordinated to the same Zn^{II} ion is about 73.7° which is much larger than those in **III-33-4**. This also indicates each metal center has a distorted tetrahedral geometry. The dihedral angle between the mean planes of two dipyrins in each ligand is ca. 19.3° . The complete overlap of the individual molecules in

the crystal leads to a single hexagonal channel (12.8 Å in diameter) in the three-dimensional packing structure of **III-36-6**. Strong F-F interactions between the neighbouring *p*-fluorophenyl groups of the adjacent molecules are observed with an F-F distance of ca. 3.5 Å, which may play a significant role in the generation of the channel in the solid state.^{80, 81} Each hexagon captures six chloroform molecules, which are located alternately above and below the mean plane through the six Zn^{II} ions to provide an overall arrangement with three above and three below (Figure 3-13).

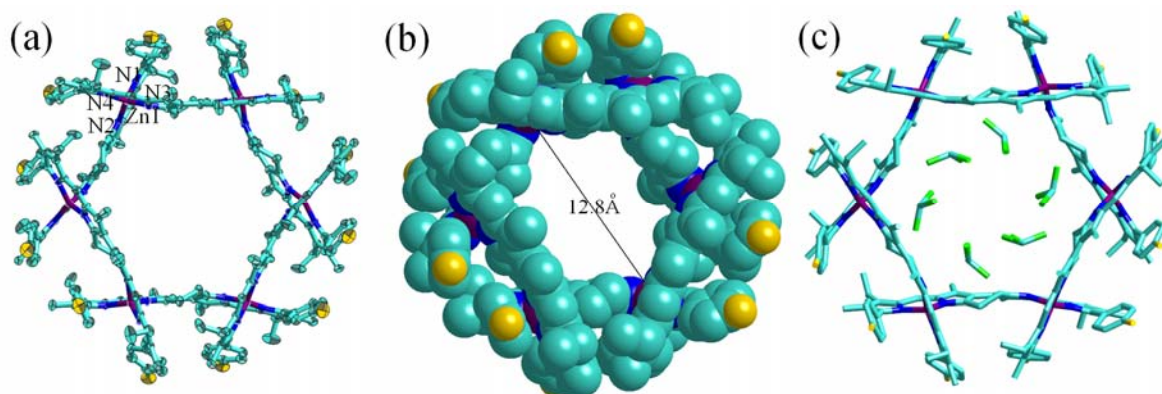


Figure 3-12 Crystal structure of Zn^{II} hexagon **III-36-6**: (a) ORTEP diagram (thermal ellipsoids are scaled to the 50% probability level); (b) space-filled representation and (c) stick representation with CHCl₃ molecules.

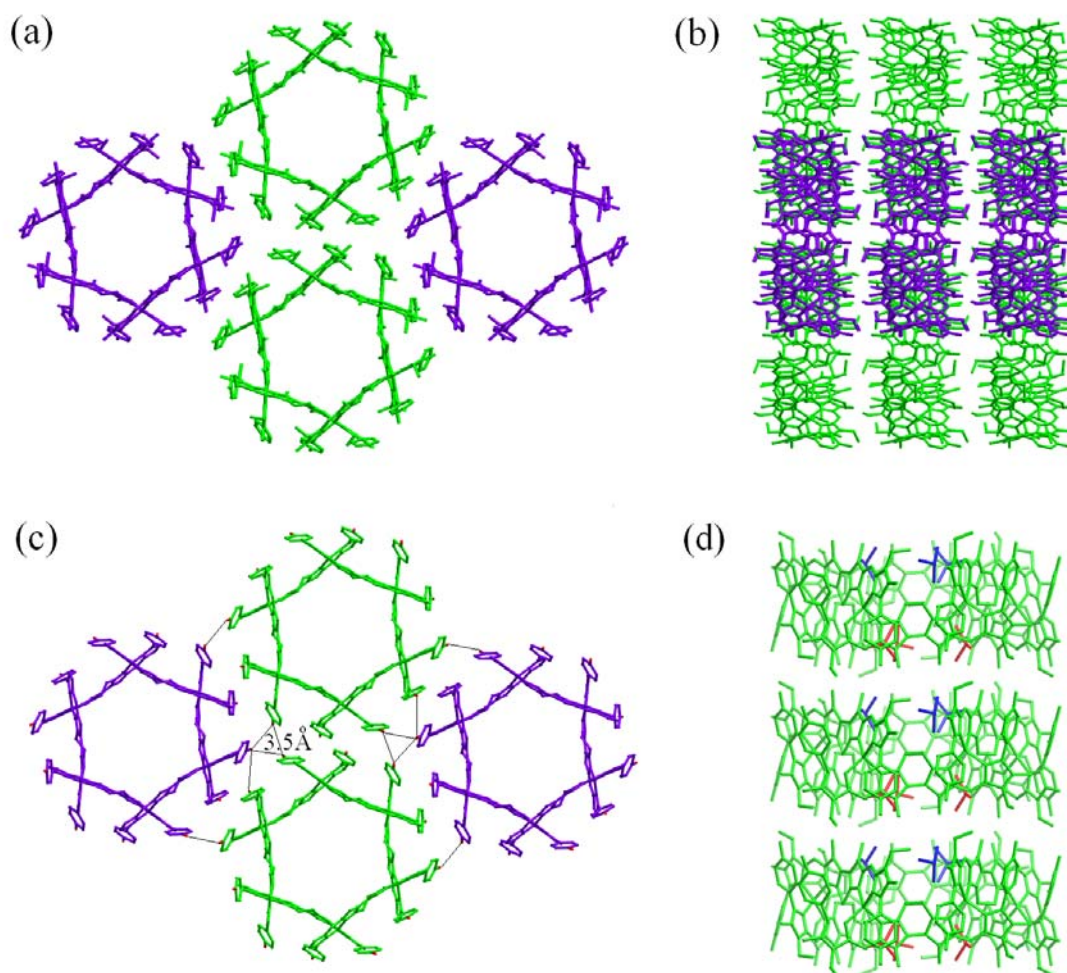


Figure 3-13 Stick packing of Zn^{II} hexagon **III-36-6**: (a) top view; (b) side view; (c) F-F interactions between neighbouring *p*-fluorophenyl groups of the adjacent molecules (alkyl groups omitted for clarity) and (d) side view (with CHCl_3 molecules in red/blue).

3.2.1.4 Electronic Absorption Spectra of Ring Fused Bisdipyrrin Metal Complexes

The ring fused bisdipyrrin metal grids and Zn^{II} hexagons are all green solids upon crystallization, but **III-27-4**, **III-29-4**, **III-31-4**, **III-32-4** and **III-35-4** form dark blue solutions when dissolved in CHCl_3 with the rest generating dark green solutions. Complex **III-27-4** through **III-36-6** were analyzed by electronic absorption spectroscopy (Figure 3-14).

Surprisingly, the absorption spectra of all complexes in chloroform show two intense bands which may receive contributions from both spin-allowed ligand-centered (LC) transitions ($\pi\text{-}\pi^*$) and metal-to-ligand charge transfer (MLCT) transitions (Table 3-1). The two bands display an almost identical $\log\epsilon$ value, but one is at longer wavelength and the other at shorter wavelength than the ligand's main absorption. It is difficult to pair the band with its corresponding transition type at this stage, but the LC transition is probably responsible for the first band while the second band may be attributed to the MLCT transition. An ascending trend of λ_{max} can be observed in the [2×2] Zn^{II} grids (**III-27-4** through **III-33-4**), which may be caused by substituent effects through the replacement of protons with an *i*-pentyl group or various aromatic rings. A large bathochromic shift (~ 19 nm) occurs with phenyl groups on the β' -position of the ligands (**III-31-4** and **III-32-4**) instead of a proton (**III-27-4**) owing to the larger π -conjugated systems extended through the aromatic rings.⁷² Remarkably, a much larger bathochromic shift (~ 44 to 50 nm) was observed when the phenyl groups were attached to the α' -position of the ligands (**III-33-4**, **III-34-4** and **III-36-4**), which may be further explained by the strong π - π interactions between the phenyl ring and the mean plane of the dipyrin in each coordination center. The wavelengths of metal-to-ligand charge transfer bands for the metal grids and hexagons are marginally-shifted (0 to 2 nm) in **III-34** and **III-36** owing to the similar conformation of each coordination center and minimum overlap between the two adjacent π -systems (coordination centers) in the Zn^{II} grids and hexagons.⁸²

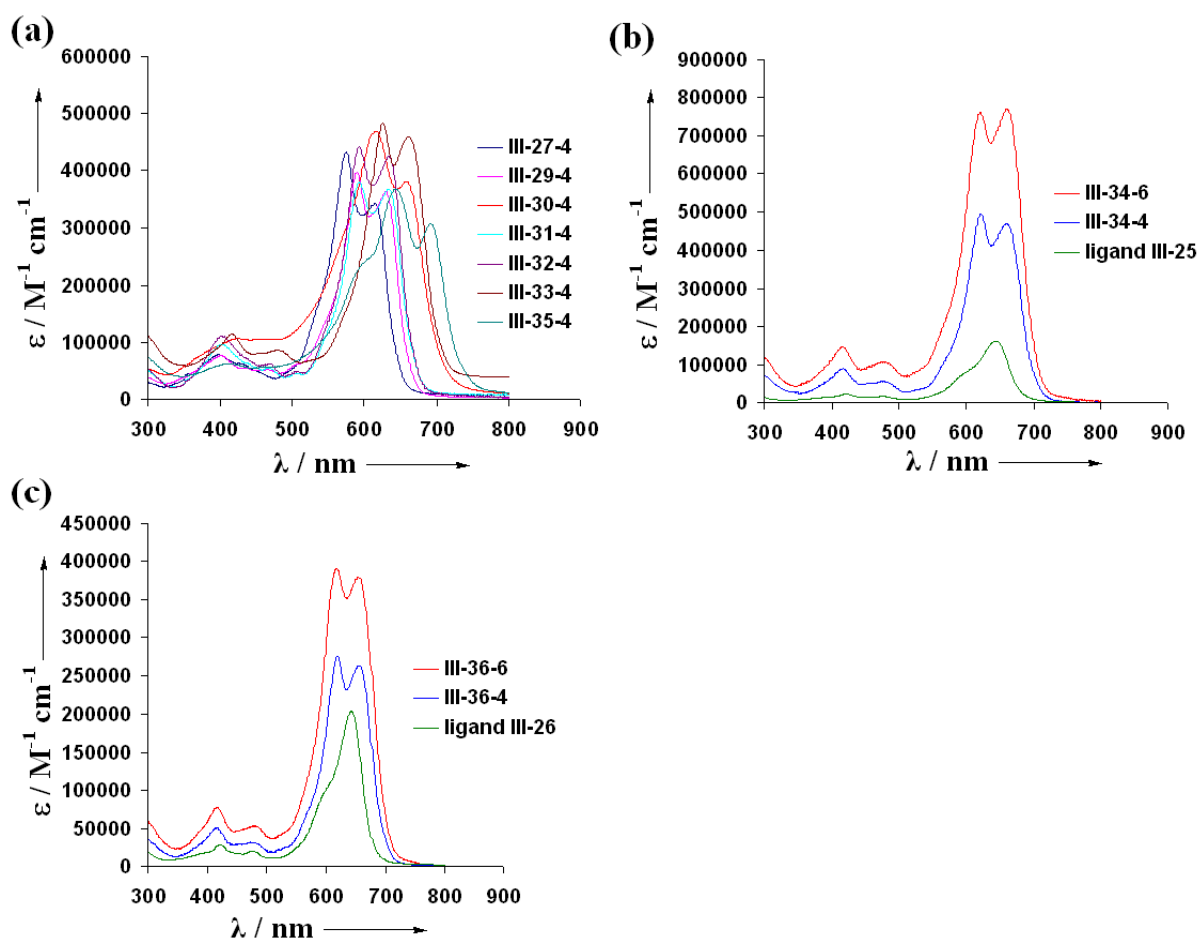


Figure 3-14 Electronic absorption spectra of cyclohexane bisdipyrrin metal complexes in chloroform: (a) III-27-4, III-29-4 through III-33-4 and III-35-4; (b) III-34 and (c) III-36.

Table 3-1 Spin-allowed ligand-centered transition band $\lambda_{\max 1}$ (nm) and metal-to-ligand charge transfer transition band $\lambda_{\max 2}$ (nm) for the metal grids and/or hexagons in chloroform.

Compound	$\lambda_{\max 1}/\log \epsilon_1$	$\lambda_{\max 2}/\log \epsilon_2$	Compound	$\lambda_{\max 1}/\log \epsilon_1$	$\lambda_{\max 2}/\log \epsilon_2$
III-24	647/5.24	—	III-32-4	594/5.64	632/5.63
III-25	644/5.21	—	III-33-4	625/5.68	661/5.66
III-26	644/5.31	—	III-34-4	623/5.69	659/5.67
III-27-4	575/5.63	613/5.53	III-34-6	622/5.88	659/5.89
III-29-4	590/5.60	629/5.56	III-35-4	643/5.56	692/5.49
III-30-4	615/5.67	658/5.58	III-36-4	620/5.44	657/5.42
III-31-4	593/5.58	632/5.56	III-36-6	618/5.59	655/5.58

3.3 Conclusions

The ring fused bisdipyrrin ligands are readily obtainable, and react with different metal ions (Zn^{II} , Co^{II} and Ni^{II}) to generate metal grids and/or hexagons. The metal grid is the only product when α' -free ring fused bisdipyrrin ligands are used while both the hexagon and the grid are formed when α' -phenyl bisdipyrrin ligands are introduced. The electronic absorption spectra of the metal grids and hexagons both exhibit two intense bands, one of which is attributed to spin-allowed ligand-centered transitions (small λ_{max}) and the other from metal-to-ligand charge transfer transitions (large λ_{max}). Structures of two of the $[2 \times 2]$ Zn^{II} grids are confirmed by X-ray analysis, one of which is shaped as a square (**III-27-4**) and the other as a rhombus (**III-33-4**). Furthermore, one solid-state structure of a Zn^{II} hexagon was revealed by X-ray analysis (**III-36-6**). The three-dimensional packing of the crystal structures of both **III-33-4** and **III-36-6** showed the complete overlap of individual molecules to achieve tunnel-like structures with different shapes and sizes. The hexagonal tunnel with a diameter of 12.8 Å in **III-36-6** renders it a potential candidate for gas storage and separation.⁵²⁻⁵⁴ In general, the metal grids solved the isomer issue which proved to be a hurdle in the purification of the tetrameric circular helicates in chapter 2, and further allowed successful crystal growth to reveal the structures for characterization.

Chapter Four
Heteroleptic Racks and Ladders

4.1 Design Strategy

meso-Unsubstituted bisdipyrrin salts through condensation have been widely investigated as the ligands for generation of metal complexes featuring double-^{45, 46} or triple-⁴⁷ helical structures. *meso*-Aryl dipyrrins, which are stable in their free-base form, are usually synthesized through oxidation of dipyrromethanes.⁷³ However, each type of the aforementioned ligands were previously treated with various metal ions to generate only homoleptic metal complexes.⁸³ No heteroleptic metal complexes based on two distinct dipyrrin ligands have been reported thus far. Inspired by the work of Lehn and Schmittl on rack-type⁴¹ (Figure 4-1) and ladder-type^{24, 25} (Figure 4-2) complexes using bipyridine/terpyridine ligands, bisdipyrrin metal racks and ladders were successfully pursued.

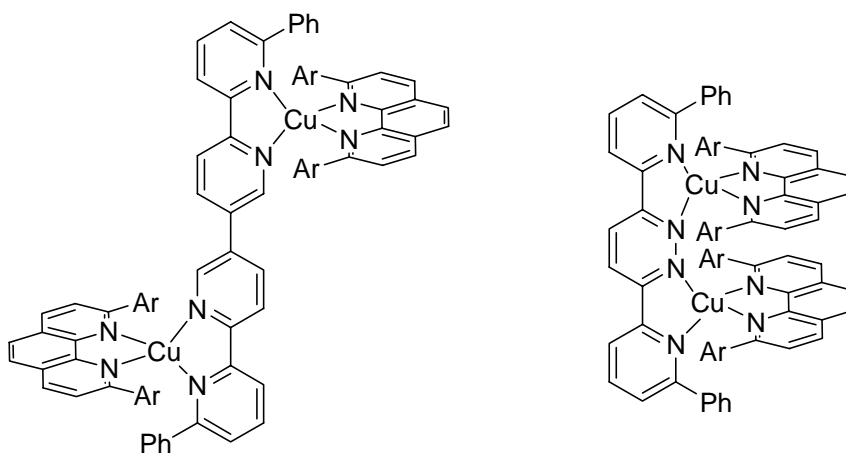


Figure 4-1 Rack-type Cu^I complexes using bipyridine ligands synthesized by Lehn (counterions omitted for clarity).

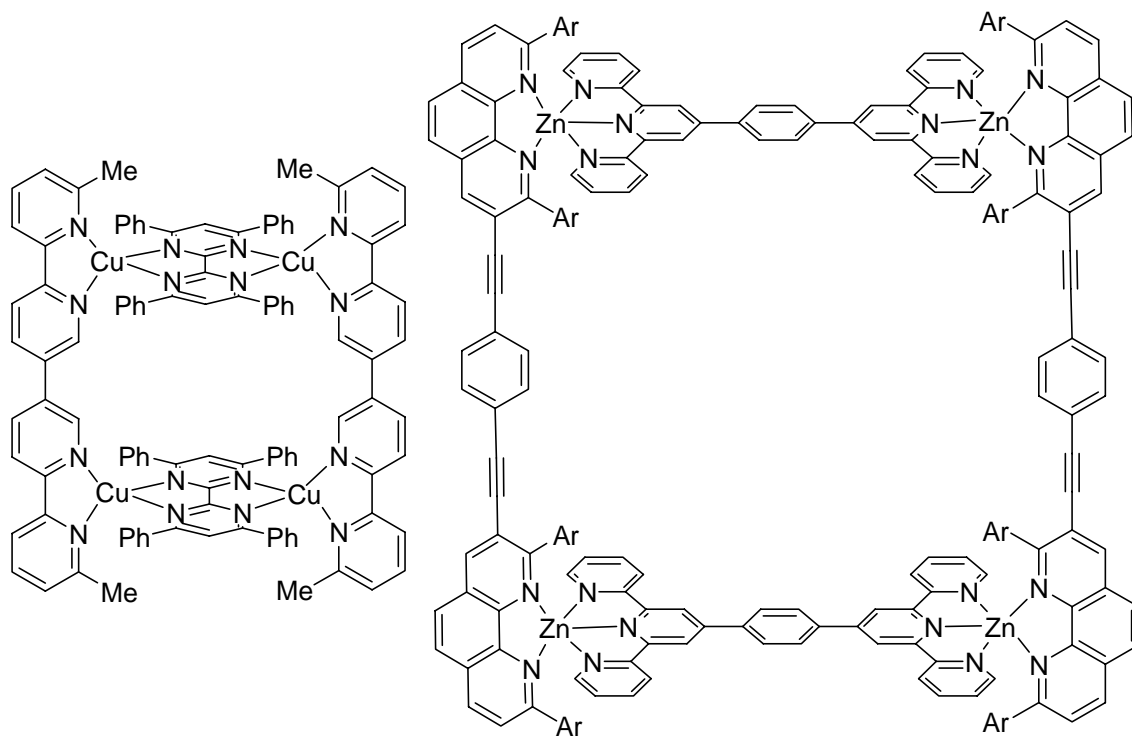


Figure 4-2 Ladder-type Cu^I and Zn^{II} complexes using bipyridine/terpyridine ligands reported by Lehn and Schmittel (counterions omitted for clarity).

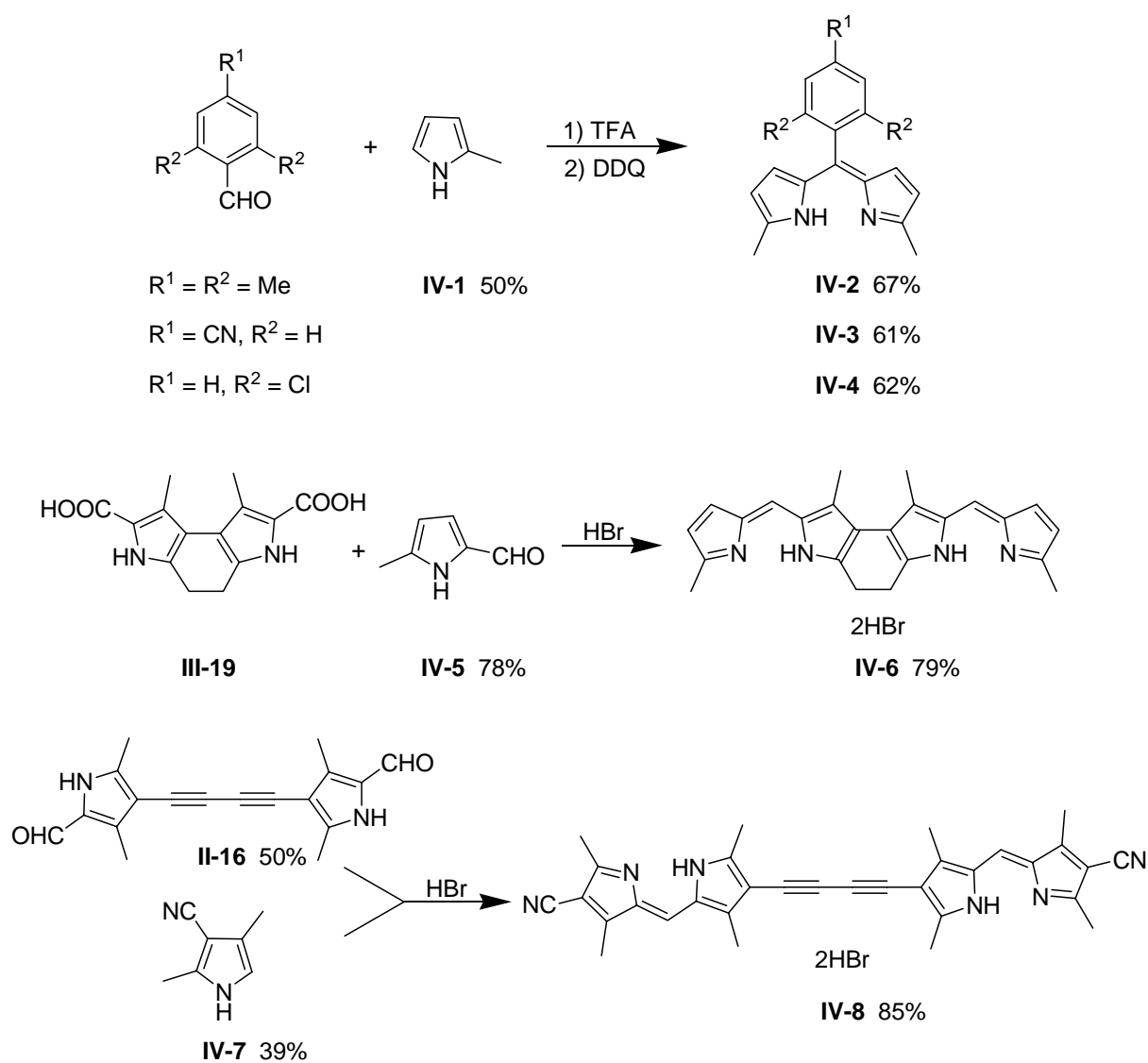
4.2 Results and Discussion

4.2.1 Rack-Type Metal Complexes

The rigid diacetylene bisdipyrrens in Chapter II and the ring fused bisdipyrrens in Chapter III, together with *meso*-aryl dipyrrens and metal ions of tetrahedral geometry such as Zn^{II} and Co^{II}, were selected for preparation of the rack-type metal complexes. It is expected that in the resulting crystal structures, the metal ions are consecutively located on opposite sides of the rigid diacetylene bisdipyrren backbone due to the two dipyrren units being anti-parallel to one other. In contrast, the metal ions are aligned on the same side of the ring fused bisdipyrren backbone owing to the parallel conformation of the two dipyrren units.

4.2.1.1 Synthesis of Rack-Type Metal Complexes

The preparation of rack-type metal complexes began with the synthesis of several *meso*-aryl dipyrrens: **IV-2** through **IV-4** (Scheme 4-1). **IV-3** was synthesized based on a previously reported procedure,⁸⁴ starting with 4-formylbenzotrile and 2-methylpyrrole.⁸⁵ Compounds **IV-2** and **-4** were obtained using the same synthetic route. The ring fused bisdipyrren ligand **IV-6** was generated by combination of **III-19** and **IV-5**⁸⁶ in the presence of HBr. Similarly, dialdehyde **II-16** was condensed with 3-cyano-2,4-dimethylpyrrole **IV-7**⁸⁷ in the presence of HBr to afford the bisdipyrren ligand **IV-8** as the HBr salt.



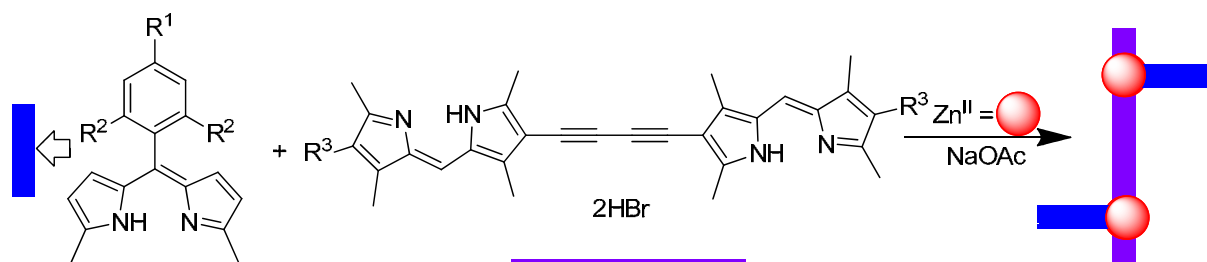
Scheme 4-1 Synthetic route to the ligands for preparation of rack-type metal complexes.

Combination of *meso*-aryl dipyrin **IV-2** and diacetylene bisdipyrin **II-22** with $\text{Zn}(\text{OAc})_2 \cdot 2\text{H}_2\text{O}$ and NaOAc generates a mixture of Zn^{II} complexes **IV-9** (Scheme 4-2). Non-polar fractions were collected from flash chromatography on silica gel eluting with dichloromethane, followed by elution through a gel permeation chromatography (GPC) column with toluene to afford three fractions. The MALDI-TOF mass spectrometry shows that the first fraction **IV-9-1** (red) is the trimeric Zn^{II} complex of **II-22**, the second fraction **IV-9-2** (orange) is

the rack-type Zn^{II} complex and the last fraction (yellow) is the dimeric Zn^{II} complex of **IV-2**. The rack-type Zn^{II} complexes **IV-10-2** and **IV-11-2** were obtained using the same synthetic route and separation procedure. However, the crude complexes **IV-10** and **IV-11** were collected from flash chromatography on silica gel eluting with CH₂Cl₂/MeOH due to the polar cyanide group attached to the diacetylene bisdipyrrin ligand **IV-8**.

Treatment of *meso*-aryl dipyrin **IV-2** and ring fused bisdipyrrin **IV-6** with Zn(OAc)₂•2H₂O and NaOAc forms a mixture of Zn^{II} complexes **IV-12** (Scheme 4-2). Non-polar fractions were collected from flash chromatography on silica gel eluting with dichloromethane, followed by elution through a GPC column with toluene to afford two fractions. The first fraction **IV-12-1** (green) is the parallel rack-type Zn^{II} complex and the second fraction (yellow) is the dimeric Zn^{II} complex of **IV-2** (confirmed by MALDI-TOF). The same procedure was used to afford rack-type Zn^{II} complexes **IV-13-1**, **IV-14-1** and **IV-15-2**. However, an extra fraction (blue) elutes from the GPC column first in the case of **IV-15**, which was confirmed to be the grid-type Zn^{II} complex **IV-15-1**, a side product due to formation of the kinetically-controlled Zn^{II} grid using α' -free bisdipyrrin ligand **III-22**. This also helps to explain why rack **IV-15-2** was obtained in a very low yield (3%). Because no Zn^{II} grids using ligand **IV-6**, which has methyl groups at the α' -positions, were observed in **IV-12** through **IV-14**, perhaps more ligand **IV-6** is available for synthesis of Zn^{II} racks. Unfortunately, racks **IV-12-1** through **IV-14-1** were still obtained in a relatively low yield (4 to 7%), which is probably caused by poor solubility of the ring fused bisdipyrrin ligand **IV-6** in common solvents.

In order to obtain the Zn^{II} rack in a high yield, the ring fused bisdipyrrin ligands should be very soluble in chloroform to make it available to react with the *meso*-aryl dipyrins and Zn^{II} ions, and should also contain very bulky substituents at the α' -position of the terminal pyrrole rings to minimize the possible formation of homoleptic Zn^{II} grids. Therefore, ligand **III-24** was selected as a potential candidate to react with ligand **IV-2**, Zn(OAc)₂•2H₂O and NaOAc to generate a mixture of Zn^{II} complexes **IV-16** (Scheme 4-2). The same separation procedure was used to purify the mixture **IV-16**. Surprisingly, three dark green fractions were collected from the GPC column in addition to the yellow fraction (the same dimeric Zn^{II} complex of **IV-2**). The first dark green fraction **IV-16-1** is the [2A+3B] type Zn^{II} complex (A = ligand **IV-2** and B = ligand **III-24**), the second one **IV-16-2** is the [2A+2B] type Zn^{II} complex and the third one **IV-16-3** is the parallel rack-type Zn^{II} complex, all of which are confirmed by MALDI-TOF mass spectrometry. The introduction of ligand **III-24** into the preparation of rack-type Zn^{II} complexes proved to be very successful due to absence of the unwanted homoleptic Zn^{II} grid and much higher yield (~17%) of rack **IV-16-3**. It seems that the zigzag-type Zn^{II} complexes of ligand **III-24** are favoured species compared to the Zn^{II} grid owing to less steric hindrance in the former than that in the latter, which is caused by the very bulky 3,5-dimethylphenyl groups at the α' -position of the terminal pyrrole rings. The formation of [2A+3B] type Zn^{II} complex **IV-16-1** and [2A+2B] type Zn^{II} complex **IV-16-2** further confirms that zigzag-type intermediates (3B and 2B type Zn^{II} complexes) exist in the reaction mixture. Ligand **IV-2** (A) acts as a stopper to the zigzag-type intermediates and allows the facile separation and further characterization of zigzag-type Zn^{II} complexes **IV-16-1** and **IV-16-2**. However, only rack **IV-17-3** and [2A+2B] type zigzag rack **IV-17-2** were formed when Co^{II} ions were introduced.



R¹ = R² = Me **IV-2**

R³ = Et **II-22**

IV-9-2 10%

R¹ = R² = Me **IV-2**

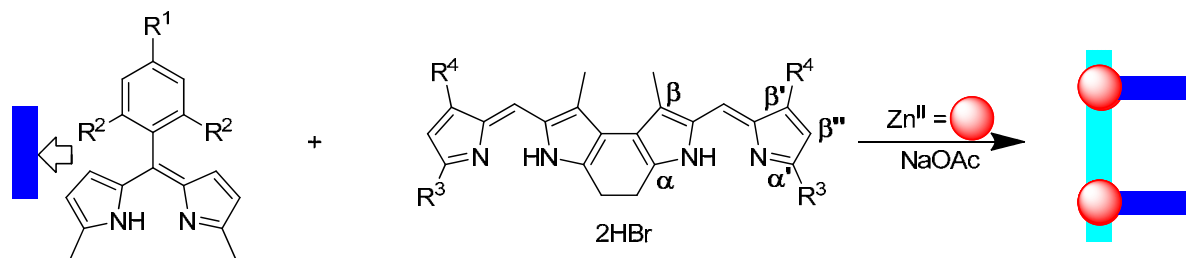
R³ = CN **IV-8**

IV-10-2 8%

R¹ = CN, R² = H **IV-3**

R³ = CN **IV-8**

IV-11-2 5%



R¹ = R² = Me **IV-2**

R³ = Me, R⁴ = H **IV-6**

IV-12-1 4%

R¹ = CN, R² = H **IV-3**

R³ = Me, R⁴ = H **IV-6**

IV-13-1 4%

R¹ = H, R² = Cl **IV-4**

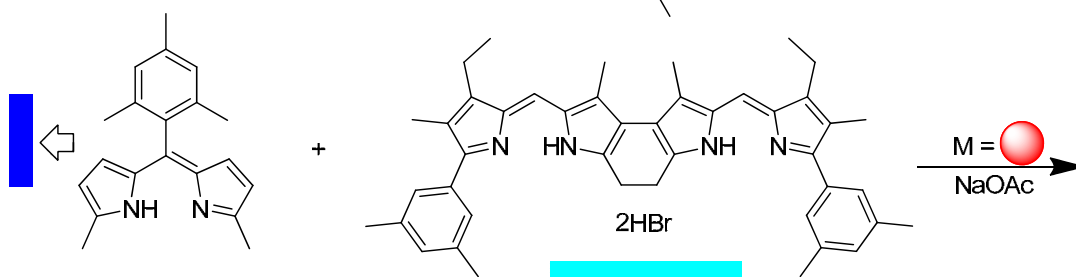
R³ = Me, R⁴ = H **IV-6**

IV-14-1 7%

R¹ = R² = Me **IV-2**

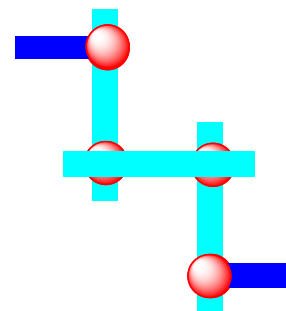
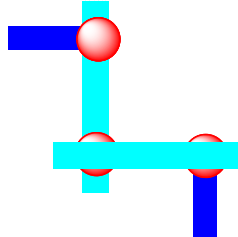
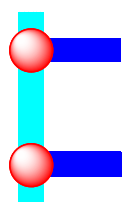
R³ = H, R⁴ =  **III-22**

IV-15-2 3%



IV-2

III-24



M = Zn^{II} **IV-16-3** 17%

IV-16-2 20%

IV-16-1 5%

M = Co^{II} **IV-17-3** 4%

IV-17-2 5%

Scheme 4-2 Synthetic route for preparation of rack-type metal complexes.

4.2.1.2 ^1H NMR Spectra of Zn^{II} Rack-Type and Zigzag Rack-Type Complexes

^1H NMR spectra of Zn^{II} rack **IV-16-3** and zigzag rack **IV-16-2** dissolved in CDCl_3 showed that the two NH signals, previously at δ 14.27 and 12.52 for **III-24**, were no longer present, which supports the generation of the Zn^{II} racks. Experiments determined that coordination of ligand **III-24** and **IV-2** with Zn^{II} ions to form rack or zigzag rack-type complexes led to upfield shifts for all ^1H signals. The *meso*-H and *para*-H signals from ligand **III-24** in **IV-16-3** shift upfield 0.1 ppm and 0.3 ppm, respectively. Remarkably, the *ortho*-H signals from ligand **III-24** in **IV-16-3** showed even further upfield shifts (0.66 ppm) owing to strong anisotropic effects (Figure 4-3). The *meta*-H signals from the mesityl groups in **IV-16-3** split into a doublet instead of the singlet in ligand **IV-2** due to differences in the surrounding chemical environment. However, the β -H signals from the dipyrin in ligand **IV-2** remain unchanged (doublet of doublets). The ^1H signals in zigzag rack **IV-16-2** can be divided into two sets, one of which belongs to the coordination site with Zn^{R} (similar chemical environment in Rack **IV-16-3**) and the other belongs to the coordination site with Zn^{G} (similar chemical environment in Grid **III-33-4**). The *para*-H, *ortho*-H and *meso*-H signals in the coordination site with Zn^{R} are either the same or marginally shifted (0.04 ppm), compared to those in rack **IV-16-3** due to the similar conformation of both coordination sites. Furthermore, the *para*-H, *ortho*-H and *meso*-H signals in the coordination site with Zn^{G} are marginally shifted (0.07 to 0.19 ppm), compared to those in grid **III-33-4** for the same reason. The *meta*-H signals from the mesityl groups in **IV-16-2** remain the same as those in **IV-16-3**. Surprisingly, another set of the β -H signals from the dipyrin in ligand **IV-2** appears while the original set remains nearly unchanged.

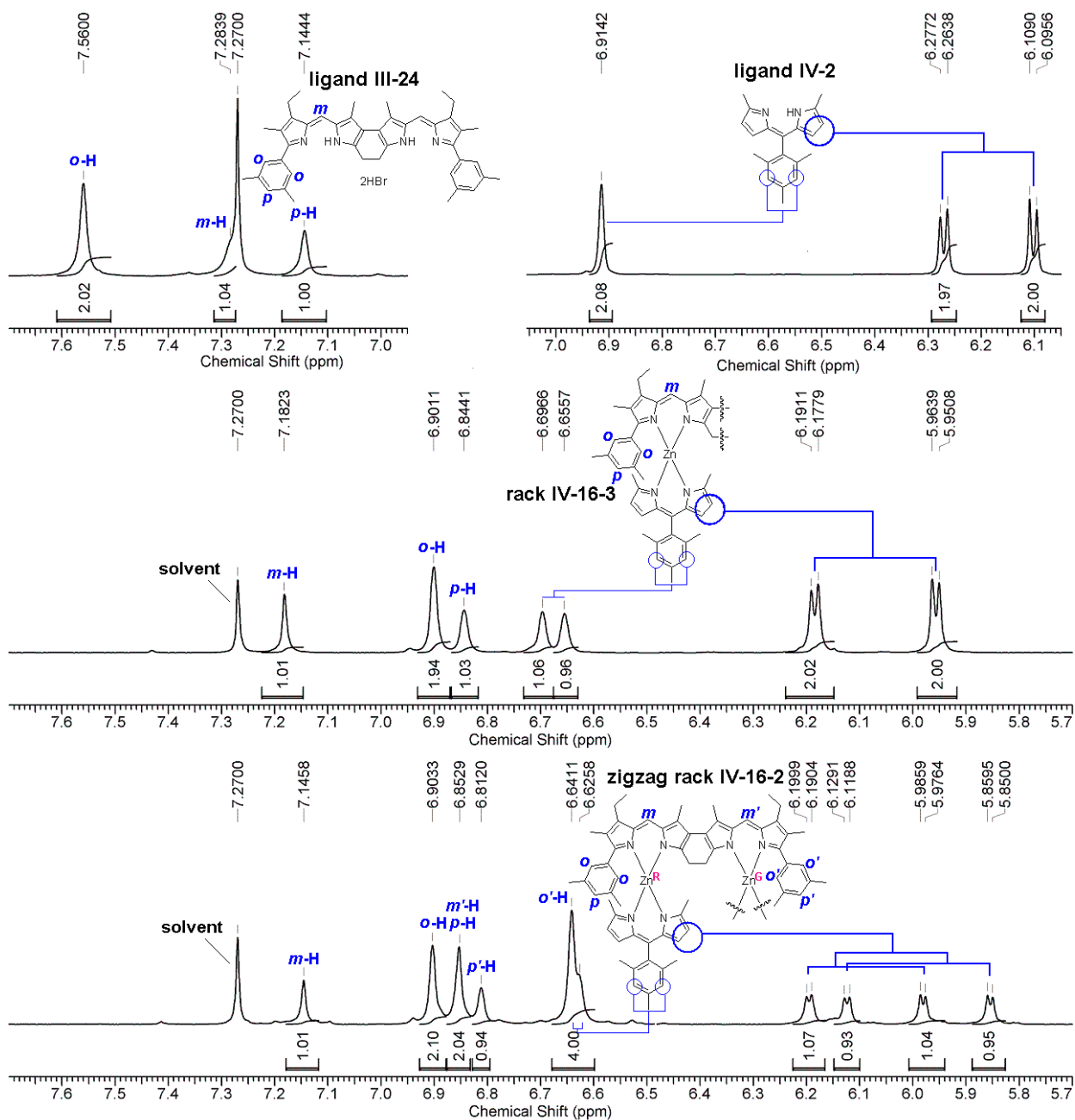


Figure 4-3 ^1H NMR spectra (aromatic region) of ligand **III-24** (400 MHz) and **IV-2** (300 MHz) (top), Zn^{II} rack **IV-16-3** (300 MHz) (middle) and zigzag Zn^{II} rack **IV-16-2** (400 MHz) (bottom) in CDCl_3 .

4.2.1.3 X-Ray Analysis of Zn^{II} Rack IV-16-3

A single crystal of **IV-16-3** was grown from slow diffusion of hexane into a chloroform solution and the structure was investigated by X-ray diffraction analysis (Figure 4-4). The material crystallizes with one half-molecule in the asymmetric unit, related to another by a 2-fold axis of rotation. **IV-16-3** is indeed a slightly distorted rack due to the repulsion between the two bulky mesityl groups at the *meso*-position in ligand **IV-2**. The distance between the two Zn^{II} ions in one molecule is 8.11 Å and the Zn-N bond lengths range from 1.97-1.99 Å, which are close to those in the Zn^{II} grid **III-33-4**. The dihedral angle between the mean planes of two dipyrins coordinated to the same Zn^{II} ion is 81.9°, which indicates each metal center has a much less distorted tetrahedral geometry than that in **III-33-4**. The dihedral angle between the mean planes of the two dipyrins within each ligand **III-24** is 11.4° owing to the sufficient flexibility of the cyclohexadiene ring. The dihedral angle between the plane of the mesityl group and the mean plane of the dipyrin in ligand **IV-2** is 84.4°. The two mesityl groups move away from each other (dihedral angle = 42.2°) due to the steric hindrance caused by the *ortho*-methyl groups oriented towards each other. Furthermore, the two mean planes of the dipyrins in ligand **IV-2** move towards each other (dihedral angle = 21.5°) owing to the bulky 3,5-dimethylphenyl groups attached to the α' -position of the terminal dipyrin rings in ligand **III-24**. The three-dimensional packing structure of **IV-16-3** exhibits no tunnel-like structure (Figure 4-5).

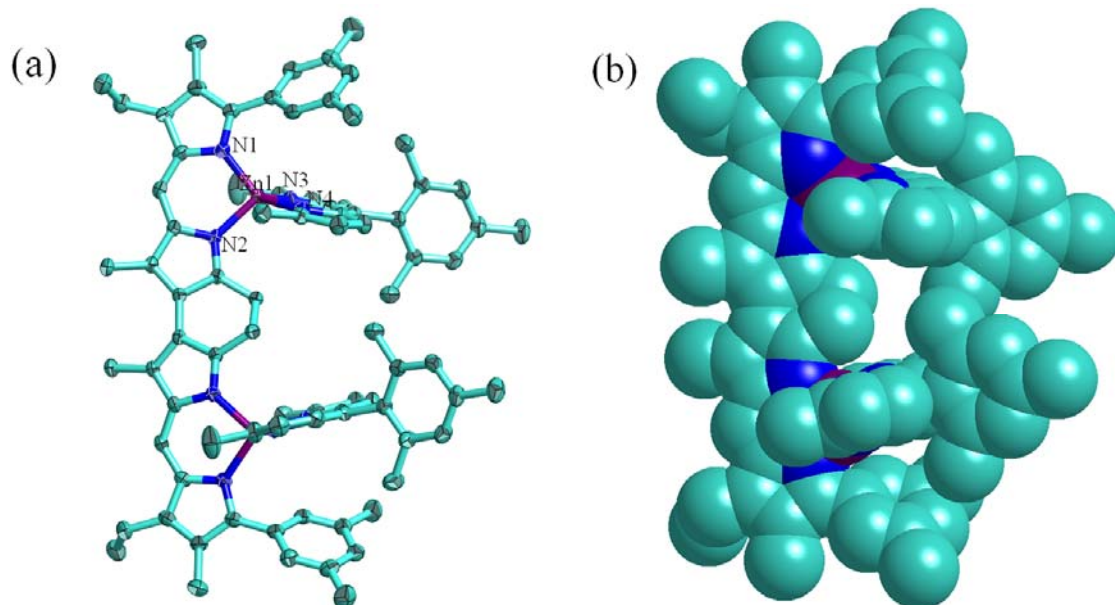


Figure 4-4 Crystal structure of Zn^{II} rack **IV-16-3**: (a) ORTEP diagram (thermal ellipsoids are scaled to the 50% probability level) and (b) space-filled representation.

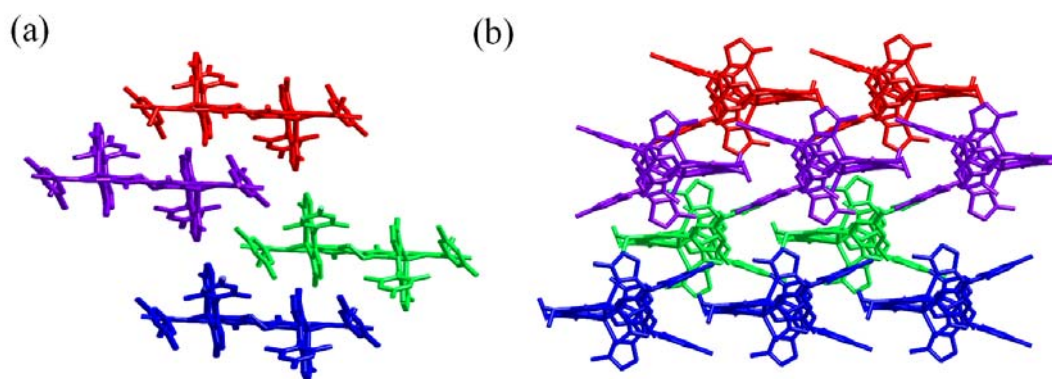


Figure 4-5 Stick-packing of Zn^{II} rack **IV-16-3**: (a) top view and (b) side view.

4.2.1.4 Electronic Absorption Spectra of Metal Racks and Zigzag Racks

The anti-parallel racks **IV-9-2** through **IV-11-2** are all red solids upon crystallization, but form red-orange solutions when dissolved in chloroform. However, the parallel racks **IV-12-1** through **IV-15-2** are all green solids upon crystallization, and generate blue solutions when dissolved in chloroform. The rack and zigzag racks from **IV-16** are all dark green in the solid form and in solution while those from **IV-17** are all dark blue. Complexes **IV-9-2** through **IV-17-2** were analyzed by electronic absorption spectroscopy (Figure 4-6). Remarkably, the absorption spectra of all Zn^{II} racks in CHCl₃ show two intense metal-to-ligand charge transfer (MLCT) transition bands (Table 4-1). The first bands peaking at 491-498 nm are attributed to MLCT transitions only engaging the *meso*-aryl dipyrin ligands **IV-2** through **IV-4**, and the shoulders of the first bands probably result from the spin-allowed ligand-centered (LC) transitions (π - π^*) involving the aforementioned ligands. Similarly, the second bands peaking at 542-546 nm for anti-parallel racks and at 627-637 nm for parallel racks may receive contributions from MLCT transitions involving the diacetylene bisdipyrin ligands (**II-22** and **IV-8**) or ring fused bisdipyrin ligands (**III-22** and **IV-6**), respectively. The LC transitions engaging diacetylene or ring fused bisdipyrin ligands are likely responsible for the shoulders of the second bands.

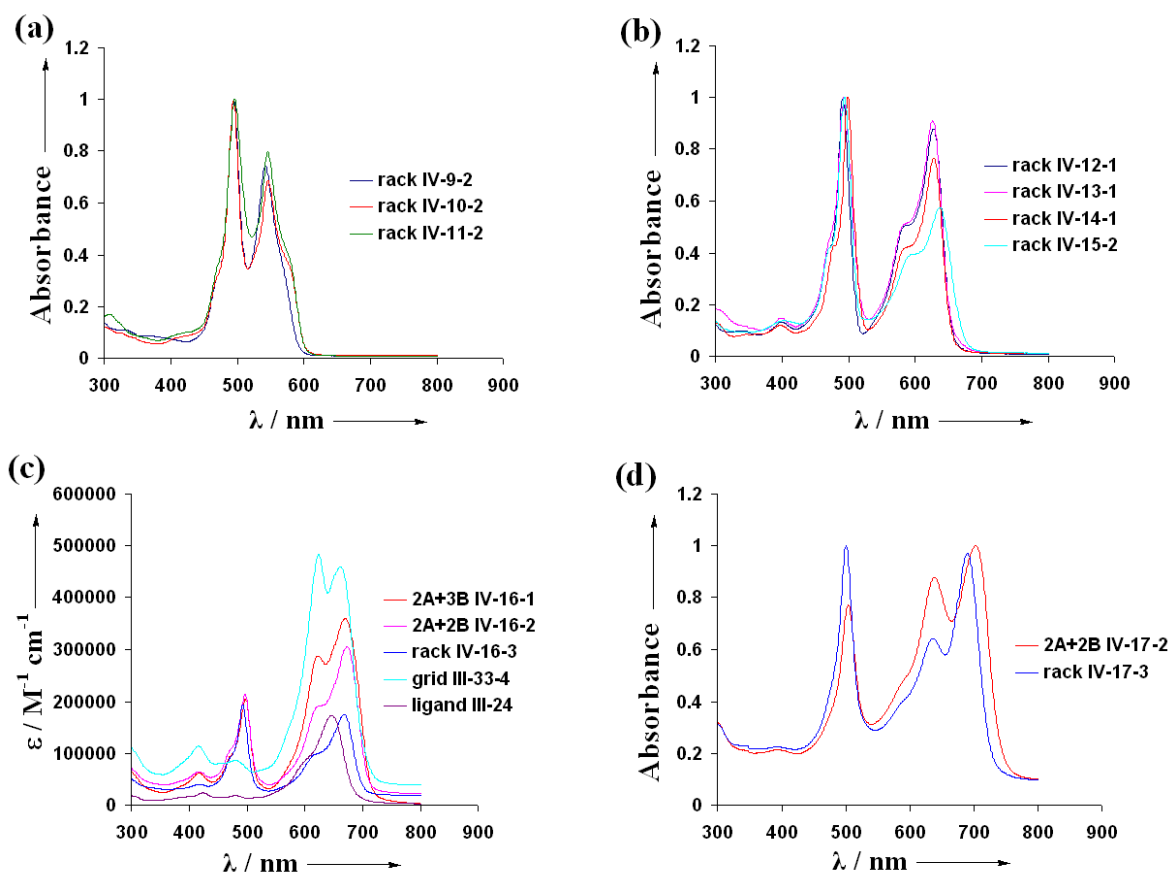


Figure 4-6 Electronic absorption spectra of rack-type Zn^{II} complexes in chloroform: (a) **IV-9-2** through **IV-11-2**; (b) **IV-12-1** through **IV-15-2**; (c) **IV-16** and (d) **IV-17**.

Table 4-1 Metal-to-ligand charge transfer transition bands λ_{max} (nm) for the Zn^{II} racks in chloroform.

Rack	λ_{max1} (nm)	λ_{max2} (nm)	Rack	λ_{max1} (nm)	λ_{max2} (nm)
IV-9-2	495	542	IV-13-1	493	627
IV-10-2	494	546	IV-14-1	498	629
IV-11-2	496	546	IV-15-2	493	637
IV-12-1	491	628			

As expected, the Zn^{II} rack **IV-16-3** and zigzag racks **IV-16-2** and **-1** all exhibit a sharp band (similar $\lambda_{\text{max}_1}/\log\epsilon_1$) with a left shoulder which is associated to the MLCT and LC transitions involving ligand **IV-2** due to the fixed number of these ligands incorporated into the complexes (Table 4-2).⁴⁰ Surprisingly, the shoulder of the second band gradually becomes a separate band with increased ratio of number of ring fused bisdipyrrin ligand **III-24** to number of Zn^{II} ions involved in the Zn^{II} racks or zigzag racks. Grid **III-33-4** which contains four Zn^{II} ions and four ligands (ratio = 1) showed two intense bands with almost identical log ϵ values, which further confirms that the second bands are attributed to MLCT transition while the shoulders receive contributions from the spin-allowed LC transitions. The wavelengths of the two intense bands in rack **IV-16-3** and zigzag racks **IV-16-2** and **-1** are marginally-shifted (1 to 5 nm), which indicates a minimal overlap between the two distinct π -systems, coordination center with Zn^R and that with Zn^G, respectively.⁸² The electronic absorption spectra of complexes **IV-16-3** through **IV-16-1** display a hyperchromic shift for the bands associated with increasing number of ligand **III-24**. By contrast, the Co^{II} rack **IV-17-3** and zigzag rack **IV-17-2** both showed three intense bands. Instead of a shoulder, a separate band appears for the LC transitions involving ligand **III-24** due to a large wavelength difference (52 nm) between the second and third bands.

Table 4-2 Metal-to-ligand charge transfer transition bands $\lambda_{\max 1}$ and $\lambda_{\max 3}$ (nm) and spin-allowed ligand-centered transition band $\lambda_{\max 2}$ (nm) for the metal racks and zigzag racks in chloroform.

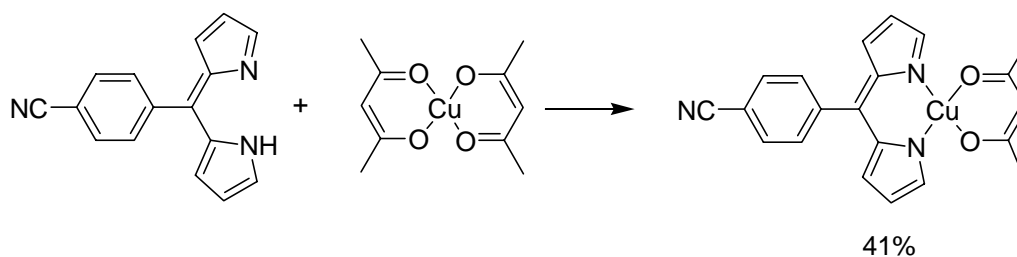
Compound	$\lambda_{\max 1}(\text{nm})/\log \epsilon_1$	$\lambda_{\max 2}(\text{nm})/\log \epsilon_2$	$\lambda_{\max 3}(\text{nm})/\log \epsilon_3$
III-24	—	647/5.24	—
IV-16-3	492/5.29	—	667/5.25
IV-16-2	496/5.33	—	672/5.48
IV-16-1	497/5.31	623/5.46	669/5.56
III-33-4	—	625/5.68	661/5.66
IV-17-3	500/—	637/—	689/—
IV-17-2	504/—	639/—	702/—

4.2.2 Rigid Ladder-Type Metal Complexes

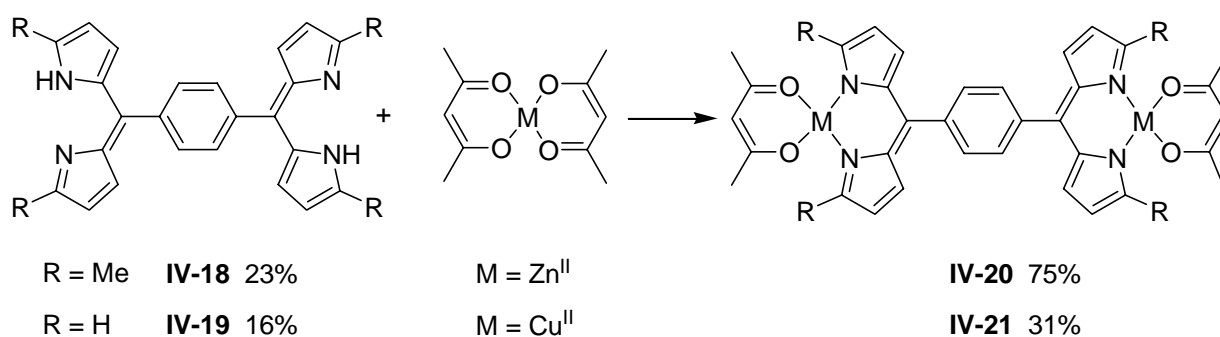
After the success of synthesizing parallel Zn^{II} racks, formation of the metal ladder using the same procedure seems but one step away. With the ring fused bisdipyrrin ligands (the rails of the ladder) in hand, we only need to find a new kind of *meso*-aryl bisdipyrrin ligand to fit the other role (the rungs of the ladder). Inspired by ligand **IV-2**, used for synthesis of Zn^{II} rack **IV-16-3**, a double *meso*-aryl dipyrin ligand **IV-18** was prepared for the ladder synthesis. Compound **IV-19** was generated based on the same idea, but with α -free pyrrole instead.

4.2.2.1 Synthesis of Rigid Ladder-Type Metal Complexes

The preparation of rigid ladder-type metal complexes began with synthesis of *meso*-phenyl bisdipyrrin ligands **IV-18**⁸² and **-19**. Combination of α -free cyclohexane bisdipyrrin ligand **III-22** with either **IV-18** and $\text{Zn}(\text{OAc})_2 \cdot 2\text{H}_2\text{O}$ or **IV-19** and $\text{Cu}(\text{OAc})_2 \cdot \text{H}_2\text{O}$ in the presence of NaOAc afforded only the metal grid of ligand **III-22**. It seems that ligand **III-22** can rapidly chelate the metal ions in the solution to generate the homoleptic grid which leaves ligands **IV-18** or **-19** to form polymers on their own. In order to overcome that obstacle, we have to link the metal ions to ligands **IV-18** or **-19** because if ligand **III-22** wants to obtain the metal ions to form the complexes, it will have no choice but to react with ligands **IV-18** or **-19** with metal ions attached to them. Inspired by Cohen's work on heteroleptic Cu^{II} dipyrin complexes which are stable in solution and easy to purify on silica gel (Scheme 4-3),⁸⁸ heteroleptic Zn^{II} (**IV-20**) and Cu^{II} (**IV-21**) bisdipyrrin complexes were prepared (Scheme 4-4). Treatment of **IV-18** with excess $\text{Zn}(\text{acac})_2$ affords the crude product which was recrystallized from $\text{CH}_2\text{Cl}_2/\text{Et}_2\text{O}$ to give the pure heteroleptic Zn^{II} bisdipyrrin complex **IV-20** in a high yield (75%). The Cu^{II} complex **IV-21** was obtained using the same synthetic route. Surprisingly, **IV-21** can be purified by simply passing it through a silica gel plug with chloroform as the eluent. However, no desired heteroleptic metal complexes were observed when **IV-18** was paired with $\text{Cu}(\text{acac})_2$ or **IV-19** with $\text{Zn}(\text{acac})_2$.



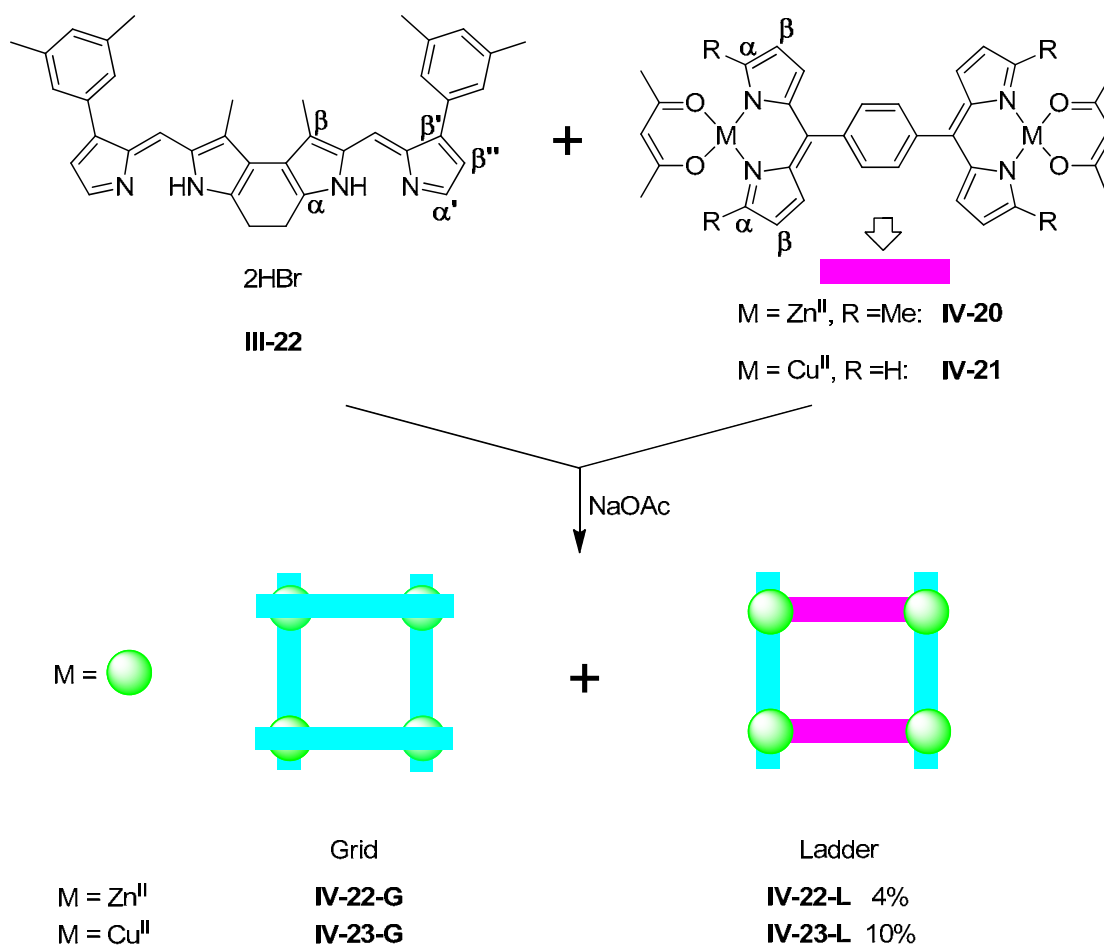
Scheme 4-3 Synthetic route for preparation of the heteroleptic Cu^{II} dipyrin complex by Cohen.



Scheme 4-4 Synthetic route for preparation of the heteroleptic Zn^{II} and Cu^{II} bisdipyrrin complexes.

Treatment of heteroleptic bisdipyrrin metal complexes **IV-20** or **IV-21** and ring fused bisdipyrrin ligand **III-22** with NaOAc in CHCl₃/MeOH forms a mixture of Zn^{II} complexes **IV-22** or a mixture of Cu^{II} complexes **IV-23** (Scheme 4-5). Non-polar fractions were collected from flash chromatography on silica gel eluting with CH₂Cl₂, followed by elution through a GPC column with toluene to afford two separate fractions for **IV-23**. The first fraction **IV-23-G** (dark blue) is the Cu^{II} grid of **III-22** and the second one **IV-23-L** (dark green) is the rigid ladder-type Cu^{II} complex, both of which are confirmed by MALDI-TOF mass spectrometry. However, the two fractions in **IV-22** always coelute on the GPC column due to the small

difference in their molecular weights and perhaps their similar conformations as well. Fortunately, these two complexes have different solubilities in dichloromethane. Thus, pure Zn^{II} ladder **IV-22-L** can be obtained by using dichloromethane to wash out the Zn^{II} grid **IV-22-G** from the mixture.



Scheme 4-5 Synthetic route for preparation of rigid ladder-type metal complexes.

Ideally, we hope that the metal-N bond is stronger than the metal-O bond in complexes **IV-20** and **IV-21**, and also that ligand **III-22** can break the metal-O bond and leave the metal-N bond intact. However, it turned out ligand **III-22** did break metal-O bonds, and unfortunately

some of the metal-N bonds as well, which explained why metal grids were always formed in the reaction. The grids using α' -free ring fused bisdipyrrin ligands prefer metal ions with tetrahedral geometry due to their square-shaped structures, which is responsible for the fact that Zn^{II} grid **IV-22-G** is more favoured than Cu^{II} grid **IV-23-G**. The Zn^{II} ladder **IV-22-L** prefers metal ions with tetrahedral geometry to ease the repulsion between the α -methyl groups from complex **IV-20** and the α -methylene groups from ligand **III-22**. The same repulsion does not exist in Cu^{II} ladder **IV-23-L**, thus, both ligands can easily adjust their conformations and arrangements to fulfill the coordination geometry the Cu^{II} ion prefers. Therefore, the ladder/grid ratio is much higher in **IV-23** than that in **IV-22**. Other than ligand **III-22**, many other α' -aryl ring fused bisdipyrrin ligands have been investigated, but no Zn^{II} or Cu^{II} ladders were observed. It is likely that the α' -aryl groups block the orientation that the heteroleptic metal complexes **IV-20** and **-21** try to adopt.

4.2.2.2 X-Ray Analysis of Cu^{II} Rigid Ladder **IV-23-L**

A single crystal of **IV-23-L** was grown from slow diffusion of hexane into a CH_2Cl_2 solution and the structure was investigated by X-ray diffraction analysis (Figure 4-7). The material crystallizes with one half molecule in the asymmetric unit related to a crystallographically equivalent fragment related by a c-glide plane. Complex **IV-23-L** is a heavily twisted ladder consisting of four Cu^{II} ions and two sets of distinct bisdipyrrin ligands. The distances between two adjacent Cu^{II} ions in one molecule are 8.14 and 12.33 Å due to the existence of two different ligands. The distance between two diagonal Cu^{II} ions in one molecule is 14.28 Å,

which is much longer than that in Zn^{II} grid **III-27-4** (11.47 Å). The Cu^{II} ladder **IV-23-L** displays significant differences in Cu-N bond length, which probably results from Jahn-Teller distortion. The dihedral angles between the mean planes of two dipyrins coordinated to the same Cu^{II} ion are 53.5 and 57.8°, which indicates each metal center has a heavily distorted tetrahedral geometry. The dihedral angle between the mean planes of two dipyrins within each ligand **III-22** is 15.8° due to the sufficient flexibility of the cyclohexadiene ring. The dihedral angle between the mean planes of two dipyrins in ligand **IV-19** is 8.9°.

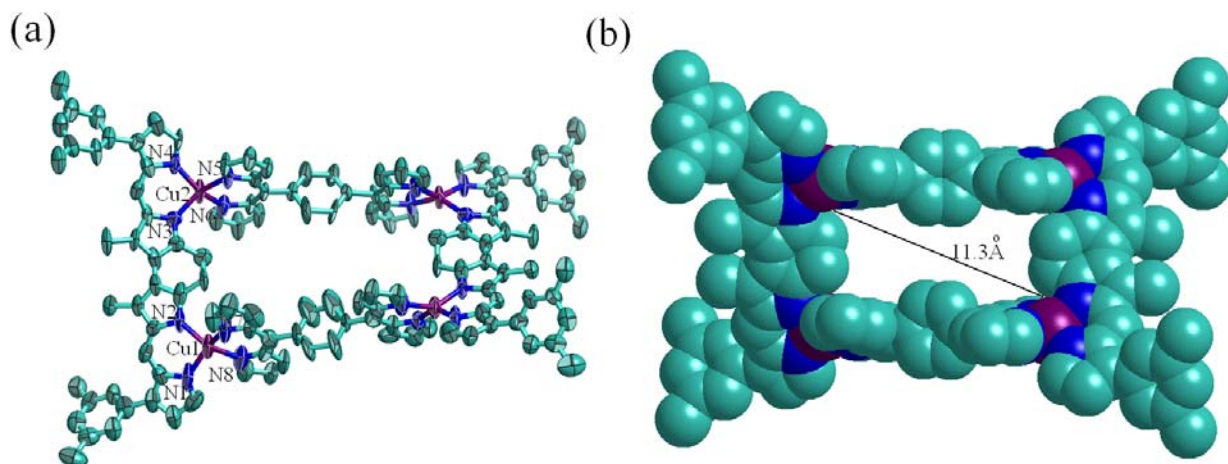


Figure 4-7 Crystal structure of Cu^{II} ladder **IV-23-L**: (a) ORTEP diagram (thermal ellipsoids are scaled to the 50% probability level) and (b) space-filled representation.

The three-dimensional packing structure of **IV-23-L** exhibits a rectangular tunnel (11.3 Å on the diagonal) along the *c* axis in the crystal (Figure 4-8). The interesting tunnel structure may receive contributions from two sets of intermolecular CH/ π interactions^{15, 89-92} between individual molecules. The first set consists of four types (A, B, C and D) intermolecular CH/ π interactions involving only the ligand **III-22** between the neighboring molecules: type A is

formed between the methyl groups from 3,5-dimethylphenyl substituents and the centroid of the mean plane of the dipyrin units belonging to the nearest molecules; type B between the *ortho*-H from 3,5-dimethylphenyl substituents and the centroid of the pyrrole rings of the same neighboring molecules; type C between the β -methyl groups from ligand **III-22** and the centroid of the mean plane of the dipyrin units belonging to the nearest molecules; type D between the methyl groups from 3,5-dimethylphenyl substituents and the centroid of the pyrrole rings belonging to the nearest molecules in adjacent layers. The second set contains one type (E) intermolecular CH/ π interactions engaging both ligands (**III-22** and **IV-19**) between the neighboring molecules: type E is formed between β -H from ligand **IV-19** and the centroid of the pyrrole rings from ligand **III-22** (Figure 4-9 and Table 4-3). As a consequence of these intermolecular interactions, a three-dimensional tunnel structure of **IV-23-L** along the *c* axis is eventually generated.

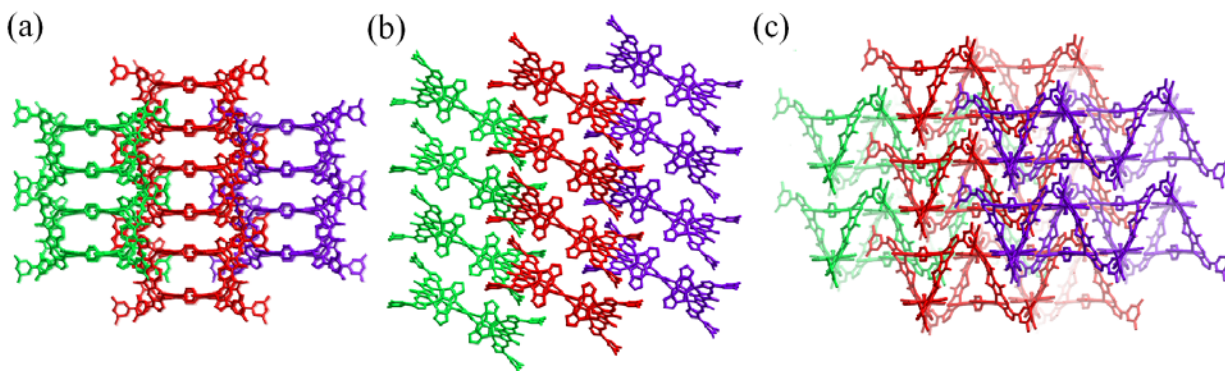


Figure 4-8 Stick-packing of Cu^{II} ladder **IV-23-L**: (a) top view; (b) and (c) side views.

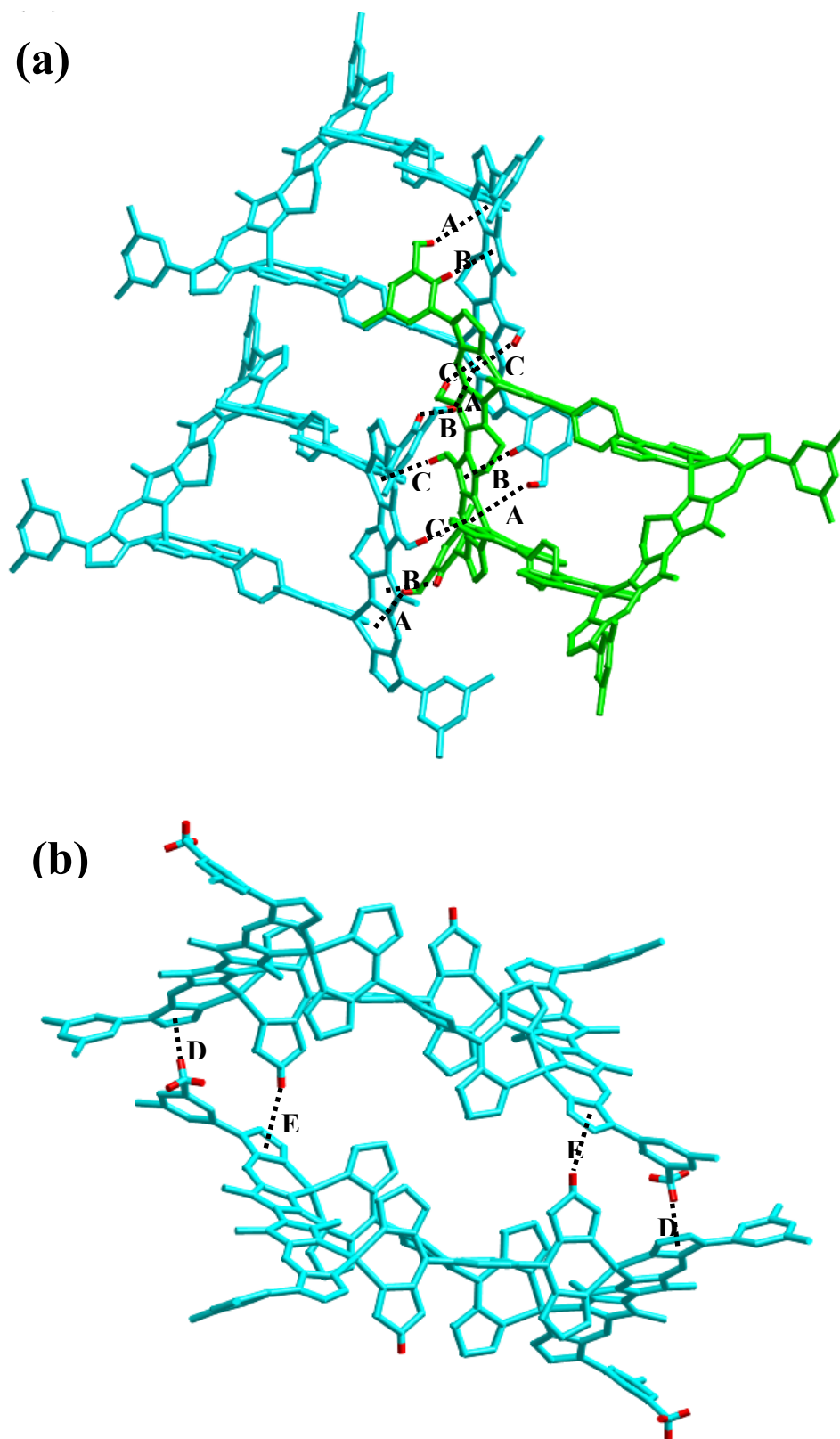


Figure 4-9 Five types of CH/ π interactions (A to E) in IV-23-L with stick representation: (a) top view and (b) side view.

Table 4-3 Intermolecular CH/ π interactions in the crystal structure of Cu^{II} rigid ladder **IV-23-L**.

CH/ π interactions	CH \cdots centroid (Å)	C \cdots centroid (Å)
Type A	2.76	3.53
Type B	2.80	3.40
Type C	2.70	3.58
Type D	3.06	3.93
Type E	3.05	3.83

4.2.2.3 Electronic Absorption Spectra of Metal Rigid Ladders

Both **IV-22-L** and **IV-23-L** are green solids upon crystallization, and form dark green solutions when dissolved in chloroform. Both ladders were analyzed by electronic absorption spectroscopy (Figure 4-10). As expected, the absorption spectra of Zn^{II} ladder **IV-22-L** in chloroform shows two intense metal-to-ligand charge transfer (MLCT) transition bands (Table 4-4). The first band peaking at 484 nm receives contributions from MLCT transitions only involving the *meso*-aryl bisdipyrrin ligand **IV-18**, and the shoulder of the first band likely results from the spin-allowed ligand-centered (LC) transitions (π - π^*) engaging the aforementioned ligand. Similarly, the second band peaking at 636 nm is attributed to MLCT transitions involving the ring fused bisdipyrrin ligand **III-22**. The LC transitions engaging ligand **III-22** are

probably responsible for the shoulder of the second band. However, the absorption spectra of Cu^{II} ladder **IV-23-L** shows no shoulder peaks, and a very broad second band which is probably attributed to the sum of effects of LC and MLCT transitions engaging ligand **III-22**.

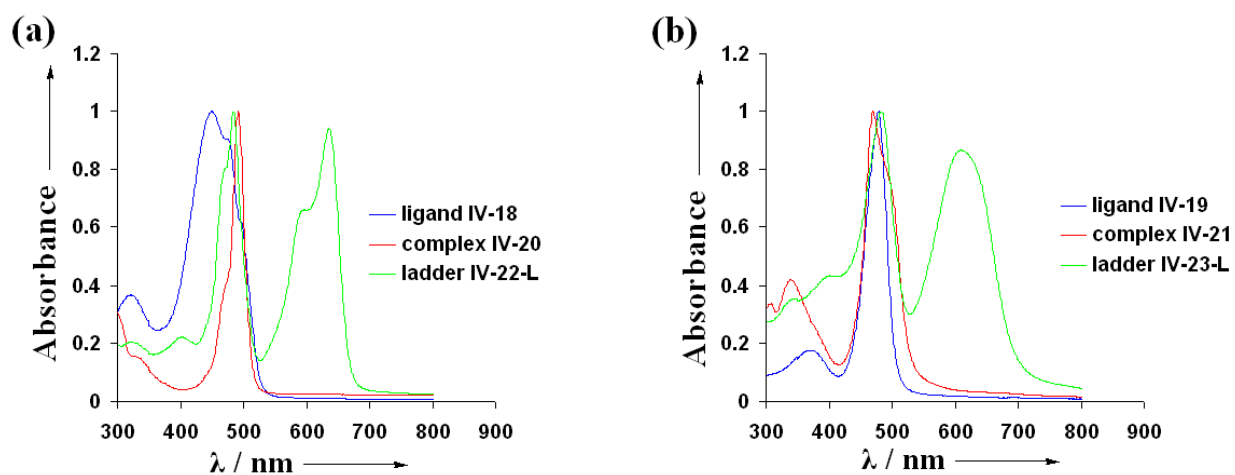


Figure 4-10 Electronic absorption spectra of rigid ladder-type metal complexes in chloroform: (a) Zn^{II} ladder **IV-22-L** with ligand **IV-18** and complex **IV-20**; (b) Cu^{II} ladder **IV-23-L** with ligand **IV-19** and complex **IV-21**.

Table 4-4 Ligand-centered transition band λ_{max} (nm) for the ligands and metal-to-ligand charge transfer transition bands λ_{max} (nm) for metal complexes in chloroform.

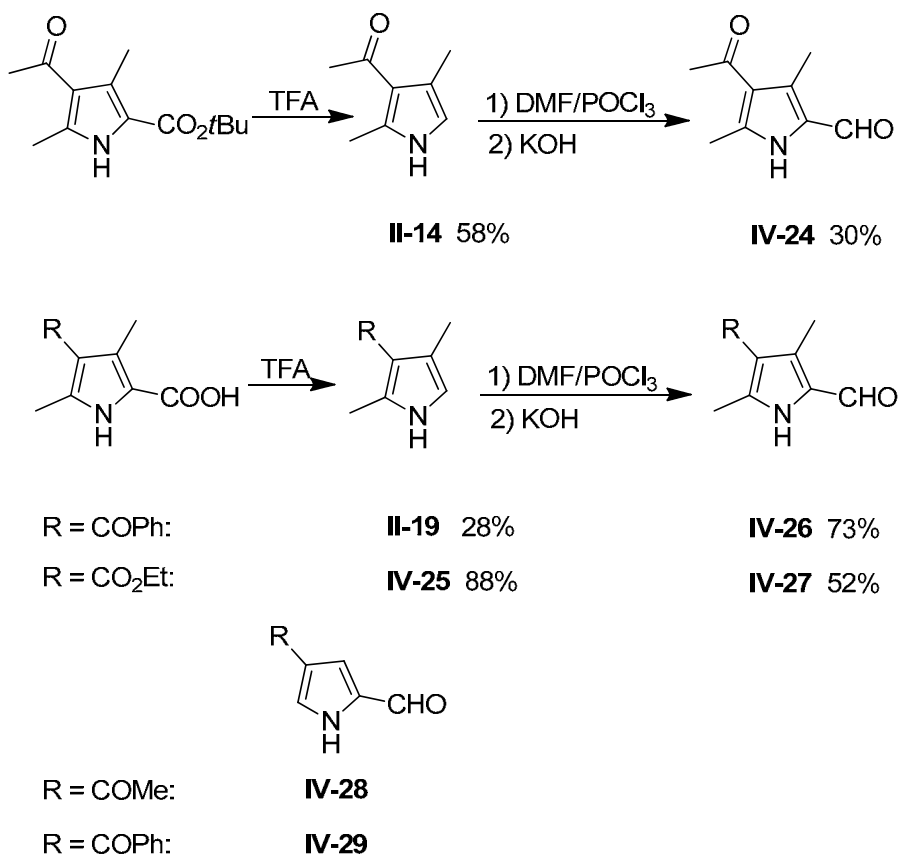
Compound	$\lambda_{\text{max}1}$ (nm)	$\lambda_{\text{max}2}$ (nm)	Compound	$\lambda_{\text{max}1}$ (nm)	$\lambda_{\text{max}2}$ (nm)
IV-18	449	—	IV-19	478	—
IV-20	491	—	IV-21	469	—
IV-22-L	484	636	IV-23-L	482	611

4.2.3 Flexible Ladder-Type Metal Complexes

The Zn^{II} ladder **IV-22-L** is very rigid, which receives contributions from the ring fused bisdipyrrin ligand **III-22**, the Zn^{II} ions which prefer perfect tetrahedral geometry and the α -methyl groups from ligand **IV-18**. At this point, we reasoned that if we introduce a flexible bisdipyrrin ligand instead of ligand **III-22**, can we obtain a double-helical ladder such as that in DNA. In order to investigate this hypothesis, several β - β' bisdipyrrin ligands linked with alkylene groups of different length were synthesized. The heteroleptic bisdipyrrin Zn^{II} and Cu^{II} complexes (**IV-20** and **IV-21**), again were selected as the source of the rungs of the ladder.

4.2.3.1 Synthesis of Flexible Ladder-Type Metal Complexes

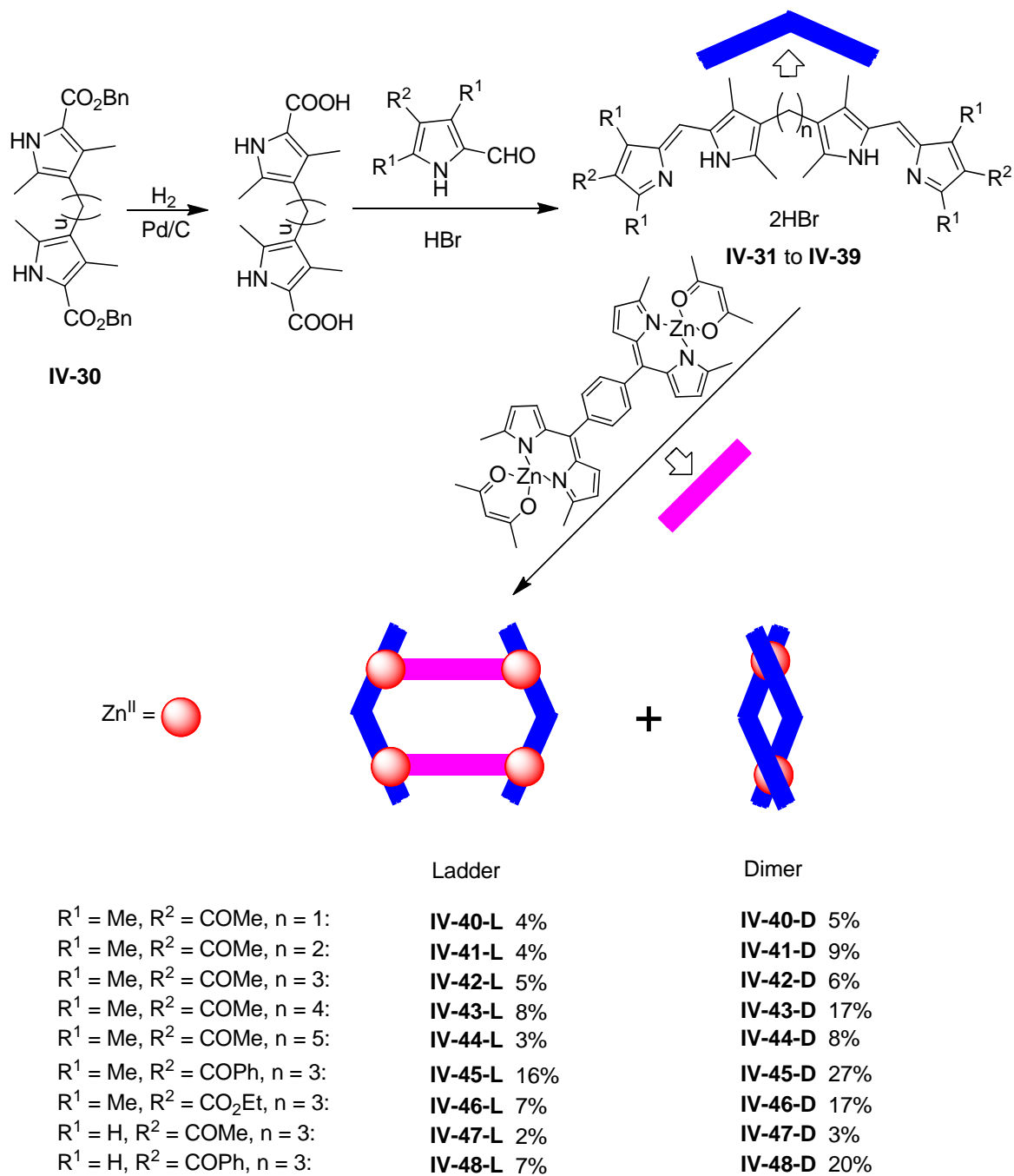
The preparation of flexible bisdipyrrins started with the synthesis of another set of pyrrole-2-carbaldehyde derivatives (Scheme 4-6). In addition to many previously synthesized pyrrole-2-carbaldehydes with attached electron-donating groups, some electron-withdrawing groups are selected to introduce to the 4-position of the pyrrole-2-carbaldehydes. Compound **IV-24** is the side product of the Vilsmeier reaction of **II-14** while **IV-26** is the main product of the Vilsmeier reaction. The same procedure was used to generate **IV-27** as a brown solid. Compound **IV-28** was synthesized by a former group member and the synthesis of **IV-29** was based on a previously reported procedure.⁹³



Scheme 4-6 Synthetic route for preparation of pyrrole-2-carbaldehyde derivatives.

A series of starting materials **IV-30** ($n = 1$ to 5) for flexible bisdipyrrins were synthesized based on the previously reported procedures.⁴⁶ Hydrogenation of **IV-30** in the presence of palladium on activated carbon as the catalyst,⁴⁶ followed by treatment of pyrrole-2-carbaldehyde derivatives **IV-24** and **IV-26** through **IV-29** with HBr formed ligands **IV-31** through **IV-39** as their HBr salts. Combination of ligands **IV-31** through **IV-39** with heteroleptic bisdipyrrin Zn^{II} complex **IV-20** and NaOAc in CH₂Cl₂/MeOH forms a mixture of Zn^{II} complexes **IV-40** through **IV-48** (Scheme 4-7). Non-polar fractions were collected from flash chromatography on neutral alumina eluting with CH₂Cl₂/MeOH, followed by elution through a GPC column with toluene to afford two yellow fractions in all cases. The first fraction is the flexible ladder-type Zn^{II} complex and the second one is the Zn^{II} double-helix of flexible bisdipyrrin ligand, both of which

are confirmed by MALDI-TOF mass spectrometry. However, the introduction of heteroleptic bisdipyrrin Cu^{II} complex **IV-21** to the reaction only led to formation of a Cu^{II} double-helix, and no positive sign of generation of the flexible ladder-type complexes was observed.



Scheme 4-7 Synthetic route for preparation of flexible ladder-type Zn^{II} complexes.

4.2.3.2 ^1H NMR Spectra of Zn^{II} Flexible Ladder-Type Complexes

The ^1H NMR spectra of Zn^{II} flexible ladders **IV-40-L**, **IV-42-L** and **IV-43-L** dissolved in CDCl_3 showed that the $\beta\text{-H}$ signals (doublet of doublets) from ligand **IV-18**, previously at δ 6.53 and 6.20 ppm for **IV-18**, were shifted and the shape of the peaks was changed as well, which supports the generation of the Zn^{II} ladders (Figure 4-11). ^1H NMR spectrum of Zn^{II} flexible ladder **IV-40-L** exhibited five sets of doublet of doublets for the $\beta\text{-H}$ signals while **IV-42-L** had three such sets and **IV-43-L** with only one. It appears that the $\beta\text{-H}$ signals in ^1H NMR spectra become simpler with increasing the length of the alkylene linker. It is thought that two isomers may exist in the solution when a methylene group was introduced as the spacer (**IV-40-L**), which causes the complexity of the signals. However, one isomer gradually dominates the other with increasing the length of the spacer, which may be responsible for the simplifying trend of the $\beta\text{-H}$ signals at the end.

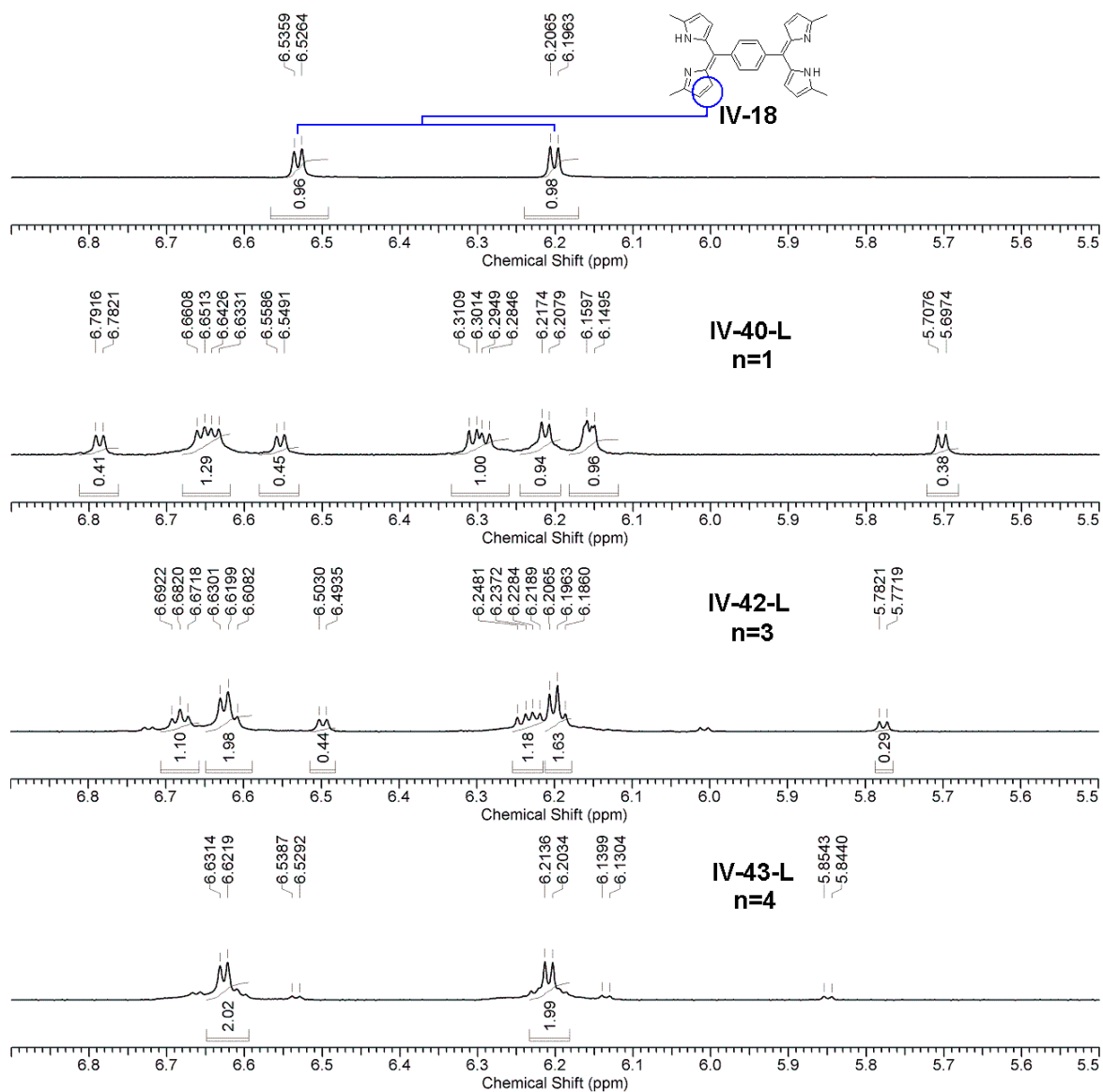


Figure 4-11 Partial ^1H NMR spectra of ligand **IV-18**, Zn^{II} ladders **IV-40-L**, **IV-42-L** and **IV-43-L** in CDCl_3 (400 MHz).

4.2.3.3 X-Ray Analysis of Zn^{II} Flexible Ladder IV-42-L

A single crystal of **IV-42-L** was grown from slow diffusion of hexane into a chloroform solution of **IV-42-L** and the structure was investigated by X-ray diffraction analysis (Figure 4-12). The material crystallizes with one half-molecule residing on an inversion centre. Surprisingly, instead of a ladder-type helicate, **IV-42-L** is a heavily twisted ladder-type mesocate consisting of four Zn^{II} ions and two sets of distinct bisdipyrrin ligands. The distances between two adjacent Zn^{II} ions in one molecule are 9.87 and 12.48 Å due to the existence of the two types of ligand. The distances between two diagonal Zn^{II} ions in one molecule are 14.61 and 16.87 Å, which are a little longer than those in Cu^{II} ladder **IV-23-L** owing to the much longer introduced linker. Unlike the Cu^{II} ladder **IV-23-L**, the Zn-N bond lengths range from 1.96-2.00 Å, which shows slight differences in the metal-N bond lengths. The dihedral angles between the mean planes of two dipyrins coordinated to the same Zn^{II} ion are 85.8 and 76.4°, which indicates one metal center has a much more distorted tetrahedral geometry than the other. The dihedral angle between the mean planes of the two dipyrins within each ligand **IV-33** is 70.6° due to the flexibility of the propylene linker. The dihedral angle between the mean planes of the two dipyrins in ligand **IV-18** is 38.0°, which is much larger than that in Cu^{II} ladder **IV-23-L** (8.9°) which is probably due to the presence of the α -methyl groups in ligand **IV-18**.

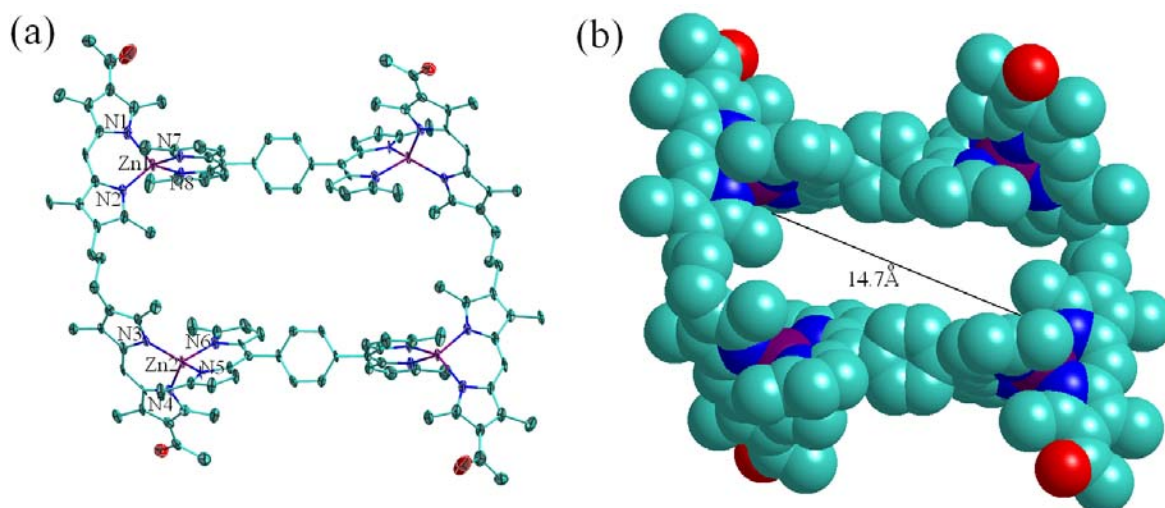


Figure 4-12 Crystal structure of Zn^{II} ladder **IV-42-L**: (a) ORTEP diagram (thermal ellipsoids are scaled to the 50% probability level) and (b) space-filled representation.

The three-dimensional packing structure of **IV-42-L**, like the Cu^{II} ladder **IV-23-L**, exhibits a much larger rectangular tunnel (14.7 Å on the diagonal) along the a axis in the crystal (Figure 4-13). This fascinating tunnel structure may receive contributions from two sets of intermolecular interactions between individual molecules. The first set consists of two types (A and B) intermolecular $\text{CH}\cdots\text{O}$ interactions⁹⁴ between the neighboring molecules: type A is formed between the *ortho*-H of phenyl spacer from ligand **IV-18** and O atom from the carbonyl group from ligand **IV-33**; type B between the β -H from ligand **IV-18** and the same aforementioned O atom. The second set contains two types (C and D) intermolecular CH/π interactions^{15, 89-92, 95} between the neighboring molecules: type C is generated between the β -H from ligand **IV-18** and the centroid of the pyrrole rings with attached carbonyl groups; type D between the β -H from ligand **IV-18** and the centroid of the pyrrole rings from ligand **IV-18** belonging to the neighboring molecules in adjacent layers (Figure 4-14 and Table 4-5). As a

consequence of these intermolecular interactions, a three-dimensional tunnel structure of **IV-42-L** along the *a* axis is eventually constructed.

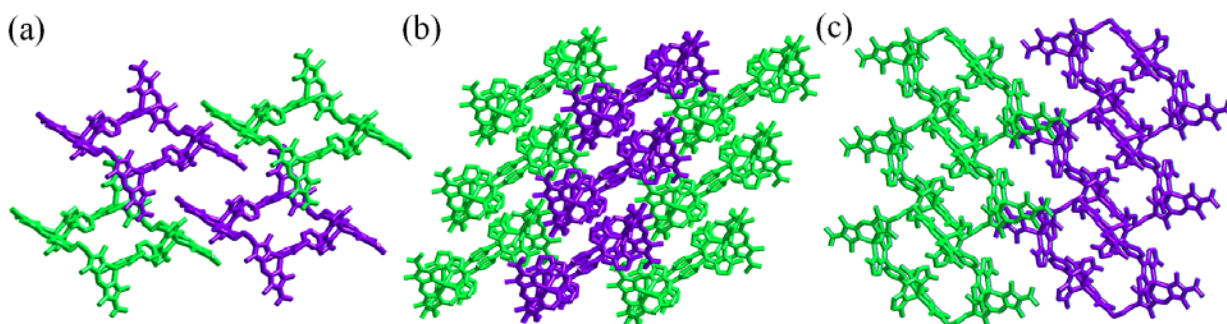
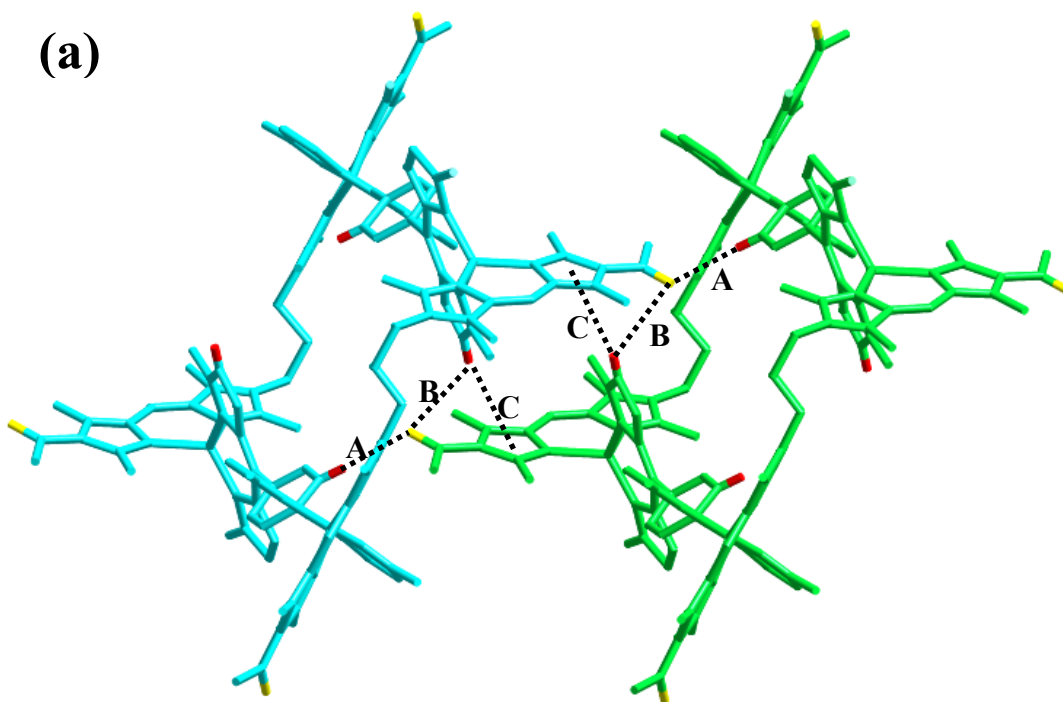


Figure 4-13 Stick-packing of Zn^{II} ladder **IV-42-L**: (a) top view; (b) and (c) side views.



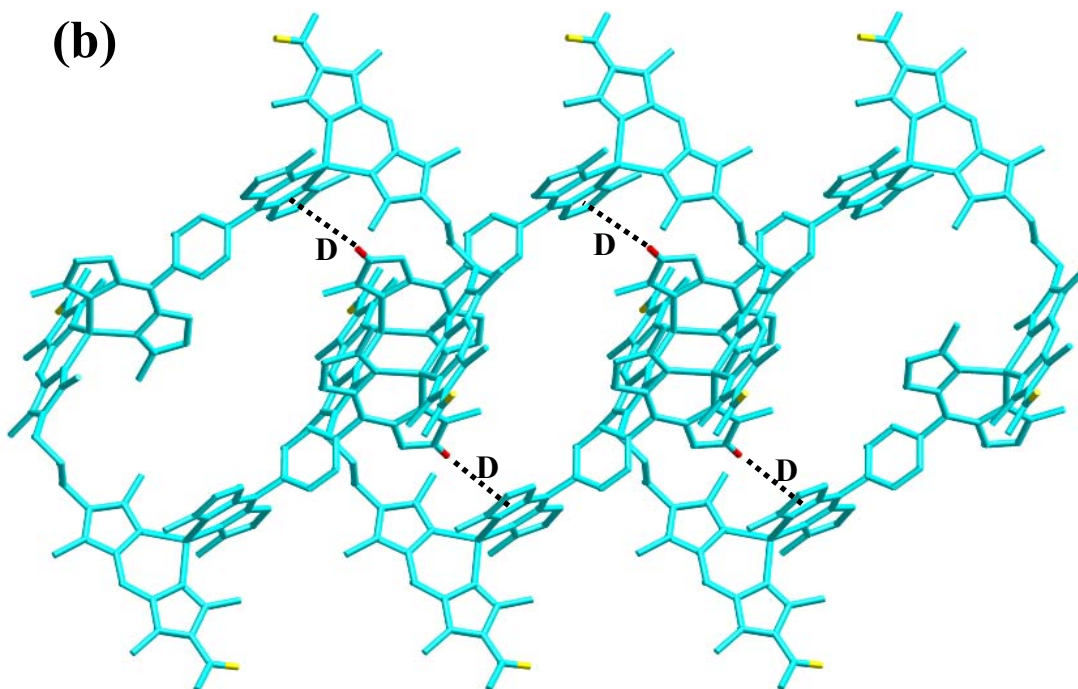


Figure 4-14 Two types of CH/O interactions (A and B) and two types of CH/ π interactions (C and D) in **IV-42-L** with stick representation: (a) top view and (b) side view.

Table 4-5 Intermolecular CH/O and CH/ π interactions in the crystal structure of Zn^{II} flexible ladder **IV-42-L**.

CH/O interactions	CH \cdots O (Å)	CH/ π interactions	CH \cdots centroid (Å)	C \cdots centroid (Å)
Type A	2.47	Type C	3.02	3.78
Type B	3.02	Type D	3.27	4.06

4.2.3.4 Electronic Absorption Spectra of Zn^{II} Flexible Ladders

The Zn^{II} flexible ladders **IV-40-L** through **IV-48-L** are all orange solids upon crystallization, but form yellow solutions when dissolved in chloroform. All the ladders were analyzed by electronic absorption spectroscopy (Figure 4-15). The absorption spectra of all the Zn^{II} ladders in chloroform exhibit one intense metal-to-ligand charge transfer (MLCT) transition band except for **IV-45-L**, which shows two instead (Table 4-6). An ascending trend of λ_{max} can be observed in the Zn^{II} ladders (**IV-40-L** through **IV-44-L**), which may be caused by substituent effects through increasing the length of the alkylene spacer in the flexible bisdipyrrin ligands. A bathochromic shift (~ 7 nm) occurs with methyl groups on the α' - and β' -position of the flexible ligands (**IV-42-L** and **IV-45-L**) instead of a proton (**IV-47-L** and **IV-48-L**) owing to the same aforementioned reason. The small difference between the wavelengths (λ_{max}) of dimer **IV-42-D** and ladder **IV-42-L** indicates a minimal overlap between two distinct ligands in the latter.⁸²

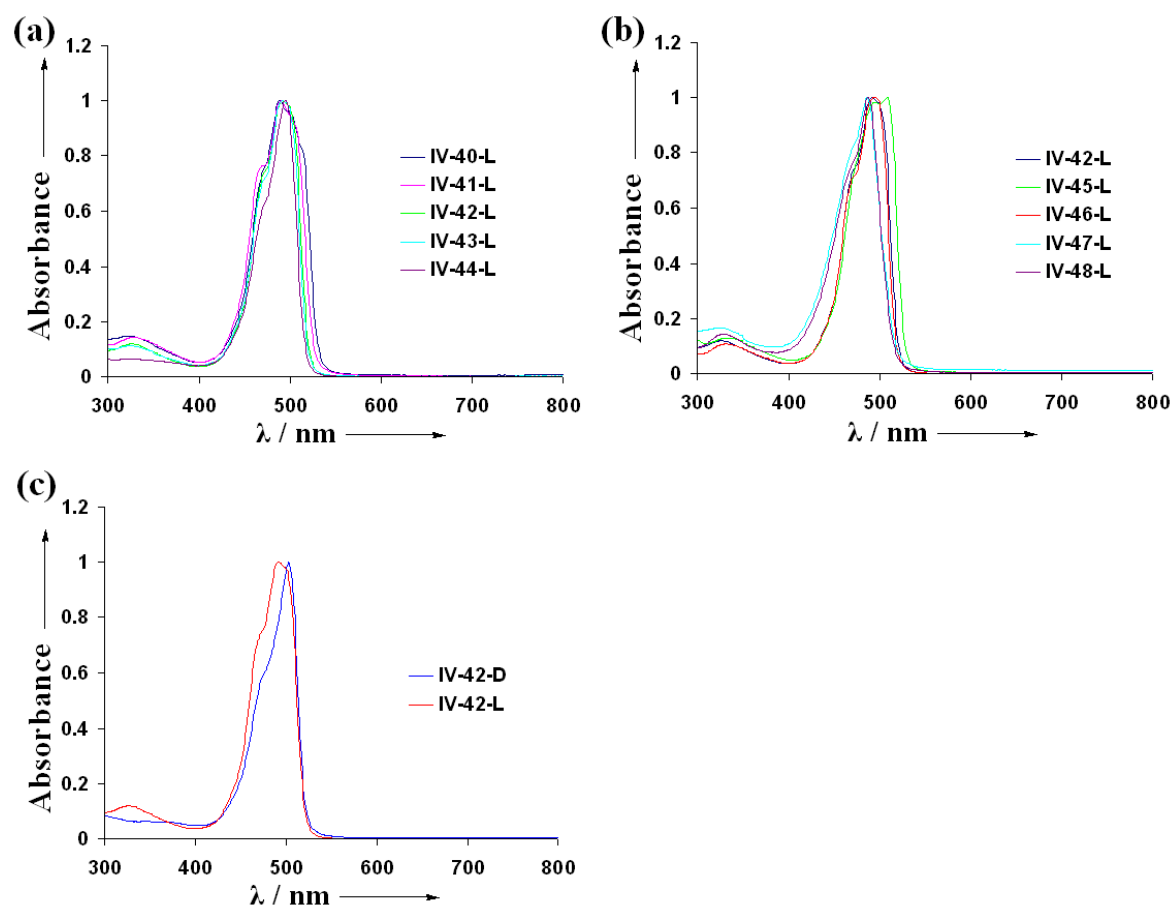


Figure 4-15 Electronic absorption spectra of flexible ladder-type Zn^{II} complexes in chloroform: (a) Zn^{II} ladder **IV-40-L** through **IV-44-L**; (b) Zn^{II} ladder **IV-42-L** and **IV-45-L** through **IV-48-L**; (c) Zn^{II} ladder **IV-42-L** and dimer **IV-42-D**.

Table 4-6 Metal-to-ligand charge transfer transition band(s) λ_{max} (nm) for Zn^{II} ladders in chloroform.

Ladder	λ_{max}	Ladder	λ_{max}	Ladder	λ_{max}
IV-40-L	489	IV-43-L	492	IV-46-L	494
IV-41-L	490	IV-44-L	495	IV-47-L	486
IV-42-L	492	IV-45-L	495/509	IV-48-L	488

4.3 Conclusions

The present results indicate the formation of well-defined heteroleptic rack-type metal complexes showing rigid linear arrangements of the metal centers when two distinct ligands were treated with Zn^{II} or Co^{II} ions. Furthermore, longer zigzag racks are obtained when ring fused bisdipyrrin ligand **III-24**, with bulky 3,5-dimethylphenyl groups attached to the α' -position of the terminal pyrrole rings, are incorporated. However, this traditional method proves to be ineffective for the synthesis of ladder-type metal complexes. Surprisingly, the introduction of heteroleptic Zn^{II} (**IV-20**) or Cu^{II} (**IV-21**) complexes as both the ligand and the metal ion source allows the easy generation of heteroleptic ladder-type metal complexes, which should be a very fruitful approach for the preparation of highly diversified assemblies. The electronic absorption spectra of the metal racks exhibit two intense peaks because the absorption spectrum of each ligand involved shows a very different λ_{max} . The same conclusion applies to rigid metal ladders as well. By contrast, the absorption spectra of the flexible metal ladders only exhibit one intense peak due to the similar λ_{max} of the two chosen ligands (except **IV-45-L**). Three crystal structures (**IV-16-3**, **IV-23-L** and **IV-42-L**) were generated through X-ray analysis. Complex **IV-16-3** is a slightly distorted rack while both **IV-23-L** and **IV-42-L** are heavily twisted ladders. The three-dimensional packing of the crystal structures of both **IV-23-L** and **IV-42-L** achieved rectangular tunnel structures with different sizes (11.3 and 14.7 Å on the diagonal, respectively).

Chapter Five
Experimental Sections

5.1 General Information

Unless otherwise noted, all starting materials and solvents were obtained from Aldrich, Fisher, Alfa Aesar or Oakwood and used without further purification. Thin layer chromatography (TLC) was performed with Merck Silica Gel 60 F254. Column chromatography was performed using silica gel from Silicycle Chemical Division (particle size: 230-400 mesh) or alumina from Fisher (neutral; 6% water added for Brockman activity III; particle size: 60-235 mesh). The gel permeation chromatography (GPC) was carried out on Bio-Beads S-X1 beads (200-400 mesh). ^1H NMR and ^{13}C NMR data were collected in d_6 -DMSO, CD_2Cl_2 or CDCl_3 on a Bruker Avance 300 MHz or a Bruker Avance 400 MHz spectrometer. Chemical shifts are reported relative to the residual non-deuterated solvent proton resonance as reference standard (d_6 -DMSO at 2.50 ppm and 39.51 ppm for ^1H NMR and ^{13}C NMR, respectively; CD_2Cl_2 at 5.32 ppm and 54.00 ppm for ^1H NMR and ^{13}C NMR, respectively; CDCl_3 at 7.27 ppm and 77.00 ppm for ^1H NMR and ^{13}C NMR).

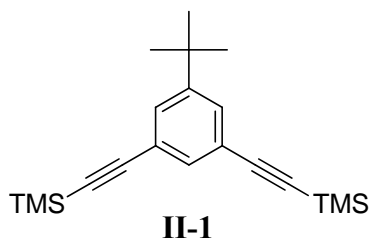
The low-resolution mass spectrometry (LRMS) and high-resolution mass spectrometry (HRMS) were taken on Kratos Concept IIHQ (EI), or Kratos MS50 (EI), or Bruker Esquire-LC (ESI) spectrometers. Mass spectra of the metal complexes were obtained by MALDI-TOF mass spectroscopy in the presence of an added matrix, 2-[(2E)-3-(4-*tert*-butylphenyl)-2-methylprop-2-enylidene]malononitrile (DCTB), on the Bruker Biflex IV instrument. UV-Visible spectra were recorded in chloroform at room temperature on Cary 5000 scan spectrophotometer. Elemental analysis was carried out on a Carlo Erba

Elemental Analyzer EA 1108.

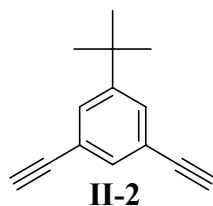
The X-ray data were obtained on a Bruker X8 APEX II diffractometer with graphite monochromated Mo-K α radiation. Data were collected and integrated using the Bruker SAINT software. The structures were solved by direct methods and refined with SHELXTL crystallographic software package of Bruker-AXS.

Besides the complexes being isolated and characterized, the remainder is composed of unidentified polymeric materials.

5.2 Experimental Procedure and Data

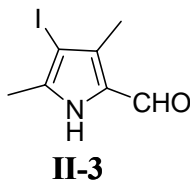


(5-tert-butyl-1,3-phenylene)bis(ethyne-2,1-diyl)bis(trimethylsilane) (II-1).⁶³ To a mixture of 1,3-dibromo-5-tert-butylbenzene (2.0 g, 6.85 mmol), CuI (40 mg, 0.2 mmol) and Pd(PPh₃)₂Cl₂ (246 mg, 0.35 mmol) in THF (25 mL) and piperidine (5 mL) was added ethynyltrimethylsilane (9.5 mL, 68.5 mmol). The reaction mixture was heated to reflux for 36 h. After removal of the organic solvent, the residue was treated with CH₂Cl₂ (50 mL). The organic layer was washed with water and brine, dried over anhydrous Na₂SO₄, and concentrated under reduced pressure to give the crude product. Flash chromatography on silica gel, eluting with hexanes, gave a pale yellow oil. Yield: 1.70 g (76%); ¹H NMR (300MHz, CD₂Cl₂) δ (ppm) 7.44 (d, *J* = 1.5 Hz, 2H, Ar-H), 7.36 (t, *J* = 1.3 Hz, 1H, Ar-H), 1.29 (s, 9H, *t*Bu), 0.24 (s, 18H, TMS).

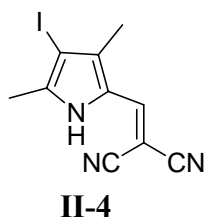


1-tert-butyl-3,5-diethynylbenzene (II-2).⁶³ To a solution of **II-1** (1.86 g, 5.70 mmol) in THF (20 mL) and MeOH (50 mL) was added KOH (0.66 g, 11.8 mmol). The reaction mixture

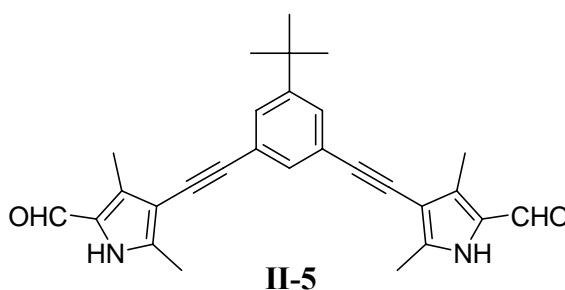
was stirred for 4 h at room temperature. After removal of the organic solvent *in vacuo*, CH₂Cl₂ (50 mL) was introduced. The organic layer was washed with water and brine, dried over anhydrous Na₂SO₄, and concentrated under reduced pressure to give the crude product. Flash chromatography on silica gel, eluting with 10% CH₂Cl₂ in hexanes, afforded a brown liquid. Yield: 1.02 g (98%); ¹H NMR (300MHz, CD₂Cl₂) δ (ppm) 7.52 (d, *J* = 1.4 Hz, 2H, Ar-H), 7.42 (t, *J* = 1.3 Hz, 1H, Ar-H), 3.13 (s, 2H, CH), 1.30 (s, 9H, *t*Bu); EI MS (M⁺): *m/z* 182. HR-EI MS (M⁺) *m/z* calcd for C₁₄H₁₄ 182.1096, found 182.1094.



4-iodo-3,5-dimethylpyrrole-2-carbaldehyde (II-3).⁶⁴ To a mixture of 3,5-dimethylpyrrole-2-carbaldehyde (0.74 g, 6 mmol) and K₂CO₃ (0.83 g, 6 mmol) in MeOH (300 mL) was added KI/I₂ (1.90/1.83 g, 11.4/7.2 mmol, dissolved in 20 mL water and 15 mL MeOH). The reaction was stirred overnight at room temperature. Saturated Na₂SO₃ was then introduced to quench the excess I₂. After removal of the organic solvent, the residue was washed with several portions of water, followed by filtration to give a white solid. Yield: 1.33 g (89%); ¹H NMR (300MHz, CD₂Cl₂) δ (ppm) 9.51 (s, 1H, CHO), 2.32 (s, 3H, CH₃), 2.26 (s, 3H, CH₃); EI MS (M⁺): *m/z* 249. HR-EI MS (M⁺) *m/z* calcd for C₇H₈NOI 248.9651, found 248.9649.

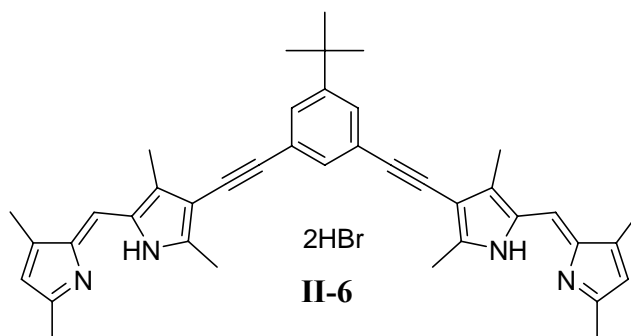


2-((4-iodo-3,5-dimethylpyrrol-2-yl)methylene)malononitrile (II-4). According to the previously reported procedure,⁶⁶ some modifications have been made for synthesis of **II-4**. To a mixture of **II-3** (1.5 g, 6 mmol) and malononitrile (0.79 g, 12 mmol) in EtOAc (20 mL) was added HNEt₂ (0.6 mL). The reaction was stirred overnight at room temperature. After removal of the organic solvent, the residue was washed with a small amount of MeOH, and filtered to give a yellow solid. Yield: 1.60 g (90%); ¹H NMR (300MHz, DMSO-*d*₆) δ (ppm) 11.56 (s, 1H, NH), 7.95 (s, 1H, CH), 2.35 (s, 3H, CH₃), 2.15 (s, 3H, CH₃); ¹³C NMR (100MHz, DMSO-*d*₆) δ (ppm) 145.1, 143.3, 139.4, 124.5, 116.2, 115.3, 76.2, 64.6, 14.7, 13.6; EI MS (M⁺): *m/z* 297. HR-EI MS (M⁺) *m/z* calcd for C₁₀H₈N₃I 296.9763, found 296.9764.



4,4'-(5-tert-butyl-1,3-phenylene)bis(ethyne-2,1-diyl)bis(3,5-dimethylpyrrole-2-carbaldehyde) (II-5). According to the previously reported procedure,⁶⁵ some modifications have been made for synthesis of **II-5**. To a mixture of **II-2** (0.40 g, 2.18 mmol), **II-4** (1.30 g, 4.36 mmol) and CuI (20 mg, 0.1 mmol) in THF (20 mL) and piperidine (10 mL) was added Pd(PPh₃)₂Cl₂

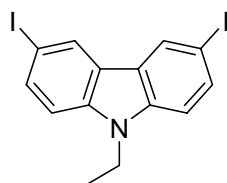
(70 mg, 0.1 mmol). The reaction mixture was purged with hydrogen at 1 atm and stirred for overnight. After removal of the organic solvent, EtOH (30 mL) was introduced, followed by addition of KOH (2.24 g, 40 mmol, dissolved in 5 mL water). The reaction mixture was refluxed for 3 h. The reaction was allowed to cool to room temperature, and then poured into 100 mL water and 100 mL CHCl₃. The organic layer was washed with water, brine and dried over anhydrous Na₂SO₄. After removal of the organic solvent, the residue was purified by flash chromatography on silica gel, eluting with 1% MeOH in CH₂Cl₂, to give a brown solid. Yield: 200 mg (22%); ¹H NMR (400MHz, DMSO-*d*₆) δ (ppm) 12.02 (br. s, 2H, NH), 9.53 (s, 2H, CHO), 7.46 (d, *J* = 1.1 Hz, 4H, Ar-H), 7.41 (t, *J* = 1.7 Hz, 2H, Ar-H), 2.37 (s, 6H, CH₃), 2.33 (s, 6H, CH₃), 1.31 (s, 9H, *t*Bu); ¹³C NMR (100MHz, DMSO-*d*₆) δ (ppm) 177.0, 151.7, 140.8, 130.3, 127.9, 127.3, 123.5, 105.3, 92.4, 83.0, 34.4, 30.8, 11.9, 9.6; EI MS (M⁺): *m/z* 424. HR-EI MS (M⁺) *m/z* calcd for C₂₈H₂₈N₂O₂ 424.2151, found 424.2149.



bisdipyririn ligand (II-6).⁶⁷ To a mixture of **II-5** (161 mg, 0.38 mmol) and 2,4-dimethylpyrrole (0.09 mL, 0.88 mmol) in THF (75 mL) and methanol (25 mL) was added 33% hydrogen bromide in acetic acid (2.0 mL). The solution quickly turned from yellow to

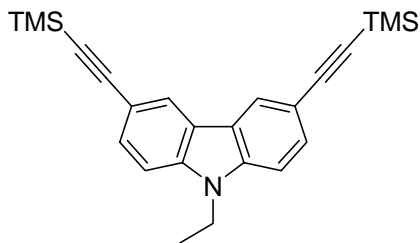
orange and then to an orange suspension. The suspension was stirred for 2 h at room temperature, and then filtered to collect the precipitate, which was rinsed with THF to give an orange solid. Yield: 250 mg (90%); $^1\text{H NMR}$ (400MHz, $\text{CDCl}_3/\text{CD}_3\text{OD} = 2/1$) δ (ppm) 7.32 (d, $J = 1.6$ Hz, 2H, Ar-H), 7.29 (m, 1H, Ar-H), 7.06 (s, 2H, *meso*-H), 6.14 (s, 2H, pyrrole-H), 2.56 (s, 6H, CH_3), 2.46 (s, 6H, CH_3), 2.32 (s, 6H, CH_3), 2.23 (s, 6H, CH_3), 1.17 (s, 9H, *t*Bu); ESI MS ($\text{M}+\text{H}$) $^+$: m/z 579.7; HR-ESI MS ($\text{M}+\text{H}$) $^+$: m/z calcd for $\text{C}_{40}\text{H}_{43}\text{N}_4$: 579.3488; found: 579.3491. UV/Vis ($\text{CHCl}_3/\text{CH}_3\text{OH} = 2/1$) λ_{max} nm (A): 501.0 (1.567).

Co^{II} bisdipyrrin complex (II-7-2).⁶⁷ To a solution of **II-6** (74 mg, 0.1 mmol) in $\text{CHCl}_3/\text{MeOH}$ (20 mL/10 mL) was added a solution of $\text{Co}(\text{OAc})_2 \cdot 4\text{H}_2\text{O}$ (37 mg, 0.15 mmol) in MeOH (1 mL). The reaction mixture was stirred for 1 h before a solution of NaOAc (82 mg, 1 mmol) in MeOH (1 mL) was added. After stirring overnight, the solvent was removed by rotary evaporation. A crude mixture of the metal complexes was obtained after filtration through a short column using silica gel and CH_2Cl_2 . The target complexes were separated by gel permeation chromatography eluting with toluene to give a green metallic solid. Yield: 11 mg (17%); MALDI-TOF calcd. 1270.5, found 1270.4 [M] $^+$; Elemental analysis (%) calcd. 8.81 (N), 75.57 (C), 6.34 (H) found 8.69 (N), 75.58 (C), 6.62 (H); UV/Vis (CHCl_3) λ_{max} nm (log ϵ): 380.0 (4.51), 516.0 (5.35).



II-8

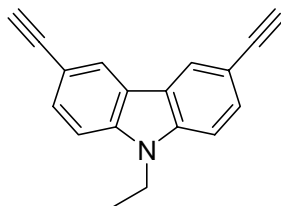
9-ethyl-3,6-diiodocarbazole (II-8). According to the previously reported procedure,⁹⁶ some modifications have been made for synthesis of **II-8**. To a solution of 9-ethylcarbazole (3.5 g, 17.9 mmol) in CHCl_3 (160 mL) and acetic acid (50 mL) was added NIS (8.4 g, 36.7 mmol). The reaction mixture was stirred overnight at room temperature. Saturated Na_2SO_3 was then introduced to quench the excess NIS. The organic layer was washed with several portions of water, saturated NaHCO_3 and brine, dried over anhydrous Na_2SO_4 , and then concentrated under reduced pressure to give the crude product. Flash chromatography on silica gel, eluting with CH_2Cl_2 , gave a yellow solid. Yield: 6.0 g (75%); ^1H NMR (300MHz, CDCl_3) δ (ppm) 8.61 (d, $J = 1.5$ Hz, 2H, carbazole-H), 7.73 (dd, $J = 8.7$ and 1.6 Hz, 2H, carbazole-H), 7.50 (d, $J = 8.6$ Hz, 2H, carbazole-H), 4.41 (q, $J = 7.2$ Hz, 2H, CH_2), 1.26 (t, $J = 7.1$ Hz, 3H, CH_3); EI MS (M^+): m/z 447. HR-EI MS (M^+) m/z calcd for $\text{C}_{14}\text{H}_{11}\text{NI}_2$ 446.8981, found 446.8977.



II-9

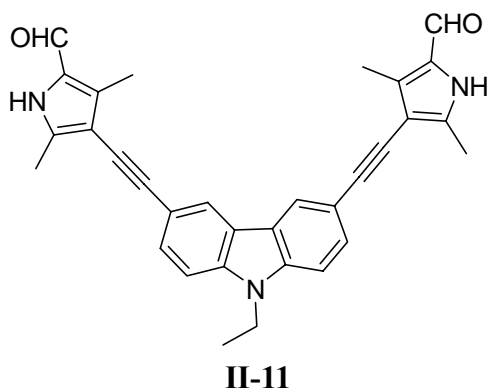
9-ethyl-3,6-bis(trimethylsilyl)ethynylcarbazole (II-9). According to the previously reported procedure,⁶³ some modifications have been made for synthesis of **II-9**. To a mixture of

II-8 (1.8 g, 4.03mmol), CuI (40 mg, 0.2 mmol) and Pd(PPh₃)₂Cl₂ (140 mg, 0.2 mmol) in THF (45 mL) and piperidine (10 mL) was added ethynyltrimethylsilane (3.4 mL, 24.2 mmol). The reaction mixture was stirred overnight at room temperature. After removal of the organic solvent, the residue was dissolved in CH₂Cl₂ (50 mL). The organic layer was washed by water and brine, dried over anhydrous Na₂SO₄, and then concentrated under reduced pressure to give the crude product. Flash chromatography on silica gel, eluting with hexanes, gave a yellow oil. Yield: 1.40 g (90%); ¹H NMR (300MHz, CDCl₃) δ (ppm) 8.21 (d, *J* = 0.9 Hz, 2H, carbazole-H), 7.59 (dd, *J* = 8.4 and 1.3 Hz, 2H, carbazole-H), 7.32 (d, *J* = 8.7 Hz, 2H, carbazole-H), 4.34 (q, *J* = 7.3 Hz, 2H, CH₂), 1.43 (t, *J* = 7.3 Hz, 3H, CH₃), 0.30 (s, 18H, TMS); EI MS (M⁺): *m/z* 387. HR-EI MS (M⁺) *m/z* calcd for C₂₄H₂₉NSi₂ 387.1839, found 387.1838.

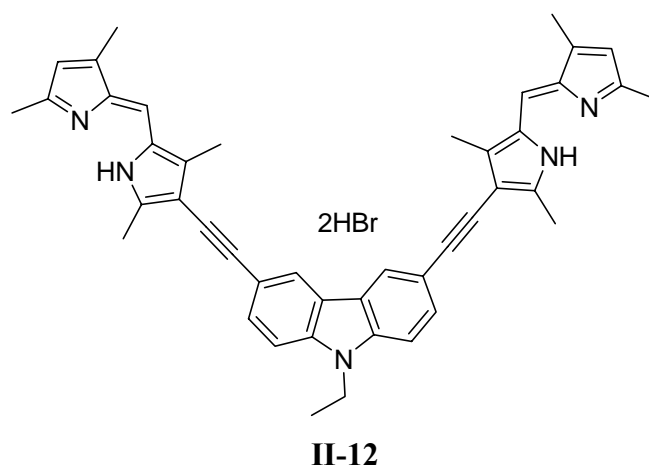


II-10

9-ethyl-3,6-diethynylcarbazole (II-10). The same procedure was used as in the synthesis of **II-2**, starting from **II-9** (2.20 g, 5.70 mmol) to afford pale yellow needles. Yield: 1.37 g (99%); ¹H NMR (300MHz, CDCl₃) δ (ppm) 8.23 (d, *J* = 0.9 Hz, 2H, carbazole-H), 7.62 (dd, *J* = 8.6 and 1.5 Hz, 2H, carbazole-H), 7.34 (d, *J* = 8.8 Hz, 2H, carbazole-H), 4.34 (q, *J* = 7.0 Hz, 2H, CH₂), 3.10 (s, 2H, CH), 1.43 (t, *J* = 7.3 Hz, 3H, CH₃); EI MS (M⁺): *m/z* 243. HR-EI MS (M⁺) *m/z* calcd for C₁₈H₁₃N 243.1048, found 243.1046.

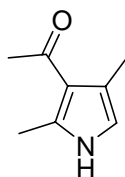


4,4'-(9-ethyl-9H-carbazole-3,6-diyl)bis(ethyne-2,1-diyl)bis(3,5-dimethyl-1H-pyrrole-2-carbaldehyde) (II-11). The same procedure was used as in the synthesis of **II-5**, starting from **II-10** (0.53 g, 2.18 mmol) to afford a brown solid. Yield: 0.39 g (37%); ^1H NMR (400MHz, $\text{DMSO-}d_6$) δ (ppm) 11.98 (br. s, 2H, NH), 9.54 (s, 2H, CHO), 8.43 (s, 2H, carbazole-H), 7.65 (d, $J = 8.7$ Hz, 2H, carbazole-H), 7.59 (dd, $J = 8.5$ and 1.8 Hz, 2H, carbazole-H), 4.47 (q, $J = 7.6$ Hz, 2H, CH_2), 2.41 (s, 6H, CH_3), 2.37 (s, 6H, CH_3), 1.33 (t, $J = 7.6$ Hz, 3H, CH_3); ^{13}C NMR (100MHz, $\text{DMSO-}d_6$) δ (ppm) 176.9, 140.2, 139.3, 129.2, 127.9, 123.7, 121.9, 113.8, 109.7, 106.1, 106.0, 93.9, 80.6, 37.2, 13.7, 12.0, 9.7; EI MS (M^+): m/z 485. HR-EI MS (M^+) m/z calcd for $\text{C}_{32}\text{H}_{27}\text{N}_3\text{O}_2$ 485.2103, found 485.2101.



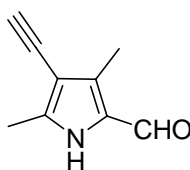
bisdipyrrin ligand (II-12). The same procedure was used as in the synthesis of **II-6**, starting from **II-11** (184 mg, 0.38 mmol) to afford a red solid. Yield: 265 mg (87%); $^1\text{H NMR}$ (400MHz, $\text{CDCl}_3/\text{CD}_3\text{OD} = 2/1$) δ (ppm) 8.07 (s, 2H, carbazole-H), 7.45 (d, $J = 8.5$ Hz, 2H, carbazole-H), 7.25 (d, $J = 8.4$ Hz, 2H, carbazole-H), 7.05 (s, 2H, *meso*-H), 6.12 (s, 2H, pyrrole-H), 2.58 (s, 6H, CH_3), 2.44 (s, 6H, CH_3), 2.34 (s, 6H, CH_3), 2.23 (s, 6H, CH_3), 1.27 (t, $J = 7.0$ Hz, 3H, CH_3); ESI MS ($\text{M}+\text{H}$) $^+$: m/z 640.8; HR-ESI MS ($\text{M}+\text{H}$) $^+$: m/z calcd for $\text{C}_{44}\text{H}_{42}\text{N}_5$: 640.3440; found: 640.3450. UV/Vis ($\text{CHCl}_3/\text{CH}_3\text{OH} = 2/1$) λ_{max} nm (A): 500.0 (0.958).

Co^{II} bisdipyrrin complex (II-13-2). The same procedure was used as in the synthesis of **II-7-2**, starting from **II-12** (80 mg, 0.1 mmol) to afford a green metallic solid. Yield: 15 mg (22%); MALDI-TOF calcd. 1392.5, found 1392.3 [M] $^+$; UV/Vis (CHCl_3) λ_{max} nm ($\log \epsilon$): 380.1 (4.63), 515.0 (5.38).



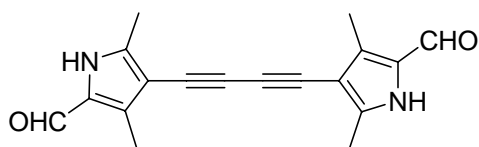
II-14

1-(2,4-dimethylpyrrol-3-yl)ethanone (II-14).⁷⁰ To *t*-butyl 4-acetyl-3,5-dimethylpyrrole-2-carboxylate (0.95 g, 4 mmol) in a 50 mL round-bottom flask was added TFA (10 mL). The reaction mixture was stirred for 2 h at room temperature. After the mixture was poured into well-stirred 500 mL ice-water, a pink solid started to precipitate. The precipitate was collected by filtration and washed with a large amount of water to remove the TFA to give a pink solid. Yield: 320 mg (58%); ¹H NMR (300MHz, DMSO-*d*₆) δ (ppm) 10.88 (br. s, 1H, NH), 6.38 (s, 1H, pyrrole-H), 2.38 (s, 3H, CH₃), 2.29 (s, 3H, CH₃), 2.14 (s, 3H, CH₃); EI MS (M⁺): *m/z* 137. HR-EI MS (M⁺) *m/z* calcd for C₈H₁₁NO 137.0841, found 137.0841.



II-15

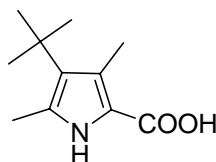
4-ethynyl-3,5-dimethylpyrrole-2-carbaldehyde (II-15). The previously reported procedure⁷¹ was used as in the synthesis of **II-15**, starting from **II-14** (9.0 g, 65.6 mmol) to afford a white solid. Yield: 2.86 g (30%); ¹H NMR (300MHz, DMSO-*d*₆) δ (ppm) 11.92 (br. s, 1H, NH), 9.49 (s, 1H, CHO), 4.12 (s, 1H, CH), 2.27 (s, 3H, CH₃), 2.24 (s, 3H, CH₃); EI MS (M⁺): *m/z* 147. HR-EI MS (M⁺) *m/z* calcd for C₉H₉NO 147.0684, found 147.0683.



II-16

4,4'-(buta-1,3-diyne-1,4-diyl)bis(3,5-dimethylpyrrole-2-carbaldehyde) (II-16).

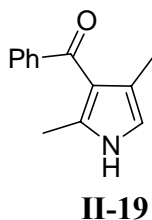
According to the previously reported procedure,⁶⁵ some modifications have been made for synthesis of **II-16**. To a mixture of **II-15** (250 mg, 1.70 mmol), Pd(PPh₃)₂Cl₂ (120 mg, 0.17 mmol) and α -chloroacetone (0.6 mL, 7.8 mmol) in THF (20 mL) was added NEt₃ (1 mL). The mixture was stirred for 1 h at room temperature. After addition of CuI (50 mg, 0.26 mmol), the reaction mixture was stirred overnight. After removal of the organic solvent, the residue was purified by flash chromatography on silica gel, eluting with 1% MeOH in CH₂Cl₂, to give a yellow solid. Yield: 125 mg (50%); ¹H NMR (300MHz, DMSO-*d*₆) δ (ppm) 12.11 (br. s, 2H, NH), 9.52 (s, 2H, CHO), 2.32 (s, 6H, CH₃), 2.29 (s, 6H, CH₃); ¹³C NMR (75MHz, DMSO-*d*₆) δ (ppm) 177.3, 142.9, 127.8, 104.1, 86.4, 77.5, 75.4, 12.1, 9.7; EI MS (M⁺): *m/z* 292. HR-EI MS (M⁺) *m/z* calcd for C₁₈H₁₆N₂O₂ 292.1212, found 292.1215.



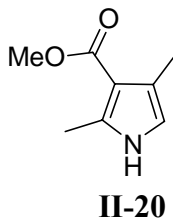
II-17

4-*t*-butyl-3,5-dimethylpyrrole-2-carboxylic acid (II-17).⁹⁷ To a solution of ethyl 4-*t*-butyl-3,5-dimethylpyrrole-2-carboxylate (0.56 g, 2.5 mmol) in EtOH (30 mL) was added KOH (1.4 g, 25 mmol, dissolved in 5 mL water). The reaction mixture was refluxed for 3 h.

After removal of the solvent, the residue was treated with 400 mL water, followed by addition of acetic acid to generate the precipitate. The precipitate was filtered and washed with several portions of water to remove excess acetic acid to give a pink solid. Yield: 385 mg (79%); ^1H NMR (300MHz, $\text{DMSO-}d_6$) δ (ppm) 11.81 (br. s, 1H, NH), 10.77 (s, 1H, COOH), 2.37 (s, 3H, CH_3), 2.27 (s, 3H, CH_3), 1.29 (s, 9H, *t*Bu); ^{13}C NMR (100MHz, CDCl_3) δ (ppm) 166.3, 129.6, 129.6, 129.3, 116.2, 33.0, 31.7, 16.5, 13.5; EI MS (M^+): m/z 195. HR-EI MS (M^+) m/z calcd for $\text{C}_{11}\text{H}_{17}\text{NO}_2$ 195.1259, found 195.1260.

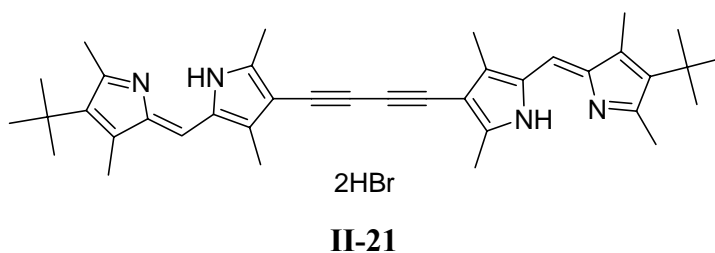


(2,4-dimethyl-1H-pyrrol-3-yl)(phenyl)methanone (II-19). The previously reported procedure⁹⁸ was used as in the synthesis of **II-19** to afford a brown solid. Yield: 305 mg (28%); ^1H NMR (300MHz, CDCl_3) δ (ppm) 8.15 (br. s, 1H, NH), 7.69 – 7.72 (m, 2H, Ar-H), 7.49 – 7.53 (m, 1H, Ar-H), 7.40 – 7.45 (m, 2H, Ar-H), 6.42 (s, 1H, pyrrole-H), 2.18 (s, 3H, CH_3), 2.00 (s, 3H, CH_3); EI MS (M^+): m/z 199. HR-EI MS (M^+) m/z calcd for $\text{C}_{13}\text{H}_{13}\text{NO}$ 199.0997, found 199.0996.

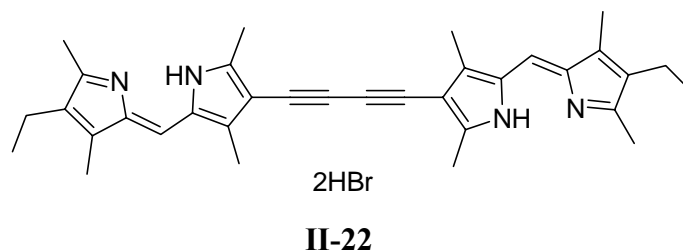


Methyl 2,4-dimethylpyrrole-3-carboxylate (II-20). The same procedure was used as in the

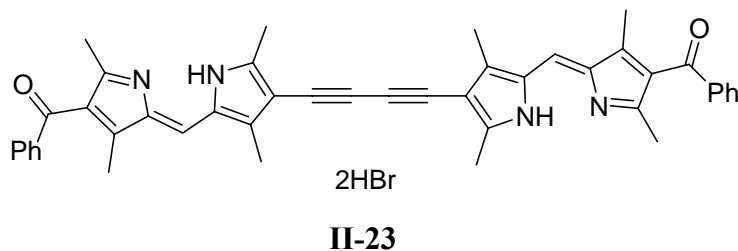
synthesis of **II-14**, starting from 2-*t*-butyl 4-methyl 3,5-dimethylpyrrole-2,4-dicarboxylate (1.01 g, 4 mmol) to afford a pink solid. Yield: 550 mg (90%); ^1H NMR (400MHz, CDCl_3) δ (ppm) 7.94 (br. s, 1H, NH), 6.36 (s, 1H, pyrrole-H), 3.81 (s, 3H, CH_3), 2.49 (s, 3H, CH_3), 2.24 (s, 3H, CH_3); EI MS (M^+): m/z 153. HR-EI MS (M^+) m/z calcd for $\text{C}_8\text{H}_{11}\text{NO}_2$ 153.0790, found 153.0788.



bisdipyrin ligand (II-21).⁶⁷ To a mixture of **II-16** (200 mg, 0.68 mmol) and **II-17** (332 mg, 1.7 mmol) in THF (75 mL) and MeOH (25 mL) at 75°C was added 33% hydrogen bromide in acetic acid (2.0 mL). The reaction mixture was stirred for 4 h at 75°C. Removal of the organic solvent gave the crude product as a red solid. Trituration of the crude solid with diethyl ether gave a red solid. Yield: 370 mg (76%); ^1H NMR (300MHz, CD_2Cl_2) δ (ppm) 13.49 (br. s, 2H, NH), 13.18 (br. s, 2H, NH), 7.18 (s, 2H, *meso*-H), 2.91 (s, 6H, CH_3), 2.73 (s, 6H, CH_3), 2.48 (s, 6H, CH_3), 2.44 (s, 6H, CH_3), 1.41 (s, 18H, *t*Bu); ^{13}C NMR (75MHz, CD_2Cl_2) δ (ppm) 159.8, 156.3, 146.5, 144.3, 138.0, 128.6, 125.4, 120.0, 110.7, 80.3, 74.8, 33.8, 31.5, 18.0, 13.7, 13.6, 11.8; ESI MS ($\text{M}+\text{H}$)⁺: m/z 559.5; Anal. Calcd. for: $\text{C}_{38}\text{H}_{38}\text{Br}_2\text{N}_4$: C, 63.34; H, 6.71; N, 7.77. Found: C, 62.96; H, 6.83; N, 7.90; UV/Vis (CHCl_3) λ_{max} nm (log ϵ): 531.0 (5.15).

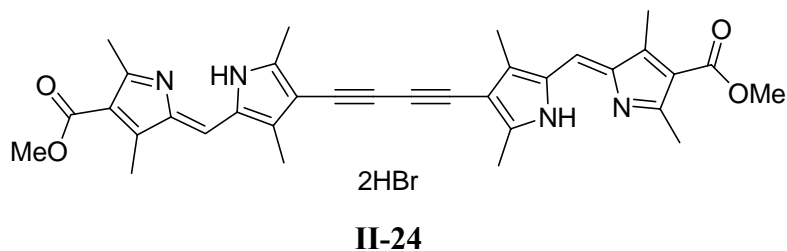


bisdipyrryn ligand (II-22). According to the previously reported procedure,⁶⁷ some modifications have been made for synthesis of **II-22**. To a mixture of **II-16** (100 mg, 0.34 mmol) and **II-18** (0.09 ml, 0.68 mmol) in THF (75 mL) and MeOH (25 mL) was added 33% hydrogen bromide in acetic acid (2.0 mL). The solution quickly turned from yellow to dark red, and then to a red suspension. The suspension was stirred for 2 h at room temperature, and then filtered to collect the precipitate, which was rinsed with THF to give a red solid. Yield: 180 mg (80%); ¹H NMR (400MHz, CDCl₃/CD₃OD = 2/1) δ (ppm) 7.01 (s, 2H, *meso*-H), 2.47 (s, 6H, CH₃), 2.43 (s, 6H, CH₃), 2.30 (q, *J* = 7.6 Hz, 4H, CH₂), 2.26 (s, 6H, CH₃), 2.15 (s, 6H, CH₃), 0.91 (t, *J* = 7.6 Hz, 6H, CH₃); ESI MS (M+H)⁺: *m/z* 503.5; HR-ESI MS (M+H)⁺: *m/z* calcd for C₃₄H₃₉N₄: 503.3175; found: 503.3177. UV/Vis (CHCl₃/CH₃OH = 2/1) λ_{max} nm (A): 525.0 (1.084).



bisdipyrryn ligand (II-23). The same procedure was used as in the synthesis of **II-22**, starting from **II-16** (100 mg, 0.34 mmol) and **II-19** (136 mg, 0.68 mmol) to give a red solid. Yield: 180 mg (65%); ¹H NMR (400MHz, CDCl₃/CD₃OD = 2/1) δ (ppm) 7.55 (d, *J* = 7.6 Hz, 4H, Ar-H), 7.46 (t, *J* = 7.5 Hz, 2H, Ar-H), 7.32 (t, *J* = 7.6 Hz, 4H, Ar-H), 7.23 (s, 2H, *meso*-H),

2.59 (s, 6H, CH₃), 2.41 (s, 6H, CH₃), 2.34 (s, 6H, CH₃), 2.15 (s, 6H, CH₃); ¹³C NMR (100MHz, CDCl₃/CD₃OD = 2/1) δ (ppm) 191.9, 160.2, 156.6, 150.0, 145.4, 137.9, 133.5, 128.8, 128.6, 128.1, 126.7, 126.0, 122.5, 112.4, 80.6, 73.4, 13.8, 13.2, 11.3, 11.1; ESI MS (M+H)⁺: *m/z* 655.6; HR-ESI MS (M+H)⁺: *m/z* calcd for C₄₄H₃₉N₄O₂: 655.3073; found: 655.3086. UV/Vis (CHCl₃/CH₃OH = 2/1) λ_{max} nm (A): 531.0 (1.141).



bisdipyrrin ligand (II-24). The same procedure was used as in the synthesis of **II-22**, starting from **II-16** (100 mg, 0.34 mmol) and **II-20** (104 mg, 0.68 mmol) to give a dark red solid. Yield: 150 mg (64%); ¹H NMR (400MHz, CDCl₃/CD₃OD = 2/1) δ (ppm) 7.27 (s, 2H, *meso*-H), 3.70 (s, 6H, CH₃), 2.70 (s, 6H, CH₃), 2.59 (s, 6H, CH₃), 2.46 (s, 6H, CH₃), 2.34 (s, 6H, CH₃); ESI MS (M+H)⁺: *m/z* 563.6; HR-ESI MS (M+H)⁺: *m/z* calcd for C₃₄H₃₅N₄O₄: 563.2658; found: 563.2667. UV/Vis (CHCl₃/CH₃OH = 2/1) λ_{max} nm (A): 522.0 (0.533).

Zn^{II} bisdipyrrin complexes (II-25).⁶⁷ To a solution of **II-21** (72 mg, 0.1 mmol) in CHCl₃/MeOH (20 mL/10 mL) was added a solution of Zn(OAc)₂•2H₂O (33 mg, 0.15 mmol) in MeOH (1 mL), followed by addition of a solution of NaOAc (82 mg, 1 mmol) in MeOH (1 mL). After stirring overnight, the solvent was removed by rotary evaporation. A crude mixture of the metal complexes was obtained after filtration through a short column using silica gel and

CH₂Cl₂. The crude compound was then purified using gel permeation chromatography eluting with toluene. The target metal complexes were obtained as dichroic red/green solids.

II-25-3 (trimer): Yield: 12 mg (19%); ¹H NMR (CDCl₃, 300 MHz) δ (ppm) 7.02 (s, 6H, *meso*-H), 2.38-2.40 (m, 36H, CH₃), 2.11-2.13 (m, 18H, CH₃), 1.95-2.00 (m, 18H, CH₃), 1.33 (s, 54H, *t*-Bu); ¹³C NMR (CD₂Cl₂, 75 MHz) δ (ppm) 162.1, 158.9, 142.2, 139.6, 138.6, 137.5, 134.9, 121.7, 109.6, 79.9, 78.4, 33.6, 31.9, 20.3, 15.4, 13.3, 11.4; MALDI-TOF calcd. 1860.9, found 1860.9 [(M)⁺]; Anal. Calcd. for: C₁₁₄H₁₃₂N₁₂Zn₃: C, 73.36; H, 7.13; N, 9.01. Found: C, 73.35; H, 7.36; N, 8.76; UV/Vis (CHCl₃) λ_{max} nm (logε): 544.0 (5.81).

II-25-4 (tetramer): Yield: 2 mg (3%); ¹H NMR (CDCl₃, 300 MHz) δ (ppm) 7.01 (s, 6H, *meso*-H), 2.37-2.39 (m, 36H, CH₃), 2.12 (s, 18H, CH₃), 1.98 (d, *J* = 7.7 Hz, 18H, CH₃), 1.33 (d, *J* = 2.5 Hz, 54H, *t*-Bu); MALDI-TOF calcd. 2481.1, found 2481.1 [(M)⁺]; UV/Vis (CHCl₃) λ_{max} nm (logε): 544.0 (5.93).

II-25-5 (pentamer): Yield: trace; MALDI-TOF calcd. 3101.4, found 3101.3 [(M)⁺];

Zn^{II} bisdipyrrin complexes (II-26). The same procedure was used as in the synthesis of **II-25**, starting from **II-22** (66 mg, 0.1 mmol) to afford dichroic red/green solids.

II-26-3 (trimer): Yield: 10 mg (17%); ¹H NMR (CDCl₃, 300 MHz) δ (ppm) 6.97 (s, 6H, *meso*-H), 2.32-2.40 (m, 30H, CH₂ and CH₃), 2.23 (s, 18H, CH₃), 1.93-2.01 (m, 36H, CH₃), 1.02 (t, *J* = 7.5 Hz, 18H, CH₃); ¹³C NMR (CDCl₃, 100 MHz) δ (ppm) 161.3, 158.9, 141.9, 139.3, 137.8, 134.0, 132.0, 121.3, 109.1, 79.4, 77.8, 17.9, 15.2, 14.8, 14.7, 11.1, 9.8; MALDI-TOF calcd. 1692.7, found 1692.8 [(M)⁺]; UV/Vis (CHCl₃) λ_{max} nm (logε): 542.0 (5.82).

II-26-4 (tetramer): Yield: 1 mg (2%); ¹H NMR (CDCl₃, 300 MHz) δ (ppm) 6.96 (s, 6H,

meso-H), 2.33-2.39 (m, 30H, CH₂ and CH₃), 2.22 (s, 18H, CH₃), 2.01 (dd, $J = 9.1, 2.4$ Hz, 18H, CH₃), 1.92 (s, 18H, CH₃), 1.02 (dt, $J = 7.4, 2.4$ Hz, 18H, CH₃); MALDI-TOF calcd. 2256.9, found 2256.9 [(M)⁺]; UV/Vis (CHCl₃) λ_{\max} nm (log ϵ): 542.0 (5.90).

II-26-5 (pentamer): Yield: trace; MALDI-TOF calcd. 2821.1, found 2821.2 [(M)⁺];

Zn^{II} bisdipyrin complexes (II-27). The same procedure was used as in the synthesis of **II-25**, starting from **II-23** (82 mg, 0.1 mmol) to afford dichroic red/green solids.

II-27-3 (trimer): Yield: 13 mg (18%); ¹H NMR (CDCl₃, 400 MHz) δ (ppm) 7.71 (dd, $J = 7.0, 1.4$ Hz, 12H, Ar-H), 7.53-7.56 (m, 6H, Ar-H), 7.43-7.47 (m, 12H, Ar-H), 7.19 (d, $J = 1.8$ Hz, 6H, *meso*-H), 2.43-2.45 (m, 18H, CH₃), 2.23 (s, 18H, CH₃), 2.02-2.09 (m, 36H, CH₃); ¹³C NMR (CDCl₃, 100 MHz) δ (ppm) 194.0, 163.6, 159.7, 147.1, 144.1, 144.0, 140.3, 136.9, 136.3, 132.3, 129.1, 128.4, 124.2, 112.4, 80.5, 77.5, 29.7, 16.8, 12.0, 11.4; MALDI-TOF calcd. 2148.6, found 2148.7 [(M)⁺]; UV/Vis (CHCl₃) λ_{\max} nm (log ϵ): 554.0 (5.68).

II-27-4 (tetramer): Yield: 7 mg (10%); ¹H NMR (CDCl₃, 300 MHz) δ (ppm) 7.71 (dd, $J = 6.9, 1.2$ Hz, 12H, Ar-H), 7.55 (dt, $J = 7.2, 1.1$ Hz, 6H, Ar-H), 7.45 (dt, $J = 7.1, 1.3$ Hz, 12H, Ar-H), 7.19 (s, 6H, *meso*-H), 2.44 (d, $J = 2.6$ Hz, 18H, CH₃), 2.22 (s, 18H, CH₃), 2.11 (d, $J = 3.9$ Hz, 18H, CH₃), 2.03 (s, 18H, CH₃); MALDI-TOF calcd. 2872.7, found 2872.6 [(M)⁺]; UV/Vis (CHCl₃) λ_{\max} nm (log ϵ): 553.0 (5.82).

II-27-5 (pentamer): Yield: 2 mg (3%); ¹H NMR (CDCl₃, 400 MHz) δ (ppm) 7.71 (d, $J = 7.6$ Hz, 12H, Ar-H), 7.54 (t, $J = 6.9$ Hz, 6H, Ar-H), 7.45 (t, $J = 7.0$ Hz, 12H, Ar-H), 7.19 (s, 6H, *meso*-H), 2.43 (s, 18H, CH₃), 2.22 (s, 18H, CH₃), 2.12 (s, 18H, CH₃), 2.01 (s, 18H, CH₃); MALDI-TOF calcd. 3590.9, found 3592.0 [(M)⁺]; UV/Vis (CHCl₃) λ_{\max} nm (log ϵ): 553.0 (5.92).

Zn^{II} bisdipyrin complexes (II-28). The same procedure was used as in the synthesis of **II-25**, starting from **II-24** (72 mg, 0.1 mmol) to afford dichroic red/green solids.

II-28-3 (trimer): Yield: 9 mg (15%); ¹H NMR (CDCl₃, 300 MHz) δ (ppm) 7.23 (t, *J* = 2.1 Hz, 6H, *meso*-H), 3.80 (d, *J* = 2.4 Hz, 18H, CH₃), 2.58 (s, 18H, CH₃), 2.42-2.45 (m, 18H, CH₃), 2.22 (s, 18H, CH₃), 1.94-2.00 (m, 18H, CH₃); ¹³C NMR (CDCl₃, 100 MHz) δ (ppm) 165.6, 163.5, 160.6, 147.3, 146.9, 136.9, 135.8, 124.3, 118.5, 112.4, 80.4, 77.5, 50.7, 17.5, 15.4, 12.2, 11.4; MALDI-TOF calcd. 1872.5, found 1872.3 [(M)⁺]; UV/Vis (CHCl₃) λ_{max} nm (logε): 545.0 (5.77).

II-28-4 (tetramer): Yield: 3 mg (5%); ¹H NMR (CDCl₃, 400 MHz) δ (ppm) 7.21-7.23 (m, 6H, *meso*-H), 3.80 (d, *J* = 3.8 Hz, 18H, CH₃), 2.58 (t, *J* = 2.6 Hz, 18H, CH₃), 2.41-2.45 (m, 18H, CH₃), 2.21 (s, 18H, CH₃), 2.01 (d, *J* = 9.7 Hz, 18H, CH₃); MALDI-TOF calcd. 2504.1, found 2504.6 [(M)⁺]; UV/Vis (CHCl₃) λ_{max} nm (logε): 544.0 (5.84).

Co^{II} bisdipyrin complexes (II-29). The same procedure was used as in the synthesis of **II-25**, starting from **II-22** (66 mg, 0.1 mmol) and Co(OAc)₂•4H₂O (38 mg, 0.15 mmol) to afford dichroic purple/green solids.

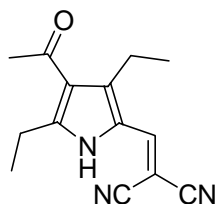
II-29-3 (trimer): Yield: 4 mg (8%); MALDI-TOF calcd. 1677.7, found 1677.7 [(M)⁺]; UV/Vis (CHCl₃) λ_{max} nm (logε): 540.0 (5.54).

II-29-4 (tetramer): Yield: 2 mg (4%); MALDI-TOF calcd. 2236.9, found 2236.9 [(M)⁺]; UV/Vis (CHCl₃) λ_{max} nm (logε): 541.0 (5.73).

Ni^{II} bisdipyrin complexes (II-30). The same procedure was used as in the synthesis of **II-25**, starting from **II-22** (66 mg, 0.1 mmol) and Ni(OAc)₂•4H₂O (38 mg, 0.15 mmol) to afford dichroic brown/green solids.

II-30-3 (trimer): Yield: 4 mg (8%); MALDI-TOF calcd. 1674.7, found 1674.9 [(M)⁺]; UV/Vis (CHCl₃) λ_{max} nm (logε): 580.0 (5.40).

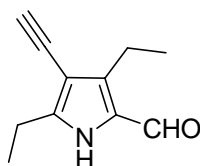
II-30-4 (tetramer): Yield: 2 mg (3%); MALDI-TOF calcd. 2232.9, found 2233.1 [(M)⁺]; UV/Vis (CHCl₃) λ_{max} nm (logε): 582.0 (5.50).



II-31

2-((4-acetyl-3,5-diethylpyrrol-2-yl)methylene)malononitrile (II-31). According to the previously reported procedure,⁷⁰ some modifications have been made for synthesis of **II-31**. To a solution of 2-((3,5-diethylpyrrol-2-yl)methylene)malononitrile (1 g, 5 mmol) in MeNO₂ (10 mL) and DCE (10 mL) at 0°C was slowly added SnCl₄ (0.62 mL, 5.3 mmol) and acetyl chloride (0.38 mL, 5.3 mmol). The reaction mixture was stirred for 5 h at room temperature. The mixture was poured into 100 mL water and 100 CH₂Cl₂, and the organic layer was washed with 10% HCl solution, water, brine and dried over anhydrous Na₂SO₄. After removal of the organic solvent, the residue was purified by flash chromatography on silica gel, eluting with CH₂Cl₂, to give a yellow solid. Yield: 0.90 g (75%); ¹H NMR (400MHz, CDCl₃) δ (ppm) 9.77 (br. s, 1H, NH), 7.50 (s, 1H, CH), 3.06 (q, *J* = 7.6 Hz, 2H, CH₂), 2.86 (q, *J* = 7.6 Hz, 2H, CH₂), 2.51 (s, 3H, NH),

CH₃), 1.37 (t, $J = 7.5$ Hz, 3H, CH₃), 1.21 (t, $J = 7.5$ Hz, 3H, CH₃); ¹³C NMR (100MHz, CDCl₃) δ (ppm) 194.1, 150.6, 144.4, 141.9, 123.5, 122.7, 116.6, 114.6, 31.0, 22.4, 18.8, 16.8, 11.4; EI MS (M⁺): m/z 241. HR-EI MS (M⁺) m/z calcd for C₁₄H₁₅N₃O 241.1215, found 241.1214.

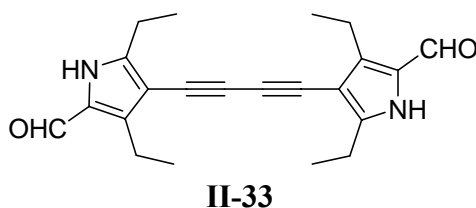


II-32

3,5-diethyl-4-ethynylpyrrole-2-carbaldehyde (II-32). According to the previously reported procedure,⁷¹ some modifications have been made for synthesis of **II-32**. To a solution of DMF (2.5 mL) cooled in an ice-water bath was slowly added POCl₃ (0.4 mL, 4 mmol). The reaction mixture was stirred for 30 min, followed by addition of **II-31** (0.90 g, 3.73 mmol, dissolved in 10 mL DMF). The mixture was heated to 40°C and stirred for 3 h. The reaction was poured into a well-stirred 200 mL ice/water to give a precipitate. The precipitate was collected by filtration to give a yellow solid. To the yellow solid (1.06 g, 4.08 mmol) in EtOH (30 mL) was added KOH (2.29 g, 40.8 mmol, dissolved in 5 mL water). The reaction mixture was refluxed for 3 h. The reaction was allowed to cool to room temperature, and was then poured into 100 mL water and 100 mL CH₂Cl₂. The organic layer was washed with water, brine and dried over anhydrous Na₂SO₄. After removal of the organic solvent, the residue was purified by flash chromatography on silica gel, eluting with 10% EtOAc in hexanes, to give a white solid. Yield: 0.38 g (53%); ¹H NMR (400MHz, CDCl₃) δ (ppm) 9.92 (br. s, 1H, NH), 9.52 (s, 1H, CHO), 3.21 (s, 1H, CH), 2.76 – 2.85 (m, 4H), 1.28 – 1.32 (m, 6H); ¹³C NMR (100MHz, CDCl₃)

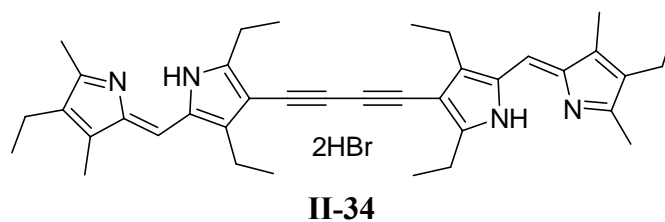
δ (ppm) 176.6, 147.7, 143.0, 126.9, 104.2, 81.2, 20.3, 18.0, 16.2, 12.7; EI MS (M^+): m/z 175.

HR-EI MS (M^+) m/z calcd for $C_{11}H_{13}NO$ 175.0997, found 175.0996.



4,4'-(buta-1,3-diyne-1,4-diyl)bis(3,5-diethyl-1H-pyrrole-2-carbaldehyde) (II-33).

According to the previously reported procedure,⁶⁵ some modifications have been made for synthesis of **II-33**. To a mixture of **II-32** (298 mg, 1.7mmol), $Pd(PPh_3)_2Cl_2$ (120 mg, 0.17mmol) and α -chloroacetone (0.6 mL, 7.8 mmol) in THF (20 mL) was added NEt_3 (1 mL). The mixture was stirred for 1 h at room temperature. After addition of CuI (50 mg, 0.26 mmol), the reaction mixture was stirred overnight. After removal of the organic solvent, the residue was purified by flash chromatography on silica gel, eluting with 1% MeOH in CH_2Cl_2 , to give a yellow solid. Yield: 143 mg (48%); 1H NMR (400MHz, $DMSO-d_6$) δ (ppm) 12.08 (br. s, 2H, NH), 9.55 (s, 2H, CHO), 2.76 (q, $J = 7.6$ Hz, 4H, CH_2), 2.67 (q, $J = 7.6$ Hz, 4H, CH_2), 1.20 (t, $J = 7.6$ Hz, 6H, CH_3), 1.19 (t, $J = 7.6$ Hz, 6H, CH_3); ^{13}C NMR (100MHz, $DMSO-d_6$) δ (ppm) 177.4, 148.5, 141.0, 127.0, 102.1, 77.4, 75.2, 19.8, 17.6, 16.2, 13.4; EI MS (M^+): m/z 348. HR-EI MS (M^+) m/z calcd for $C_{22}H_{24}N_2O_2$ 348.1838, found 348.1843.



bisdipyririn ligand (II-34). The same procedure was used as in the synthesis of **II-22**, starting from **II-33** (118 mg, 0.34 mmol) and **II-18** (0.09 mL, 0.68 mmol) to give a dark red solid. Yield: 200 mg (82%); ^1H NMR (400MHz, CDCl_3) δ (ppm) 13.46 (br. s, 2H, NH), 13.12 (br. s, 2H, NH), 7.08 (s, 2H, *meso*-H), 3.18 (q, $J = 7.6$ Hz, 4H, CH_2), 2.83 (q, $J = 7.6$ Hz, 4H, CH_2), 2.73 (s, 6H, CH_3), 2.46 (q, $J = 7.6$ Hz, 4H, CH_2), 2.31 (s, 6H, CH_3), 1.46 (t, $J = 7.4$ Hz, 6H, CH_3), 1.31 (t, $J = 7.6$ Hz, 6H, CH_3), 1.09 (t, $J = 7.6$ Hz, 6H, CH_3); ^{13}C NMR (100MHz, CDCl_3) δ (ppm) 161.7, 159.4, 152.3, 143.8, 132.6, 128.1, 123.6, 119.3, 108.3, 79.9, 74.1, 21.2, 19.6, 17.2, 16.2, 14.2, 13.8, 13.2, 10.1; ESI MS ($\text{M}+\text{H}$) $^+$: m/z 559.6; HR-ESI MS ($\text{M}+\text{H}$) $^+$: m/z calcd for $\text{C}_{38}\text{H}_{47}\text{N}_4$: 559.3801; found: 559.3802. UV/Vis (CHCl_3) λ_{max} nm (log ϵ): 529.0 (5.17).

Zn^{II} bisdipyririn complexes (II-35). The same procedure was used as in the synthesis of **II-25**, starting from **II-34** (72 mg, 0.1 mmol) to afford dichroic red/green solids.

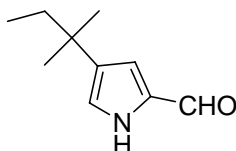
II-35-3 (trimer): Yield: 7 mg (12%); ^1H NMR (300MHz, CDCl_3) δ (ppm) 6.97 (s, 6H, *meso*-H), 2.75-2.81 (m, 12H, CH_2), 2.24-2.38 (m, 42H, CH_2 and CH_3), 2.00 (s, 18H, CH_3), 1.23-1.33 (m, 30H, CH_2 and CH_3), 0.99-1.04 (m, 18H, CH_3), 0.74 (ddt, $J = 12.7$, 6.3 and 1.7 Hz, 18H, CH_3); ^{13}C NMR (100MHz, CDCl_3) δ (ppm) 165.1, 160.6, 149.0, 139.7, 137.4, 133.1, 131.8, 121.2, 107.4, 79.6, 77.8, 23.7, 19.4, 17.9, 16.5, 14.8, 13.2, 13.0, 9.9; MALDI-TOF calcd. 1860.9, found 1860.8 [M] $^+$; UV/Vis (CHCl_3) λ_{max} nm (log ϵ): 546.0 (5.82).

II-35-4 (tetramer): Yield: 8 mg (13%); ^1H NMR (300MHz, CDCl_3) δ (ppm) 6.97 (s, 8H, *meso*-H), 2.75-2.81 (m, 16H, CH_2), 2.33-2.36 (m, 32H, CH_2), 2.23 (s, 24H, CH_3), 1.95 (s, 24H, CH_3), 1.24-1.33 (m, 40H, CH_2 and CH_3), 1.01 (dt, $J = 7.4$ and 3.1 Hz, 24H, CH_3), 0.78 (q, $J = 7.2$ Hz, 24H, CH_3); ^{13}C NMR (75MHz, CDCl_3) δ (ppm) 164.5, 149.4, 139.2, 137.5, 132.9, 131.9, 121.2, 107.0, 79.5, 77.2, 29.7, 23.7, 19.4, 17.9, 16.5, 14.9, 14.7, 13.3, 9.9; MALDI-TOF calcd. 2481.1, found 2481.1 $[(\text{M})^+]$; UV/Vis (CHCl_3) λ_{max} nm (log ϵ): 543.0 (5.93).

Co^{II} bisdipyrin complexes (II-36). The same procedure was used as in the synthesis of **II-29**, starting from **II-34** (72 mg, 0.1 mmol) to afford dichroic purple/green solids.

II-36-3 (trimer): Yield: 15 mg (24%); MALDI-TOF calcd. 1845.9, found 1846.0 $[(\text{M})^+]$; UV/Vis (CHCl_3) λ_{max} nm (log ϵ): 544.0 (5.66); Anal. Calcd. for: $\text{C}_{114}\text{H}_{132}\text{Co}_3\text{N}_{12}$: C, 74.13; H, 7.20; N, 9.10. Found: C, 74.06; H, 7.31; N, 9.16.

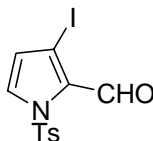
II-36-4 (tetramer): Yield: 7 mg (12%); MALDI-TOF calcd. 2461.2, found 2461.4 $[(\text{M})^+]$; UV/Vis (CHCl_3) λ_{max} nm (log ϵ): 541.0 (5.74).



III-2

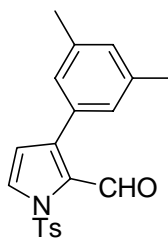
4-*t*-pentylpyrrole-2-carbaldehyde (III-2). According to the previously reported procedure,⁷⁴ some modifications have been made for synthesis of **III-2**. To a suspension of anhydrous AlCl_3 (1.6 g, 12 mmol) in DCE (3 mL) cooled to 0°C was added pyrrole-2-carbaldehyde (0.95 g, 10 mmol). The reaction mixture was stirred for 20 min,

followed by addition of 2-chloro-2-methylbutane (1.6 mL, 13 mmol). The mixture was stirred for 4 h at room temperature before being poured into a well-stirred mixture of 200 ml water and 50 mL CH₂Cl₂. The organic layer was washed with water, saturated NaHCO₃, brine and concentrated to give a dark brown oil. The crude oil was purified by flash chromatography on silica gel, eluting with 10% EtOAc in hexanes, to give a brown oil. Yield: 1.1 g (67%); ¹H NMR (300MHz, CDCl₃) δ (ppm) 10.30 (br. s, 1H, NH), 9.44 (s, 1H, CHO), 7.03 (s, 1H, Ar-H), 6.91 (d, *J* = 1.3 Hz, 1H, Ar-H), 1.21 - 1.31 (m, 11H, CH₂ CH₃); ¹³C NMR (75MHz, CDCl₃) δ (ppm) 179.2, 132.4, 123.1, 119.0, 111.3, 36.9, 31.6, 28.6; EI MS (M⁺): *m/z* 165. HR-EI MS (M⁺) *m/z* calcd for C₁₀H₁₅NO 165.1154, found 165.1152.



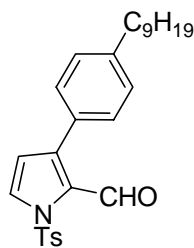
III-3

3-iodo-1-tosylpyrrole-2-carbaldehyde (III-3). **III-3** was synthesized based on the previously reported procedure.⁷⁵ Yield: 6.01 g (42%); ¹H NMR (300MHz, CD₂Cl₂) δ (ppm) 9.78 (s, 1H, CHO), 7.83 (d, *J* = 8.7 Hz, 2H, Ar-H), 7.66 (d, *J* = 3.5 Hz, 1H, pyrrole-H), 7.36 (d, *J* = 7.9 Hz, 2H, Ar-H), 6.63 (d, *J* = 3.5 Hz, 1H, Pyrrole-H), 2.43 (s, 3H, CH₃); EI MS (M⁺): *m/z* 375. HR-EI MS (M⁺) *m/z* calcd for C₁₂H₁₀INO₃S 374.9426, found 374.9420.



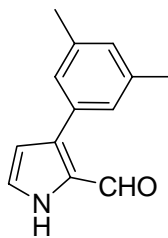
III-4

3-(3,5-dimethylphenyl)-1-tosylpyrrole-2-carbaldehyde (III-4). According to the previously reported procedure,⁷⁵ some modifications have been made for synthesis of **III-4**. To a mixture of 3,5-dimethylphenylboronic acid (0.4 g, 2.70 mmol), Pd(PPh₃)₂Cl₂ (77 mg, 0.11 mmol) and **III-3** (0.85 g, 2.26 mmol) in DME (35 mL) was added K₂CO₃ (0.97 g, 7.0 mmol, dissolved in minimum amount of water). The reaction mixture was heated to reflux and stirred for 5 h. The reaction mixture was allowed to cool, and the organic solvent was then removed *in vacuo*. The residue was treated with EtOAc (100 mL) and thoroughly washed with several portions of water and brine. The organic layer was dried over anhydrous Na₂SO₄ and concentrated under reduced pressure. Flash chromatography on silica gel, eluting with 10% EtOAc in hexanes, afforded an off-white solid. Yield: 0.58 g (73%); ¹H NMR (300MHz, CDCl₃) δ (ppm) 9.58 (s, 1H, CHO), 7.96 (d, *J* = 8.4 Hz, 2H, Ar-H), 7.84 (d, *J* = 3.0 Hz, 1H, pyrrole-H), 7.35 (d, *J* = 8.4 Hz, 2H, Ar-H), 7.04 (s, 1H, Ar-H), 7.01 (s, 2H, Ar-H), 6.48 (d, *J* = 3.1 Hz, 1H, pyrrole-H), 2.44 (s, 3H, CH₃), 2.14 (s, 6H, CH₃); ¹³C NMR (75MHz, CDCl₃) δ (ppm) 178.4, 145.3, 144.3, 138.2, 135.3, 132.2, 130.4, 129.7, 129.6, 128.5, 128.1, 127.4, 112.8, 21.7, 21.2; EI MS (M⁺): *m/z* 353. HR-EI MS (M⁺) *m/z* calcd for C₂₀H₁₉NO₃S 353.1086, found 353.1085.



III-5

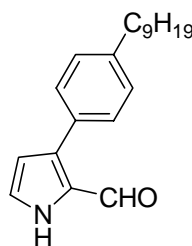
3-(4-nonylphenyl)-1-tosylpyrrole-2-carbaldehyde (III-5). The same procedure was used as in the synthesis of **III-4**, starting from 4-nonylphenylboronic acid (0.67 g, 2.70 mmol) to afford a yellow oil. Yield: 0.80 g (78%); EI MS (M^+): m/z 451. HR-EI MS (M^+) m/z calcd for $C_{27}H_{33}NO_3S$ 451.2181, found 451.2195.



III-6

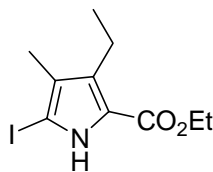
3-(3,5-dimethylphenyl)pyrrole-2-carbaldehyde (III-6). According to the previously reported procedure,⁷⁵ some modifications have been made for synthesis of **III-6**. To a solution of **III-4** (0.47 g, 1.33 mmol) in THF (20 mL) and MeOH (15 mL) was added KOH (0.37 g, 6.65 mmol). The reaction mixture was heated to 60°C and stirred for 1 h. The mixture was allowed to cool, and the organic solvent was then removed *in vacuo*. The residue was treated with EtOAc (100 mL) and thoroughly washed with several portions of water and brine. The organic layer was dried over anhydrous Na_2SO_4 and concentrated under reduced pressure. Flash chromatography on silica gel, eluting with 20% EtOAc in hexanes, gave a brown solid. Yield: 0.23 g (87%); 1H NMR (300MHz, $CDCl_3$) δ (ppm) 9.79 (br. s, 1H, NH), 9.65 (s, 1H, CHO), 7.13 (s, 3H, Ar-H), 7.04 (s, 1H, Ar-H), 6.44 (t, $J = 2.4$ Hz, 1H, pyrrole-H), 2.39 (s, 6H, CH_3);

^{13}C NMR (75MHz, CDCl_3) δ (ppm) 180.0, 138.3, 137.4, 133.5, 129.4, 128.8, 127.1, 125.4, 111.5, 21.3; EI MS (M^+): m/z 199. HR-EI MS (M^+) m/z calcd for $\text{C}_{13}\text{H}_{13}\text{NO}$ 199.0997, found 199.0997.



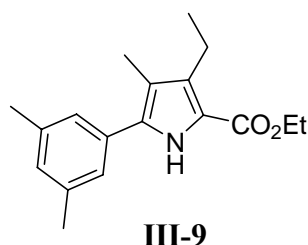
III-7

3-(4-nonylphenyl)pyrrole-2-carbaldehyde (III-7). The same procedure was used as in the synthesis of **III-6**, starting from **III-5** (0.38 g, 0.84 mmol) and KOH (0.24 g, 4.2 mmol) to afford a brown solid. Yield: 0.23 g (92%); EI MS (M^+): m/z 297. HR-EI MS (M^+) m/z calcd for $\text{C}_{20}\text{H}_{27}\text{NO}$ 297.2093, found 297.2094.

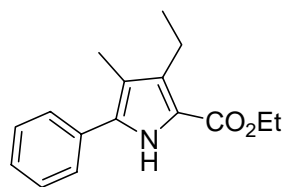


III-8

ethyl 3-ethyl-5-iodo-4-methylpyrrole-2-carboxylate (III-8). **III-8** was synthesized based on the previously reported procedure.⁹⁹ ^1H NMR (300MHz, CDCl_3) δ (ppm) 8.77 (br. s, 1H, NH), 4.32 (q, $J = 7.2$ Hz, 2H, CH_2), 2.78 (q, $J = 7.4$ Hz, 2H, CH_2), 1.99 (s, 3H, CH_3), 1.36 (t, $J = 7.0$ Hz, 3H, CH_3), 1.11 (t, $J = 7.4$ Hz, 3H, CH_3); EI MS (M^+): m/z 307. HR-EI MS (M^+) m/z calcd for $\text{C}_{10}\text{H}_{14}\text{INO}_2$ 307.0069, found 307.0059.

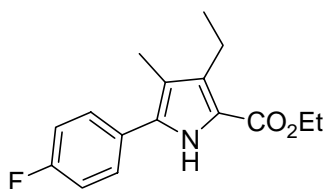


ethyl 5-(3,5-dimethylphenyl)-3-ethyl-4-methylpyrrole-2-carboxylate (III-9). According to the previously reported procedure,¹⁰⁰ some modifications have been made for synthesis of **III-9**. To a mixture of **III-8** (1.0 g, 3.26 mmol), 3,5-dimethylphenylboronic acid (0.6 g, 4 mmol) and Pd(PPh₃)₂Cl₂ (140 mg, 0.2 mmol) in DME (30 mL) was added K₂CO₃ (1.38 g, 10 mmol, dissolved in minimum amount of water). The mixture was heated to 85°C and stirred for 3 h. The reaction was allowed to cool, and the organic solvent was then removed *in vacuo*. The residue was treated with EtOAc (100 mL) and thoroughly washed with several portions of water and brine. The organic layer was dried over anhydrous Na₂SO₄ and concentrated under reduced pressure. Flash chromatography on silica gel, eluting with 20% EtOAc in hexanes, afforded a yellow solid. Yield: 0.85 g (92%); ¹H NMR (300MHz, CDCl₃) δ (ppm) 8.81 (br. s, 1H, NH), 7.10 (s, 2H, Ar-H), 6.99 (s, 1H, Ar-H), 4.35 (q, *J* = 7.1 Hz, 2H, CH₂), 2.83 (q, *J* = 7.4 Hz, 2H, CH₂), 2.38 (s, 6H, CH₃), 2.17 (s, 3H, CH₃), 1.39 (t, *J* = 7.3 Hz, 3H, CH₃), 1.19 (t, *J* = 7.5 Hz, 3H, CH₃); ¹³C NMR (75MHz, CDCl₃) δ (ppm) 161.6, 138.3, 134.6, 133.1, 132.4, 129.1, 125.1, 117.8, 116.9, 59.8, 21.3, 18.4, 15.0, 14.5, 9.8; EI MS (M⁺): *m/z* 285. HR-EI MS (M⁺) *m/z* calcd for C₁₈H₂₃NO₂ 285.1729, found 285.1730.



III-10

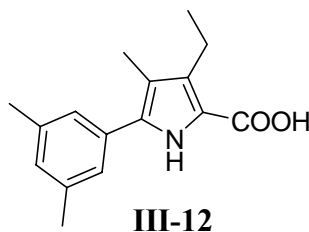
ethyl 3-ethyl-4-methyl-5-phenylpyrrole-2-carboxylate (III-10). The same procedure was used as in the synthesis of **III-9**, starting from phenylboronic acid (0.49 g, 4 mmol) to afford a yellow solid. Yield: 0.59 g (70%); ^1H NMR (300MHz, CD_2Cl_2) δ (ppm) 8.86 (br. s, 1H, NH), 7.31 - 7.50 (m, 5H, Ar-H), 4.30 (q, $J = 7.0$ Hz, 2H, CH_2), 2.81 (q, $J = 7.0$ Hz, 2H, CH_2), 2.16 (s, 3H, CH_3), 1.36 (t, $J = 7.0$ Hz, 3H, CH_3), 1.15 (t, $J = 7.0$ Hz, 3H, CH_3); EI MS (M^+): m/z 257. HR-EI MS (M^+) m/z calcd for $\text{C}_{16}\text{H}_{19}\text{NO}_2$ 257.1416, found 257.1418.



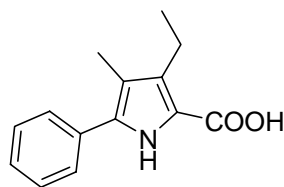
III-11

ethyl 3-ethyl-5-(4-fluorophenyl)-4-methylpyrrole-2-carboxylate (III-11). The same procedure was used as in the synthesis of **III-9**, starting from 4-fluorophenylboronic acid (0.56 g, 4 mmol) to afford an off-white solid. Yield: 0.78 g (87%); ^1H NMR (300MHz, CDCl_3) δ (ppm) 8.92 (br. s, 1H, NH), 7.42 - 7.46 (m, 2H, Ar-H), 7.13 (t, $J = 8.8$ Hz, 2H, Ar-H), 4.32 (q, $J = 7.1$ Hz, 2H, CH_2), 2.81 (q, $J = 7.6$ Hz, 2H, CH_2), 2.14 (s, 3H, CH_3), 1.37 (t, $J = 7.1$ Hz, 3H, CH_3), 1.18 (t, $J = 7.5$ Hz, 3H, CH_3); ^{13}C NMR (75MHz, CDCl_3) δ (ppm) 163.7, 161.6, 160.4, 134.5, 129.1, 129.0, 117.0, 115.9, 115.6, 59.9, 18.5, 15.0, 14.5, 9.6; EI MS (M^+): m/z 275. HR-EI MS

(M⁺) *m/z* calcd for C₁₆H₁₈NO₂F 275.1322, found 275.1321.

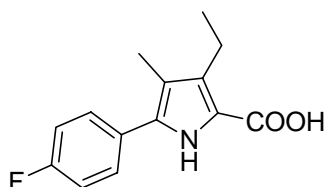


5-(3,5-dimethylphenyl)-3-ethyl-4-methylpyrrole-2-carboxylic acid (III-12). According to the previously reported procedure,¹⁰⁰ some modifications have been made for synthesis of **III-12**. To a solution of **III-9** (0.71 g, 2.5 mmol) in EtOH (30 mL) was added KOH (1.4 g, 25 mmol, dissolved in 5 mL water). The reaction mixture was refluxed for 3 h. After removal of the solvent, the residue was treated with 400 mL water, followed by addition of acetic acid to give a precipitate. The precipitate was filtered and washed with several portions of water to remove excess acetic acid to afford a grey solid. Yield: 0.50 g (78%); ¹H NMR (300MHz, CDCl₃) δ (ppm) 8.87 (s, 1H, COOH), 7.11 (s, 2H, Ar-H), 7.01 (s, 1H, Ar-H), 2.86 (q, *J* = 7.6 Hz, 2H, CH₂), 2.38 (s, 6H, CH₃), 2.18 (s, 3H, CH₃), 1.20 (t, *J* = 7.4 Hz, 3H, CH₃); ¹³C NMR (75MHz, CDCl₃) δ (ppm) 166.3, 138.4, 136.8, 134.6, 132.2, 132.1, 129.4, 125.2, 117.5, 21.3, 18.4, 15.0, 9.8; EI MS (M⁺): *m/z* 257. HR-EI MS (M⁺) *m/z* calcd for C₁₆H₁₉NO₂ 257.1416, found 257.1417.



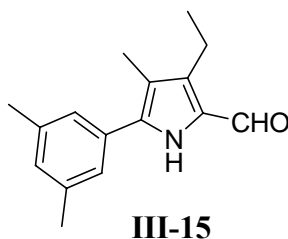
III-13

3-ethyl-4-methyl-5-phenylpyrrole-2-carboxylic acid (III-13). The same procedure was used as in the synthesis of **III-12**, starting from **III-10** (0.64 g, 2.5 mmol) to afford a grey solid. Yield: 0.44 g (76%); ^1H NMR (300MHz, CDCl_3) δ (ppm) 9.00 (s, 1H, COOH), 7.40 - 7.48 (m, 5H, Ar-H), 2.84 (q, $J = 7.5$ Hz, 2H, CH_2), 2.17 (s, 3H, CH_3), 1.18 (t, $J = 7.5$ Hz, 3H, CH_3); ^{13}C NMR (75MHz, CDCl_3) δ (ppm) 166.2, 136.4, 133.9, 128.7, 127.5, 127.3, 125.5, 117.5, 117.4, 18.4, 15.0, 9.8; EI MS (M^+): m/z 229. HR-EI MS (M^+) m/z calcd for $\text{C}_{14}\text{H}_{15}\text{NO}_2$ 229.1103, found 229.1103.

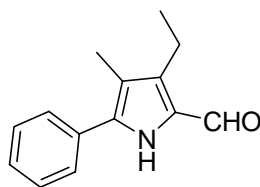


III-14

3-ethyl-5-(4-fluorophenyl)-4-methylpyrrole-2-carboxylic acid (III-14). The same procedure was used as in the synthesis of **III-12**, starting from **III-11** (0.69 g, 2.5 mmol) to afford a grey solid. Yield: 0.57 g (92%); ^1H NMR (300MHz, CDCl_3) δ (ppm) 8.96 (s, 1H, COOH), 7.43 - 7.48 (m, 2H, Ar-H), 7.14 (t, $J = 8.8$ Hz, 2H, Ar-H), 2.86 (q, $J = 7.5$ Hz, 2H, CH_2), 2.15 (s, 3H, CH_3), 1.20 (t, $J = 7.5$ Hz, 3H, CH_3); ^{13}C NMR (75MHz, CDCl_3) δ (ppm) 166.5, 163.9, 160.6, 136.9, 129.2, 129.1, 117.6, 116.0, 115.7, 18.4, 15.0, 9.7; EI MS (M^+): m/z 247. HR-EI MS (M^+) m/z calcd for $\text{C}_{14}\text{H}_{14}\text{NO}_2\text{F}$ 247.1009, found 247.1008.

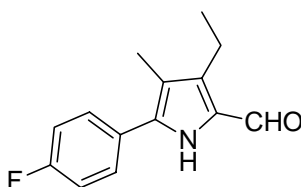


5-(3,5-dimethylphenyl)-3-ethyl-4-methylpyrrole-2-carbaldehyde (III-15). According to the previously reported procedure,⁷⁶ some modifications have been made for synthesis of **III-15**. To a 50 mL round-bottom flask was added **III-12** (0.42 g, 1.65 mmol) and TFA (3 mL). The reaction mixture was stirred for 15 mins before cooling to 0°C. The mixture was stirred for an additional 15 mins after slow addition of TMOF (2 mL) at 0°C. The reaction was poured into a well-stirred mixture of ice-water and CH₂Cl₂. The organic layer was washed with water, saturated NaHCO₃ and brine, dried over anhydrous Na₂SO₄ and filtered. After removal of the organic solvent, the residue was purified by flash chromatography on silica gel, eluting with 30% EtOAc in hexanes, to give an off-white solid. Yield: 0.36 g (90%); ¹H NMR (300MHz, CDCl₃) δ (ppm) 9.62 (s, 1H, CHO), 9.11 (br. s, 1H, NH), 7.13 (s, 2H, Ar-H), 7.02 (s, 1H, Ar-H), 2.78 (q, *J* = 7.6 Hz, 2H, CH₂), 2.37 (s, 6H, CH₃), 2.18 (s, 3H, CH₃), 1.26 (t, *J* = 7.7 Hz, 3H, CH₃); ¹³C NMR (75MHz, CDCl₃) δ (ppm) 176.8, 139.1, 138.4, 137.3, 131.6, 129.9, 128.1, 125.2, 117.6, 21.3, 17.2, 16.5, 9.7; EI MS (M⁺): *m/z* 241. HR-EI MS (M⁺) *m/z* calcd for C₁₆H₁₉NO 241.1467, found 241.1467.



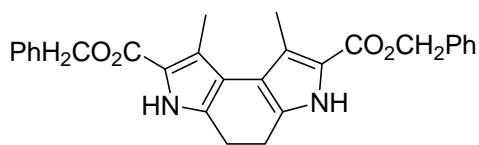
III-16

3-ethyl-4-methyl-5-phenylpyrrole-2-carbaldehyde (III-16). The same procedure was used as in the synthesis of **III-15**, starting from **III-13** (0.38 g, 1.65 mmol) to afford an off-white solid. Yield: 0.28 g (80%); ^1H NMR (300MHz, CDCl_3) δ (ppm) 9.64 (s, 1H, CHO), 9.24 (br. s, 1H, NH), 7.35 - 7.53 (m, 5H, Ar-H), 2.79 (q, $J = 7.4$ Hz, 2H, CH_2), 2.19 (s, 3H, CH_3), 1.27 (t, $J = 7.7$ Hz, 3H, CH_3); ^{13}C NMR (75MHz, CDCl_3) δ (ppm) 176.9, 139.1, 137.0, 131.7, 128.8, 128.3, 128.1, 127.4, 117.7, 17.2, 16.5, 9.7; EI MS (M^+): m/z 213. HR-EI MS (M^+) m/z calcd for $\text{C}_{14}\text{H}_{15}\text{NO}$ 213.1154, found 213.1155.



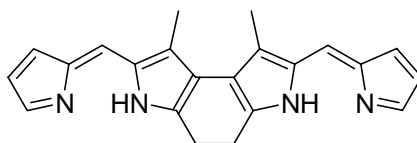
III-17

3-ethyl-5-(4-fluorophenyl)-4-methylpyrrole-2-carbaldehyde (III-17). The same procedure was used as in the synthesis of **III-15**, starting from **III-14** (0.41 g, 1.65 mmol) to afford a yellow solid. Yield: 0.35 g (92%); ^1H NMR (300MHz, CDCl_3) δ (ppm) 9.62 (s, 1H, CHO), 9.41 (br. s, 1H, NH), 7.46 - 7.52 (m, 2H, Ar-H), 7.15 (t, $J = 8.6$ Hz, 2H, Ar-H), 2.78 (q, $J = 7.6$ Hz, 2H, CH_2), 2.15 (s, 3H, CH_3), 1.26 (t, $J = 7.6$ Hz, 3H, CH_3); ^{13}C NMR (75MHz, CDCl_3) δ (ppm) 176.9, 164.1, 160.9, 139.2, 136.2, 129.4, 129.3, 116.0, 115.7, 17.2, 16.5, 9.6; EI MS (M^+): m/z 231. HR-EI MS (M^+) m/z calcd for $\text{C}_{14}\text{H}_{14}\text{NOF}$ 231.1059, found 231.1059.



III-18

dihydropyrrolo[3,2-e]indole (III-18). **III-18** was synthesized based on the previously reported procedure to afford an off-white solid.⁷⁷ Yield: 9.0 g (36%); ¹H NMR (300MHz, DMSO-*d*₆) δ (ppm) 11.55 (br. s, 2H, NH), 7.32 - 7.46 (m, 10H, Ar-H), 5.27 (s, 4H, CH₂), 2.70 (s, 4H, CH₂), 2.46 (s, 6H, CH₃); EI MS (M⁺): *m/z* 454; Anal. Calcd. for: C₂₈H₂₆N₂O₄: C, 73.99; H, 5.77; N, 6.16. Found: C, 74.39; H, 5.87; N, 6.50.

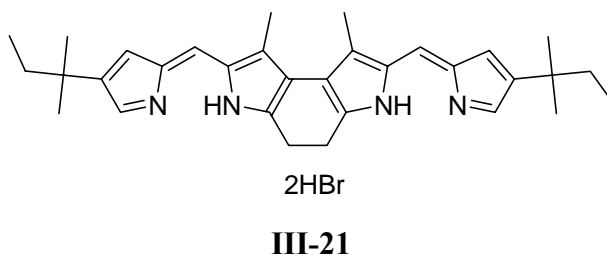


2HBr

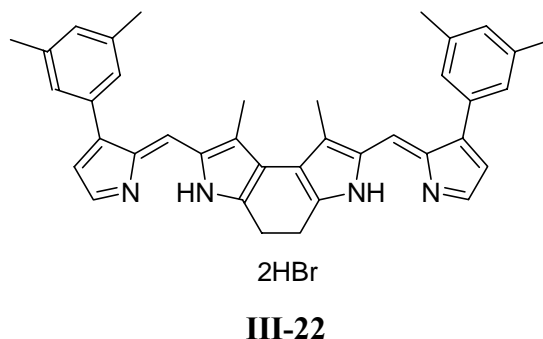
III-20

bisdipyrin ligand (III-20). According to the previously reported procedure,⁴⁶ some modifications have been made for synthesis of **III-20**. To a mixture of **III-18** (227 mg, 0.50 mmol) and 10 mol % palladium on activated carbon (50 mg) in a 250 mL round-bottom flask was added THF (75 mL) and MeOH (25 mL). The mixture was purged with hydrogen at 1 atm and stirred for overnight. The reaction mixture was then filtered through Celite to remove the catalyst. The filtrate was collected in a 250 mL round-bottom flask, and then **III-1** (48 mg, 0.50 mmol) was added, followed by the addition of 33% hydrogen bromide in acetic acid (1.0 mL). The solution immediately turned from colourless to dark purple. The solution was stirred for 1 h,

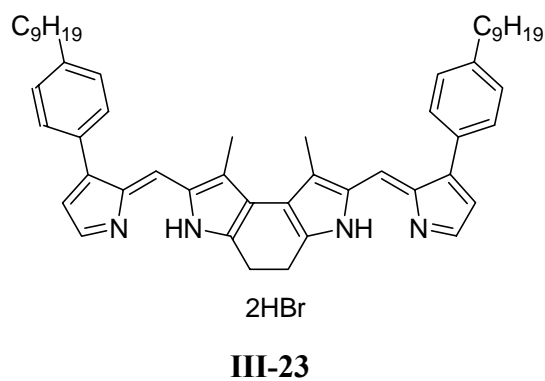
and the organic solvent was then removed *in vacuo* to give black solid. The black solid was redissolved in CHCl₃ (75 mL) and MeOH (25 mL), and **III-1** (48 mg, 0.50 mmol) was added, followed by the addition of 33% hydrogen bromide in acetic acid (1.0 mL). The reaction mixture was stirred for 4 h at room temperature. Removal of the solvent *in vacuo* gave the crude product. To this crude product was added just enough chloroform and methanol to form a homogeneous solution, and then diethyl ether was added to precipitate the product, which was collected by filtration and rinsed with more diethyl ether to give a black solid. Yield: 200 mg (80%); ESI MS (M+H)⁺: *m/z* 341.3; HR-ESI MS (M+H)⁺: *m/z* calcd for C₂₂H₂₁N₄: 341.1766; found: 341.1758. UV/Vis (CHCl₃/CH₃OH = 2/1) λ_{max} nm (A): 583.0 (1.115).



bisdipyrrin ligand (III-21). The same procedure was used as in the synthesis of **III-20**, starting from **III-2** (83 mg, 0.5 mmol) to afford a black solid. Yield: 275 mg (86%); ESI MS (M+H)⁺: *m/z* 481.4; HR-ESI MS (M+H)⁺: *m/z* calcd for C₃₂H₄₁N₄: 481.3331; found: 481.3338. UV/Vis (CHCl₃/CH₃OH = 2/1) λ_{max} nm (A): 598.0 (0.837).

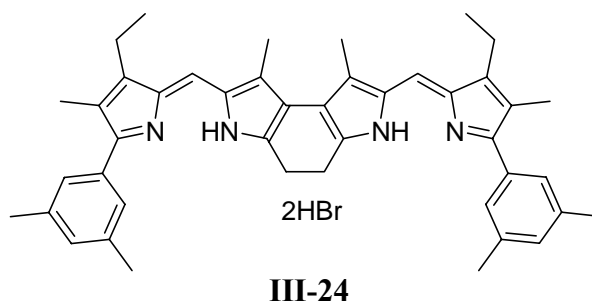


bisdipyririn ligand (III-22). The same procedure was used as in the synthesis of **III-20**, starting from **III-6** (100 mg, 0.5 mmol) to afford a black solid. Yield: 300 mg (84%); ESI MS (M+H)⁺: *m/z* 549.5; HR-ESI MS (M+H)⁺: *m/z* calcd for C₃₈H₃₇N₄: 549.3018; found: 549.3026. UV/Vis (CHCl₃) λ_{max} nm (A): 608 (0.607) and 668.0 (0.564).

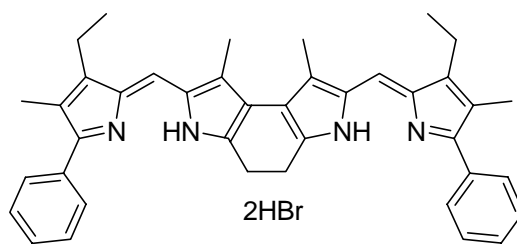


bisdipyririn ligand (III-23). The same procedure was used as in the synthesis of **III-20**, starting from **III-7** (149 mg, 0.5 mmol) to afford a dark brown solid. Yield: 150 mg (36%); ¹H NMR (400MHz, CDCl₃) δ (ppm) 14.20 (br. s, 2H, NH), 13.56 (br. s, 2H, NH), 7.82 (s, 2H, pyrrole-H), 7.45 (s, 2H, *meso*-H), 7.37 (dd, *J* = 15.7, 7.8 Hz, 8H, Ar-H), 6.65 (s, 2H, pyrrole-H), 3.55 (s, 4H, CH₂), 2.70 (t, *J* = 7.8 Hz, 4H, CH₂), 2.50 (s, 6H, CH₃), 1.69 (t, *J* = 6.6 Hz, 4H, CH₂), 1.29 (s, 24H, CH₂), 0.89 (t, *J* = 6.0 Hz, 6H, CH₃); ¹³C NMR (100MHz, CDCl₃) δ (ppm) 159.4, 149.1, 144.7, 139.5, 137.6, 130.4, 129.8, 129.6, 129.3, 126.0, 125.7, 121.4, 114.9, 35.8, 31.9,

31.3, 29.5, 29.5, 29.4, 29.3, 22.7, 22.2, 14.1, 13.4; ESI MS (M+H)⁺: *m/z* 745.5; HR-ESI MS (M+H)⁺: *m/z* calcd for C₅₂H₆₅N₄: 745.5209; found: 745.5229. UV/Vis (CHCl₃) λ_{max} nm (A): 607.0 (1.082).

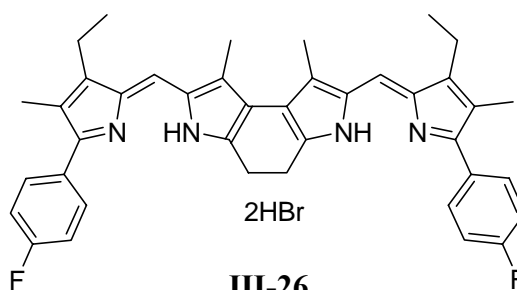


bisdipyririn ligand (III-24). The same procedure was used as in the synthesis of **III-20**, starting from **III-15** (121 mg, 0.5 mmol) to afford a black solid. Yield: 346 mg (87%); ¹H NMR (400MHz, CDCl₃) δ (ppm) 14.27 (br. s, 2H, NH), 12.52 (br. s, 2H, NH), 7.56 (s, 4H, Ar-H), 7.28 (s, 2H, Ar-H), 7.14 (s, 2H, *meso*-H), 3.50 (s, 4H, CH₂), 2.78 (d, *J* = 7.0 Hz, 4H, CH₂), 2.65 (s, 6H, CH₃), 2.44 (s, 12H, CH₃), 2.20 (s, 6H, CH₃), 1.24 (t, *J* = 7.6 Hz, 6H, CH₃); ¹³C NMR (100MHz, CDCl₃) δ (ppm) 156.0, 154.8, 150.4, 138.1, 134.3, 132.8, 128.1, 128.0, 127.8, 126.9, 123.5, 120.8, 119.3, 29.6, 22.2, 21.3, 18.9, 16.2, 10.7; ESI MS (M+H)⁺: *m/z* 633.6; HR-ESI MS (M+H)⁺: *m/z* calcd for C₄₄H₄₉N₄: 633.3957; found: 633.3943. UV/Vis (CHCl₃) λ_{max} nm (logε): 647.0 (5.24).



III-25

bisdipyrrin ligand (III-25). The same procedure was used as in the synthesis of **III-20**, starting from **III-16** (107 mg, 0.5 mmol) to afford a black solid. Yield: 300 mg (81%); ^1H NMR (400MHz, CDCl_3) δ (ppm) 14.25 (br. s, 2H, NH), 12.55 (br. s, 2H, NH), 7.91 (d, $J = 6.5$ Hz, 4H, Ar-H), 7.51 - 7.56 (m, 6 H, Ar-H), 7.34 (s, 2H, *meso*-H), 3.48 (s, 4H, CH_2), 2.76 (q, $J = 7.6$ Hz, 4H, CH_2), 2.67 (s, 6H, CH_3), 2.17 (s, 6H, CH_3), 1.20 (t, $J = 7.1$ Hz, 6H, CH_3); ^{13}C NMR (100MHz, CDCl_3) δ (ppm) 156.2, 154.0, 150.7, 134.8, 130.8, 130.1, 128.5, 128.4, 128.1, 126.9, 123.4, 120.8, 120.0, 22.1, 18.7, 16.1, 13.6, 10.6; ESI MS ($\text{M}+\text{H}$) $^+$: m/z 577.5; HR-ESI MS ($\text{M}+\text{H}$) $^+$: m/z calcd for $\text{C}_{40}\text{H}_{41}\text{N}_4$: 577.3331; found: 577.3329. UV/Vis (CHCl_3) λ_{max} nm (log ϵ): 644 (5.21).



III-26

bisdipyrrin ligand (III-26). The same procedure was used as in the synthesis of **III-20**, starting from **III-17** (116 mg, 0.5 mmol) to afford a black solid. Yield: 350 mg (90%); ^1H NMR (400MHz, CDCl_3) δ (ppm) 14.25 (br. s, 2H, NH), 12.61 (br. s, 2H, NH), 7.93 (s, 4H, Ar-H), 7.32

(s, 2H, *meso*-H), 7.22 (t, $J = 7.6$ Hz, 4H, Ar-H), 3.48 (s, 4H, CH₂), 2.77 (d, $J = 5.9$ Hz, 4H, CH₂), 2.66 (s, 6H, CH₃), 2.16 (s, 6H, CH₃), 1.23 (br. s, 6H, CH₃); ¹³C NMR (100MHz, CDCl₃) δ (ppm) 156.5, 152.9, 150.6, 134.9, 132.4, 132.3, 128.2, 126.8, 124.6, 123.3, 119.9, 116.0, 115.7, 22.2, 18.8, 16.1, 13.6, 10.6; ESI MS (M+H)⁺: m/z 613.5; HR-ESI MS (M+H)⁺: m/z calcd for C₄₀H₃₉N₄F₂: 613.3143; found: 613.3148. UV/Vis (CHCl₃) λ_{\max} nm (log ϵ): 644.0 (5.31).

Zn^{II} bisdipyrrin complex (III-27-4). According to the previously reported procedure,⁶⁷ some modifications have been made for synthesis of **III-27-4**. To a solution of **III-20** (50 mg, 0.1 mmol) in CHCl₃/MeOH (20 mL/10 mL) was added a solution of Zn(OAc)₂·2H₂O (33 mg, 0.15 mmol) in MeOH (1 mL), followed by addition of a solution of NaOAc (82 mg, 1 mmol) in MeOH (1 mL). After stirring overnight, the solvent was removed by rotary evaporation. The crude compound was purified by flash chromatography on silica gel, eluting with CH₂Cl₂, to give the target Zn^{II} complex as a dark green solid. Yield: 8 mg (19%); ¹H NMR (300MHz, CDCl₃) δ (ppm) 7.18 (s, 8H, pyrrole-H), 7.16 (s, 8H, pyrrole-H), 6.99 (d, $J = 3.5$ Hz, 8H, *meso*-H), 6.34 (dd, $J = 3.7, 1.4$ Hz, 8H, pyrrole-H), 2.53 (s, 24H, CH₃), 2.28 (dq, $J = 10.6, 6.6$ Hz, 16H, CH₂); ¹³C NMR (75MHz, CDCl₃) δ (ppm) 164.2, 145.4, 140.1, 138.0, 133.7, 128.4, 126.7, 123.4, 115.3, 25.0, 13.1; MALDI-TOF calcd. 1615.2, found 1615.2 [(M)⁺]; Anal. Calcd. for: C₈₈H₇₂N₁₆Zn₄: C, 65.44; H, 4.49; N, 13.88. Found: C, 65.33; H, 4.59; N, 13.63; UV/Vis (CHCl₃) λ_{\max} nm (log ϵ): 575.0 (5.63) and 613.0 (5.53).

Co^{II} bisdipyrrin complex (III-28-4). The same procedure was used as in the synthesis of **III-27-4**, starting from **III-20** (50 mg, 0.1 mmol) and Co(OAc)₂•4H₂O (38 mg, 0.15 mmol) to afford a dark purple solid. Yield: 9 mg (21%); MALDI-TOF calcd. 1589.4, found 1589.4 [(M)⁺]; UV/Vis (CHCl₃) λ_{max} nm (A): 570.0 (1.011) and 645.0 (0.842).

Zn^{II} bisdipyrrin complex (III-29-4). The same procedure was used as in the synthesis of **III-27-4**, starting from **III-21** (64 mg, 0.1 mmol) to afford a dark green solid. Yield: 9 mg (17%); Anal. Calcd. for: C₁₂₈H₁₅₂N₁₆Zn₄: C, 70.64; H, 7.04; N, 10.30. Found: C, 70.41; H, 7.24; N, 10.00; UV/Vis (CHCl₃) λ_{max} nm (logε): 590.0 (5.60) and 629.0 (5.56).

Ni^{II} bisdipyrrin complex (III-30-4). The same procedure was used as in the synthesis of **III-27-4**, starting from **III-21** (64 mg, 0.1 mmol) and Ni(OAc)₂•4H₂O (38 mg, 0.15 mmol) to afford a dark brown solid. Yield: 3 mg (5%); Anal. Calcd. for: C₁₂₈H₁₅₂N₁₆Ni₄: C, 71.52; H, 7.13; N, 10.43. Found: C, 71.78; H, 7.29; N, 10.32; UV/Vis (CHCl₃) λ_{max} nm (logε): 615.0 (5.67) and 658.0 (5.58).

Zn^{II} bisdipyrrin complex (III-31-4). The same procedure was used as in the synthesis of **III-27-4**, starting from **III-22** (71 mg, 0.1 mmol). The crude compound collected from flash chromatography on silica gel, was then purified using gel permeation chromatography eluting with toluene. The target Zn^{II} complex was obtained as a dark green solid. Yield: 7 mg (11%); ¹H NMR (300MHz, CD₂Cl₂) δ (ppm) 7.34 (s, 8H, Ar-H), 7.16 (d, *J* = 0.8 Hz, 8H, Pyrrole-H), 7.11 (s, 16H, Ar-H), 7.01 (s, 8H, *meso*-H), 6.41 (d, *J* = 1.5 Hz, 8H, Pyrrole-H), 2.46 (s, 24H, CH₃),

2.38 (s, 64H, CH₂ and CH₃); ¹³C NMR (75MHz, CD₂Cl₂) δ (ppm) 164.8, 144.5, 144.1, 141.0, 138.7, 136.5, 135.8, 134.5, 129.1, 127.6, 126.5, 124.2, 115.2, 30.3, 25.9, 21.7, 13.4; MALDI-TOF calcd. 2448.4, found 2448.5 [(M)⁺]; UV/Vis (CHCl₃) λ_{max} nm (logε): 593.0 (5.58) and 632.0 (5.56).

Zn^{II} bisdipyrin complex (III-32-4). The same procedure was used as in the synthesis of **III-31-4**, starting from **III-23** (83 mg, 0.1 mmol) to afford a dark green solid. Yield: 10 mg (13%); ¹H NMR (300MHz, CD₂Cl₂) δ (ppm) 6.88-7.50 (m, 48H), 6.40 (s, 8H, Pyrrole-H), 2.67 (s, 16H, CH₂), 2.41-2.45 (m, 24H, CH₃), 1.27-1.38 (m, 128H, CH₂), 0.89-0.91 (m, 24H, CH₃); ¹³C NMR (100MHz, CDCl₃) δ (ppm) 163.9, 144.4, 143.5, 141.7, 140.4, 135.3, 133.5, 129.1, 128.6, 126.0, 123.4, 114.7, 35.8, 31.9, 31.5, 29.7, 29.6, 29.6, 29.4, 25.2, 22.7, 14.1, 13.2; MALDI-TOF calcd. 3233.9, found 3233.9 [(M)⁺]; Anal. Calcd. for: C₂₀₈H₂₄₈N₁₆Zn₄: C, 77.25; H, 7.73; N, 6.93. Found: C, 77.14; H, 7.91; N, 6.68; UV/Vis (CHCl₃) λ_{max} nm (logε): 594.0 (5.64) and 632.0 (5.63).

Zn^{II} bisdipyrin complex (III-33-4). The same procedure was used as in the synthesis of **III-31-4**, starting from **III-24** (79 mg, 0.1 mmol) to afford a dark green solid. Yield: 5 mg (7%); ¹H NMR (400MHz, CDCl₃) δ (ppm) 6.74 (s, 8H, *meso*-H), 6.63 (s, 8H, Ar-H), 6.57 (s, 16H, Ar-H), 2.50-2.58 (m, 16H, CH₂), 2.45 (s, 24H, CH₃), 2.14-2.20 (m, 16H, CH₂), 1.99 (s, 48H, CH₃), 1.88 (s, 24H, CH₃), 1.13 (t, *J* = 7.6 Hz, 24H, CH₃); ¹³C NMR (100MHz, CDCl₃) δ (ppm) 160.7, 157.2, 142.9, 138.3, 136.6, 135.7, 129.5, 128.3, 126.0, 122.6, 121.1, 120.5, 29.7, 25.3, 21.1, 18.4, 16.1, 13.0, 10.1; MALDI-TOF calcd. 2785.0, found 2784.7 [(M)⁺]; UV/Vis (CHCl₃)

λ_{\max} nm (log ϵ): 625.0 (5.68) and 661.0 (5.66).

Zn^{II} bisdipyrrin complexes (III-34). The same procedure was used as in the synthesis of **III-31-4**, starting from **III-25** (74 mg, 0.1 mmol) to afford dark green solids.

III-34-4 (grid): Yield: 6 mg (10%); ¹H NMR (400MHz, CDCl₃) δ (ppm) 6.90-7.02 (m, 40H, Ar-H), 6.74 (s, 8H, *meso*-H), 2.53-2.64 (m, 16H, CH₂), 2.43 (s, 24H, CH₃), 2.11 (d, $J = 4.1$ Hz, 16H, CH₂), 1.90 (s, 24H, CH₃), 1.16 (t, $J = 7.6$ Hz, 24H, CH₃); ¹³C NMR (100MHz, CDCl₃) δ (ppm) 161.1, 156.5, 143.4, 138.6, 135.8, 135.6, 130.2, 128.0, 127.3, 126.3, 122.8, 121.0, 29.7, 25.2, 18.4, 16.6, 12.9, 10.2; MALDI-TOF calcd. 2560.6, found 2560.8 [(M)⁺]; UV/Vis (CHCl₃) λ_{\max} nm (log ϵ): 623.0 (5.69) and 659.0 (5.67).

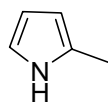
III-34-6 (hexamer): Yield: 1 mg (1%); ¹H NMR (400MHz, CDCl₃) δ (ppm) 7.02 (dd, $J = 8.7$ and 1.5 Hz, 24H, Ar-H), 6.97 (d, $J = 7.0$ Hz, 12H, Ar-H), 6.88 (t, $J = 7.4$ Hz, 24H, Ar-H), 6.73 (s, 12H, *meso*-H), 2.62-2.70 (m, 24H, CH₂), 2.27 (s, 36H, CH₃), 1.88-2.00 (m, 60H, CH₂ and CH₃), 1.19 (t, $J = 7.4$ Hz, 36H, CH₃); MALDI-TOF calcd. 3840.9, found 3840.4 [(M)⁺]; UV/Vis (CHCl₃) λ_{\max} nm (log ϵ): 623.0 (5.88) and 659.0 (5.89).

Co^{II} bisdipyrrin complex (III-35-4). The same procedure was used as in the synthesis of **III-31-4**, starting from **III-25** (74 mg, 0.1 mmol) and Co(OAc)₂•4H₂O (38 mg, 0.15 mmol) to afford a dark purple solid. Yield: 7 mg (11%); MALDI-TOF calcd. 2533.0, found 2533.0 [(M)⁺]; UV/Vis (CHCl₃) λ_{\max} nm (log ϵ): 643.0 (5.56) and 692.0 (5.49).

Zn^{II} bisdipyririn complexes (III-36). The same procedure was used as in the synthesis of **III-31-4**, starting from **III-26** (77 mg, 0.1 mmol) to afford dark green solids.

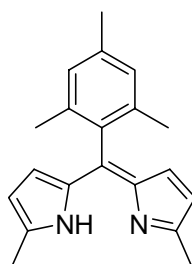
III-36-4 (grid): Yield: 6 mg (9%); ¹H NMR (400MHz, CDCl₃) δ (ppm) 6.88 (dd, *J* = 7.9 and 5.5 Hz, 16H, Ar-H), 6.81 (s, 8H, *meso*-H), 6.61 (t, *J* = 8.6 Hz, 16H, Ar-H), 2.56-2.65 (m, 16H, CH₂), 2.49 (s, 24H, CH₃), 2.15 (s, 16H, CH₂), 1.88 (s, 24H, CH₃), 1.17 (t, *J* = 7.5 Hz, 24H, CH₃); ¹³C NMR (100MHz, CDCl₃) δ (ppm) 161.0, 155.7, 144.0, 138.5, 135.7, 131.6, 130.8, 129.6, 122.8, 121.2, 121.1, 114.3, 114.1, 29.7, 25.3, 18.4, 16.5, 12.8, 10.1; MALDI-TOF calcd. 2704.5, found 2704.3 [(M)⁺]; UV/Vis (CHCl₃) λ_{max} nm (logε): 620.0 (5.44) and 657.0 (5.42).

III-36-6 (hexamer): Yield: 2 mg (2%); ¹H NMR (400MHz, CDCl₃) δ (ppm) 6.95 (dd, *J* = 8.5 and 5.6 Hz, 24H, Ar-H), 6.79 (s, 12H, *meso*-H), 6.57 (t, *J* = 8.5 Hz, 24H, Ar-H), 2.69 (q, *J* = 7.0 Hz, 24H, CH₂), 2.32 (s, 36H, CH₃), 1.96-1.99 (m, 60H, CH₂ and CH₃), 1.19 (t, *J* = 7.6 Hz, 36H, CH₃); MALDI-TOF calcd. 4056.8, found 4056.4 [(M)⁺]; UV/Vis (CHCl₃) λ_{max} nm (logε): 618.0 (5.59) and 655.0 (5.58).



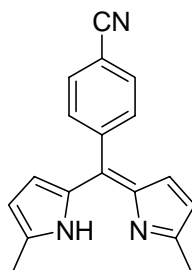
IV-1

2-methylpyrrole (IV-1). **IV-1** was synthesized based on the previously reported procedure, starting with pyrrole-2-carboxaldehyde (9.5 g, 0.10 mol) to afford a colourless liquid.⁸⁵ Yield: 4.3 g (50%); ¹H NMR (400MHz, CD₂Cl₂) δ (ppm) 7.96 (br. s, 1H, NH), 6.63 (s, 1H, pyrrole-H), 6.08 (d, *J* = 3.0 Hz, 1H, pyrrole-H), 5.88 (s, 1H, pyrrole-H), 2.28 (s, 3H, CH₃); ¹³C NMR (100MHz, CD₂Cl₂) δ (ppm) 128.0, 116.6, 108.8, 106.3, 13.1; EI MS (M⁺): *m/z* 81.



IV-2

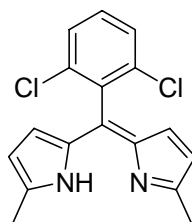
meso-mesityl dipyrriin ligand (IV-2). The same procedure was used as in the synthesis of **IV-3**, starting with 2,4,6-trimethylbenzaldehyde (222 mg, 1.5 mmol) and **IV-1** (260 mg, 3.21 mmol) to afford a brown powder. Yield: 291 mg (67%); ^1H NMR (300MHz, CDCl_3) δ (ppm) 6.91 (s, 2H, Ar-H), 6.27 (d, $J = 4.0$ Hz, 2H, pyrrole-H), 6.10 (d, $J = 4.0$ Hz, 2H, pyrrole-H), 2.45 (s, 6H, CH_3), 2.36 (s, 3H, CH_3), 2.12 (s, 6H, CH_3); ^{13}C NMR (100MHz, CD_2Cl_2) δ (ppm) 153.5, 139.6, 137.0, 137.0, 136.8, 133.6, 127.6, 127.5, 117.4, 21.1, 19.8, 16.3; ESI MS ($\text{M}+\text{H}$) $^+$: m/z 291.2; HR-ESI MS ($\text{M}+\text{H}$) $^+$: m/z calcd for $\text{C}_{20}\text{H}_{23}\text{N}_2$: 291.1861; found: 291.1869. UV/Vis (CHCl_3) λ_{max} nm ($\log \epsilon$): 450.0 (4.50) and 479.0 (4.46).



IV-3

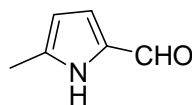
meso-4-cyanophenyl dipyrriin ligand (IV-3). **IV-3** was synthesized based on the previously reported procedure,⁸⁴ starting with 4-formylbenzonitrile (197 mg, 1.5 mmol) and **IV-1** (260 mg, 3.21 mmol) to afford a brown powder. Yield: 250 mg (61%); ^1H NMR (300MHz, CD_2Cl_2) δ

(ppm) 7.73 (d, $J = 8.6$ Hz, 2H, Ar-H), 7.56 (d, $J = 8.5$ Hz, 2H, Ar-H), 6.33 (d, $J = 4.0$ Hz, 2H, pyrrole-H), 6.18 (d, $J = 4.2$ Hz, 2H, pyrrole-H), 2.43 (s, 6H, CH₃); ESI MS (M+H)⁺: m/z 274.2; HR-ESI MS (M+H)⁺: m/z calcd for C₁₈H₁₆N₃: 274.1344; found: 274.1349. UV/Vis (CHCl₃) λ_{\max} nm (A): 483.0 (1.407).



IV-4

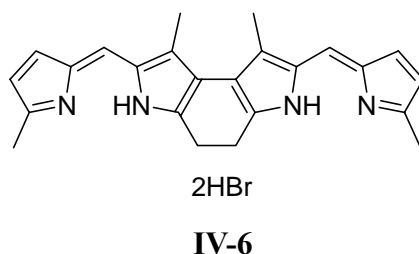
meso-2,6-dichlorophenyl dipyrriin ligand (IV-4). The same procedure was used as in the synthesis of **IV-3**, starting with 2,6-dichlorobenzaldehyde (262 mg, 1.5 mmol) and **IV-1** (260 mg, 3.21 mmol) to afford a brown powder. Yield: 296 mg (62%); ¹H NMR (300MHz, CD₂Cl₂) δ (ppm) 7.43-7.46 (m, 2H, Ar-H), 7.32-7.37 (m, 1H, Ar-H), 6.22 (d, $J = 4.1$ Hz, 2H, pyrrole-H), 6.15 (d, $J = 4.1$ Hz, 2H, pyrrole-H), 2.43 (s, 6H, CH₃); ESI MS (M+H)⁺: m/z 317.2; HR-ESI MS (M+H)⁺: m/z calcd for C₁₇H₁₅N₂³⁵Cl₂: 317.0612; found: 317.0610. UV/Vis (CHCl₃) λ_{\max} nm (A): 490.0 (1.366).



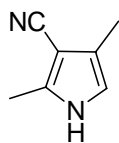
IV-5

5-methylpyrrole-2-carbaldehyde (IV-5). According to the previously reported procedure,⁸⁶ some modifications have been made for synthesis of **IV-5**. To a mixture of DMF (4.5 mL, 0.057

mol) and DCE (19 mL) cooled to -50°C was slowly added POCl_3 (4.2 mL, 0.045 mol). The reaction mixture was warmed to 0°C and stirred for 30 min, followed by addition of **IV-1** (3.36 g, 0.041 mol, dissolved in 14 mL DCE). The mixture was stirred for 1 h at 0°C before heating to reflux for 30 min. The reaction mixture was allowed to cool to room temperature and NaOAc (18.4 g, 0.225 mol, dissolved in 100 mL water) was slowly added. After refluxing for an additional hour, the mixture was cooled to room temperature. The organic layer was washed with water and brine. After removal of the organic solvent *in vacuo*, the residue was purified by flash chromatography on silica gel, eluting with 20% EtOAc in hexanes, to give an off-white solid.⁸⁶ Yield: 3.5 g (78%); ^1H NMR (300MHz, CDCl_3) δ (ppm) 10.60 (br. s, 1H, NH), 9.35 (s, 1H, CHO), 6.92 (t, $J = 3.2$ Hz, 1H, pyrrole-H), 6.07 (t, $J = 3.0$ Hz, 1H, pyrrole-H), 2.39 (s, 3H, CH_3); EI MS (M^+): m/z 109. HR-EI MS (M^+) m/z calcd for $\text{C}_6\text{H}_7\text{NO}$ 109.0528, found 109.0528.

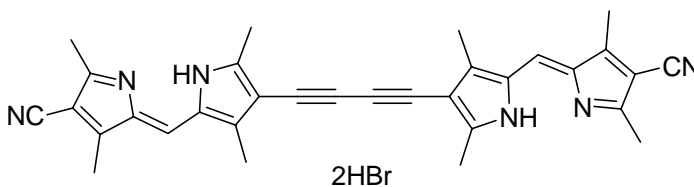


bisdipyririn ligand (IV-6). The same procedure was used as in the synthesis of **III-20**, starting from **IV-5** (54 mg, 0.5 mmol) to afford a black solid. Yield: 210 mg (79%); ESI MS ($\text{M}+\text{H}$)⁺: m/z 369.3; HR-ESI MS ($\text{M}+\text{H}$)⁺: m/z calcd for $\text{C}_{24}\text{H}_{25}\text{N}_4$: 369.2079; found: 369.2090. UV/Vis ($\text{CHCl}_3/\text{CH}_3\text{OH} = 2/1$) λ_{max} nm (A): 590.0 (0.777).



IV-7

3-cyano-2,4-dimethylpyrrole (IV-7). IV-7 was synthesized based on the previously reported procedures,¹⁰¹ starting with 2-(2-cyano-1-methylvinylamino)-N-methoxy-N-methylacetamide⁸⁷ (0.68 g, 3.72 mmol) to afford a white solid. Yield: 0.17 g (39%); ¹H NMR (400MHz, CDCl₃) δ (ppm) 7.98 (br. s, 1H, NH), 6.38 (d, *J* = 1.2 Hz, 1H, pyrrole-H), 2.39 (s, 3H, CH₃), 2.15 (s, 3H, CH₃), 1.57 (s, 3H, CH₃); EI MS (M⁺): *m/z* 120.



IV-8

bisdipyrrin ligand (IV-8). The same procedure was used as in the synthesis of **II-22**, starting from **II-16** (100 mg, 0.34 mmol) and **IV-7** (82 mg, 0.68 mmol) to give a red solid. Yield: 190 mg (85%); ¹H NMR (400MHz, CDCl₃/CD₃OD = 2/1) δ (ppm) 7.22 (s, 2H, *meso*-H), 2.62 (s, 6H, CH₃), 2.58 (s, 6H, CH₃), 2.36 (s, 12H, CH₃); ESI MS (M+H)⁺: *m/z* 497.3; UV/Vis (CHCl₃/CH₃OH = 2/1) λ_{max} nm (A): 527.0 (0.973).

rack complex (IV-9-2). To a solution of **IV-2** (26 mg, 0.09 mmol) and **II-22** (27 mg, 0.04 mmol) in CHCl₃/MeOH (20 mL/10 mL) was added a solution of Zn(OAc)₂·2H₂O (33 mg, 0.15 mmol) in MeOH (1 mL), followed by addition of a solution of NaOAc (41 mg, 0.5 mmol) in

MeOH (1 mL). After stirring overnight, the solvent was removed by rotary evaporation. The residue was purified by flash chromatography on silica gel, eluting with CH₂Cl₂, to give the crude complex which was then purified using gel permeation chromatography eluting with toluene. The target Zn^{II} rack complex was obtained as a dark red solid. Yield: 5 mg (10%); ¹H NMR (400MHz, CDCl₃) δ (ppm) 7.02 (s, 2H, *meso*-H), 6.92 (s, 4H, Ar-H), 6.42 (d, *J* = 3.8 Hz, 4H, pyrrole-H), 6.10 (d, *J* = 4.1 Hz, 4H, pyrrole-H), 2.41 (s, 6H, CH₃), 2.38 (q, *J* = 7.6 Hz, 4H, CH₂), 2.37 (s, 6H, CH₃), 2.25 (s, 6H, CH₃), 2.13 (s, 6H, CH₃), 2.11 (s, 6H, CH₃), 2.11 (s, 6H, CH₃), 2.03 (s, 6H, CH₃), 2.02 (s, 12H, CH₃), 1.04 (t, *J* = 7.6 Hz, 6H, CH₃); ¹³C NMR (100MHz, CDCl₃) δ (ppm) 161.4, 158.7, 143.4, 142.1, 139.4, 138.5, 137.9, 136.8, 136.8, 136.5, 135.7, 134.2, 132.1, 131.3, 127.5, 127.4, 121.3, 116.9, 79.3, 77.8, 29.7, 21.1, 19.6, 17.9, 16.6, 15.1, 14.8, 14.7, 11.1, 9.9; MALDI-TOF calcd. 1206.5, found 1206.5 [(M)⁺]; UV/Vis (CHCl₃) λ_{max} nm (A): 495.0 (1.011) and 542.0 (0.750).

rack complex (IV-10-2). The same procedure was used as in the synthesis of **IV-9-2**, starting from **IV-2** (26 mg, 0.09 mmol) and **IV-8** (26 mg, 0.04 mmol) to give a dark red solid. Yield: 4 mg (8%); ¹H NMR (400MHz, CDCl₃) δ (ppm) 7.16 (s, 2H, *meso*-H), 6.92 (d, *J* = 3.2 Hz, 4H, Ar-H), 6.45 (d, *J* = 3.8 Hz, 4H, pyrrole-H), 6.12 (d, *J* = 4.1 Hz, 4H, pyrrole-H), 2.49 (s, 6H, CH₃), 2.46 (s, 6H, CH₃), 2.37 (s, 6H, CH₃), 2.17 (s, 6H, CH₃), 2.16 (s, 6H, CH₃), 2.11 (s, 6H, CH₃), 2.10 (s, 6H, CH₃), 2.00 (s, 12H, CH₃); MALDI-TOF calcd. 1200.4, found 1200.5 [(M)⁺]; UV/Vis (CHCl₃) λ_{max} nm (A): 494.0 (0.969) and 546.0 (0.664).

rack complex (IV-11-2). The same procedure was used as in the synthesis of **IV-9-2**, starting from **IV-3** (25 mg, 0.09 mmol) and **IV-8** (26 mg, 0.04 mmol) to give a dark red solid. Yield: 2 mg (5%); $^1\text{H NMR}$ (400MHz, CDCl_3) δ (ppm) 7.74 (tt, $J = 6.4$ and 2.0 Hz, 4H, Ar-H), 7.58 (dt, $J = 8.3$ and 1.4 Hz, 4H, Ar-H), 7.16 (s, 2H, *meso*-H), 6.43 (d, $J = 4.1$ Hz, 4H, pyrrole-H), 6.21 (d, $J = 4.1$ Hz, 4H, pyrrole-H), 2.48 (s, 6H, CH_3), 2.46 (s, 6H, CH_3), 2.15 (s, 6H, CH_3), 2.14 (s, 6H, CH_3); MALDI-TOF calcd. 1166.3, found 1166.4 $[(\text{M})^+]$; UV/Vis (CHCl_3) λ_{max} nm (A): 496.0 (1.037) and 546.0 (0.827).

rack complex (IV-12-1). The same procedure was used as in the synthesis of **IV-9-2**, starting from **IV-2** (26 mg, 0.09 mmol) and **IV-6** (21 mg, 0.04 mmol) to give a dark blue solid. Yield: 2 mg (4%); $^1\text{H NMR}$ (400MHz, CDCl_3) δ (ppm) 7.11 (s, 2H, *meso*-H), 7.00 (d, $J = 3.5$ Hz, 2H, pyrrole-H), 6.92 (s, 2H, Ar-H), 6.86 (s, 2H, Ar-H), 6.40 (d, $J = 3.8$ Hz, 4H, pyrrole-H), 6.22 (d, $J = 3.5$ Hz, 2H, pyrrole-H), 6.08 (d, $J = 4.1$ Hz, 4H, pyrrole-H), 2.58 (s, 6H, CH_3), 2.43 (s, 4H, CH_2), 2.38 (s, 6H, CH_3), 2.11 (s, 6H, CH_3), 2.10 (s, 6H, CH_3), 2.02 (s, 6H, CH_3), 1.93 (s, 6H, CH_3); MALDI-TOF calcd. 1072.4, found 1072.5 $[(\text{M})^+]$; UV/Vis (CHCl_3) λ_{max} nm (A): 491.0 (1.085) and 628.0 (0.952).

rack complex (IV-13-1). The same procedure was used as in the synthesis of **IV-9-2**, starting from **IV-3** (25 mg, 0.09 mmol) and **IV-6** (21 mg, 0.04 mmol) to give a dark blue solid. Yield: 2 mg (4%); $^1\text{H NMR}$ (400MHz, CDCl_3) δ (ppm) 7.72 (ddd, $J = 16.5$, 8.8 and 1.5 Hz, 4H, Ar-H), 7.57 (d, $J = 8.5$ Hz, 4H, Ar-H), 7.12 (s, 2H, *meso*-H), 7.00 (d, $J = 3.8$ Hz, 2H, pyrrole-H), 6.40 (d, $J = 4.1$ Hz, 4H, pyrrole-H), 6.22 (d, $J = 3.8$ Hz, 2H, pyrrole-H), 6.17 (d, $J = 4.1$ Hz, 4H,

pyrrole-H), 2.59 (s, 6H, CH₃), 2.53 (s, 4H, CH₂), 2.05 (s, 12H, CH₃), 2.01 (s, 6H, CH₃); MALDI-TOF calcd. 1038.3, found 1038.3 [(M)⁺]; UV/Vis (CHCl₃) λ_{max} nm (A): 493.0 (1.181) and 627.0 (1.074).

rack complex (IV-14-1). The same procedure was used as in the synthesis of **IV-9-2**, starting from **IV-4** (29 mg, 0.09 mmol) and **IV-6** (21 mg, 0.04 mmol) to give a dark blue solid. Yield: 3 mg (7%); ¹H NMR (400MHz, CDCl₃) δ (ppm) 7.41 (ddd, *J* = 10.3, 7.9 and 1.2 Hz, 4H, Ar-H), 7.32 (t, *J* = 8.0 Hz, 2H, Ar-H), 7.11 (s, 2H, *meso*-H), 6.99 (d, *J* = 3.5 Hz, 2H, pyrrole-H), 6.38 (d, *J* = 3.8 Hz, 4H, pyrrole-H), 6.22 (d, *J* = 3.8 Hz, 2H, pyrrole-H), 6.15 (d, *J* = 4.1 Hz, 4H, pyrrole-H), 2.59 (s, 6H, CH₃), 2.52 (s, 4H, CH₂), 2.10 (s, 6H, CH₃), 2.04 (s, 12H, CH₃); MALDI-TOF calcd. 1124.1, found 1124.3 [(M)⁺]; UV/Vis (CHCl₃) λ_{max} nm (A): 498.0 (1.044) and 629.0 (0.797).

rack complex (IV-15-2). The same procedure was used as in the synthesis of **IV-9-2**, starting from **IV-2** (26 mg, 0.09 mmol) and **III-22** (28 mg, 0.04 mmol) to give a dark blue solid. Yield: 2 mg (3%); ¹H NMR (400MHz, CDCl₃) δ (ppm) 7.41 (s, 2H, *meso*-H), 7.38 (s, 2H, pyrrole-H), 7.19 (s, 4H, Ar-H), 7.03 (s, 2H, Ar-H), 6.94 (s, 2H, Ar-H), 6.81 (s, 2H, Ar-H), 6.53 (d, *J* = 1.5 Hz, 2H, pyrrole-H), 6.41 (d, *J* = 4.1 Hz, 4H, pyrrole-H), 6.09 (d, *J* = 3.8 Hz, 4H, pyrrole-H), 2.49 (s, 6H, CH₃), 2.41-2.43 (m, 16H, CH₂ and CH₃), 2.38 (s, 6H, CH₃), 2.20 (s, 6H, CH₃), 2.05 (s, 12H, CH₃), 1.88 (s, 6H, CH₃); MALDI-TOF calcd. 1252.5, found 1252.6 [(M)⁺]; UV/Vis (CHCl₃) λ_{max} nm (A): 493.0 (1.531) and 637.0 (0.878).

Zn^{II} complexes (IV-16). The same procedure was used as in the synthesis of **IV-9-2**, starting from **IV-2** (26 mg, 0.09 mmol) and **III-24** (28 mg, 0.04 mmol) to give dark green solids.

IV-16-3 (rack): Yield: 9 mg (17%); ¹H NMR (300MHz, CDCl₃) δ (ppm) 7.18 (s, 2H, *meso*-H), 6.90 (s, 4H, Ar-H), 6.84 (s, 2H, Ar-H), 6.70 (s, 2H, Ar-H), 6.66 (s, 2H, Ar-H), 6.19 (d, *J* = 3.9 Hz, 4H, pyrrole-H), 5.96 (d, *J* = 4.0 Hz, 4H, pyrrole-H), 2.78 (q, *J* = 7.3 Hz, 4H, CH₂), 2.59 (s, 6H, CH₃), 2.33 (s, 6H, CH₃), 2.11 (s, 4H, CH₂), 2.09 (s, 6H, CH₃), 2.03 (s, 12H, CH₃), 1.98 (s, 12H, CH₃), 1.81 (s, 6H, CH₃), 1.71 (s, 6H, CH₃), 1.28 (t, *J* = 7.3 Hz, 6H, CH₃); ¹³C NMR (75MHz, CDCl₃) δ (ppm) 161.9, 158.0, 157.8, 144.5, 142.8, 139.2, 138.0, 137.0, 136.8, 136.7, 136.4, 135.9, 135.7, 135.4, 130.9, 130.3, 129.2, 127.3, 127.1, 126.1, 123.3, 121.8, 121.2, 116.5, 29.7, 24.4, 21.1, 21.1, 19.8, 19.4, 18.6, 16.7, 16.5, 13.0, 10.4; MALDI-TOF calcd. 1340.4, found 1340.5 [(M)⁺]; UV/Vis (CHCl₃) λ_{max} nm (logε): 492.0 (5.29) and 667.0 (5.25).

IV-16-2 (zigzag rack 2A+2B): Yield: 16 mg (20%); ¹H NMR (400MHz, CDCl₃) δ (ppm) 7.15 (s, 2H, *meso*-H), 6.90 (s, 4H, Ar-H), 6.85 (s, 4H, Ar-H), 6.81 (s, 2H, *meso*-H), 6.64 (s, 8H, Ar-H), 6.20 (d, *J* = 3.8 Hz, 2H, pyrrole-H), 6.13 (d, *J* = 4.1 Hz, 2H, pyrrole-H), 5.98 (d, *J* = 3.8 Hz, 2H, pyrrole-H), 5.86 (d, *J* = 3.8 Hz, 2H, pyrrole-H), 2.77 (q, *J* = 7.6 Hz, 4H, CH₂), 2.60-2.67 (m, 4H, CH₂), 2.54 (s, 6H, CH₃), 2.47 (s, 6H, CH₃), 2.38 (s, 6H, CH₃), 2.09 (s, 6H, CH₃), 2.08 (s, 6H, CH₃), 2.01-2.03 (m, 8H, CH₂), 1.98 (s, 12H, CH₃), 1.97 (s, 12H, CH₃), 1.94 (s, 6H, CH₃), 1.91 (s, 6H, CH₃), 1.84 (s, 6H, CH₃), 1.76 (s, 6H, CH₃), 1.27 (t, *J* = 7.2 Hz, 6H, CH₃), 1.19 (t, *J* = 7.3 Hz, 6H, CH₃); ¹³C NMR (100MHz, CDCl₃) δ (ppm) 162.7, 160.7, 158.2, 157.6, 157.3, 157.1, 144.0, 143.5, 142.6, 139.3, 138.4, 138.0, 137.9, 137.0, 136.8, 136.8, 136.4, 135.9, 135.8, 135.7, 135.6, 135.4, 130.8, 130.6, 129.7, 129.7, 129.0, 128.5, 127.2, 126.2, 126.1, 123.7, 122.4, 121.4, 121.2, 120.9, 120.7, 116.7, 116.4, 29.7, 24.7, 24.5, 21.1, 21.1, 19.5, 19.4, 18.6, 18.5, 16.7, 16.7,

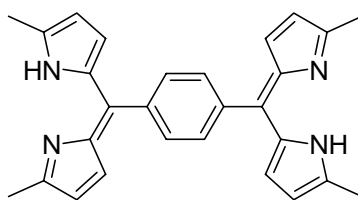
16.4, 16.4, 12.9, 12.8, 10.4, 10.4; MALDI-TOF calcd. 2036.7, found 2036.7 [(M)⁺]; UV/Vis (CHCl₃) λ_{max} nm (logε): 496.0 (5.33) and 672.0 (5.48).

IV-16-1 (zigzag rack 2A+3B): Yield: 6 mg (5%); MALDI-TOF calcd. 2732.9, found 2732.9 [(M)⁺]; UV/Vis (CHCl₃) λ_{max} nm (logε): 497.0 (5.31), 623.0 (5.46) and 669.0 (5.56).

Co^{II} complex (IV-17). The same procedure was used as in the synthesis of **IV-9-2**, starting from **IV-2** (26 mg, 0.09 mmol), **III-24** (28 mg, 0.04 mmol) and Co(OAc)₂•4H₂O (38 mg, 0.15 mmol) to give dark blue solids.

IV-17-3 (rack): Yield: 2 mg (4%); MALDI-TOF calcd. 1326.6, found 1326.6 [(M)⁺]; UV/Vis (CHCl₃) λ_{max} nm (A): 500.0 (1.000), 637.0 (0.641) and 689.0 (0.970).

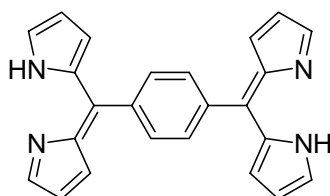
IV-17-2 (zigzag rack 2A+2B): Yield: 3.9 mg (4.8%); MALDI-TOF calcd. 2017.3, found 2017.3 [(M)⁺]; UV/Vis (CHCl₃) λ_{max} nm (A): 504.0 (0.893), 639.0 (1.017) and 702.0 (1.159).



IV-18

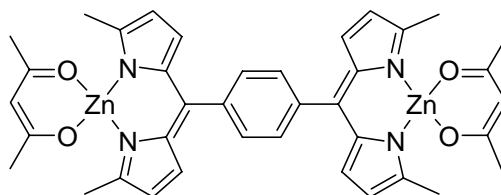
1,4-bis((Z)-(5-methyl-1H-pyrrol-2-yl)(5-methyl-2H-pyrrol-2-ylidene)methyl)benzene (IV-18). **IV-18** was synthesized based on a previously reported procedure,⁸² starting with terephthalaldehyde (1.96 g, 14.6 mmol) and 2-methylpyrrole (5.23g, 64.5 mmol) to afford a dark brown solid. Yield: 1.44 g (23%); ¹H NMR (400 MHz, CDCl₃) δ (ppm) 7.52 (s, 4H, Ar-H), 6.53 (d, *J* = 3.8 Hz, 4H, β-dipyrromethene), 6.20 (d, *J* = 4.1 Hz, 4H, β-dipyrromethene), 2.47 (s, 12H,

CH₃); ¹³C NMR (75 MHz, CD₂Cl₂) δ (ppm) 154.56, 140.35, 138.25, 138.10, 130.54, 129.26, 118.10, 16.57; Anal. Calcd. for: C₂₈H₂₆N₄·H₂O: C, 77.04; H, 6.46; N, 12.83. Found: C, 76.62; H, 6.09; N, 12.50. UV/Vis (CHCl₃) λ_{max} nm (A): 449.0 (0.972).



IV-19

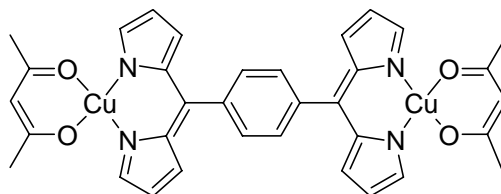
1,4-bis((Z)-(1H-pyrrol-2-yl)(2H-pyrrol-2-ylidene)methyl)benzene (IV-19). The same procedure was used as in the synthesis of **IV-18**, starting with terephthalaldehyde (3.35 g, 25 mmol) and pyrrole (87 ml, 1.25 mol) to afford a dark brown solid. Yield: 1.46 g (16%); ¹H NMR (300 MHz, CD₂Cl₂) δ (ppm) 7.56-7.76 (m, 8H, α-dipyrromethane and Ar-H), 6.67-6.73 (m, 4H, β-dipyrromethene), 6.43-6.49 (m, 4H, β-dipyrromethene); LR-ESI MS (M+H)⁺: *m/z* calcd for C₂₄H₁₉N₄: 363.5; found: 363.2; UV/Vis (CHCl₃) λ_{max} nm (A): 478.0 (1.007).



IV-20

heteroleptic Zn^{II} complex (IV-20). To a solution of Zinc(II) acetylacetonate (1.03 g, 3.9 mmol) in CHCl₃ (50 mL) was added dropwise **IV-18** (110 mg, 0.26 mmol, dissolved in 30 mL CHCl₃). The reaction mixture was stirred for 4 hours and the solvent was removed *in vacuo*. The crude product was purified by recrystallization from CH₂Cl₂/Et₂O to afford bright red crystals.

Yield: 147 mg (75%); ^1H NMR (300 MHz, CD_2Cl_2) δ (ppm) 7.45 (s, 4H, Ar-H), 6.58 (d, $J = 3.88$ Hz, 4H, β -dipyrromethene), 6.25 (d, $J = 4.11$ Hz, 4H, β -dipyrromethene), 5.55 (s, 2H, CH-acetylacetonate), 2.31 (s, 12H, CH_3 -dipyririn), 2.06 (s, 12H, CH_3 -acetylacetonate); ^{13}C NMR (75 MHz, CD_2Cl_2) δ (ppm) 194.8, 160.0, 144.7, 139.7, 139.4, 134.3, 129.9, 117.7, 100.5, 28.5, 17.2; MALDI-TOF calcd. 746.5, found 746.3 $[(\text{M})^+]$; UV/Vis (CHCl_3) λ_{max} nm (A): 491.0 (1.450).

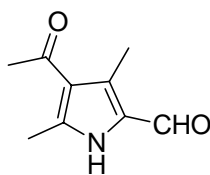


IV-21

heteroleptic Cu^{II} complex (IV-21). According to the previously reported procedure,⁸⁸ some modifications have been made for synthesis of **IV-21**. To a solution of copper(II) acetylacetonate (1.11 g, 4.24 mmol) in CHCl_3 (100 mL) was added **IV-19** (257 mg, 0.71 mmol, dissolved in 20 mL CHCl_3). The reaction mixture was stirred for 2 h at room temperature. The mixture was passed then through a silica gel pad. The organic solution was collected and concentrated under reduced pressure to give **IV-21** as a red solid. Yield: 152 mg (31%); MALDI-TOF calcd. 684.1, found 684.4 $[(\text{M})^+]$; UV/Vis (CHCl_3) λ_{max} nm (A): 308.0 (0.423), 339.0 (0.526) and 469.0 (1.249).

Zn^{II} rigid ladder (IV-22-L). To a solution of **III-22** (39 mg, 0.055 mmol) and **IV-20** (37 mg, 0.05 mmol) in CHCl₃/MeOH (20 mL/10 mL) was added a solution of NaOAc (27 mg, 0.33 mmol) in MeOH (1 mL). After stirring overnight, the solvent was removed by rotary evaporation. The residue was purified by flash chromatography on silica gel eluting with CH₂Cl₂/hexanes (3/2) to give the crude product which was then purified using gel permeation chromatography eluting with toluene, followed by washing with CH₂Cl₂ to afford the target Zn^{II} rigid ladder as a dark green solid. Yield: 2 mg (4%); MALDI-TOF calcd. 2180.7, found 2180.8 [(M)⁺]; UV/Vis (CHCl₃) λ_{max} nm (A): 484 (1.252) and 636 (1.178).

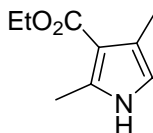
Cu^{II} rigid ladder (IV-23-L). The same procedure was used as in the synthesis of **IV-22-L**, starting from **III-22** (39 mg, 0.055 mmol) and **IV-21** (34 mg, 0.05 mmol) to give a dark green solid. Yield: 5 mg (10%); MALDI-TOF calcd. 2064.6, found 2064.8 [(M)⁺]; UV/Vis (CHCl₃) λ_{max} nm (A): 482.0 (1.232) and 611.0 (1.067).



IV-24

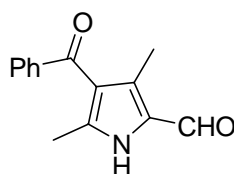
4-acetyl-3,5-dimethylpyrrole-2-carbaldehyde (IV-24). According to the previously reported procedure,⁷¹ some modifications have been made for synthesis of **IV-24**. To DMF (5 mL), cooled in an ice-water bath, was slowly added POCl₃ (0.27 mL, 2.8 mmol). The reaction mixture was stirred for 30 min, followed by addition of **II-14** (274 mg, 2 mmol, dissolved in 20

mL DCE). The mixture was heated to 85°C and stirred for 3 h. The reaction was allowed to cool to 0°C, followed by slow addition of K₂CO₃ (2.76 g, 20 mmol, dissolved in 10 mL water), and then heated to 85°C for another 2 h. The mixture was cooled to room temperature, and the organic layer was then washed with water and brine. After removal of the organic layer, the residue was purified by flash chromatography on silica gel eluting with 40% EtOAc in hexanes to give **IV-24** as a yellow solid. Yield: 100 mg (30%); ¹H NMR (400MHz, CDCl₃) δ (ppm) 9.67 (s, 1H, CHO), 9.55 (br. s, 1H, NH), 2.58 (s, 6H, CH₃), 2.47 (s, 3H, CH₃); EI MS (M⁺): *m/z* 165. HR-EI MS (M⁺) *m/z* calcd for C₉H₁₁NO₂ 165.0790, found 165.0788.



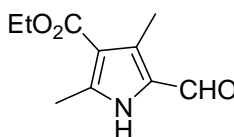
IV-25

ethyl 2,4-dimethylpyrrole-3-carboxylate (IV-25). The same procedure was used as in the synthesis of **II-19**, starting from 4-(ethoxycarbonyl)-3,5-dimethyl-1H-pyrrole-2-carboxylic acid (0.84 g, 4 mmol) to afford a brown solid. Yield: 0.62 g (88%); ¹H NMR (400MHz, CDCl₃) δ (ppm) 7.88 (br. s, 1H, NH), 6.36 (s, 1H, pyrrole-H), 4.28 (q, *J* = 7.1 Hz, 2H, CH₂), 2.50 (s, 3H, CH₃), 2.25 (s, 3H, CH₃), 1.36 (t, *J* = 7.2 Hz, 3H, CH₃); EI MS (M⁺): *m/z* 167. HR-EI MS (M⁺) *m/z* calcd for C₉H₁₃NO₂ 167.0946, found 167.0943.



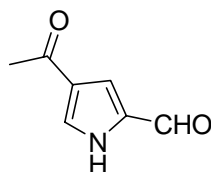
IV-26

4-benzoyl-3,5-dimethylpyrrole-2-carbaldehyde (IV-26). The same procedure was used as in the synthesis of **IV-24**, starting from **II-19** (0.40 g, 2 mmol) to afford a yellow solid. Yield: 330 mg (73%); ^1H NMR (300MHz, CDCl_3) δ (ppm) 10.22 (br. s, 1H, NH), 9.63 (s, 1H, CHO), 7.72-7.74 (m, 2H, Ar-H), 7.55-7.60 (m, 1H, Ar-H), 7.45-7.50 (m, 2H, Ar-H), 2.30 (s, 3H, CH_3), 2.29 (s, 3H, CH_3); EI MS (M^+): m/z 227. HR-EI MS (M^+) m/z calcd for $\text{C}_{14}\text{H}_{13}\text{NO}_2$ 227.0946, found 227.0941.



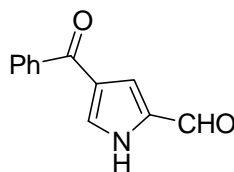
IV-27

ethyl 5-formyl-2,4-dimethylpyrrole-3-carboxylate (IV-27). The same procedure was used as in the synthesis of **IV-24**, starting from **IV-25** (0.33 g, 2 mmol) to afford a white solid. Yield: 200 mg (52%); ^1H NMR (300MHz, CDCl_3) δ (ppm) 10.51 (br. s, 1H, NH), 9.60 (s, 1H, CHO), 4.31 (q, $J = 7.0$ Hz, 2H, CH_2), 2.59 (s, 3H, CH_3), 2.56 (s, 3H, CH_3), 1.37 (t, $J = 7.0$ Hz, 3H, CH_3); EI MS (M^+): m/z 195. HR-EI MS (M^+) m/z calcd for $\text{C}_{10}\text{H}_{13}\text{NO}_3$ 195.0895, found 195.0903.



IV-28

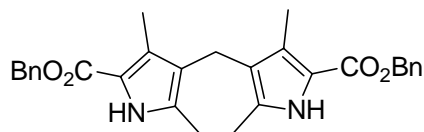
4-acetylpyrrole-2-carbaldehyde (IV-28). IV-28 was synthesized based on a previous reported procedure.¹⁰² ¹H NMR (300 MHz, DMSO-*d*₆) δ (ppm) 12.70 (br. s, 1H, NH), 9.57 (s, 1H, CHO), 7.90 (s, 1H, Pyrrole-H), 7.39 (d, *J* = 1.4 Hz, 1H, Pyrrole-H), 2.39 (s, 3H, CH₃); EI MS (M⁺): *m/z* 137. HR-EI MS (M⁺) *m/z* calcd for C₇H₇NO₂ 137.0477, found 137.0478.



IV-29

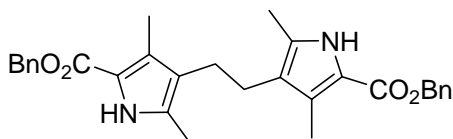
4-benzoyl-1H-pyrrole-2-carbaldehyde (IV-29). IV-29 was synthesized based on a previously reported procedure.⁹³ ¹H NMR (300 MHz, DMSO-*d*₆) δ (ppm) 12.86 (br. s, 1H, NH), 9.62 (s, 1H, CHO), 7.80-7.82 (m, 2H, Ar-H), 7.75 (s, 1H, Pyrrole-H), 7.61-7.67 (m, 1H, Ar-H), 7.52-7.57 (m, 2H, Ar-H), 7.46 (d, *J* = 1.3 Hz, 1H, Pyrrole-H); EI MS (M⁺): *m/z* 199. HR-EI MS (M⁺) *m/z* calcd for C₁₂H₉NO₂ 199.0633, found 199.0636.

dibenzyl β - β' linked bis(pyrrole-2-carboxylate) (IV-30). IV-30 ($n = 1$ to 5) were synthesized based on previously reported procedures.⁴⁶



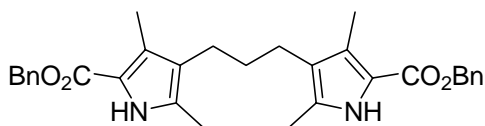
IV-30, n = 1

IV-30, n = 1: ¹H NMR (300 MHz, DMSO-*d*₆) δ (ppm) 11.07 (br. s, 2H, NH), 7.31-7.43 (m, 10H, Ar-H), 5.22 (s, 4H, CH₂), 3.36 (s, 2H, CH₂), 2.08 (s, 6H, CH₃), 2.00 (s, 6H, CH₃); EI MS (M^+): m/z 470.3. HR-EI MS (M^+) m/z calcd for C₂₉H₃₀N₂O₄ 470.2206, found 470.2209.



IV-30, n = 2

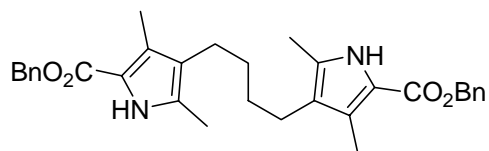
IV-30, n = 2: ¹H NMR (300 MHz, DMSO-*d*₆) δ (ppm) 11.04 (br. s, 2H, NH), 7.31-7.43 (m, 10H, Ar-H), 5.23 (s, 4H, CH₂), 2.35 (s, 4H, CH₂), 2.10 (s, 6H, CH₃), 1.91 (s, 6H, CH₃); EI MS (M^+): m/z 484.3. HR-EI MS (M^+) m/z calcd for C₃₀H₃₂N₂O₄ 484.2362, found 484.2363.



IV-30, n = 3

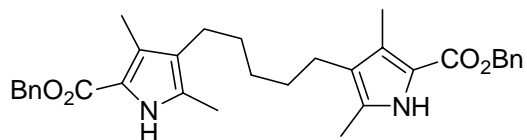
IV-30, n = 3: ¹H NMR (300 MHz, DMSO-*d*₆) δ (ppm) 11.07 (br. s, 2H, NH), 7.31-7.43 (m, 10H, Ar-H), 5.23 (s, 4H, CH₂), 2.28 (t, $J = 7.5$ Hz, 4H, CH₂), 2.13 (s, 6H, CH₃), 2.09 (s, 6H, CH₃),

1.37-1.47 (m, 2H, CH₂); EI MS (M⁺): *m/z* 498.4. HR-EI MS (M⁺) *m/z* calcd for C₃₁H₃₄N₂O₄ 498.2519, found 498.2521.



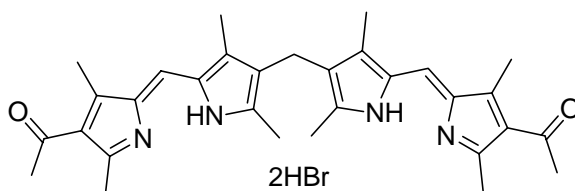
IV-30, n = 4

IV-30, n = 4: ¹H NMR (300 MHz, DMSO-*d*₆) δ (ppm) 11.07 (br. s, 2H, NH), 7.31-7.43 (m, 10H, Ar-H), 5.23 (s, 4H, CH₂), 2.26-2.30 (m, 4H, CH₂), 2.15 (s, 6H, CH₃), 2.09 (s, 6H, CH₃), 1.32-1.37 (m, 4H, CH₂); EI MS (M⁺): *m/z* 512.1. HR-EI MS (M⁺) *m/z* calcd for C₃₂H₃₆N₂O₄ 512.2675, found 512.2678.



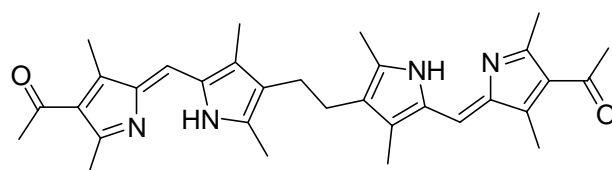
IV-30, n = 5

IV-30, n = 5: ¹H NMR (300 MHz, DMSO-*d*₆) δ (ppm) 11.07 (br. s, 2H, NH), 7.31-7.43 (m, 10H, Ar-H), 5.23 (s, 4H, CH₂), 2.28 (t, *J* = 7.5 Hz, 4H, CH₂), 2.15 (s, 6H, CH₃), 2.10 (s, 6H, CH₃), 1.22-1.37 (m, 6H, CH₂); EI MS (M⁺): *m/z* 526.2. HR-EI MS (M⁺) *m/z* calcd for C₃₃H₃₈N₂O₄ 526.2832, found 526.2832.



IV-31

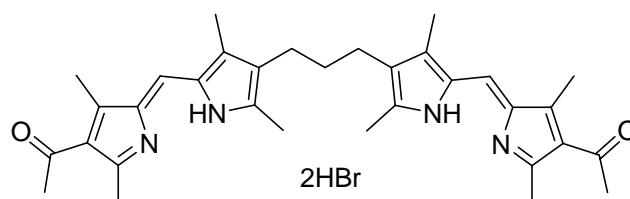
β - β' linked bisdipyrin ligand (IV-31). According to the previously reported procedure,⁴⁶ some modifications have been made for synthesis of **IV-31**. To a mixture of **IV-30** ($n = 1$) (235 mg, 0.5 mmol) and 10 mol % palladium on activated carbon (50 mg) in a 250 mL round-bottom flask was added THF (75 mL) and MeOH (25 mL). The mixture was stirred overnight under a hydrogen atmosphere at 1 atm. The reaction mixture was then filtered through Celite to remove the catalyst. The filtrate was collected in a 250 mL round-bottom flask, and then **IV-24** (165 mg, 1.0 mmol) was added, followed by the addition of 33% hydrogen bromide in acetic acid (1.5 mL). The solution immediately turned from colourless to dark orange. The reaction mixture was stirred for 2 h at room temperature, and then the organic solvent was removed *in vacuo* to give the crude product. Trituration of the crude product with diethyl ether gave **IV-31** as a red solid. Yield: 260 mg (79%); ¹H NMR (400MHz, CDCl₃/CD₃OD = 2/1) δ (ppm) 7.23 (s, 2H, *meso*-H), 2.65 (s, 6H, CH₃), 2.40 (s, 6H, CH₃), 2.38 (s, 2H, CH₂), 2.35 (s, 6H, CH₃), 2.32 (s, 6H, CH₃), 2.14 (s, 6H, CH₃); ESI MS (M+H)⁺: m/z 497.4; HR-ESI MS (M+H)⁺: m/z calcd for C₃₁H₃₇N₄O₂: 497.2917; found: 497.2922; UV/Vis (CHCl₃/CH₃OH = 2/1) λ_{\max} nm (A): 486.0 (0.868).



2HBr

IV-32

β - β' linked bisdipyrrin ligand (IV-32). The same procedure was used as in the synthesis of **IV-31**, starting from **IV-30** ($n = 2$) (242 mg, 0.5 mmol) to afford a red solid. Yield: 300 mg (89%); ^1H NMR (400MHz, $\text{CDCl}_3/\text{CD}_3\text{OD} = 2/1$) δ (ppm) 7.20 (s, 2H, *meso*-H), 2.62 (s, 6H, CH_3), 2.50 (s, 4H, CH_2), 2.40 (s, 6H, CH_3), 2.31 (s, 6H, CH_3), 2.22 (s, 6H, CH_3), 2.07 (s, 6H, CH_3); ESI MS ($\text{M}+\text{H}$) $^+$: m/z 511.4; HR-ESI MS ($\text{M}+\text{H}$) $^+$: m/z calcd for $\text{C}_{32}\text{H}_{39}\text{N}_4\text{O}_2$: 511.3073; found: 511.3060. UV/Vis ($\text{CHCl}_3/\text{CH}_3\text{OH} = 2/1$) λ_{max} nm (A): 492.0 (0.682).

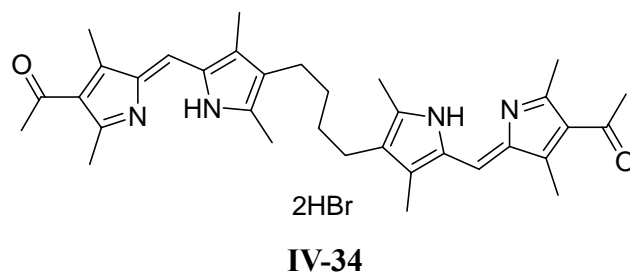


2HBr

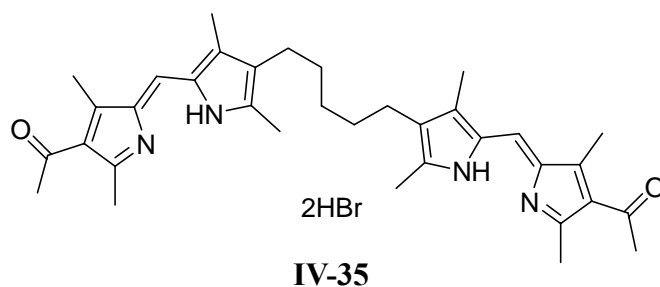
IV-33

β - β' linked bisdipyrrin ligand (IV-33). The same procedure was used as in the synthesis of **IV-31**, starting from **IV-30** ($n = 3$) (249 mg, 0.5 mmol) to afford an orange solid. Yield: 310 mg (90%); ^1H NMR (400MHz, $\text{CDCl}_3/\text{CD}_3\text{OD} = 2/1$) δ (ppm) 7.17 (s, 2H, *meso*-H), 2.66 (s, 6H, CH_3), 2.47 (s, 6H, CH_3), 2.39 (s, 6H, CH_3), 2.31-2.37 (m, 10H, CH_2 and CH_3), 2.16 (s, 6H, CH_3), 1.42-1.49 (m, 2H, CH_2); ^{13}C NMR (100MHz, $\text{CDCl}_3/\text{CD}_3\text{OD} = 2/1$) δ (ppm) 194.8, 159.9, 153.5, 145.5, 144.5, 130.3, 128.6, 126.3, 124.6, 120.8, 30.8, 29.0, 23.2, 14.9, 12.7, 12.1, 9.8; ESI MS ($\text{M}+\text{H}$) $^+$: m/z 525.4; HR-ESI MS ($\text{M}+\text{H}$) $^+$: m/z calcd for $\text{C}_{33}\text{H}_{41}\text{N}_4\text{O}_2$: 525.3230; found:

525.3240. UV/Vis (CHCl₃/CH₃OH = 2/1) λ_{\max} nm (A): 487.0 (1.340).

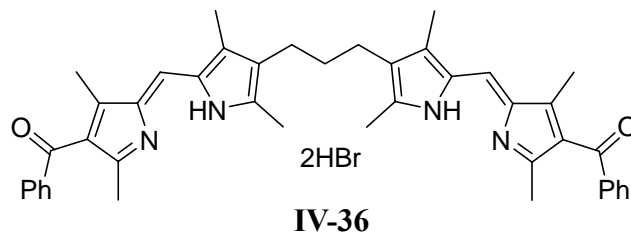


β - β' linked bisdipyrrin ligand (IV-34). The same procedure was used as in the synthesis of **IV-31**, starting from **IV-30** ($n = 4$) (256 mg, 0.5 mmol) to afford an orange solid. Yield: 332 mg (95%); ¹H NMR (400MHz, CDCl₃/CD₃OD = 2/1) δ (ppm) 7.16 (s, 2H, *meso*-H), 2.63 (s, 6H, CH₃), 2.45 (s, 6H, CH₃), 2.39 (s, 6H, CH₃), 2.31 (s, 10H, CH₂ and CH₃), 2.15 (s, 6H, CH₃), 1.33 (s, 4H, CH₂); ESI MS (M+H)⁺: m/z 539.4; HR-ESI MS (M+H)⁺: m/z calcd for C₃₄H₄₃N₄O₂: 539.3386; found: 539.3395. UV/Vis (CHCl₃/CH₃OH = 2/1) λ_{\max} nm (A): 483.0 (1.146).

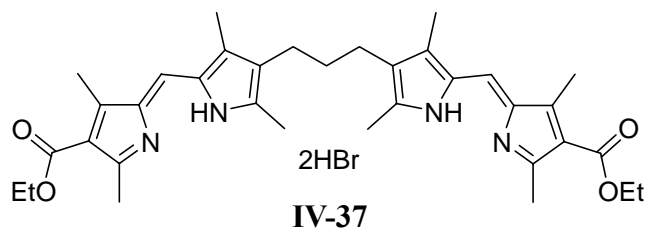


β - β' linked bisdipyrrin ligand (IV-35). The same procedure was used as in the synthesis of **IV-31**, starting from **IV-30** ($n = 5$) (263 mg, 0.5 mmol) to afford an orange solid. Yield: 330 mg (92%); ¹H NMR (400MHz, CDCl₃/CD₃OD = 2/1) δ (ppm) 7.16 (s, 2H, *meso*-H), 2.64 (s, 6H,

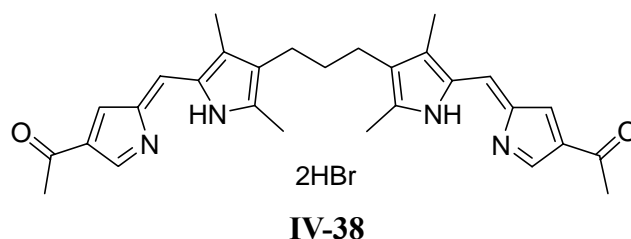
CH₃), 2.46 (s, 6H, CH₃), 2.39 (s, 6H, CH₃), 2.26-2.31 (m, 10H, CH₂ and CH₃), 2.16 (s, 6H, CH₃), 1.28-1.35 (m, 4H, CH₂), 1.14-1.20 (m, 2H, CH₂); ESI MS (M+H)⁺: *m/z* 553.5; HR-ESI MS (M+H)⁺: *m/z* calcd for C₃₅H₄₅N₄O₂: 553.3543; found: 553.3533. UV/Vis (CHCl₃/CH₃OH = 2/1) λ_{max} nm (A): 481.0 (0.956).



β-β' linked bisdipyrin ligand (IV-36). The same procedure was used as in the synthesis of **IV-31**, starting from **IV-30** (*n* = 3) (249 mg, 0.5 mmol) and **IV-26** (227 mg, 1.0 mmol) to afford a red solid. Yield: 330 mg (81%); ¹H NMR (400MHz, CDCl₃/CD₃OD = 2/1) δ (ppm) 12.75 (br. s, 2H, NH), 12.50 (br. s, 2H, NH), 7.51 (d, *J* = 7.6 Hz, 4H, Ar-H), 7.42 (t, *J* = 7.3 Hz, 2H, Ar-H), 7.30 (d, *J* = 7.6 Hz, 4H, Ar-H), 7.14 (s, 2H, *meso*-H), 2.48 (s, 6H, CH₃), 2.33-2.38 (m, 10H, CH₂ and CH₃), 2.17 (s, 6H, CH₃), 2.10 (s, 6H, CH₃), 1.43-1.50 (m, 2H, CH₂); ¹³C NMR (100MHz, CDCl₃/CD₃OD = 2/1) δ (ppm) 192.4, 159.3, 152.3, 145.2, 143.7, 138.3, 133.0, 130.1, 128.6, 128.4, 128.2, 126.4, 124.9, 120.7, 29.0, 23.2, 13.4, 12.6, 11.1, 9.7; ESI MS (M+H)⁺: *m/z* 649.5; HR-ESI MS (M+H)⁺: *m/z* calcd for C₄₃H₄₅N₄O₂: 649.3543; found: 649.3528. UV/Vis (CHCl₃/CH₃OH = 2/1) λ_{max} nm (A): 491.0 (0.489).

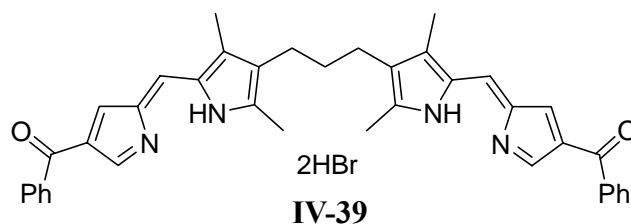


β - β' linked bisdipyrin ligand (IV-37). The same procedure was used as in the synthesis of **IV-31**, starting from **IV-30** ($n = 3$) (249 mg, 0.5 mmol) and **IV-27** (195 mg, 1.0 mmol) to afford an orange solid. Yield: 340 mg (91%); $^1\text{H NMR}$ (400MHz, $\text{CDCl}_3/\text{CD}_3\text{OD} = 2/1$) δ (ppm) 7.15 (s, 2H, *meso*-H), 4.13 (q, $J = 7.5$ Hz, 4H, CH_2), 2.63 (s, 6H, CH_3), 2.45 (s, 6H, CH_3), 2.40 (s, 6H, CH_3), 2.34 (t, $J = 7.8$ Hz, 4H, CH_2), 2.16 (s, 6H, CH_3), 1.46 (t, $J = 7.3$ Hz, 2H, CH_2), 1.18 (t, $J = 7.2$ Hz, 6H, CH_3); ESI MS ($\text{M}+\text{H}$) $^+$: m/z 585.4; HR-ESI MS ($\text{M}+\text{H}$) $^+$: m/z calcd for $\text{C}_{35}\text{H}_{45}\text{N}_4\text{O}_4$: 585.3441; found: 585.3428. UV/Vis ($\text{CHCl}_3/\text{CH}_3\text{OH} = 2/1$) λ_{max} nm (A): 485.0 (1.255).



β - β' linked bisdipyrin ligand (IV-38). The same procedure was used as in the synthesis of **IV-31**, starting from **IV-30** ($n = 3$) (249 mg, 0.5 mmol) and **IV-28** (137 mg, 1.0 mmol) to afford an orange solid. Yield: 266 mg (84%); $^1\text{H NMR}$ (400MHz, $\text{CDCl}_3/\text{CD}_3\text{OD} = 2/1$) δ (ppm) 7.79 (s, 4H, pyrrole-H), 7.55 (s, 2H, *meso*-H), 2.50 (s, 6H, CH_3), 2.36 (t, $J = 7.5$ Hz, 4H, CH_2), 2.30 (s, 6H, CH_3), 2.16 (s, 6H, CH_3), 1.44-1.45 (m, 2H, CH_2); $^{13}\text{C NMR}$ (100MHz, $\text{CDCl}_3/\text{CD}_3\text{OD} = 2/1$) δ (ppm) 193.6, 166.3, 148.6, 134.7, 132.5, 132.2, 129.9, 127.6, 126.5, 125.1, 28.5, 26.9, 23.2, 13.3, 9.8; ESI MS ($\text{M}+\text{H}$) $^+$: m/z 469.3; HR-ESI MS ($\text{M}+\text{H}$) $^+$: m/z calcd for $\text{C}_{29}\text{H}_{33}\text{N}_4\text{O}_2$:

469.2604; found: 469.2611. UV/Vis (CHCl₃/CH₃OH = 2/1) λ_{max} nm (A): 468.0 (0.572).



β - β' linked bisdipyrin ligand (IV-39). The same procedure was used as in the synthesis of **IV-31**, starting from **IV-30** ($n = 3$) (249 mg, 0.5 mmol) and **IV-29** (199 mg, 1.0 mmol) to afford an orange solid. Yield: 358 mg (95%); ¹H NMR (400MHz, CDCl₃/CD₃OD = 2/1) δ (ppm) 7.80 (s, 2H, pyrrole-H), 7.69 (s, 2H, pyrrole-H), 7.63 (d, $J = 7.3$ Hz, 4H, Ar-H), 7.55 (s, 2H, *meso*-H), 7.42 (t, $J = 7.3$ Hz, 2H, Ar-H), 7.32 (d, $J = 7.6$ Hz, 4H, Ar-H), 2.49 (s, 6H, CH₃), 2.40 (t, $J = 7.8$ Hz, 4H, CH₂), 2.20 (s, 6H, CH₃), 1.43-1.51 (m, 2H, CH₂); ESI MS (M+H)⁺: m/z 593.4; HR-ESI MS (M+H)⁺: m/z calcd for C₃₉H₃₇N₄O₂: 593.2917; found: 593.2906. UV/Vis (CHCl₃/CH₃OH = 2/1) λ_{max} nm (A): 471.0 (0.813).

Zn^{II} flexible ladder (IV-40-L). To a solution of **IV-31** (27 mg, 0.04 mmol) and **IV-20** (20 mg, 0.027 mmol) in CHCl₃/MeOH (20 mL/10 mL) was added a solution of NaOAc (41 mg, 0.5 mmol) in MeOH (1 mL). After stirring overnight, the solvent was removed by rotary evaporation. The residue was purified by flash chromatography on neutral alumina eluting with CH₂Cl₂/MeOH to give the crude product which was then purified using gel permeation chromatography eluting with toluene to afford two separate fractions. The target Zn^{II} ladder was obtained as a yellow solid. Yield: 1 mg (4%); ¹H NMR (400MHz, CDCl₃) δ (ppm) 7.53-7.55 (m,

4H, Ar-H), 7.44-7.48 (m, 4H, Ar-H), 7.22 (d, $J = 7.5$ Hz, 4H, meso-H), 6.79 (d, $J = 3.8$ Hz, 2H, pyrrole-H), 6.66 (d, $J = 3.8$ Hz, 2H, pyrrole-H), 6.64 (d, $J = 3.8$ Hz, 2H, pyrrole-H), 6.56 (d, $J = 3.8$ Hz, 2H, pyrrole-H), 6.31 (d, $J = 3.8$ Hz, 2H, pyrrole-H), 6.29 (d, $J = 3.8$ Hz, 2H, pyrrole-H), 6.22 (d, $J = 3.8$ Hz, 2H, pyrrole-H), 6.16 (d, $J = 4.1$ Hz, 2H, pyrrole-H), 5.71 (d, $J = 4.1$ Hz, 2H, pyrrole-H), 2.60 (s, 12H, CH₃), 2.45-2.48 (m, 28H, CH₂ and CH₃), 2.34 (s, 6H, CH₃), 2.31 (s, 6H, CH₃), 1.95-2.11 (m, 24H, CH₃), 1.52 (s, 12H, CH₃); MALDI-TOF calcd. 2076.7, found 2076.6 [(M)⁺]; UV/Vis (CHCl₃) λ_{\max} nm (A): 489.0 (0.630).

Zn^{II} Dimer (IV-40-D). The Zn^{II} dimer was obtained as a yellow solid. Yield: 1 mg (5%); ¹H NMR (400MHz, CDCl₃) δ (ppm) 7.10 (s, 4H, meso-H), 2.53 (s, 12H, CH₃), 2.43 (s, 12H, CH₃), 2.32 (d, $J = 9.4$ Hz, 4H, CH₂), 2.29 (s, 12H, CH₃), 2.27 (s, 12H, CH₃), 1.43 (s, 12H, CH₃); MALDI-TOF calcd. 1116.4, found 1116.5 [(M)⁺]; UV/Vis (CHCl₃) λ_{\max} nm (A): 468.0 (0.405) and 519.0 (0.949).

Zn^{II} flexible ladder (IV-41-L). The same procedure was used as in the synthesis of IV-40-L, starting from IV-32 (27 mg, 0.04 mmol) to afford a yellow solid. Yield: 1 mg (4%); MALDI-TOF calcd. 2104.7, found 2104.7 [(M)⁺]; UV/Vis (CHCl₃) λ_{\max} nm (A): 490.0 (0.523).

Zn^{II} Dimer (IV-41-D). The Zn^{II} dimer was obtained as a yellow solid. Yield: 2 mg (9%); ¹H NMR (400MHz, CDCl₃) δ (ppm) 7.10 (s, 4H, meso-H), 2.50 (s, 12H, CH₃), 2.36-2.38 (m, 20H, CH₂ and CH₃), 2.31 (s, 12H, CH₃), 1.99 (s, 12H, CH₃), 1.40 (s, 12H, CH₃); MALDI-TOF calcd. 1144.4, found 1144.5 [(M)⁺]; UV/Vis (CHCl₃) λ_{\max} nm (A): 465.0 (0.793) and 516.0 (1.460).

Zn^{II} flexible ladder (IV-42-L). The same procedure was used as in the synthesis of **IV-40-L**, starting from **IV-33** (27 mg, 0.04 mmol) to afford a yellow solid. Yield: 2 mg (5%); ¹H NMR (400MHz, CDCl₃) δ (ppm) 7.50-7.57 (m, 8H, Ar-H), 7.17-7.21 (m, 4H, meso-H), 6.68 (t, *J* = 4.1 Hz, 3H, pyrrole-H), 6.61-6.63 (m, 4H, pyrrole-H), 6.50 (d, *J* = 3.8 Hz, 1H, pyrrole-H), 6.22-6.25 (m, 3H, pyrrole-H), 6.19-6.21 (m, 4H, pyrrole-H), 5.78 (d, *J* = 3.8 Hz, 1H, pyrrole-H), 2.56-2.59 (m, 12H, CH₃), 2.42-2.47 (m, 18H, CH₃), 2.29-2.34 (m, 20H, CH₂ and CH₃), 2.25 (s, 6H, CH₃), 2.14 (s, 6H, CH₃), 2.03 (s, 12H, CH₃), 1.92-1.98 (s, 12H, CH₃), 1.79 (s, 3H, CH₃), 1.69 (s, 3H, CH₃); MALDI-TOF calcd. 2140.0, found 2139.8 [(M)⁺]; UV/Vis (CHCl₃) λ_{max} nm (A): 492.0 (1.080).

Zn^{II} Dimer (IV-42-D). The Zn^{II} dimer was obtained as a yellow solid. Yield: 1 mg (6%); ¹H NMR (400MHz, CDCl₃) δ (ppm) 7.15 (d, *J* = 7.3 Hz, 4H, *meso*-H), 2.55 (d, *J* = 4.3 Hz, 12H, CH₃), 2.42 (s, 12H, CH₃), 2.26-2.33 (m, 20H, CH₂ and CH₃), 2.22 (s, 12H, CH₃), 1.79 (s, 6H, CH₃), 1.69 (s, 6H, CH₃), 1.51 (t, *J* = 7.0 Hz, 4H, CH₂); MALDI-TOF calcd. 1172.5, found 1172.7 [(M)⁺]; UV/Vis (CHCl₃) λ_{max} nm (A): 503.0 (1.275).

Zn^{II} flexible ladder (IV-43-L). The same procedure was used as in the synthesis of **IV-40-L**, starting from **IV-34** (28 mg, 0.04 mmol) to afford a yellow solid. Yield: 2 mg (8%); ¹H NMR (400MHz, CDCl₃) δ (ppm) 7.47-7.59 (m, 8H, Ar-H), 7.17-7.20 (m, 4H, meso-H), 6.63 (t, *J* = 3.8 Hz, 8H, pyrrole-H), 6.21 (t, *J* = 3.8 Hz, 8H, pyrrole-H), 2.58-2.60 (m, 12H, CH₃), 2.47 (s, 12H, CH₃), 2.41-2.44 (m, 12H, CH₃), 2.37-2.38 (m, 12H, CH₃), 2.25-2.30 (m, 24H, CH₃), 2.17-2.19 (m, 8H, CH₂), 2.05 (s, 12H, CH₃), 1.39-1.45 (m, 8H, CH₂); MALDI-TOF calcd.

2168.0, found 2168.2 [(M)⁺]; UV/Vis (CHCl₃) λ_{max} nm (A): 492.0 (1.319).

Zn^{II} Dimer (IV-43-D). The Zn^{II} dimer was obtained as a yellow solid. Yield: 4 mg (17%); ¹H NMR (400MHz, CDCl₃) δ (ppm) 7.15 (s, 4H, *meso*-H), 2.55 (s, 12H, CH₃), 2.42 (s, 12H, CH₃), 2.30-2.36 (m, 8H, CH₂), 2.25 (s, 12H, CH₃), 2.15-2.18 (m, 12H, CH₃), 1.79-1.86 (m, 12H, CH₃), 1.48 (s, 12H, CH₃); MALDI-TOF calcd. 1204.2, found 1204.4 [(M)⁺]; UV/Vis (CHCl₃) λ_{max} nm (A): 502.0 (1.326).

Zn^{II} flexible ladder (IV-44-L). The same procedure was used as in the synthesis of IV-40-L, starting from IV-35 (28 mg, 0.04 mmol) to afford a yellow solid. Yield: 1 mg (3%); MALDI-TOF calcd. 2196.1, found 2196.0 [(M)⁺]; UV/Vis (CHCl₃) λ_{max} nm (A): 495.0 (1.167).

Zn^{II} Dimer (IV-44-D). The Zn^{II} dimer was obtained as a yellow solid. Yield: 2 mg (8%); ¹H NMR (400MHz, CDCl₃) δ (ppm) 7.16 (s, 4H, *meso*-H), 2.55 (d, *J* = 2.9 Hz, 12H, CH₃), 2.42 (s, 12H, CH₃), 2.23-2.30 (m, 32H, CH₂ and CH₃), 1.81 (d, *J* = 3.8 Hz, 12H, CH₃), 1.30-1.35 (m, 8H, CH₂), 1.17-1.23 (m, 4H, CH₂); MALDI-TOF calcd. 1228.5, found 1228.6 [(M)⁺]; UV/Vis (CHCl₃) λ_{max} nm (A): 496.0 (0.988).

Zn^{II} flexible ladder (IV-45-L). The same procedure was used as in the synthesis of IV-40-L, starting from IV-36 (32 mg, 0.04 mmol) to afford a yellow solid. Yield: 5 mg (16%); MALDI-TOF calcd. 2388.2, found 2388.1 [(M)⁺]; UV/Vis (CHCl₃) λ_{max} nm (A): 495.0 (1.160) and 509.0 (1.181).

Zn^{II} Dimer (IV-45-D). The Zn^{II} dimer was obtained as a yellow solid. Yield: 8 mg (27%); ¹H NMR (400MHz, CDCl₃) δ (ppm) 7.69 (d, *J* = 7.9 Hz, 8H, Ar-H), 7.50 (t, *J* = 7.3 Hz, 4H,

Ar-H), 7.42 (t, $J = 7.4$ Hz, 8H, Ar-H), 7.10 (d, $J = 2.0$ Hz, 4H, *meso*-H), 2.31-2.37 (m, 8H, CH₂), 2.27 (s, 12H, CH₃), 2.21 (d, $J = 6.4$ Hz, 12H, CH₃), 2.01 (d, $J = 4.1$ Hz, 12H, CH₃), 1.86 (s, 6H, CH₃), 1.76 (s, 6H, CH₃), 1.52-1.55 (m, 4H, CH₂); MALDI-TOF calcd. 1424.4, found 1424.4 [(M)⁺]; UV/Vis (CHCl₃) λ_{\max} nm (A): 511.0 (1.417).

Zn^{II} flexible ladder (IV-46-L). The same procedure was used as in the synthesis of IV-40-L, starting from IV-37 (32 mg, 0.04 mmol) to afford a yellow solid. Yield: 2 mg (7%); ¹H NMR (400MHz, CDCl₃) δ (ppm) 7.49-7.56 (m, 8H, Ar-H), 7.15-7.19 (m, 4H, *meso*-H), 6.68 (t, $J = 3.8$ Hz, 3H, pyrrole-H), 6.61-6.62 (m, 4H, pyrrole-H), 6.50 (d, $J = 3.8$ Hz, 1H, pyrrole-H), 6.18-6.24 (m, 7H, pyrrole-H), 5.78 (d, $J = 3.8$ Hz, 1H, pyrrole-H), 4.23-4.32 (m, 8H, CH₂), 2.56-2.58 (m, 12H, CH₃), 2.40 (s, 6H, CH₃), 2.28-2.32 (m, 20H, CH₂ and CH₃), 2.23 (s, 6H, CH₃), 2.14 (s, 6H, CH₃), 2.03 (s, 12H, CH₃), 1.92-1.97 (s, 12H, CH₃), 1.79 (s, 3H, CH₃), 1.68 (s, 3H, CH₃), 1.33-1.35 (m, 4H, CH₂), 0.89-0.91 (m, 12H, CH₃); MALDI-TOF calcd. 2252.8, found 2252.7 [(M)⁺]; UV/Vis (CHCl₃) λ_{\max} nm (A): 494.0 (0.728).

Zn^{II} Dimer (IV-46-D). The Zn^{II} dimer was obtained as a yellow solid. Yield: 5 mg (17%); ¹H NMR (400MHz, CDCl₃) δ (ppm) 7.13 (d, $J = 6.8$ Hz, 4H, *meso*-H), 4.25 (q, $J = 7.1$ Hz, 8H, CH₂), 2.55 (d, $J = 3.5$ Hz, 12H, CH₃), 2.25-2.33 (m, 20H, CH₂ and CH₃), 2.21 (d, $J = 2.9$ Hz, 12H, CH₃), 1.78 (s, 6H, CH₃), 1.67 (s, 6H, CH₃), 1.50 (t, $J = 6.7$ Hz, 4H, CH₂), 0.89 (t, $J = 6.7$ Hz, 12H, CH₃); MALDI-TOF calcd. 1292.5, found 1292.7 [(M)⁺]; UV/Vis (CHCl₃) λ_{\max} nm (A): 499.0 (1.284).

Zn^{II} flexible ladder (IV-47-L). The same procedure was used as in the synthesis of **IV-40-L**, starting from **IV-38** (25 mg, 0.04 mmol) to afford a yellow solid. Yield: 1 mg (2%); MALDI-TOF calcd. 2027.7, found 2027.9 [(M)⁺]; UV/Vis (CHCl₃) λ_{max} nm (A): 486.0 (0.876).

Zn^{II} Dimer (IV-47-D). The Zn^{II} dimer was obtained as a yellow solid. Yield: 0.6 mg (2.8%); ¹H NMR (400MHz, CDCl₃) δ (ppm) 7.68 (s, 4H, pyrrole-H), 7.34 (s, 4H, pyrrole-H), 7.11 (s, 4H, *meso*-H), 2.40 (s, 12H, CH₃), 2.27-2.31 (m, 8H, CH₂), 2.24 (s, 12H, CH₃), 1.69 (s, 12H, CH₃), 1.49-1.52 (m, 4H, CH₂); MALDI-TOF calcd. 1060.3, found 1060.5 [(M)⁺]; UV/Vis (CHCl₃) λ_{max} nm (A): 483.0 (1.164).

Zn^{II} flexible ladder (IV-48-L). The same procedure was used as in the synthesis of **IV-40-L**, starting from **IV-39** (30 mg, 0.04 mmol) to afford a yellow solid. Yield: 2 mg (7%); MALDI-TOF calcd. 2276.0, found 2275.8 [(M)⁺]; UV/Vis (CHCl₃) λ_{max} nm (A): 488.0 (0.913).

Zn^{II} Dimer (IV-48-D). The Zn^{II} dimer was obtained as a yellow solid. Yield: 5 mg (20%); ¹H NMR (400MHz, CDCl₃) δ (ppm) 7.85 (d, *J* = 7.0 Hz, 8H, Ar-H), 7.72 (t, *J* = 7.9 Hz, 4H, pyrrole-H), 7.49-7.53 (m, 4H, Ar-H), 7.42-7.46 (m, 12H, Ar-H and pyrrole-H), 7.13 (s, 4H, *meso*-H), 2.23-2.31 (m, 20H, CH₂ and CH₃), 1.70 (s, 12H, CH₃), 1.52 (t, *J* = 7.0 Hz, 4H, CH₂); MALDI-TOF calcd. 1308.4, found 1308.8 [(M)⁺]; UV/Vis (CHCl₃) λ_{max} nm (A): 488.0 (1.195).

5.3 Crystal Data

Table 5-1 Crystal data and structure refinement for **II-7-2**.

Temperature	-100.0 ± 0.1 °C
Empirical Formula	C ₈₅ H ₈₅ N ₈ CO ₂ Cl ₁₅
Formula Weight	1868.22
Crystal Colour, Habit	red, plate
Crystal Dimensions	0.08 × 0.20 × 0.35 mm
Crystal System	triclinic
Lattice Type	primitive
Lattice Parameters	a = 16.7103(16) Å b = 17.1894(16) Å c = 18.881(3) Å α = 101.334(7) ^o β = 101.137(7) ^o γ = 116.285(5) ^o V = 4519(1) Å ³
Space Group	<i>P</i> -1 (#2)
Z value	2
Reflections collected	11798
Independent reflections	7582
Goodness of Fit Indicator	1.05
Final R Indices [<i>I</i> > 2σ(<i>I</i>)]	R1 = 0.083, wR2 = 0.221
R indices (all data)	R1 = 0.133, wR2 = 0.256

Table 5-2 Crystal data and structure refinement for **II-13-2**.

Temperature	-100.0 ± 0.1 °C
Empirical Formula	C ₉₀ H ₈₀ N ₁₀ Co ₂ Cl ₃
Formula Weight	1632.20
Crystal Colour, Habit	red, plate
Crystal Dimensions	0.12 × 0.50 × 0.50 mm
Crystal System	triclinic
Lattice Type	primitive
Lattice Parameters	a = 13.5936(9) Å b = 18.5791(12) Å c = 24.3507(17) Å α = 90.743(3)° β = 92.110(2)° γ = 102.012(3)° V = 6009.9(7) Å ³
Space Group	<i>P</i> -1 (#2)
Z value	2
Reflections collected	15694
Independent reflections	7524
Goodness of Fit Indicator	0.95
Final R Indices [I > 2σ(I)]	R1 = 0.081, wR2 = 0.205
R indices (all data)	R1 = 0.136, wR2 = 0.221

Table 5-3 Crystal data and structure refinement for **II-25-3**.

Temperature	-100.0 ± 0.1 °C
Empirical Formula	C ₁₁₄ H ₁₃₂ N ₁₂ Zn ₃
Formula Weight	1866.43
Crystal Colour, Habit	red, prism
Crystal Dimensions	0.08 × 0.12 × 0.25 mm
Crystal System	trigonal
Lattice Type	R-centered
Lattice Parameters	a = 19.650(1) Å b = 19.650 Å c = 60.258(4) Å α = 90.0° β = 90.0° γ = 120.0° V = 20150(2) Å ³
Space Group	<i>R</i> - 3 <i>c</i> (#167)
Z value	6
Reflections collected	3960
Independent reflections	2954
Goodness of Fit Indicator	1.06
Final R Indices [<i>I</i> > 2σ(<i>I</i>)]	R1 = 0.037, wR2 = 0.091
R indices (all data)	R1 = 0.054, wR2 = 0.095

Table 5-4 Crystal data and structure refinement for **II-26-3**.

Temperature	-100.0 ± 0.1 °C
Empirical Formula	C _{112.5} H _{132.5} N ₁₂ Zn ₃
Formula Weight	1848.92
Crystal Colour, Habit	red, tablet
Crystal Dimensions	0.12 × 0.18 × 0.50 mm
Crystal System	monoclinic
Lattice Type	primitive
Lattice Parameters	a = 15.887(3) Å b = 18.761(3) Å c = 21.673(3) Å α = 90.0° β = 92.527(5)° γ = 90.0° V = 6453.6(18) Å ³
Space Group	<i>P</i> 2/ <i>c</i> (#13)
Z value	2
Reflections collected	8444
Independent reflections	5325
Goodness of Fit Indicator	1.05
Final R Indices [<i>I</i> > 2σ(<i>I</i>)]	R1 = 0.069, wR2 = 0.186
R indices (all data)	R1 = 0.106, wR2 = 0.204

Table 5-5 Crystal data and structure refinement for **II-35-3**.

Temperature	-100.0 ± 0.1 °C
Empirical Formula	C ₁₁₅ H ₁₃₄ N ₁₂ Zn ₃ Cl ₂
Formula Weight	1951.35
Crystal Colour, Habit	red, tablet
Crystal Dimensions	0.20 × 0.20 × 0.35 mm
Crystal System	monoclinic
Lattice Type	primitive
Lattice Parameters	a = 14.9377(18) Å b = 37.901(5) Å c = 23.225(3) Å α = 90.0° β = 92.749(4)° γ = 90.0° V = 13134(3) Å ³
Space Group	<i>P</i> 2 ₁ / <i>c</i> (#14)
Z value	4
Reflections collected	17934
Independent reflections	9602
Goodness of Fit Indicator	1.08
Final R Indices [<i>I</i> > 2σ(<i>I</i>)]	R1 = 0.101, wR2 = 0.286
R indices (all data)	R1 = 0.153, wR2 = 0.319

Table 5-6 Crystal data and structure refinement for **III-27-4**.

Temperature	-100.0 ± 0.1 °C
Empirical Formula	C ₉₀ H ₇₄ N ₁₆ Zn ₄ Cl ₆
Formula Weight	1853.83
Crystal Colour, Habit	green, prism
Crystal Dimensions	0.13 × 0.25 × 0.45 mm
Crystal System	monoclinic
Lattice Type	primitive
Lattice Parameters	a = 15.3033(13) Å b = 31.095(3) Å c = 17.7059(15) Å α = 90.0° β = 99.366(4)° γ = 90.0° V = 8313.2(12) Å ³
Space Group	<i>P</i> 2 ₁ / <i>n</i> (#14)
Z value	4
Reflections collected	10815
Independent reflections	6388
Goodness of Fit Indicator	1.07
Final R Indices [<i>I</i> > 2σ(<i>I</i>)]	R1 = 0.085, wR2 = 0.193
R indices (all data)	R1 = 0.159, wR2 = 0.253

Table 5-7 Crystal data and structure refinement for **III-33-4**.

Temperature	-100.0 ± 0.1 °C
Empirical Formula	C ₂₀₆ H ₂₅₄ N ₁₆ Zn ₄
Formula Weight	3215.73
Crystal Colour, Habit	green, prism
Crystal Dimensions	0.40 × 0.44 × 0.55 mm
Crystal System	monoclinic
Lattice Type	primitive
Lattice Parameters	a = 24.936(3) Å b = 12.9012(17) Å c = 28.201(4) Å α = 90.0° β = 95.206(6)° γ = 90.0° V = 9035(2) Å ³
Space Group	<i>P</i> 2/n (#13)
Z value	2
Reflections collected	21591
Independent reflections	12724
Goodness of Fit Indicator	1.07
Final R Indices [I > 2σ(I)]	R1 = 0.058, wR2 = 0.158
R indices (all data)	R1 = 0.105, wR2 = 0.180

Table 5-8 Crystal data and structure refinement for **III-36-6**.

Temperature	-170.0 ± 0.1 °C
Empirical Formula	C ₂₄₃ H ₂₁₉ N ₂₄ F ₁₂ Cl ₉ Zn ₆
Formula Weight	4414.69
Crystal Colour, Habit	green, tablet
Crystal Dimensions	0.11 × 0.22 × 0.40 mm
Crystal System	trigonal
Lattice Type	primitive
Lattice Parameters	a = 24.236(2) Å b = 24.236(2) Å c = 11.8480(6) Å α = 90.0° β = 90.0° γ = 120.0° V = 6026.8(6) Å ³
Space Group	<i>P</i> -3 (#147)
Z value	1
Reflections collected	7126
Independent reflections	5647
Goodness of Fit Indicator	1.09
Final R Indices [I > 2σ(I)]	R1 = 0.062, wR2 = 0.171
R indices (all data)	R1 = 0.081, wR2 = 0.186

Table 5-9 Crystal data and structure refinement for **IV-16-3**.

Temperature	-100.0 ± 0.1 °C
Empirical Formula	C ₈₄ H ₈₈ N ₈ Zn ₂
Formula Weight	1340.36
Crystal Colour, Habit	green, tablet
Crystal Dimensions	0.16 × 0.38 × 0.60 mm
Crystal System	monoclinic
Lattice Type	C-centered
Lattice Parameters	a = 19.3999(7) Å b = 12.7918(5) Å c = 28.5681(11) Å α = 90.0° β = 92.966(2)° γ = 90.0° V = 9035(2) Å ³
Space Group	<i>C</i> 2/ <i>c</i> (#15)
Z value	4
Reflections collected	8511
Independent reflections	6289
Goodness of Fit Indicator	1.06
Final R Indices [<i>I</i> > 2σ(<i>I</i>)]	<i>R</i> 1 = 0.044, <i>wR</i> 2 = 0.102
R indices (all data)	<i>R</i> 1 = 0.072, <i>wR</i> 2 = 0.115

Table 5-10 Crystal data and structure refinement for **IV-23-L**.

Temperature	-100.0 ± 0.1 °C
Empirical Formula	C ₁₃₀ H ₁₁₂ N ₁₆ Cu ₄ Cl ₁₂
Formula Weight	2577.92
Crystal Colour, Habit	black, prism
Crystal Dimensions	0.15 × 0.30 × 0.50 mm
Crystal System	monoclinic
Lattice Type	C-centered
Lattice Parameters	a = 35.898(4) Å b = 15.203(2) Å c = 24.481(3) Å α = 90.0° β = 100.757(3)° γ = 90.0° V = 13126(3) Å ³
Space Group	C 2/c (#15)
Z value	4
Reflections collected	6922
Independent reflections	2990
Goodness of Fit Indicator	1.06
Final R Indices [I > 2σ(I)]	R1 = 0.105, wR2 = 0.291
R indices (all data)	R1 = 0.187, wR2 = 0.350

Table 5-11 Crystal data and structure refinement for **IV-42-L**.

Temperature	-100.0 ± 0.1 °C
Empirical Formula	C ₁₃₆ H ₁₄₆ N ₁₆ O ₄ Zn ₄ Cl ₂₄
Formula Weight	3180.97
Crystal Colour, Habit	orange, plate
Crystal Dimensions	0.15 × 0.20 × 0.25 mm
Crystal System	triclinic
Lattice Type	primitive
Lattice Parameters	a = 12.6924(16) Å b = 14.3388(14) Å c = 22.438(3) Å α = 105.588(8) ^o β = 96.193(7) ^o γ = 110.661(6) ^o V = 3586.2(8) Å ³
Space Group	<i>P</i> -1 (#2)
Z value	1
Reflections collected	9205
Independent reflections	5960
Goodness of Fit Indicator	1.05
Final R Indices [<i>I</i> > 2σ(<i>I</i>)]	<i>R</i> 1 = 0.074, w <i>R</i> 2 = 0.193
R indices (all data)	<i>R</i> 1 = 0.116, w <i>R</i> 2 = 0.211

Chapter Six
Conclusions and Future Work

6.1 Conclusions

In this study, the spacer linking two dipyrin units proved to be the key factor for generation of homoleptic metal complexes (circular helicates and grids). Unlike bipyridine ligands, bisdipyrin ligands with alkylene groups as the spacers always favour double- or triple-helicates upon metalation. Introduction of a diacetylene group or a fused ring system as the spacer to afford a linear rigid ligand successfully overcame the aforementioned obstacle, and led to formation of circular helicates or grids/hexagons, respectively. Grids and hexagons with channels in their solid states have been specially designed and generated. It was found that generation of the channels was driven by several noncovalent interactions such as π - π stacking, CH/ π and F-F interactions. Therefore, porous grids and hexagons using bisdipyrin ligands are poised for future study of their potential application in gas storage and separation,⁵¹⁻⁵⁴ catalysis⁵⁵,⁵⁶ and drug release.^{57, 58}

Heteroleptic bisdipyrin metal complexes (racks and ladders) both possess two distinct ligands. The key to their syntheses is to bypass the formation of homoleptic metal complexes. Bulky substituents attached to the α' -position of the terminal pyrrole rings in ring fused ligands proved to prefer zigzag metal complexes to grids, which allows the generation of racks and zigzag racks without unwanted grids. However, the synthesis of ladders using the same strategy appeared unsuccessful. Therefore, another crucial factor for synthesis of ladders emerged, which is the synthesis of an intermediate acting as both the ligand and the metal ion source. Two heteroleptic metal (Zn^{II} or Cu^{II}) complex intermediates were synthesized. The Cu^{II} complex

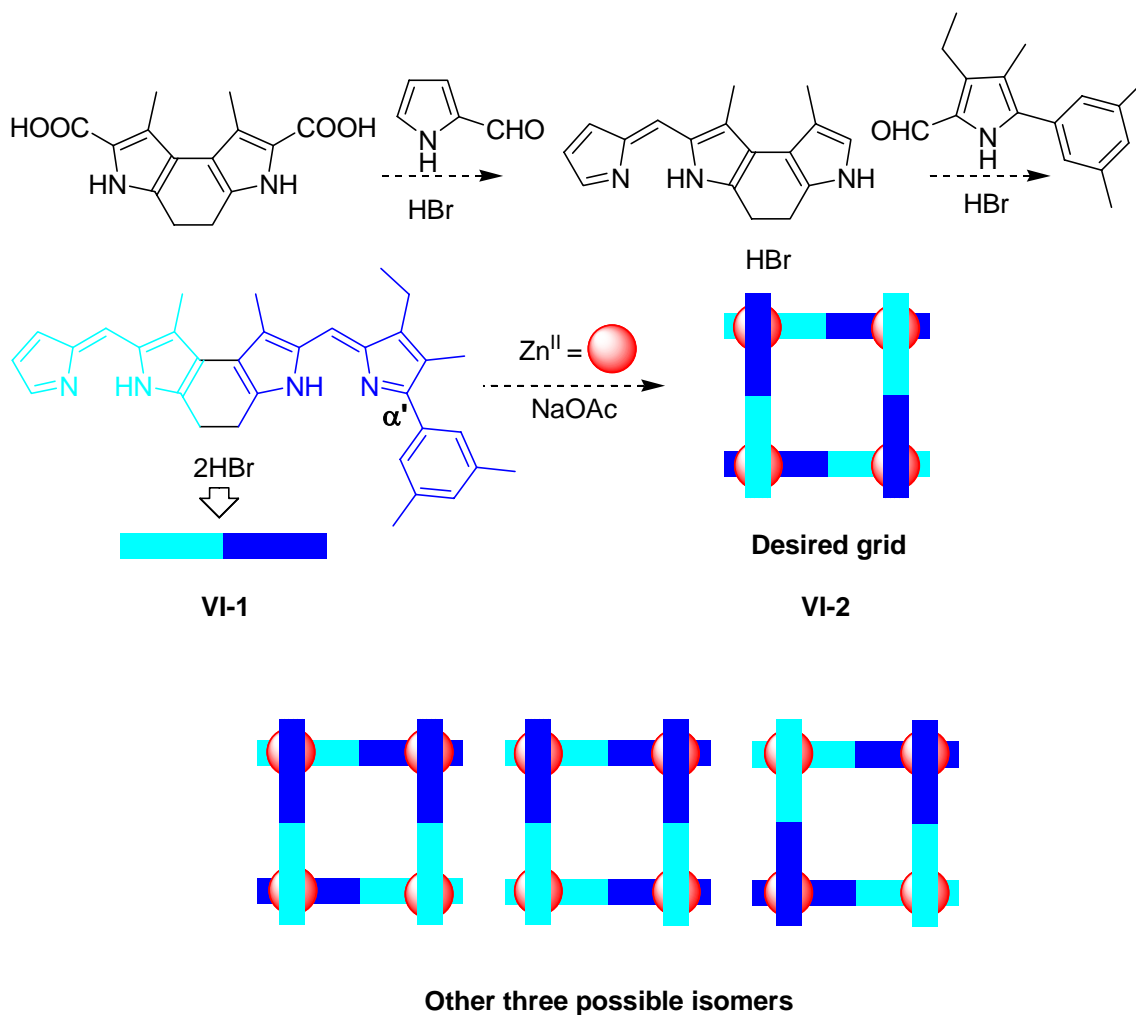
paired with ring fused ligands which prefer the metal ions with tetrahedral geometry such as Zn^{II} ions afforded the desired ladders and trace amounts of the unwanted grids. However, the Zn^{II} complex teamed with alkylene-linked ligands gave a small amount of the expected ladders and large amounts of homoleptic double-helicates since the ligands lacked a geometry preference for metal ions. In short, it appears that controlled synthesis of heteroleptic racks and ladders is feasible, which opens a path to fabrication of multicomponent supramolecular architectures using bisdipyrrin ligands to imitate complex and diverse biological systems.⁵⁹⁻⁶¹

6.2 Future Work

Myriad supramolecular systems in nature, ribosomes for example, fulfill diverse and sophisticated biological functions through noncovalent interactions of covalent building blocks.¹⁰³ Inspired by these biological processes, many artificial supramolecular systems have been designed and generated for various potential applications. Although synthetically attractive due to their high symmetry, homoleptic architectures are not the most important structures for diverse and complex biological systems. The larger the variety of components involved, such as in heteroleptic systems, the more information can be stored in the architectures. Minimizing the production of homoleptic structures during the synthesis of desired heteroleptic structures is the difficulty that has most limited progress in this area.

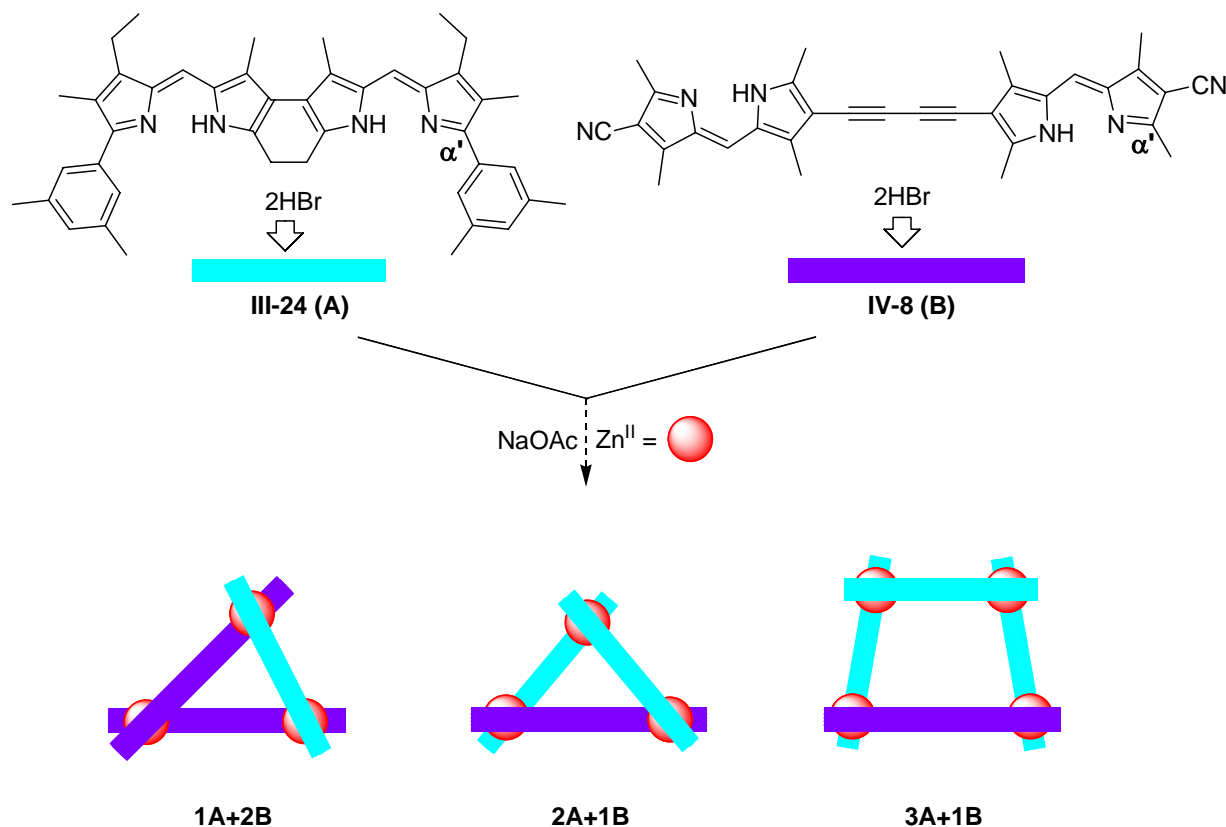
Inspired from the successful synthesis of homoleptic grids and hexagons in chapter 3, an unsymmetric ring fused bisdipyrrin ligand **VI-1** can be designed. The self-assembly of this unsymmetric ligand can theoretically afford four grids in the presence of Zn^{II} . However, the

introduction of a bulky 3,5-dimethylphenyl group at the α' -position of one terminal pyrrole ring may favour only one isomer **VI-2** because of the other three suffering at least one unfavourable steric interaction caused by two these bulky groups at a single coordination centre (Scheme 6-1).¹⁰⁴



Scheme 6-1 Synthetic route for preparation of unsymmetric ring fused bisdipyrrin ligand and its corresponding Zn^{II} grid.

With the successful controlled synthesis of heteroleptic racks **IV-16** in hand, we could explore more complicated systems with more information stored by replacing dipyrin ligand **IV-2** with bisdipyrrin ligand **IV-8** (Scheme 6-2). The diacetylene spacer in **IV-8** allows the two dipyrin units to adjust themselves to fulfill their roles in different architectures by rotation. Therefore, two triangles (**1A+2B** and **2A+1B**) and one trapezoid **3A+1B** are expected to form since ligand **III-24** prefers zigzag complexes to grids. More optimizations on the structure of ligand **IV-8**, such as introduction of bulky substituents at the α' -position, may surpass the generation of triangle **1A+2B** owing to unfavourable steric hindrance to afford an even more controlled reaction.



Scheme 6-2 Synthetic route for preparation of heteroleptic Zn^{II} complexes using bisdipyrrin ligand **III-24** and **IV-8**.

References

1. J. M. Lehn, *Supramolecular Chemistry-Concepts and Perspectives*, VCH, Weinheim, 1995.
2. G. M. Whitesides and B. Grzybowski, *Science*, 2002, **295**, 2418-2421.
3. J. S. Lindsey, *New J. Chem.*, 1991, **15**, 153-180.
4. D. P. Funeriu, J.-M. Lehn, G. Baum and D. Fenske, *Chem.--Eur. J.*, 1997, **3**, 99-104.
5. P. N. W. Baxter, *Compr. Supramol. Chem.*, 1996, **9**, 165-211.
6. M. Ruben, J. Rojo, F. J. Romero-Salguero, L. H. Uppadine and J.-M. Lehn, *Angew. Chem., Int. Ed.*, 2004, **43**, 3644-3662.
7. A. R. Pease, J. O. Jeppesen, J. F. Stoddart, Y. Luo, C. P. Collier and J. R. Heath, *Acc. Chem. Res.*, 2001, **34**, 433-444.
8. C. Joachim, J. K. Gimzewski and A. Aviram, *Nature*, 2000, **408**, 541-548.
9. A. El-Ghayouy, A. Harriman, A. De Cian, J. Fischer and R. Ziessel, *J. Am. Chem. Soc.*, 1998, **120**, 9973-9974.
10. G. Rapenne, J.-P. Sauvage, B. T. Patterson and F. R. Keene, *Chem. Commun.*, 1999, 1853-1854.
11. G. Baum, E. C. Constable, D. Fenske, C. E. Housecroft and T. Kulke, *Chem.--Eur. J.*, 1999, **5**, 1862-1873.
12. S. L. Larson, S. M. Hendrickson, S. L. Ferrere, D. L. Derr and C. M. Elliott, *J. Am. Chem. Soc.*, 1995, **117**, 5881-5882.
13. C. Bonnefous, N. Bellec and R. P. Thummel, *Chem. Commun.*, 1999, 1243-1244.

14. F. Tuna, J. Hamblin, A. Jackson, G. Clarkson, N. W. Alcock and M. J. Hannon, *Dalton Trans.*, 2003, 2141-2148.
15. L. J. Childs, N. W. Alcock and M. J. Hannon, *Angew. Chem., Int. Ed.*, 2002, **41**, 4244-4247.
16. T. Bark, M. Duggeli, H. Stoeckli-Evans and A. Von Zelewsky, *Angew. Chem., Int. Ed.*, 2001, **40**, 2848-2851.
17. O. Mamula, A. Von Zelewsky and G. Bernardinelli, *Angew. Chem., Int. Ed.*, 1998, **37**, 290-293.
18. G. S. Hanan, D. Volkmer, U. S. Schubert, J.-M. Lehn, G. Baum and D. Fenske, *Angew. Chem., Int. Ed. Engl.*, 1997, **36**, 1842-1844.
19. P. N. W. Baxter, R. G. Khoury, J.-M. Lehn, G. Baum and D. Fenske, *Chem.--Eur. J.*, 2000, **6**, 4140-4148.
20. L. Zhao, Z. Xu, L. K. Thompson, S. L. Heath, D. O. Miller and M. Ohba, *Angew. Chem., Int. Ed.*, 2000, **39**, 3114-3117.
21. A. R. Stefankiewicz and J.-M. Lehn, *Chem.--Eur. J.*, 2009, **15**, 2500-2503.
22. G. S. Hanan, C. R. Arana, J.-M. Lehn and D. Fenske, *Angew. Chem., Int. Ed. Engl.*, 1995, **34**, 1122-1124.
23. J. Ramirez, A.-M. Stadler, G. Rogez, M. Drillon and J.-M. Lehn, *Inorg. Chem.*, 2009, **48**, 2456-2463.
24. P. N. Baxter, G. S. Hanan and J.-M. Lehn, *Chem. Commun.*, 1996, 2019-2020.
25. M. Schmittel, V. Kalsani, R. S. K. Kishore, H. Coelfen and J. W. Bats, *J. Am. Chem. Soc.*, 2005, **127**, 11544-11545.

26. J.-M. Lehn, *Proc. Natl. Acad. Sci. U. S. A.*, 2002, **99**, 4763-4768.
27. R. Kramer, J. M. Lehn, A. De Cian and J. Fischer, *Angew. Chem., Int. Ed. Engl.*, 1993, **32**, 703-706.
28. P. N. W. Baxter, J.-M. Lehn, B. O. Kneisel and D. Fenske, *Chem. Commun.*, 1997, 2231-2232.
29. J.-M. Lehn, *Science*, 2002, **295**, 2400-2403.
30. M. T. Youinou, N. Rahmouni, J. Fischer and J. A. Osborn, *Angew. Chem., Int. Ed. Engl.*, 1992, **31**, 733-735.
31. S. Toyota, C. R. Woods, M. Benaglia, R. Haldimann, K. Warnmark, K. Hardcastle and J. S. Siegel, *Angew. Chem., Int. Ed.*, 2001, **40**, 751-754.
32. A. M. Garcia, F. J. Romero-Salguero, D. M. Bassani, J.-M. Lehn, G. Baum and D. Fenske, *Chem.--Eur. J.*, 1999, **5**, 1803-1808.
33. D. L. Reger, M. F. Huff, A. L. Rheingold and B. S. Haggerty, *J. Am. Chem. Soc.*, 1992, **114**, 579-584.
34. J. Hausmann, G. B. Jameson and S. Brooker, *Chem. Commun.*, 2003, 2992-2993.
35. P. N. W. Baxter, J.-M. Lehn, J. Fischer and M.-T. Youinou, *Angew. Chem., Int. Ed. Engl.*, 1994, **33**, 2284-2287.
36. M. Barboiu, G. Vaughan, R. Graff and J.-M. Lehn, *J. Am. Chem. Soc.*, 2003, **125**, 10257-10265.
37. L. Shimoni-Livny, J. P. Glusker and C. W. Bock, *Inorg. Chem.*, 1998, **37**, 1853-1867.
38. C. Janiak, *Dalton*, 2000, 3885-3896.
39. G. S. Hanan, C. R. Arana, J.-M. Lehn, G. Baum and D. Fenske, *Chem.--Eur. J.*, 1996, **2**,

- 1292-1302.
40. A.-M. Stadler, F. Puntoriero, S. Campagna, N. Kyritsakas, R. Welter and J.-M. Lehn, *Chem.--Eur. J.*, 2005, **11**, 3997-4009.
 41. H. Sleiman, P. N. W. Baxter, J.-M. Lehn, K. Airola and K. Rissanen, *Inorg. Chem.*, 1997, **36**, 4734-4742.
 42. W. R. McWhinnie and J. D. Miller, *Advan. Inorg. Chem. Radiochem.*, 1969, **12**, 135-215.
 43. E. C. Constable, *Advan. Inorg. Chem. Radiochem.*, 1986, **30**, 69-121.
 44. F. Puntoriero, S. Campagna, A.-M. Stadler and J.-M. Lehn, *Coord. Chem. Rev.*, 2008, **252**, 2480-2492.
 45. Y. Zhang, A. Thompson, S. J. Rettig and D. Dolphin, *J. Am. Chem. Soc.*, 1998, **120**, 13537-13538.
 46. A. Thompson and D. Dolphin, *J. Org. Chem.*, 2000, **65**, 7870-7877.
 47. Z. Zhang and D. Dolphin, *Chem. Commun.*, 2009, 6931-6933.
 48. A. Thompson, S. J. Rettig and D. Dolphin, *Chem. Commun.*, 1999, 631-632.
 49. J. Xu, T. N. Parac and K. N. Raymond, *Angew. Chem., Int. Ed.*, 1999, **38**, 2878-2882.
 50. T. E. Wood, A. C. Ross, N. D. Dalgleish, E. D. Power, A. Thompson, X. Chen and Y. Okamoto, *J. Org. Chem.*, 2005, **70**, 9967-9974.
 51. K. S. Park, Z. Ni, A. P. Cote, J. Y. Choi, R. Huang, F. J. Uribe-Romo, H. K. Chae, M. O'Keeffe and O. M. Yaghi, *Proc. Natl. Acad. Sci. U. S. A.*, 2006, **103**, 10186-10191.
 52. A. G. Wong-Foy, A. J. Matzger and O. M. Yaghi, *J. Am. Chem. Soc.*, 2006, **128**, 3494-3495.
 53. R. Banerjee, A. Phan, B. Wang, C. Knobler, H. Furukawa, M. O'Keeffe and O. M. Yaghi,

- Science*, 2008, **319**, 939-943.
54. J. L. C. Rowsell and O. M. Yaghi, *J. Am. Chem. Soc.*, 2006, **128**, 1304-1315.
55. C. J. Hastings, D. Fiedler, R. G. Bergman and K. N. Raymond, *J. Am. Chem. Soc.*, 2008, **130**, 10977-10983.
56. D. Fiedler, D. H. Leung, R. G. Bergman and K. N. Raymond, *Acc. Chem. Res.*, 2005, **38**, 349-358.
57. P. Horcajada, C. Serre, M. Vallet-Regi, M. Sebban, F. Taulelle and G. Ferey, *Angew. Chem., Int. Ed.*, 2006, **45**, 5974-5978.
58. P. Horcajada, C. Serre, G. Maurin, N. A. Ramsahye, F. Balas, M. Vallet-Regi, M. Sebban, F. Taulelle and G. Ferey, *J. Am. Chem. Soc.*, 2008, **130**, 6774-6780.
59. A. Langner, S. L. Tait, N. Lin, C. Rajadurai, M. Ruben and K. Kern, *Proc. Natl. Acad. Sci. U. S. A.*, 2007, **104**, 17927-17930.
60. N. Christinat, R. Scopelliti and K. Severin, *Angew. Chem., Int. Ed.*, 2008, **47**, 1848-1852.
61. M. Schmittel and K. Mahata, *Angew. Chem., Int. Ed.*, 2008, **47**, 5284-5286.
62. T. E. Wood, N. D. Dalgleish, E. D. Power, A. Thompson, X. Chen and Y. Okamoto, *J. Am. Chem. Soc.*, 2005, **127**, 5740-5741.
63. Y. Tobe, J. Kishi, I. Ohki and M. Sonoda, *J. Org. Chem.*, 2003, **68**, 3330-3332.
64. C.-W. Wan, A. Burghart, J. Chen, F. Bergstroem, L. B. A. Johansson, M. F. Wolford, T. G. Kim, M. R. Topp, R. M. Hochstrasser and K. Burgess, *Chem.--Eur. J.*, 2003, **9**, 4430-4441.
65. D. H. Cho, J. H. Lee and B. H. Kim, *J. Org. Chem.*, 1999, **64**, 8048-8050.
66. J. B. Paine, III, R. B. Woodward and D. Dolphin, *J. Org. Chem.*, 1976, **41**, 2826-2835.

67. L. Ma, J.-Y. Shin, B. O. Patrick and D. Dolphin, *CrystEngComm*, 2008, **10**, 1539-1541.
68. J. Ramirez, A.-M. Stadler, N. Kyritsakas and J.-M. Lehn, *Chem. Commun.*, 2007, 237-239.
69. S. Dong, Z. Li and J. Qin, *J. Phys. Chem. B*, 2009, **113**, 434-441.
70. J. Regourd, A. A.-S. Ali and A. Thompson, *J. Med. Chem.*, 2007, **50**, 1528-1536.
71. D. T. Kozhich, L. V. Akimenko, A. F. Mironov and R. P. Evstigneeva, *Zh. Org. Khim.*, 1977, **13**, 2604-2608.
72. Y. Murakami and K. Sakata, *Bull. Chem. Soc. Jpn.*, 1974, **47**, 3025-3028.
73. C. Bruckner, V. Karunaratne, S. J. Rettig and D. Dolphin, *Can. J. Chem.*, 1996, **74**, 2182-2193.
74. L. S. Liebeskind and W. Liu, (Emory University, USA). Application: WO 2001, p. 34 pp.
75. L. Ghosez, C. Franc, F. Denonne, C. Cuisinier and R. Touillaux, *Can. J. Chem.*, 2001, **79**, 1827-1839.
76. H. M. G. Al-Hazimi, A. H. Jackson, D. W. Knight and T. D. Lash, *J. Chem. Soc., Perkin Trans. 1*, 1987, 265-276.
77. T. D. Lash, J. R. Bellettini and S. J. Voiles, *J. Heterocycl. Chem.*, 1993, **30**, 525-528.
78. H.-C. Wu, P. Thanasekaran, C.-H. Tsai, J.-Y. Wu, S.-M. Huang, Y.-S. Wen and K.-L. Lu, *Inorg. Chem.*, 2006, **45**, 295-303.
79. X.-H. Bu, H. Liu, M. Du, K. M.-C. Wong, V. W.-W. Yam and M. Shionoya, *Inorg. Chem.*, 2001, **40**, 4143-4149.
80. S. R. Halper and S. M. Cohen, *Angew. Chem., Int. Ed.*, 2004, **43**, 2385-2388.
81. S. R. Halper and S. M. Cohen, *Inorg. Chem.*, 2005, **44**, 4139-4141.

82. Q. Miao, J.-Y. Shin, B. O. Patrick and D. Dolphin, *Chem. Commun.*, 2009, 2541-2543.
83. T. E. Wood and A. Thompson, *Chem. Rev.*, 2007, **107**, 1831-1861.
84. W. Qin, M. Baruah, M. Van der Auweraer, F. C. De Schryver and N. Boens, *J. Phys. Chem. A*, 2005, **109**, 7371-7384.
85. M. M. C. Lo and G. C. Fu, *J. Am. Chem. Soc.*, 2002, **124**, 4572-4573.
86. J. T. Hunt, T. Mitt, R. Borzilleri, J. Gullo-Brown, J. Fagnoli, B. Fink, W.-C. Han, S. Mortillo, G. Vite, B. Wautlet, T. Wong, C. Yu, X. Zheng and R. Bhide, *J. Med. Chem.*, 2004, **47**, 4054-4059.
87. A. Alberola, A. G. Ortega, M. L. Sadaba and C. Sanudo, *Tetrahedron*, 1999, **55**, 6555-6566.
88. S. R. Halper, M. R. Malachowski, H. M. Delaney and S. M. Cohen, *Inorg. Chem.*, 2004, **43**, 1242-1249.
89. E. M. Garcia-Frutos, G. Henrich, E. Gutierrez, A. Monge and B. Gomez-Lor, *J. Org. Chem.*, 2010, **75**, 1070-1076.
90. Z. Ciunik, T. Ruman, M. Lukasiewicz and S. Wolowiec, *J. Mol. Struct.*, 2004, **690**, 175-180.
91. O. Seneque, O. Reinaud and M. Giorgi, *Chem. Commun.*, 2001, 984-985.
92. D. Sredojevic, G. A. Bogdanovic, Z. D. Tomic and S. D. Zaric, *CrystEngComm*, 2007, **9**, 793-798.
93. A. Mai, S. Massa, R. Ragno, I. Cerbara, F. Jesacher, P. Loidl and G. Brosch, *J. Med. Chem.*, 2003, **46**, 512-524.
94. H. B. Tanh Jeazet, K. Gloe, T. Doert, O. N. Kataeva, A. Jaeger, G. Geipel, G. Bernhard, B.

- Buechner and K. Gloe, *Chem. Commun.*, 2010, **46**, 2373-2375.
95. H. Suezawa, T. Yoshida, Y. Umezawa, S. Tsuboyama and M. Nishio, *Eur. J. Inorg. Chem.*, 2002, 3148-3155.
96. H.-P. Zhou, Y.-P. Tian, J.-Y. Wu, J.-Z. Zhang, D.-M. Li, Y.-M. Zhu, Z.-J. Hu, X.-T. Tao, M.-H. Jiang and Y. Xie, *Eur. J. Inorg. Chem.*, 2005, 4976-4984.
97. A. Costela, I. Garcia-Moreno, M. Pintado-Sierra, F. Amat-Guerri, R. Sastre, M. Liras, F. Lopez Arbeloa, J. Banuelos Prieto and I. Lopez Arbeloa, *J. Phys. Chem. A*, 2009, **113**, 8118-8124.
98. A. Alberola, J. M. Andres, A. Gonzalez, R. Pedrosa and M. Vicente, *Heterocycles*, 1989, **29**, 1983-1991.
99. J. L. Sessler, M. J. Cyr, V. Lynch, E. McGhee and J. A. Ibers, *J. Am. Chem. Soc.*, 1990, **112**, 2810-2813.
100. C. K. Chang and N. Bag, *J. Org. Chem.*, 1995, **60**, 7030-7032.
101. T. Ueno, Y. Urano, H. Kojima and T. Nagano, *J. Am. Chem. Soc.*, 2006, **128**, 10640-10641.
102. H. J. Anderson, C. E. Loader and A. Foster, *Can. J. Chem.*, 1980, **58**, 2527-2530.
103. B. S. Schuwirth, M. A. Borovinskaya, C. W. Hau, W. Zhang, A. Vila-Sanjurjo, J. M. Holton and J. H. D. Cate, *Science*, 2005, **310**, 827-834.
104. L. Zhao, B. H. Northrop, Y.-R. Zheng, H.-B. Yang, H. J. Lee, Y. M. Lee, J. Y. Park, K.-W. Chi and P. J. Stang, *J. Org. Chem.*, 2008, **73**, 6580-6586.